

**Regulation of type IV pili formation and function by
the small GTPase MglA in *Myxococcus xanthus***

Dissertation

zur Erladung des Doktorgrades
der Naturwissenschaften
(Dr. rer. nat)

dem Fachbereich Biologie
der Philipps-Universität Marburg
vorgelegt von

Anna Potapova
aus Ekaterinburg, Russland

Marburg an der Lahn, September 2019

Die Untersuchungen zur vorliegenden Arbeit wurden von September 2014 bis September 2019 am Max-Planck-Institut für terrestrische Mikrobiologie unter der Leitung von Prof. Dr. Lotte Søgaard-Andersen durchgeführt.

Vom Fachbereich Biologie der Philipps-Universität Marburg als Dissertation
angenommen am: ____ . ____ . _____

Erstgutachterin: Prof. Dr. Lotte Søgaard-Andersen

Zweitgutachter: Prof. Dr. Martin Thanbichler

Weitere Mitglieder der Prüfungskommission:

Prof. Dr. Lars-Oliver Essen

Priv. Doz. Dr. Christof Taxis

Tag der mündlichen Prüfung: ____ . ____ . ____

Die während der Promotion erzielten Ergebnisse sind zum Teil in folgenden Originalpublikationen veröffentlicht worden:

Spatial control of the GTPase MglA by localized RomR–RomX GEF and MglB GAP activities enables *Myxococcus xanthus* motility.

Szadkowski D, Harms A, Carreira L, Wigbers M, **Potapova A**, Wuichet K, Keilberg D, Gerland U & Søgaard-Andersen L. Nature Microbiology 2019 May. doi: 10.1038/s41564-019-0451-4.

The small GTPase MglA in concert with the SgmX scaffold protein stimulate type IV pili formation and function in *Myxococcus xanthus*.

Potapova A, Szadkowski D, Carreira L & Søgaard-Andersen L (Manuscript in preparation).

TABLE OF CONTENTS

TABLE OF CONTENTS	4
ABSTRACT	7
ZUSAMMENFASSUNG	8
ABBREVIATIONS	10
1 INTRODUCTION	11
1.1 Type IV pili.....	11
1.1.1 T4P biogenesis	11
1.1.2 Biological functions of T4P	16
1.1.3 Regulation of T4P formation, function & localization.....	18
1.2 Introduction of <i>Myxococcus xanthus</i>	26
1.2.1 Life cycle of <i>M. xanthus</i>	27
1.2.2 Motility in <i>M. xanthus</i>	28
1.2.3 Polarity of <i>M. xanthus</i> cells & its regulation	35
1.2.4 Regulation of T4P-dependent motility in <i>M. xanthus</i>	38
1.3 Scope of this study	41
2 RESULTS	43
2.1 Roles of MglA, MglB & RomR in T4P dependent motility	43
2.1.1 MglA stimulates formation & function of T4P	43
2.1.2 MglB & RomR indirectly affect formation of T4P	45
2.2 Parts of T4PM depend on the polarity proteins but are not connected physically.....	52
2.2.1 PilB localizes independently on MglA/MglB/RomR	52
2.2.2 PilT localizes independently on MglA/MglB/RomR	55
2.2.3 MglA regulates localization of PilM	57
2.2.4 MglA and RomR regulate localization of PilQ	59
2.2.5 The polarity module does not interact to PilB/PilT/PilM in bacterial two hybrid assay	62
2.3 Identification of SgmX.....	63
2.3.1 Characterization of SgmX	64
2.3.2 SgmX is important for T4P-dependent motility	67
2.3.3 SgmX interacts to MglA-GTP <i>in vitro</i>	69
2.3.4 SgmX stimulates T4P formation downstream of MglA.....	71
2.3.5 SgmX stimulates polar binding of PilB.....	72
2.3.6 SgmX regulates polar localization of MglA	73

2.3.7 SgmX localizes dynamically at the leading pole	76
2.3.8 MXAN_5763-5765 proteins are not essential in <i>M. xanthus</i>	79
2.4 Novel protein regulators might link MglA to the T4P machine	80
2.4.1 T4P-dependent motility-related interaction candidates of MglA-mVenus	80
2.4.2 PilB-mCherry & MglA-mVenus have common potential interaction partners.....	83
2.4.3 SgmX-mVenus & mCherry-PilM are not soluble in <i>in vivo</i> pull down	85
3 DISCUSSION.....	86
3.1 MglA has a diverse effects of the T4P formation and function.....	86
3.2 MglB & RomR indirectly affect localization of T4P	87
3.3 MglA affects localization of the T4PM proteins	88
3.4 SgmX is a novel effector of MglA-GTP in stimulating the T4P-dependent motility.....	89
3.5 MglA-based interaction scaffold.....	92
3.6 SgmX-independent activity of MglA and its other potential effector proteins	93
4 MATERIALS & METHODS.....	96
4.1 Chemicals and equipment	96
4.2 Media	98
4.3 Microbiological methods	100
4.3.1 <i>E. coli</i> strains.....	100
4.3.2 <i>M. xanthus</i> strains	100
4.3.3 Cultivation and storage of bacterial strains	103
4.3.4 Bacterial two hybrid assay (BACTH)	103
4.3.5 Motility assays for <i>M. xanthus</i>	104
4.3.6 Methylcellulose-associated assay	104
4.3.7 Congo red dye binding assay	105
4.3.8 T4P shear-off assay	105
4.3.9 Microscopy and analysis of fluorescence microscopy images	105
4.4 Molecular biology methods	106
4.4.1 Oligonucleotides and plasmids.....	106
4.4.2 Plasmid construction	110
4.4.3 Construction of in-frame deletion mutants	112
4.4.4 DNA isolation of <i>E. coli</i> and <i>M. xanthus</i>	113
4.4.5 Polymerase chain reaction	114
4.4.6 Agarose gel electrophoresis	115
4.4.7 Restriction and ligation of DNA fragments	116
4.4.8 Preparation and transformation of chemically competent <i>E. coli</i> cells.....	116

4.4.9 Transformation of <i>E. coli</i> cells for BACTH system	116
4.4.10 Preparation and transformation of electrocompetent <i>M. xanthus</i> cells	117
4.5 Biochemical methods.....	117
4.5.1 Purification of proteins.....	117
4.5.2 SDS polyacrylamide gel electrophoresis (SDS-PAGE).....	118
4.5.3 Immunoblot analysis	119
4.5.4 GTPase assay	119
4.5.5 Pull down experiments	120
4.5.6 Co-Immunoprecipitation (Co-IP).....	120
4.5.7 Liquid chromatography-mass spectrometry (LC-MS)	121
4.6 Transmission electron microscopy.....	122
4.7 Bioinformatic analyses and statistics	122
5 SUPPLEMENTARY DATA	123
6 REFERENCES	125
ACKNOWLEDGEMENTS.....	143
CURRICULUM VITAE	145
ERKLÄRUNG	147
EINVERSTÄNDNISERKLÄRUNG.....	148

ABSTRACT

Myxococcus xanthus cells are rod-shaped and move in the direction of their long axis, using two distinct motility systems. Adventurous gliding (A-) depends on the Agl/Glt motility complexes that assemble at the leading pole, adhere to the substratum, and disassemble at the lagging pole. Social (S-) motility depends on type IV pili (T4P) that localize at the leading cell pole. T4P are anchored in the cell envelope and pull cells forward through cycles of extension, surface adhesion and retraction powered by the T4P machine. This machine includes 10 proteins spanning the outer membrane, periplasm, inner membrane and cytoplasm. Most of the proteins in the machine form stationary complexes at the two poles while the two ATPases PilB and PilT localize mostly at the leading and lagging pole, respectively. *M. xanthus* cells occasionally stop and resume movement in the opposite direction. These reversals are regulated by the Frz chemosensory system. During reversals the old lagging pole becomes the new leading and *vice versa*, the two motility systems invert polarity and after a reversal, T4P are formed at the new leading pole. Thus, T4P can assemble at both poles but at any point in time, T4P only assemble at one pole. The mechanism(s) underlying unipolar T4P formation during cell movement remains unknown.

The small GTPase MglA is essential for motility in *M. xanthus*. MglA cycles between the active MglA-GTP state, which is essential for motility, and the inactive MglA-GDP state. MglA is activated by the RomR/RomX complex, which has guanine nucleotide exchange factor (GEF) activity, and is inhibited by MglB, which is a GTPase activating protein (GAP). MglA-GTP mostly localizes to the leading pole while MglB as well as RomR/RomX localize in bipolar, asymmetric pattern with the large cluster at the lagging pole. RomR/RomX recruits MglA-GTP to the leading pole while MglB excludes MglA-GTP from the lagging pole by converting MglA-GTP to MglA-GDP. Among these four proteins, only MglA is essential for T4P-dependent motility. However, the precise function of MglA for the T4P-dependent motility remains unclear.

Here, we demonstrate that MglA-GTP stimulates T4P formation and function while MglB ensures T4P unipolarity by excluding MglA-GTP from the lagging pole. Moreover, we identify the TPR domain-containing protein SgmX and show that it is important for T4P formation. Epistasis analyses support that MglA-GTP and SgmX act in the same genetic pathway and that SgmX acts downstream of MglA-GTP. *In vitro* analyses support that SgmX interacts directly with MglA-GTP. Additionally, SgmX stimulates polar accumulation of the PilB extension ATPase. Based on these findings, we propose a model in which MglA-GTP stimulates T4P assembly via direct interaction with SgmX, which in turn interacts with PilB to stimulate T4P extension.

ZUSAMMENFASSUNG

Die stäbchenförmigen Zellen von *Myxococcus xanthus* bewegen sich durch zwei Motilitätssysteme entlang ihrer Längsachse fort. Abenteuerliches Gleiten („adventurous gliding“) ist abhängig von den Agl/Glt Komplexen, die am führenden Zellpol zusammengebaut werden, sich an das Substrat anheften und am nachfolgenden Zellpol abgebaut werden. Soziale Motilität ist auf Typ 4 Pili (T4P) angewiesen, die am führenden Zellpol lokalisieren. T4P sind in der Zellhülle verankert und ziehen die Zellen durch einen Kreislauf aus Extension, Oberflächenanheftung und Retraktion nach vorne. Dieser Prozess wird durch den T4P Apparat angetrieben, der aus zehn Proteine besteht und sich über die äußere Membran, das Periplasma, die innere Membran sowie das Zytoplasma erstreckt. Die meisten dieser Proteine bilden unbewegliche Komplexe an den zwei Polen, während die zwei ATPasen PilB und PilT hauptsächlich am führenden beziehungsweise am nachfolgenden Zellpol lokalisieren. *M. xanthus* Zellen halten gelegentlich an und bewegen sich anschließend in die entgegen entgegengesetzte Richtung weiter. Diese Zellumkehrungen werden durch das Frz chemosensorische System reguliert. Während dieser Umkehrung wird der ehemals nachfolgende Zellpol zum neuen führenden Pol und andersherum und die zwei Motilitätssysteme stellen ihre Polaritäten um. Nach der Zellumkehrung werden T4P am neuen führenden Pol gebildet. Folglich können T4P an beiden Zellpolen gebildet werden, aber sind stets nur ein an einem der beiden Pole zu finden. Der Mechanismus, der zur einpoligen Ausbildung von T4P während der Bewegung der Zelle führt, ist nicht bekannt.

Die kleine GTPase MglA ist essentiell für die Fortbewegung von *M. xanthus*. MglA zirkuliert zwischen dem inaktiven MglA-GDP Zustand und dem aktiven MglA-GTP Zustand, der unentbehrlich für die Fortbewegung ist. MglA wird durch den RomR/RomX Komplex aktiviert, der die Aktivität eines Guanin-Nukleotid-Faktor besitzt, und durch das GTPase aktivierende Protein MglB gehemmt.

Während sich MglA-GTP meistens am führenden Zellpol befindet, lokalisieren MglB und der RomR/RomX Komplex bipolar und asymmetrisch mit einem großen Cluster am nachfolgenden Zellpol. RomR/RomX rekrutiert MglA-GTP zum führenden Pol während MglB MglA-GTP vom nachfolgenden Pol ausgrenzt, indem es MglA-GTP zu MglA-GDP umsetzt. Von diesen Proteinen ist nur MglA essentiell für T4P-abhängiger Motilität, wobei hier die genaue Funktion von MglA noch unbekannt ist.

Unsere Ergebnisse zeigen, dass MglA-GTP die Bildung und Funktion von T4P stimuliert, während MglB die Einpolarität von T4P durch Ausschluss von MglA-GTP vom nachfolgenden Zellpol

gewährleistet. Außerdem identifizieren wir das Protein SgmX mit TPR-Domäne und zeigen, dass es eine wichtige Rolle bei der Bildung von T4P übernimmt. Epistase-Analysen unterstützen die Vermutung, dass MglA-GTP und SgmX im selben genetischen Signalweg beteiligt sind, wobei SgmX nach MglA-GTP agiert. In vitro Untersuchungen befürworten eine direkte Interaktion zwischen SgmX und MglA-GTP. SgmX stimuliert zudem die polare Anreicherung der Extensions-ATPase PilB. Anhand dieser Ergebnisse schlagen wir ein Modell vor, in dem MglA-GTP durch direkte Interaktion mit SgmX den Zusammenbau von T4P stimuliert. SgmX wiederum interagiert mit PilB, um die Extension von T4P anzuregen.

ABBREVIATIONS

aa	amino acids
ATP/ADP	adenosin tri-/diphosphate
BACTH	Bacterial Adenylate Cyclase-based Two-Hybrid
bp	base pairs
cAMP	3',5'-cyclic monophosphate
c-di-GMP	bis-(3'-5')-cyclic dimeric guanosine monophosphate
CTT	casitone Tris medium
DNA	deoxyribonucleic acid
DMSO	dimethyl sulfoxide
DTT	dithiothreitol
EDTA	ethylenediaminetetraacetic acid
ECM	extracellular matrix
EPS	exopolysaccharides
FAs	focal adhesions
GAP	GTPase activating proteins
GEF	guanine nucleotide exchange factor
GTP/GDP	guanosine tri-/diphosphate
h	hours
IM	inner membrane
IPTG	isopropyl β -D-1-thiogalaktopyranoside
kDa	kilodalton
LPS	lipopolysaccharides
MCP	methyl-accepting chemotaxis protein
min	minutes
MOPS	3-(N-morpholino) propanesulfonic acid
OD	optical density
OM	outer membrane
pN	piconewton
PG	peptidoglycan
s	seconds
SDS-PAGE	sodium dodecyl sulfate polyacrilamide gel electrophoresis
sfGFP	super-folded green fluorescent protein
T2SS	type 2 secretion system
T4P(M)	type 4 pili (machine)
TEM	transmission electron microscopy
TPR	tetra-trico peptide
WT	wild type
X-gal	5-Brom-4-chlor-3-indoxyl- β -D-galactopyranosid

1 INTRODUCTION

1.1 Type IV pili

Type IV pili (T4P) are ubiquitous thin filamentous structures found in numerous Gram-positive and Gram-negative bacteria (Pelicic, 2008). T4P are several micrometers long and 5-8 nm in width and perform their function by means of rapid extension, surface adhesion and subsequent retraction. A force of up to 150 pN is generated during retractions that help to propel the cell forward. The T4P fiber is generally composed of major pilin subunits that are incorporated or removed from the pilus base at rate of ≈ 1000 subunits per second (Clausen et al., 2009; Merz et al., 2000; Skerker and Berg, 2001). The formation and function of T4P depends on the T4P machine (T4PM), which consists of a set of conserved proteins that localize in the outer membrane (OM), periplasm, inner membrane (IM) and cytoplasm. In different organisms a broad range of functions involves T4P. For example, T4P function in surface sensing, surface adhesion and colonization, motility, biofilm formation, host cell interaction, predation, virulence gene induction, DNA uptake and protein secretion (Berry and Pelicic, 2015; Burrows, 2012; Craig et al., 2019; Pelicic, 2008).

1.1.1 T4P biogenesis

The main building block of T4P, the major pilin subunit, is synthesized as a precursor prepilin that contains an N-terminal class III signal peptide (Szabo et al., 2007). This signal peptide starts with a leader peptide of variable length, which is consisting of hydrophilic and neutral residues and ends with a conserved glycine (Berry and Pelicic, 2015; Szabo et al., 2007). The leader peptide is cleaved by the PilD leader peptidase resulting in formation of the mature pilin (Nunn and Lory, 1991). Different lengths of the mature pilin and leader peptide provide the basis for classifying pilins into type IVa and type IVb pilins. In particular, type IVa pilins have a short leader peptide and mature protein of 150-160 aa in length, while type IVb pilins are characterized by longer leader peptides and either long (180-200 aa) or very short (40-50 aa) mature proteins. Nevertheless, both classes of pilins fold into similar structures (Giltner et al., 2012; Pelicic, 2008). The mature major pilin has a characteristic “lollipop” shape, consisting of a N-terminal kinked α -helix that contains a conserved part of 21 highly hydrophobic residues and is followed by a C-terminal β -strand rich globular domain (Kolappan et al., 2016; Wang et al., 2017) (Fig. 1A).

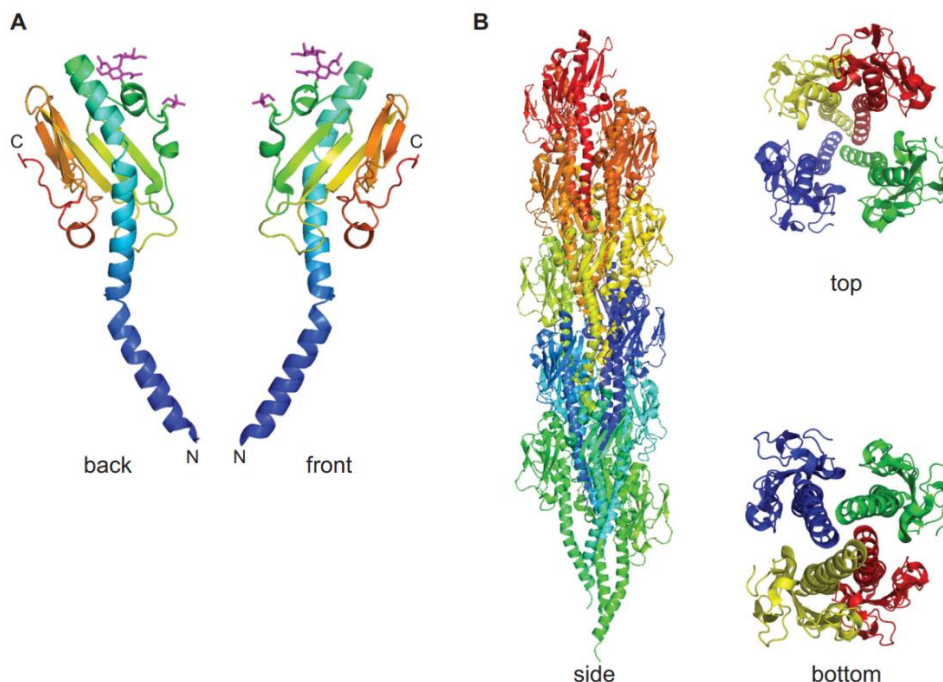


Figure 1 Common structural features of pilin subunit and assembled T4P illustrated with an example of *N. gonorrhoeae* T4aP (Berry and Pelicic, 2015).

(A) The structure of full-length PilE protomer. The protein is rainbow-colored from N-terminus (blue) to C-terminus (red).

(B) Side, top and bottom view of the pilus filament arrangement, obtained by combination of cryo-EM and X ray crystallography. Each single pilin subunit has a separate color.

Due to the hydrophobic N-terminal α -helix, the prepilins remain in the membrane as bitopic proteins, with the charged leader peptide in the cytoplasm and the C-terminal domain in the periplasm (Strom and Lory, 1987). Cleavage of the leader peptide by the dedicated prepilin peptidase occurs after the conserved Gly on the cytoplasmic side of the membrane, and leaves the mature pilin as a membrane protein with no remaining domain in the cytoplasm (Lemkul and Bevan, 2011).

The major pilins form an inner-membrane (IM) reservoir and are incorporated from this reservoir into the growing pilus. All obtained crystal structures, describing pilin assembly in the pilus filament, show that T4P are helical polymers in which the α 1N-helices provide the principal polymerization interface that are buried within the filament core, parallel to the filament axis (Craig et al., 2003; Hartung et al., 2011; Parge et al., 1995) (Fig. 1B).

The T4P biogenesis machinery that underlie T4P extension and retraction, comprise a conserved set of proteins. The simplest T4P machines present in bacteria contain (i) an ATPase that powers pilus assembly; (ii) an IM platform protein that transduces chemical energy from ATP hydrolysis to mechanical energy for pilin extrusion; (iii) a secretin that forms a channel in the OM

for the growing pilus; (iv) a prepilin processing peptidase, and (v) a major pilin and one or more pilin-like proteins (often named minor pilins) (Fig. 2) (Craig et al., 2019; Pelicic, 2008).

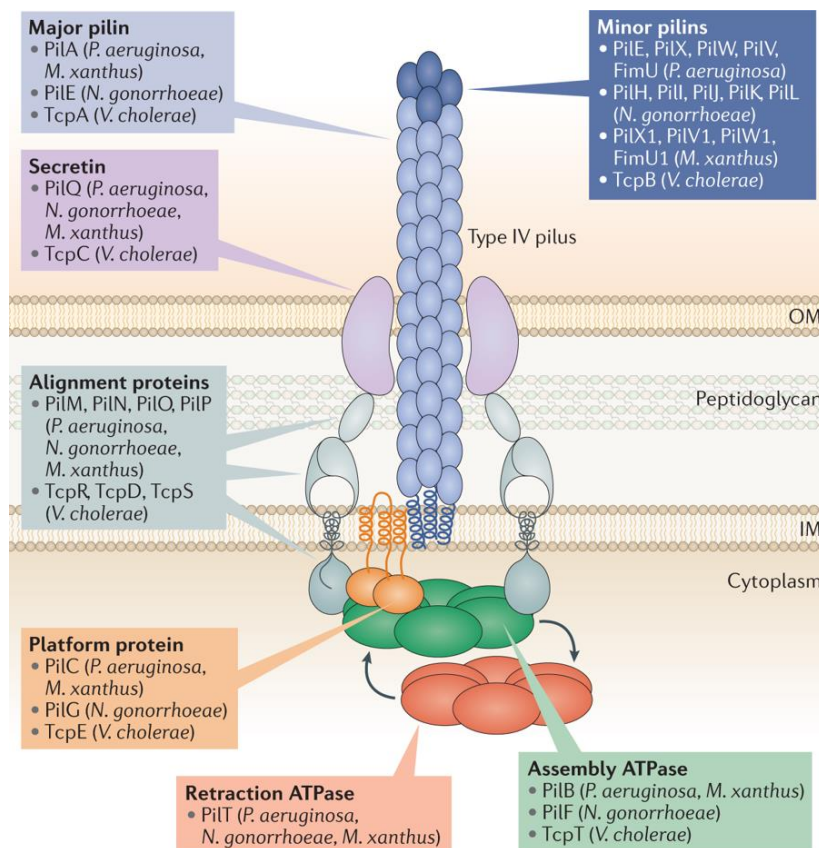


Figure 2 Architecture of the T4P machine (Craig et al., 2019). Major and minor pilins, secretin protein, platform protein and assembly ATPase represent the necessary machine components, while retraction ATPase and proteins of the alignment complex are more specific and are mostly found in T4aP systems. Names of the corresponding proteins from different species indicated in brackets.

Systematic genetic analyses identified a full set of genes encoding T4P biogenesis proteins in several model organisms. Interestingly, the number and organization of the genes varies for T4aP and T4bP systems. In bacteria producing T4aP, biogenesis genes are high in number and often scattered throughout the genome (up to 18 genes), while T4bP biogenesis genes are less numerous (10-12 genes) and are typically clustered (Alm and Mattick, 1997; Pelicic, 2008).

While the simplest T4P systems are limited to the five core components, more complex systems can contain a second retraction ATPase and four proteins, comprising a cytoplasm-IM-periplasmic alignment complex. This complex is formed by the periplasmic PiIP, IM PiIO, PiIN and cytoplasmic PiIM by means of direct protein-protein interactions (Friedrich et al., 2014; Georgiadou et al., 2012; Karupiah and Derrick, 2011; Leighton et al., 2015; Tammam et al.,

2013). In detail, PilP is connected to the secretin pore in the periplasm, and is interacting with IM PilON complex. PilN, in turn, interacts with cytoplasmic PilM, whereas PilM was shown to interact with the IM platform protein and the PilB ATPase on the cytoplasmic face (Bischof et al., 2016; Georgiadou et al., 2012) (Fig. 2). Thus, the function of the alignment complex is to stabilize the formation of the pilus at the platform protein and to translocate the energy, generated by the ATPases to the OM secretin channel (Berry and Pelicic, 2015; Leighton et al., 2015). Lack of any of the proteins from the alignment complex as well as any of the five core proteins described above leads to decrease or a complete loss of T4P formation (Bulyha et al., 2009; Hospenthal et al., 2017; Karuppiah et al., 2010; Martin et al., 1995; Rumszauer et al., 2006; Takhar et al., 2013) (Fig. 2).

Generally, the T4P machine of either type functions as follows. The hexameric extension ATPase (often referred to as PilB) binds the platform protein (and protein of an alignment complex for T4aP machine) at the cytoplasmic side (Bischof et al., 2016; Chang et al., 2016; Salzer et al., 2014b; Takhar et al., 2013). Binding and sequential ATP hydrolysis is hypothesized to result in significant conformational changes in the ATPase that are transferred to platform protein due to direct interactions (Bischof et al., 2016; Chang et al., 2016; McCallum et al., 2017; Nivaskumar et al., 2014; Savvides, 2007; Takhar et al., 2013). It has been suggested that the ATPase drives the rotation of the platform protein and “scoops” pilin subunits from the IM reservoir onto the base of the growing pilus (Chang et al., 2016; McCallum et al., 2017). Alternatively, pilin subunits have been suggested to be added at three active sites at the base of the filament (Craig et al., 2006). For the disassembly, the extension ATPase is released from the base of the T4P machinery, then the retraction ATPase (often referred to as PilT) binds to the base and is thought to stimulate the reverse process by causing the transfer of pilins from the base of the shrinking pilus back into the IM. Importantly, all of the proteins, building the T4P machine, except the PilC platform protein, were shown to oligomerize to form ring-like structures of different size (Chang et al., 2017; Chang et al., 2016). PilC was shown in some species to form a dimer (Bischof et al., 2016; Karuppiah et al., 2010).

Systems lacking a retraction ATPase are suggested to occasionally stop and reverse the assembly due to interruption of ATP or pilin subunits supply (Ng et al., 2016). This mode of retraction is spontaneous and less efficient than ATPase powered, therefore, not all the T4P-dependent functions might be fulfilled by systems lacking retraction ATPases (Craig et al., 2019; Ellison et al., 2018; Ellison et al., 2017). Genomes of *M. xanthus*, *P. aeruginosa* and *Neisseria* spp. encode a number of minor pilins that show high structural similarity to the major pilin but

accumulate in low amounts (Alm et al., 1996b; Chang et al., 2016; Jonsson et al., 1991). Low abundant minor pilins are thought to form a priming complex that initiates T4P assembly and eventually places itself at the tip of growing pilus (Ng et al., 2016; Nguyen et al., 2015). Some systems also incorporate minor pilins throughout the pilus supporting its dynamic structure and modulating functions (Giltner et al., 2010; Helaine et al., 2007; Nguyen et al., 2015). Gene clusters, encoding the minor pilins were also shown to contain *pilY/pilC* genes (Alm et al., 1996b; Carbonnelle et al., 2006). PilC1/2 of *Neisseria* and PilY1 of *P. aeruginosa* are predicted to be associated with the OM and to be involved in T4P adhesion and biogenesis (Alm et al., 1996b; Carbonnelle et al., 2005; Wolfgang et al., 1998b). Later studies reported that function of PilC is associated with T4P retraction, while PilY1 is important for T4P formation and surface attachment (Giltner et al., 2010; Wolfgang et al., 1998b).

Recent findings describe an archaeal system, named archaellum, that shares a similar protein core with T4P, and has likely diversified from the common ancestor prototype system (Albers and Jarrell, 2018). Unlike Gram-negative bacteria, archaea are surrounded by a single membrane and a proteinaceous cell wall called an S-layer (Daum and Gold, 2018). Therefore, the archaellum system is missing a PilQ-like conduit protein (Briegel et al., 2017; Daum et al., 2017). Instead, the growing filament is build on a membrane platform protein out of archaellins, which are processed in a similar fashion as the major and minor pilins and incorporated in the membrane (Albers and Jarrell, 2018). The platform protein in the membrane is additionally stabilized by an accessory proteins, which form a ring around it (Banerjee et al., 2012). Assembly of the archaellum is powered by an ATPase, which also triggers the function of the filament (Chaudhury et al., 2016). Archaellum functions as a propeller-type machine, similar to the bacterial flagellum, and its rotation is dependent on ATP hydrolysis (Reindl et al., 2013). The switch from the assembly to rotation occurs upon binding the cytoplasmic regulator (Meshcheryakov and Wolf, 2016).

Proteins of T4aP and T4bP systems share similarity with the proteins of the type 2 secretion systems (T2SS) of Gram-negative bacteria (Peabody et al., 2003). T2SS are used to translocate folded proteins (toxins, effectors and hydrolytic enzymes) from the periplasmic space across the OM to the extracellular milieu (Korotkov et al., 2012). To do so, a short periplasmic pseudopilus, formed by pseudopilin protomers, acts as a piston to push the proteins through the OM secretin (Hobbs and Mattick, 1993; Shevchik et al., 1997). Extension of the pseudopilus is stimulated by a hexameric secretion ATPase (Korotkov et al., 2012; Planet et al., 2001; Thomassin et al., 2017).

1.1.2 Biological functions of T4P

T4P are associated with an amazing number of biological processes, such as motility, cell-cell contact, surface colonization, biofilm formation, DNA uptake, prey invasion, and protein secretion (Chen and Dubnau, 2004; Craig et al., 2004; Evans et al., 2007; Hager et al., 2006; Klausen et al., 2003; Mattick, 2002; O'Toole and Kolter, 1998). Important properties of the T4P, which promote these various functions are the ability of T4P to bind different substrates, adhere to multiple surfaces and to retract.

T4P adhesion helps colonization of different biotic (host cells and extracellular matrix in commensals and pathogens) and abiotic (plastic, glass, metal etc.) surfaces (Craig et al., 2019). This function is highly relevant for human pathogens using T4P as a key virulence factor. Interestingly, major as well as minor pilins might provide steady attachment. In particular, *N. meningitidis* uses minor pilins to tightly attach to brain endothelial cells allowing the bacteria to eventually cross the blood-brain barrier (Coureuil et al., 2009). The N-terminal domain of the *P. aeruginosa* PilY1 demonstrated the ability for calcium-dependent integrin binding (Johnson et al., 2011). The major pilin PilA1 from Gram-positive *Rumonicoccus albus* promotes adhesion to cellulose in the gastrointestinal tract of ruminants (Rakotoarivonina et al., 2002).

Pilus-pilus contacts lead to formation of cell aggregates or micro-colonies in liquid environment by making use of pilus retraction. Later, on the surface, these aggregates can evolve into biofilms (O'Toole and Kolter, 1998). Formation of micro-colonies is stimulated by both major and minor pilins (Chiang et al., 1995; Helaine et al., 2005). Formation of T4P bundles also occurs upon pilus-pilus contact. This function is common for the enteropathogenic *E. coli* (EPEC) and helps tethering cells to each other and to the epithelial cells during host colonization (Donnenberg et al., 1997).

One of the key functions of T4P is to support surface-dependent motility via pilus retraction. This type of motility is commonly known as twitching or social motility and characterized by jerky cell movement. This allows cells to glide along the surface or even “walk”, positioning cells upright by tethering the T4P to the surface.

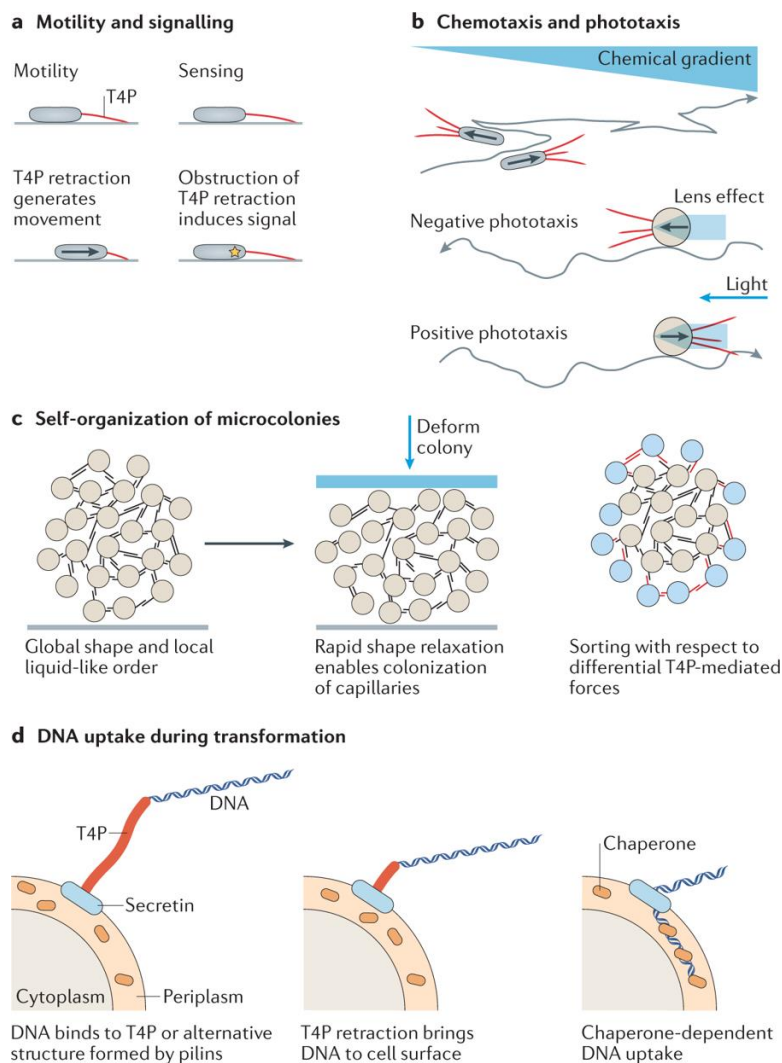


Figure 3 Retraction-dependent activities of piliated cells (Craig et al., 2019).

(A) Twitching motility and associated surface sensing

(B); Motility related chemotaxis and positive and negative phototaxis

(C) Microcolony formation

(D) DNA uptake, facilitated by cycles of T4P extension, adhesion and retraction.

The direction of twitching motility is often defined by sensing external signals. For example, cells of *P. aeruginosa* move by means of actively extruding and retracting T4P towards increasing concentrations of DMSO or succinate. Remarkably, *P. aeruginosa* cells can occasionally switch the movement direction, undergoing forced reversals that are caused by changes in gradient of the mentioned chemicals (Oliveira et al., 2016). The cyanobacterium *Synechocystis sp. PCC 6803* can detect the position of a light source and regulate motility as a function of light intensity, wavelength and direction (Chau et al., 2017; Wilde and Mullineaux, 2017). To do so, cells of *Synechocystis sp. PCC 6803* tend to arrange the localization of the PilB extension ATPase at the cell side closest to the light source, mediating T4P formation and movement towards the light source (Schuergers et al., 2015). Interestingly, the same bacterial species is capable of negative phototaxis during illumination with single spectral blue light at intensities comparable to sunlight. In this case T4P are predominantly assembled at the pole opposite the light source (Nakane and Nishizaka, 2017) (Fig. 3A, B).

In many species, T4P retraction controls important properties of microcolonies including local order of cells in the colony, colony viscosity and shape (Bonazzi et al., 2018; Welker et al., 2018). As mentioned above, microcolony formation is initiated by pilus-pilus interactions, while the retraction of pili brings cells physically closer to each other. Once the pilus-pilus bonds are disrupted, bacteria break away from each other, which results in fluid-like behavior of the microcolony (Welker et al, 2018). Minor alteration in pilus density, functionality of the retraction motor, or changes in post-translational pilin modifications leads to a switch from liquid-like to glass-like state, thus, lowering behavioral flexibility of the colony (Welker et al, 2018; Bonazzi et al, 2018) (Fig. 3C).

In addition to T4P-dependent motility, T4P are important for DNA uptake during natural transformation. During this process, the extended pilus binds extracellular DNA possibly via major or minor pilins and transports it during retraction across the OM to the periplasm (Chen and Dubnau, 2004; Stingl et al., 2010) (Fig. 3D). Retraction is crucial for DNA uptake (Wolfgang et al., 1998a). Along with DNA transport, T4P forming systems of *V. cholerae*, *E. coli* and *Dichelobacter nodosus* function as secretion systems, transporting exoproteins from the periplasm to the extracellular milieu (Han et al., 2007; Kirn et al., 2003; Yuen et al., 2013).

1.1.3 Regulation of T4P formation, function & localization

In different bacteria, the functionality, the number of T4P and their position over the cell surface are regulated. In this chapter, a number of common and unique regulatory factors and mechanisms that affect listed T4P-associated parameters at different levels will be described.

C-di-GMP and cAMP

Among the most wide spread motility regulation factors are the second messengers c-di-GMP (bis-(3'-5')-cyclic dimeric GMP) and cAMP (3', 5'-cyclic monophosphate). C-di-GMP has been reported to be involved in regulation of developmental transitions, synthesis of virulence factors, adherence to surfaces, biofilm formation and motility (Hengge, 2009; Römling et al., 2013). cAMP activity regulates type 3 secretion, carbon metabolism, virulence gene regulation, bacteriophage sensitivity, motility and biofilm formation (McDonough and Rodriguez, 2011).

Cyclic di-GMP is synthesized from two GTP molecules by diguanylate cyclases (DGCs) that have a GGDEF domain and is degraded by phosphodiesterases (PDEs) with either an EAL or an HD-GYP domain (Hengge, 2009). Cyclic di-GMP exerts a regulatory action through binding to diverse receptors including PilZ domain proteins, transcription factors, riboswitches and

enzymatically inactive variants of GGDEF, EAL or HD-GYP domain proteins (Guzzo et al., 2013; Sondermann et al., 2012).

Regulation of T4P dependent motility by c-di-GMP was described for *P. aeruginosa*, *Xanthomonas spp*, *M. xanthus*, *V. cholerae* and *Clostridium perfringens* (Dunger et al., 2016; Guzzo et al., 2013; Hendrick et al., 2017; Jones et al., 2015; Skotnicka et al., 2016). Further, a large protein network operating with intra- and extracellular levels of cAMP was reported for *P. aeruginosa*. Those regulatory mechanisms involve a range of proteins and protein-protein interactions, which will be described below.

In 2015, Jones et al. showed direct binding of c-di-GMP to the extension ATPase MshE in the human pathogen *Vibrio cholerae* (Jones et al., 2015). Cells of *V. cholerae* possess the type IVa mannose-sensitive hemagglutinin pili (MshA), important for initial attachment and biofilm formation (Watnick et al., 1999). It was demonstrated that high concentrations of c-di-GMP increase the production of the MshA pilus. Later on, it was shown that the N-terminal domain of MshE has the capacity to bind c-di-GMP via the MshEN domain. Presence of the c-di-GMP-binding domain was not shown for the pilus retraction ATPases - PilT and PilU of *V. cholerae*, suggesting that the retraction process is not modulated upon the direct binding of c-di-GMP (Jones et al., 2015).

The Gram-positive pathogen *C. perfringens* forms T4P that mediate motility and biofilm formation. The genome of *C. perfringens* encodes two homologs of the PilB extension ATPase and of the PilC IM platform protein, and three homologs of the major pilin PilA. Recently, one of the PilB homologues of *C. perfringens*, PilB2 was shown to bind c-di-GMP by means of the slightly modified MshEN-like domain. Additionally, c-di-GMP stimulates polymerization of PilA2 in a PilB2- and PilC2-dependent manner. However, possible implications for T4P dependent motility were not described yet (Hendrick et al., 2017).

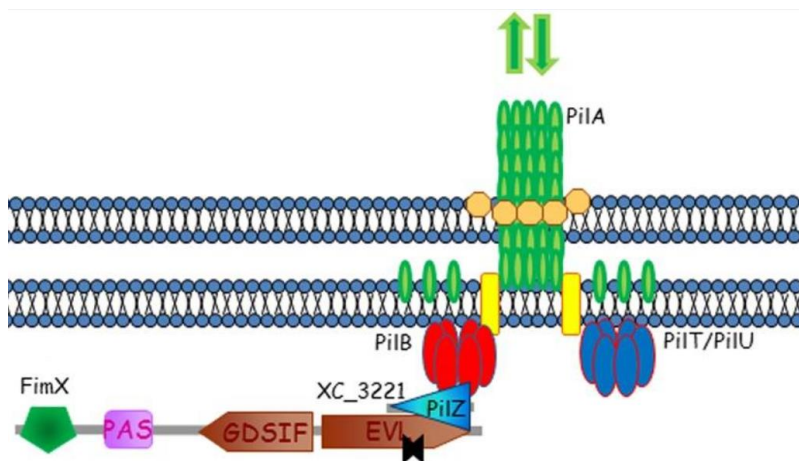


Figure 4 c-di-GMP regulation of T4P motility in *Xanthomonas* (Römling et al., 2013). See the description in the text.

Detailed studies of c-di-GMP regulation in *X. axonopodis*, *X. citri* and *X. campestris* lead to the following model of pilus biogenesis and twitching motility regulation (Guzzo et al., 2013; Guzzo et al., 2009; Römling et al., 2013) (Fig. 4). *Xanthomonas* contains the large FimX protein that binds c-di-GMP with its EAL domain and interacts with the PilZ protein (Guzzo et al., 2013). The interaction with c-di-GMP bound FimX triggers the PilZ-domain protein to interact with the extension ATPase PilB and to stimulate its function (Guzzo et al., 2013; Guzzo et al., 2009; Qi et al., 2012; Yang et al., 2014).

In *P. aeruginosa* unipolar T4P formation depends on c-di-GMP as well as cAMP. *P. aeruginosa* uses the degenerate GGDEF-EAL domain protein FimX for the assembly of the pilus at the leading pole (Jain et al., 2017; Kazmierczak et al., 2006; Laventie et al., 2019). The T4P machineries are assembled at the two poles in *P. aeruginosa* and localize PilB at both poles as well (Carter et al., 2017; Chiang et al., 2005). However, T4P are formed predominantly at the leading pole only during movement (Cowles et al., 2013; Skerker and Berg, 2001; Weiss, 1971). FimX is localized at the leading cell pole that also contains T4P and interacts directly with the PilB extension ATPase (but not with the PilT retraction ATPase) and this interaction is crucial for T4P extension. Moreover, polar localization of PilB depends on FimX, whereas localization of FimX depends on PilB and a number of membrane T4PM proteins (Jain et al., 2017). As in *Xanthomonas* spp., FimX binds c-di-GMP via its degenerate EAL domain with high affinity and this binding is crucial for its function in stimulating the T4P assembly (Guzzo et al., 2013; Jain et al., 2017; Kazmierczak et al., 2006; Navarro et al., 2009). FimW, which is encoded by a gene located immediately next to *fimX*, binds c-di-GMP and is important for the assembly and adherence of T4P. However, while upright “walking” by means of T4P was abolished, cells still

displayed twitching motility in absence of FimW arguing that FimX and FimW control distinct aspects of T4P activity (Laventie et al., 2019). *P. aeruginosa* also has a PilZ-like protein, which is important for pilus extension (Alm et al., 1996a). However, this protein was reported to not bind c-di-GMP (Merighi et al., 2007).

P. aeruginosa genome encodes a number of minor pilins, such as FimU, PilV, PilW, PilX, PilE, and a putative adhesin PilY1 (Alm et al., 1996b). The minor pilins have been shown to be important for pilus assembly and to be incorporated into the pilus fiber. The precise mechanism and implications of these incorporations are not well understood. Studies, carried out on the PilY1, PilW and PilX, revealed double regulatory role for those proteins. Thus, additionally to being a building block of the pilus, PilW, -X and -Y1 are able to repress swarming when levels of c-di-GMP are elevated. Absence of the c-di-GMP phosphodiesterase BifA leads to increased level of intracellular c-di-GMP, hyper-biofilm formation and repression of swarming motility. Combined deletion background of $\Delta bifA$ with $\Delta pilW$ or $\Delta pilX$, partially decreases swarming repression and those effects occur independently of PilW/X function in pilus assembly (Kuchma et al., 2012).

Cyclic AMP is synthesized from ATP by adenylate cyclases and it is degraded into AMP by phosphodiesterases. cAMP is produced in bacterial cells in response to carbon starvation and activates its receptor, the transcription factor CAP (catabolite activating protein) that further regulates transcription of multiple genes (Harman, 2001).

Extensive studies by Inclan et al, 2016 and Buensuceso et al, 2017 described a large regulatory system in *P. aeruginosa* that connects the T4P machine to the Chp chemosensory system and is capable of activation of the virulence factor regulator (Vfr). Subsequently, Vfr in a cAMP-dependent manner modulates the expression of various genes (Fig. 5) (Buensuceso et al., 2017; Inclan et al., 2016; Luo et al., 2015). Among the genes regulated by Vfr are, in particular, *pilBTU*, which encode the ATPases for T4P extension and retraction, and *pilMNOPQ*, which encode the proteins of the alignment complex. Activity of the Chp system is triggered by T4P retraction, hence, T4P-dependent motility is positively regulated upon the mechanical contact of the cells to the surface (Inclan et al., 2016).

The Chp chemosensory system of *P. aeruginosa* is similar to the well-studied Che system in *E. coli* and has been reported to control twitching motility and intracellular levels of cAMP (Darzins, 1993; Whitchurch et al., 2004). Key components of the Chp system include a transmembrane methyl-accepting chemotaxis protein (MCP) PilJ, a hybrid histidine kinase ChpA and two CheY-like response regulators PilG and PilH (Whitchurch et al., 2005; Whitchurch et al., 2004). The cytoplasmic FimL protein, via the large FimV protein is connected to the T4P machine.

FimV contains a periplasmic segment, one transmembrane domain, a putative peptidoglycan (PG)-binding LysM domain and a coiled-coil domain. The cytoplasmic part of FimV contains three tetratricopeptide (TPR) repeats that are, as well as the coiled-coil domain, predicted to be involved in protein-protein interactions. FimL is connected to FimV as well as the PilG response regulator (Fig. 5). Consistently all three proteins were shown to have an impact on T4P formation and twitching motility (Buensuceso et al., 2017; Fulcher et al., 2010; Inclan et al., 2016; Luo et al., 2015; Persat et al., 2015).

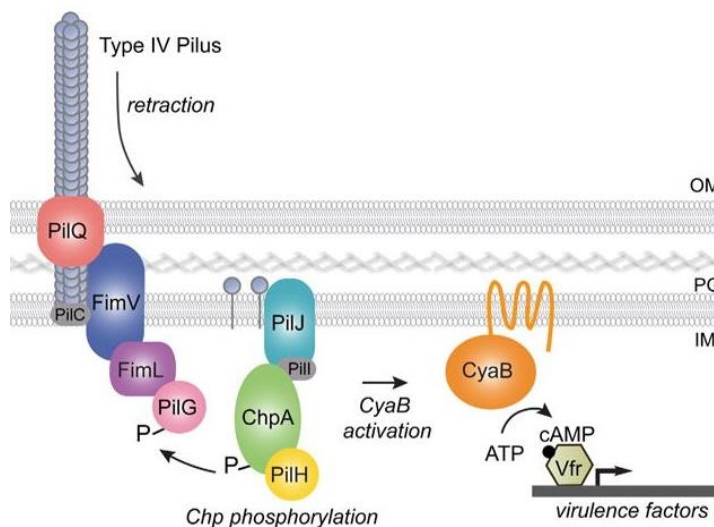


Figure 5 Model of surface-activated regulation of cAMP/Vfr-dependent virulence factors from *P. aeruginosa* (Inclan et al., 2016). See the description in the text.

The cAMP-dependent regulation mechanism described above involves the Chp chemotaxis system that is required for twitching motility and surface piliation in *P. aeruginosa*. In particular, the Chp system serves as conductor of the signal cascade initiated upon pilus retraction for further activation of the CyaB adenylate cyclase. Previously, deletions of *pilJ*, *pilG*, *pilI* and *chpA* that encode MCP, adaptor protein, histidine kinase and response regulator, respectively, have been shown to result in significantly reduced levels of surface pili (Darzins, 1993, 1994; DeLange et al., 2007; Leech and Mattick, 2006). Additionally, it is known that the functions of ChpA and PilG are connected to PilB and drive T4P extension, while the function of PilH is connected to PilT to facilitate retraction (Fig. 5). Moreover, Bertrand et al revealed the hierarchy, where ChpA, PilG and PilB act upstream of PilH, PilT and PilU (Bertrand et al., 2010). Preliminary, most of the effects given by proteins of the Chp system are eventually connected to further cAMP level regulation, but precise mechanisms are currently subjects for the research (Leighton et al., 2015).

The regulatory role of FimV is not limited to stimulating the T4P formation by transferring T4P retraction signal to CyaB and activation of the Vfr. FimV has also been shown to localize FimL, PilG, T4P structural components PilNMOPQ and PilRS two-component system to the pole (Buensuceso et al., 2017).

Absence of the minor pilins-associated PilY1 protein leads to a T4P stability and biogenesis defect. Therefore, its constant production is crucial for the assembly of functional T4P. It has been shown that expression of *pilY1* is activated by the DNA-binding response regulator AlgR, a part of the FimS-AlgR two-component system. The function of FimS-AlgR, in turn, is triggered by the Chp chemosensory system, with MCP PilJ likely interacting directly with FimS (Belete et al., 2008; Luo et al., 2015; Whitchurch et al., 1996).

Role of the PilY1 in swarming repression is similar to the ones of PilW and PilX minor pilins. It was found that repression effect of PilY1 specifically requires the SadC diguanylate cyclase that functions downstream of the PilY1. The PilY1-dependent signal transmission happens via the PilMNOP alignment complex further to SadC localized in the IM (Kuchma et al., 2010).

Photo- and chemotaxis

The mechanism described above for T4P formation regulation in *P. aeruginosa* involves a chemotaxis system. At least two chemotaxis systems were reported to be associated with T4P-dependent motility regulation in *M. xanthus* (see 1.2.2 and 1.2.3). Two bacterial species, described below, were shown to employ combination of photo- and chemotaxis to trigger directed movement by means of T4P.

Light regulated T4P formation and phototaxis-regulated T4P-dependent motility has been observed in cyanobacteria. A unique regulatory network, involving both chemo- and phototaxis, was elucidated recently for *Nostoc punctiforme* (Cho et al., 2017). *N. punctiforme* utilizes T4P-dependent motility to form long specialized filaments named hormogonia and to facilitate phototaxis (Ruan, 2013). Directed hormogonium movement is provided by T4P, whose function is stimulated by hormogonium polysaccharide (HPS). Accumulation of HPS is stimulated by functional T4P and is helpful only in filament movement but not for single cell movement (Khayatan et al., 2015; Risser and Meeks, 2013). Movement of the hormogonium works along the long axis of rod-shaped cells. These cells are oriented pole to pole and every pole has a functional machine for T4P assembly (Bhaya et al., 2000b; Khayatan et al., 2015).

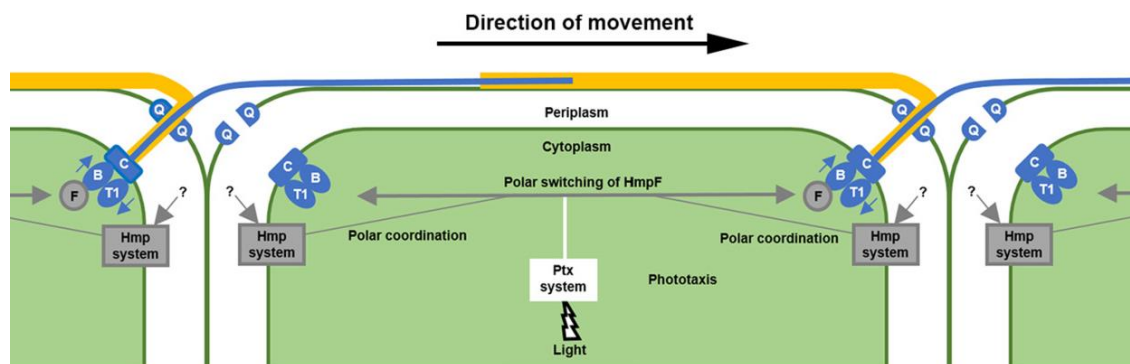


Figure 6 Model describing the regulatory interactions between T4P (blue), hormohonium polysaccharide (HPS, yellow), Hmp chemotaxis system (grey) and Ptx phototaxis control system (white) in *N. punctiforme* (Cho et al., 2017).

Hmp proteins, which are predicted to comprise a chemosensory system, regulate coordinated polarity and motility in *N. punctiforme*. The partial homologue of SMC (**S**tructural **M**aintenance of **C**hromosomes) protein, HmpF, is essential for extracellular PilA and HPS accumulation. HmpF localizes dynamically to the leading cell pole and was proposed to interact directly with the PilB extension ATPase that together with the retraction ATPase PilT remains static at both poles during movement. Therefore, HmpF likely activates PilB at the leading pole, relocates to the opposite pole shortly prior to a reversal, and stimulates PilB activity at the new leading pole. Coordinated localization of HmpF to one pole only, in turn, is regulated by the HmpB-E proteins, which represent the homologs of well-described elements of the Che system from *E. coli* (CheY, CheW, MCP, and CheA). In order to set a direction of movement, relocation of HmpF from one pole to another is triggered by a light signal, sensed by the Ptx phototaxis system (Campbell et al., 2015; Cho et al., 2017) (Fig. 6). Although the precise sequence of events is not known, it was speculated that the Hmp and the Ptx systems act by analogy with other chemosensory systems. Activation of kinase activity from the respective CheA homologs for the Hmp and Ptx system on one side of the cell results in the establishment of a concentration gradient of phospho-CheY. This phospho-CheY then prevents binding of HmpF to the T4P system, thus, driving localization of HmpF to the opposite pole (Cho et al., 2017).

The cyanobacterium *Synechocystis* sp. PCC6803 also possesses chemotaxis and phototaxis systems. Here, PilG, H, I, J, PilL-C and PilL-N represent chemotaxis proteins, while the phototaxis system is named Pix (Bhaya et al., 2001; Yoshihara et al., 2002; Yoshihara et al., 2000). Most of the studies in *S. sp.* PCC6803 are concentrated on the function of Pix system that involves activity of the blue-light receptor PixD and the response regulator PixE. These two proteins together mediate positive and negative motility responses to light of a difference wavelength. Initially, spherical cells of *Synechocystis* sp. PCC6803 extend T4P from any region

of the cell surface resulting in 360° range of motion for each individual cell (Bhaya et al., 2000a). Therefore, limited regional activation or inactivation of T4P is needed to provide directed movement. During light stimulation, the signal cascade starts with sensing light by the Pix proteins and only after a certain delay, an asymmetric localization of the extension ATPase is achieved. Thus, blue-light dependent negative phototaxis is achieved by breaking the PixD/PixE protein complex as the primary event (Nakane and Nishizaka, 2017; Tanaka et al., 2012; Yuan and Bauer, 2008).

MglA Ras-like GTPase

Small GTPases regulate multiple processes in eukaryotic as well as prokaryotic organisms such as growth, polarity and differentiation. They share a structural core, the G domain, which binds GDP or GTP and carries out GTP hydrolysis (Vetter and Wittinghofer, 2001). Slow intrinsic GTP/GDP turnover is commonly stimulated by GTPase activating proteins (GAPs) and the GDP bound state of the protein is the off-state. By contrast, the GTP-bound form is the active form, and exchange of GDP to GTP is stimulated by guanine nucleotide exchange factors (GEFs). This form of the protein interacts with downstream effectors to stimulate downstream processes (Bos et al., 2007). Small GTPases of the Ras superfamily are additionally divided into five subfamilies: Ras, Rho, Rab, Arf/Arl and Ran (Cox and Der, 2010; Vetter and Wittinghofer, 2001). Several T4P carrying bacteria use small GTPases of the Ras subfamily for regulatory purposes.

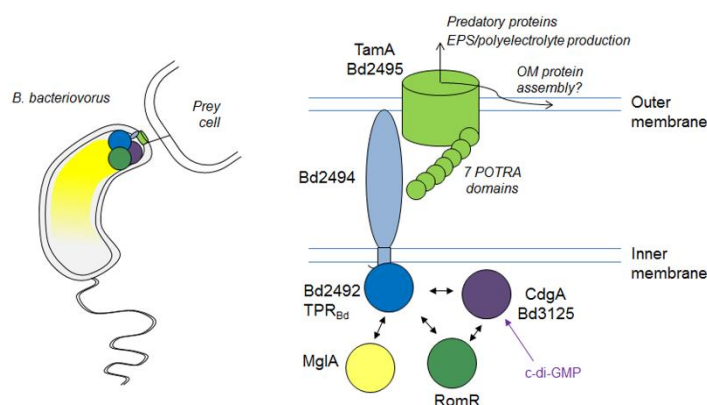


Figure 7 Model for *B. bacteriovorus* predatory-pole regulation during prey-invasion (Milner et al., 2014).

In the predatory deltaproteobacterium *B. bacteriovorus* T4P mediate prey invasion but not motility. Motility, in turn, is driven either by flagella in liquid media or by gliding motility on surfaces (Evans et al., 2007; Lambert et al., 2006; Lambert et al., 2011). Predation is regulated by a protein hub including the small Ras-like GTPase MglA, a c-di-GMP receptor protein CdgA, a TPR domain protein Bd2492 and the RomR protein (Milner et al., 2014) (Fig. 7).

Gliding of *B. bacteriovorus* has been described to be under control of c-di-GMP (Hobley et al., 2012). Interestingly, the c-di-GMP receptor CdgA was found to increase prey invasion showing a link between regulations of these two processes. MglA of *B. bacteriovorus* stimulates formation of T4P, triggers prey invasion and is associated with changes in gliding reversal behavior, however, it is not required for gliding *per se* (Milner et al., 2014). MglA is thought to be locked in the GTP bound form, interacts with the TPR domain protein Bd2492, which is important for prey invasion. Bd2492, in turn, interacts with RomR and both proteins together interact with CdgA. All four proteins are localized in asymmetric fashion and co-exist at the prey-invasive pole (Fig. 7). Furthermore, it was speculated that Bd2492 interacts with the TamAB-like (parts of translocation assembly module) proteins, encoded next to *bd2492*. The two proteins are hypothesized to localize in the IM and OM and were found to be essential in *B. bacteriovorus* (Milner et al., 2014).

An MglA homologue has also been identified in *Thermus thermophilus*. *T. thermophilus* uses unipolar T4P for twitching motility. Additionally, naturally competent *T. thermophilus* DNA uptake is mediated by the DNA translocator that shares components with T4P (Salzer et al., 2014a; Salzer et al., 2014b). Together with its GAP, named MglB, MglA localizes T4P to one pole and stimulates T4P-mediated twitching motility, adherence and biofilm formation, therefore, regulating colony formation. Colonies, formed by *mgl* single mutants and a double mutant are increased in size, which happens likely due to an uncontrolled assembly/disassembly of the T4P at both cell poles. Yet, general level of produced pili was not affected in absence of MglA or MglB (Salzer et al., 2015).

1.2 Introduction of *Myxococcus xanthus*

Species of myxobacteria represent a group of microorganisms that display complex multicellular behavior, such as collective movement, predation and development. Effective collective work of bacterial cells requires highly coordinated self-recognition, spatial morphogenesis, cell differentiation, division of labor, intercellular communication, and cooperation among individual cells (Claessen et al., 2014; Lyons and Kolter, 2015). Among the best characterized representatives of the myxobacteria, the soil-dwelling δ -proteobacterium *Myxococcus xanthus* is commonly used as a model organism for studying multicellular behavior.

Over evolution *M. xanthus* undergone extensive gene duplication, leading to formation of one of the largest bacterial genomes of ≈ 9.1 Mbp that encodes over 7500 genes (Goldman et al., 2006). This gene abundance supports diverse types of cellular behavior, affording a complex life cycle and making *M. xanthus* one of the most thrilling bacterial model organism.

1.2.1 Life cycle of *M. xanthus*

M. xanthus exhibits a complex life cycle comprised of two phases – cooperative predation and multicellular development. Both multicellular processes are mediated by the coordinated movement of cells, which use two motility systems that will be described below (Munoz-Dorado et al., 2016). On a solid surface in presence of nutrients cells move in a regulated manner and form multicellular biofilms, known as swarms (Fig. 8). When swarms make contact with prey, they penetrate the colony and lyse cells. Successful preying requires close proximity to the prey that is additionally stimulated by cell reversals. These reversals are responsible for individual *M. xanthus* cells becoming trapped in prey micro-colonies until prey-lysis is complete (Keane and Berleman, 2016; McBride and Zusman, 1996). While preying and in conditions with limited nutrients, high cell densities may lead to another way of behavior named rippling. During rippling, cells accumulate in an equispaced, ridge-like structures, separated by troughs of low cell density (Fig. 8). The ridge-like structures move coordinately and synchronously as travelling waves over the surface (Berleman and Kirby, 2007; Shimkets and Kaiser, 1982). Rippling commonly serves to maximize predation efficiency and nutrient scavenging, however it is not always necessary for predation (Berleman et al., 2006; Berleman et al., 2008; Pérez et al., 2014).

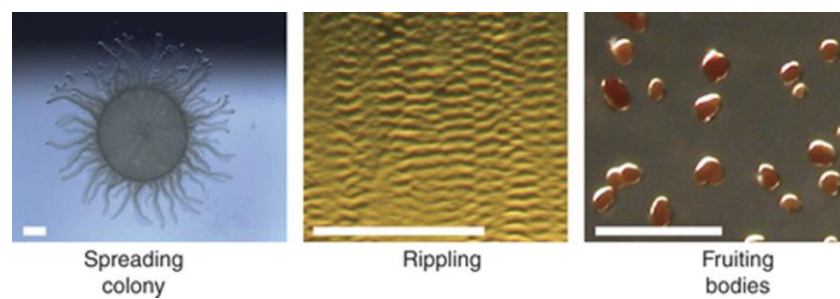


Figure 8 The three cellular patterns formed by *M. xanthus* cells (Konovalova et al., 2010).

M. xanthus exposes two preying strategies. The first strategy resembles frontal attack with groups of cells continuously penetrating the prey colony, lysing the cells inside. The second strategy is referred to as the wolf-pack attack. In this case, *M. xanthus* cells surround the colony of the prey and ripple before lysing the cells inside (Berleman et al., 2008; Pérez et al., 2014).

The social predation behavior in the absence of nutrients or in response to the complete lysis and digestion of prey cells, transits into a developmental program that culminates in the formation of multicellular, spore-filled fruiting bodies (Berleman and Kirby, 2007; Konovalova et al., 2010) (Fig. 8, 9). Fruiting body formation includes two invariable morphological processes – aggregation of cells (which is complete in 24h) and sporulation (spore maturation is over approximately 72h after the onset of starvation) (Konovalova et al., 2010; Muller et al., 2010).

During *M. xanthus* development, sporulating cells are found within the fruiting bodies, while cells outside the fruiting body become “peripheral rods” that make up 4-30% of developing cells and function as a distinct cell type. Peripheral rods differ from the sporulating cells with respect to gene expression, protein accumulation and cellular morphology. Moreover, peripheral rods keep the ability to sense cells of prey even as a part of fruiting body (O'Connor and Zusman, 1991a, b). Completing the life cycle, spores germinate in the presence of high nutrient concentrations (Fig. 9).

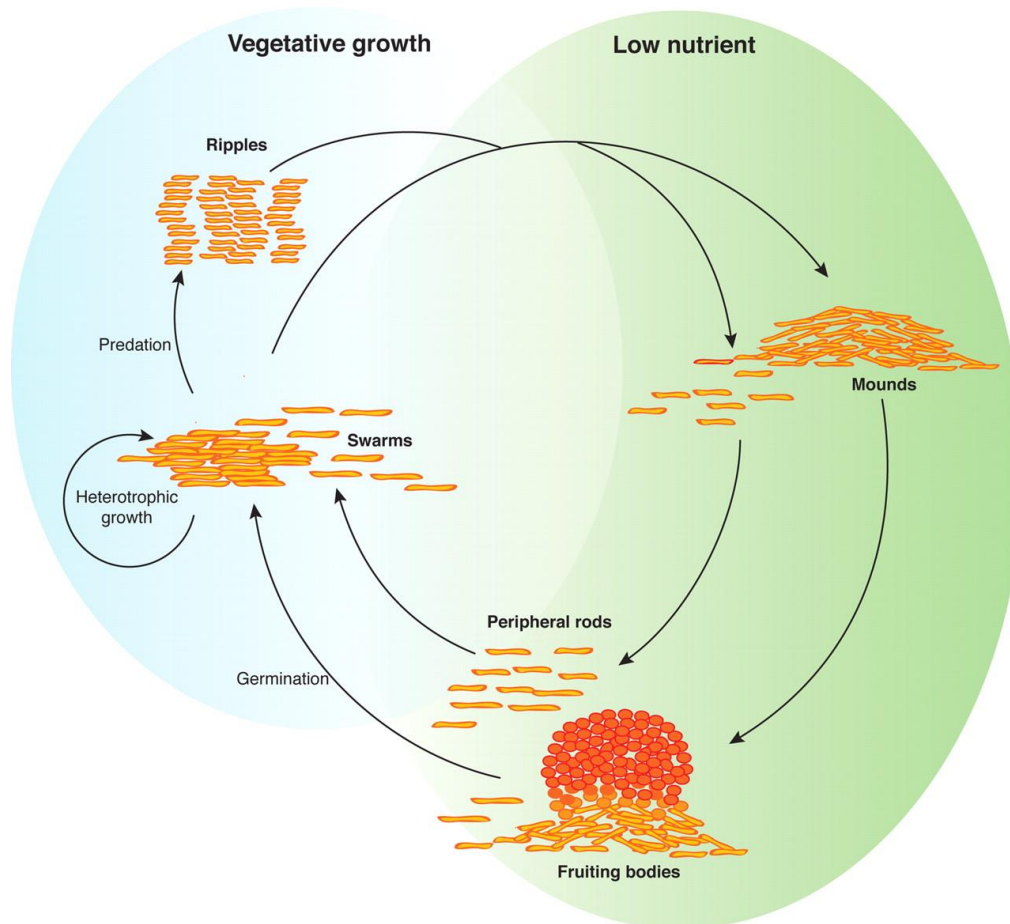


Figure 9 Life cycle of *M. xanthus* (Mauriello, 2010).

Formation of all the described above cellular patterns crucially depends on directed cell movements and its regulation (Keilberg and Søgaaard-Andersen, 2014; Leonardy et al., 2008; Starruss et al., 2012).

1.2.2 Motility in *M. xanthus*

Rod-shaped cells of *M. xanthus* move in the direction of their long axis with defined front and rear poles by means of two motility systems. While on a soft surface groups of cells move

using T4P, on a solid surface single cells glide, powered by gliding motility complexes. Occasionally, cells reverse their direction of movement in a process stimulated by the Frz chemosensory system (Blackhart and Zusman, 1985).

1.2.2.1 Gliding motility

Gliding motility of *M. xanthus* cells is an example of surface appendage-independent cell motility and is powered by the Agl/Glt motility complexes. Over 40 proteins were identified as important for gliding motility in *M. xanthus*, among which at least 14 proteins comprise the Agl/Glt complex. This machine is represented by the Agl-Glt complexes and contain two protein subcomplexes, accordingly. The Agl subcomplex contains the AglR, -S and -Q proteins, that are homologous to the stator proteins that drive flagellar rotation, and form an IM proton-conducting channel. The remaining 11 proteins of the machine comprise the Glt subcomplex, and are localized in the cytoplasm, IM, periplasm and OM (Balagam et al., 2014; Jakobczak et al., 2015; Luciano et al., 2011; Nan et al., 2010; Sun et al., 2011). Association of the two subcomplexes likely happens via AglR and GltG (Luciano et al., 2011) (Fig. 10). During movement, Agl/Glt complexes assemble at the leading pole, adhere to the substratum, and stay stationary with respect to the substratum, disassembling once they reach the lagging pole (Mignot, 2007). Additionally to the 14 Agl/Glt proteins, a few more proteins are incorporated into the Agl/Glt complexes including AglZ, MglA, RomR and RomX, and MreB (Szadkowski et al., 2019; Treuner-Lange et al., 2015). Together all mentioned proteins comprise gliding motility machinery, which are also often referred to as focal adhesions (FAs) (Fig. 10).

The arrangement and interactions between individual proteins in the Agl/Glt complexes are not known, but the following model has been proposed. The three Agl proteins form a molecular motor powered by the proton motive force (PMF). AglR is a homologue of TolQ/ExbB/MotA, while AglQ and AglS are homologous to TolR/ExbD/MotB with all three proteins localized in the IM. Absence of any of the Agl proteins causes paralysis of the gliding motility complexes (Sun et al., 2011).

The Glt subcomplex spans from the cytoplasm to the OM, and includes the large cytoplasmic GltI protein, which contains 23 TPR repeats. GltI was suggested to serve as a link to AglZ and MglA in the cytoplasm, however, it is not known which direct interactions connect GltI to the remaining 10 Glt proteins (Nan et al., 2010; Treuner-Lange et al., 2015). Most likely, one or both integral IM GltG/-J proteins link GltI to the Agl/Glt complex. GltG/-J enter the periplasmic space with C-terminal region containing TonBC domains and are likely involved in interaction to GltF. Among experimentally confirmed direct interactions, GltG was found to bind AglR, thus,

likely transmitting PMF energy to the Glt subcomplex (Faure et al., 2016; Gresock et al., 2015; Islam and Mignot, 2015).

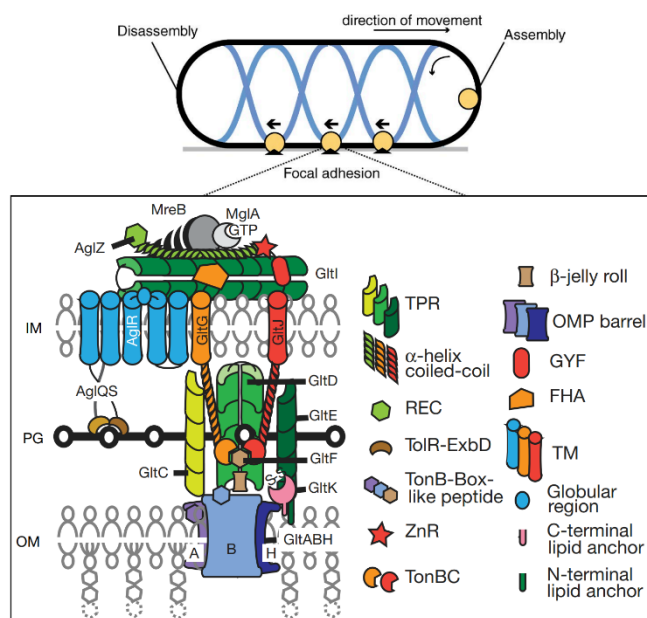


Figure 10 *M. xanthus* gliding motility machinery (Faure et al., 2016; Treuner-Lange et al., 2015). Predicted domains of the indicated proteins are assigned on the right in the box.

Three proteins GltD, E and F are predicted to localize in the periplasmic space and connect IM to OM Glt components. In particular, GltD was found to localize in Agl/Glt complexes and displayed high affinity for proteins of IM and OM (Luciano et al., 2011; Nan et al., 2010). Localization of GltE and GltF was also confirmed by fluorescence microscopy and fractionation experiments. GltE was abundant in the IM and periplasm and suggested to provide protein-protein interactions via its TPR motifs and C-terminal coiled-coil domain (Luciano et al., 2011)

Five Glt proteins have been assigned as OM components: GltA, B, C, H and K. GltA, B and H are OM β -barrel proteins. GltA and GltB interact directly and stabilize each other (Berleman et al., 2014; Jakobczak et al., 2015; Luciano et al., 2011). Together, GltA and GltB also interact and stabilize GltC, a soluble protein containing TPR domains (Berleman et al., 2014; Jakobczak et al., 2015; Kahnt et al., 2010). GltK is located on the periplasmic face of the OM and has been reported to be important for the integration of GltA and GltB to the OM (Jakobczak et al., 2015).

Three cytoplasmic proteins assure the correct function of the Agl/Glt complexes. AglZ accumulates at the leading pole as well as in the Agl/Glt complexes. AglZ oligomer was suggested to serve as a platform for Agl/Glt complex assembly. AglZ interacts directly with the small GTPase MglA, which is essential for gliding in *M. xanthus* and the two proteins co-localize (Treuner-Lange et al., 2015; Yang et al., 2004). Finally, MglA-GTP and AglZ both interact with the essential MreB

cytoskeletal protein that is important for PG cell wall synthesis (Mauriello et al, 2010; Treuner-Lange et al, 2015). MreB forms dynamic helical trajectories along the cell body and provides the scaffold for the gliding motors, whereas the gliding machinery, in turn, drives the movement of MreB itself (Fu et al., 2018; Mauriello, 2010; Treuner-Lange et al., 2015) (Fig. 10).

The model for the gliding machinery function, includes the following sequence of events. MglA-GTP is connected to the MreB cytoskeleton and AglZ and at the leading pole stimulates the assembly of the Agl-Glt complexes via contact to GltI, which in turn recruits IM GltJ and GltG, where the latter provides the connection to the AglRQS motor. On the periplasmic face of the IM, GltJ/G interact to GltD/-E/-F forming a subcomplex. The AglRQS motor moves this Glt subcomplex directionally towards the lagging pole. Once this subcomplex engages the OM GltA/-B/-C/-H/-K module, the entire apparatus adheres to the substratum and is, therefore, fixed with respect to the surface (Islam and Mignot, 2015) (Fig. 10). Strong interaction to the surface is mediated by the extracellular matrix slime (ECM), composed of the secreted polysaccharides, the OM vesicles and tubes (Burchard, 1982; Ducret et al., 2013; Ducret et al., 2012). Additionally, one or more specific adhesion molecules have been proposed to strengthen surface interaction.

1.2.2.2 T4P-dependent motility

A version of twitching motility, mediated by the T4P in *M. xanthus*, is often referred to as social motility and allows groups of cells to move on soft surfaces. T4P-dependent motility was shown to involve the T4P biogenesis machine, and exopolysaccharides (EPS) together with the lipopolysaccharide (LPS) O-antigen.

T4P machine of *M. xanthus*

Composition and architecture of the protein complex providing T4P formation and function are relatively well understood and are similar to the other known T4aP machineries (T4aPMs) (Fig. 2, 11). Complex localization and protein stability studies allowed to propose an outside-in assembly pathway of the T4aPM that in case of *M. xanthus* will be referred as to T4PM from now on. Thus, assembly starts with the OM PilQ that serves as an assembly platform and further proceeds through the periplasm (PilP) and IM (PilN, -O, -C) towards cytoplasm (PilM) (Friedrich et al., 2014). Described model of the T4PM assembly relies on a number of observations, which will be listed below. Additionally, some unique features of the *M. xanthus* T4PM will be noted.

Insertion of the PilQ oligomer and formation of PilQ multimers in *M. xanthus* requires the Tgl pilotin protein. PilQ and Tgl accumulate independently of the rest of the Pil proteins and are necessary for the accumulation and stability of a few other T4aPM components (Friedrich et al.,

2014). The peptidoglycan binding protein TsaP forms a ring-like structure around PilQ multimer to further stabilize it in the OM (Fig. 11). Cells, lacking TsaP, were shown to assemble less T4P and minor displacement of the OM secretin pore with respect to the periplasmic T4PM components (Chang et al., 2016; Siewering et al., 2014).

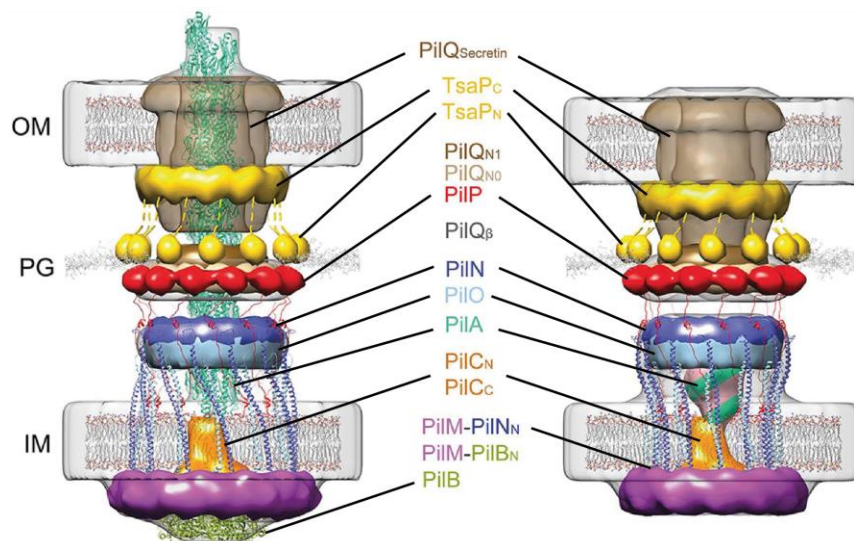


Figure 11 Architecture of the pilated (left) and empty (right) T4PM of *M. xanthus* (Chang et al., 2016).

Accumulation of the PilM/N/O/P parts of the alignment complex occurs in a PilQ/Tgl-dependent manner and is interdependent as PilM does not accumulate without PilP/N/O, PilN without PilP/O and PilO was not found in $\Delta pilP$ (Friedrich et al., 2014). Moreover, the PilN-M interaction has been shown to be necessary for the stability of PilM (Bischof et al., 2016; Friedrich et al., 2014). Although PilC accumulates independently of the other T4aPM proteins, its localization depends on PilO and PilN (Friedrich et al., 2014).

T4aPM is assembled at both poles (Bulyha et al., 2009; Chang et al., 2016; Friedrich et al., 2014). Pilus extension/retraction is triggered by incorporation of the PilB/PilT ATPases at the basis of the machine, respectively. Consequently, absence of PilB leads to the non-piliated phenotype, while absence of PilT, causes the hyper-piliation (Bulyha et al., 2009; Chang et al., 2016; Jakovljevic et al., 2008). Interestingly, PilT contains several paralogs in the genome, whose role in the motility of *M. xanthus* remains elusive (Clausen et al., 2009).

M. xanthus cells move uni-directionally and while moving they form T4aP at the leading cell pole only. Accordingly, PilB and PilT ATPases were shown to localize mostly unipolar with PilB found predominantly at the leading pole, where it stimulates pilus assembly. PilT localizes mainly at the lagging cell pole and spontaneously accumulates at the leading pole to stimulate the retraction (Bulyha et al., 2013; Bulyha et al., 2009). PilB and PilT occupy the same location at

the basis of the pilus in a mutually exclusive manner, providing assembly/disassembly (Chang et al., 2016). Accumulation, stability and localization of PilB and PilT does not depend on any other component of the T4aPM (Friedrich et al., 2014). To initiate extension of the pilus, PilB interacts with PilM and PilC. Binding to PilC causes stimulation of the ATPase activity of PilB and PilB, in turn, triggers rotation of the PilC dimer (Bischof et al., 2016; Chang et al., 2016). Rotation of PilC mediates 1-start assembly of the pilus when one step during rotation is thought to coincide with incorporation of the one PilA molecule from the IM pool (Chang et al., 2016).

Genome of *M. xanthus* encodes 10 minor pilins, divided between three clusters in the genome. Lack of nine out of ten minor pilins causes similar T4P-dependent motility defect to single $\Delta pilA$ deletion, leading to absence of surface T4P formed (Chang et al., 2016).

Exopolysaccharides and lipopolysaccharide O-antigen

In addition to T4P, EPS and lipopolysaccharide (LPS) O-antigen are important for T4P-dependent motility. EPS is comprised of the monosaccharides mannose, galactosamine, galactose, glucosamine, N-acetylated-amine sugars, glucose, rhamnose and xylose (Behmlander and Dworkin, 1994; Sutherland and Thomson, 1975). Biosynthesis of EPS in *M. xanthus* was suggested to include three steps: synthesis of monosaccharides in the cytoplasm, membrane-associated assembly of the monosaccharides into polysaccharides and transport of the polysaccharides to the cell surface (Lu et al., 2005). EPS serves as an anchoring substance for T4P on nearby cells, thus, promoting cell-cell and cell-surface contacts. Therefore, EPS allows *M. xanthus* to act as a multicellular organism, influencing social motility and, eventually, fruiting body formation, and overall accomplishing biological task that single cell cannot manage to perform alone (Berleman et al., 2016; Li et al., 2003; Shimkets, 1986a, b). Lack of EPS leads to a defect in T4P-dependent motility by suppressing retraction, although T4P can still be assembled (Hu et al., 2011; Li et al., 2003). In the opposite situation, absence of surface T4P results in a severe defect in the EPS production, thus, a mutual regulation between these two processes was predicted (Black et al., 2006; Yang et al., 2010). Interestingly, addition of purified EPS to an EPS-negative mutant restores T4P retraction in some cases (Li et al., 2003).

The T4P, sheared off the cells surface, bind purified EPS *in vitro* and a truncated version of the PilA major pilin specifically recognizes N-acetyl-glucosaminyl sugar residues of EPS trails under native conditions (Hu et al., 2012; Li et al., 2003). Moreover, Yang et al in 2010 were able to show that cells containing IM pool of PilA but unable to assemble T4P displayed stronger EPS defect than the *pilA* deletion strain. This observation allowed to hypothesize that the amount of

PilA in the membrane is a key regulatory factor for EPS production rather than the complete lack of intracellular PilA (Yang et al., 2010).

EPS production and regulation involves a number of proteins encoded by the chemotaxis-like *dif* operon, *eps* operon, which contains genes associated with carbohydrate-transport and biosynthesis, the transcriptional regulator *nla24* and DnaK homologue SglK (Lancero et al., 2004; Lu et al., 2005; Yang et al., 1998; Yang et al., 2000). Specifically, the gene products of the *eps* locus are homologous to glycosyltransferases (*epsD*), endoglucanases (*epsB*), serine acetyltransferases (*epsC*) and UDP-N-acetyl-mannosamine transferases (*epsA*) (Lu et al., 2005). One ORF in the *eps* locus *epsI* encodes an NtrC-like protein Nla24 that has been shown to influence gliding and T4P-dependent motility, as well as EPS biogenesis and fruiting body formation (Lancero et al., 2004; Lu et al., 2005).

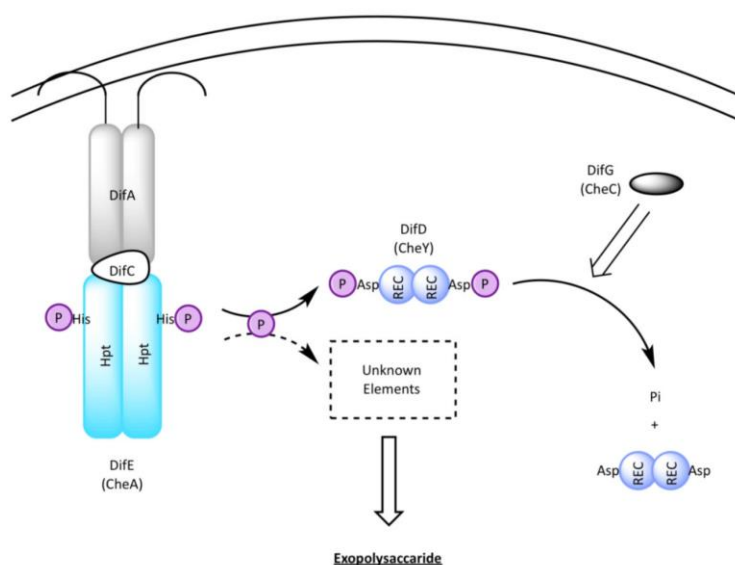


Figure 12 Schematic diagram of the Dif chemosensory pathway in *M. xanthus* (He and Bauer, 2014). See the description in the text.

Proteins encoded by the *dif* operon, comprise the Dif chemosensory pathway, which provides complex regulation of EPS production. DifA (MCP), DifC (coupling protein) and DifE (CheA-type histidine kinase) form a transmembrane complex that positively regulates EPS production via the DifE kinase. DifE, in turn, interacts directly and phosphorylates the EpsW response regulator that is likely an intermediate in the further regulatory cascade (Black et al., 2015; Black et al., 2006). DifD, a CheY-like substrate of DifE phosphorylation, functions as a phosphate sink to negatively regulate EPS production. DifG, a homologue of the CheC phosphatase, is a negative regulator that can dephosphorylate DifD-phosphate (Black et al.,

2010; Black and Yang, 2004) (Fig. 12). Construction of numerous double mutants suggests an activity of T4P upstream of the Dif pathway and showed that together they likely regulate EPS via the PilB assembly ATPase (Black et al., 2017; Black et al., 2006).

The last component, important for T4P-dependent motility, is the LPS O-antigen that commonly represents a selective barrier between the environment and periplasmic space (Yang et al., 2008). LPS O-antigen is not only important for T4P-dependent motility, but also for gliding motility (Fink and Zissler, 1989b; Kaplan et al., 1991; Pérez-Burgos et al., 2019; Yang et al., 2008; Youderian and Hartzell, 2006). O-antigen is a distal repeating polysaccharide and represents a part of LPS, additionally to hydrophobic lipid A and nonrepeating core oligosaccharide region (Raetz and Whitfield, 2002). This structure of LPS is also present in *M. xanthus* (Fink and Zissler, 1989a). Genes related to O-antigen synthesis are found in two different loci (Kaplan et al., 1991; Pérez-Burgos et al., 2019; Yang et al., 2008; Youderian and Hartzell, 2006). Specific carbohydrate composition of *M. xanthus* LPS includes glucose, mannose, rhamnose, arabinose, xylose, galactosamine, glucosamine, KDO (2-keto-3-deoxyoctulosonic acid), 3-O-methylpentose and 6-O-methylgalactosamine (Ashton, 1993). Five of those monosaccharides are common for EPS and LPS (Behmlander and Dworkin, 1994).

1.2.3 Polarity of *M. xanthus* cells & its regulation

Cells of *M. xanthus* execute two types of motility to move uni-directionally with well-defined leading and lagging poles. For the gliding motility this means that Agl/Glt complexes are assembled at the leading pole and disassembled at the lagging pole, while for T4P-dependent motility, pili are assembled at the leading and not lagging pole (Fig. 13). When cells switch direction of movement, the polarity of both motility systems is inverted with old lagging pole become new leading and vice versa. Front-rear polarity is defined and maintained by four proteins that will be described below (Keilberg and Søgaard-Andersen, 2014; Leonardy et al., 2008; Schumacher and Søgaard-Andersen, 2017).

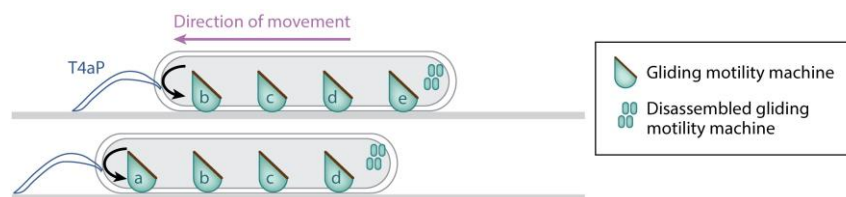


Figure 13 Front-rear polarity of *M. xanthus* cells is defined while movement (Schumacher and Søgaard-Andersen, 2017).

1.2.3.1 Polarity module & reversals

Polarity of *M. xanthus* cells is determined and supported by a complex of four proteins. The small Ras-like GTPase MglA is a key protein and is essential for gliding and T4P-dependent motility (Hodgkin and Kaiser, 1979). Interaction partners of MglA that assure pole definition are the MglB GAP and the RomR/RomX GEF complex (Keilberg et al., 2012; Leonardy et al., 2007; Leonardy et al., 2010; Miertzschke et al., 2011; Szadkowski et al., 2019; Zhang et al., 2010; Zhang et al., 2012).

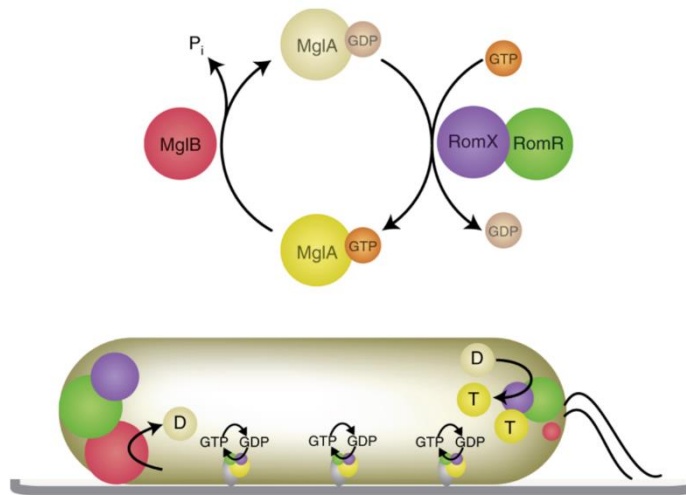


Figure 14 Model of front-rear polarity module in *M. xanthus* cells. Upper panel shows MglA GTPase cycle, while lower one represents localization of every mentioned protein inside the cell. Protein complexes along the cell body represent AgI/Glt gliding motility complexes. T4P are formed at the leading cell pole (Szadkowski et al., 2019).

MglA exists in the inactive GDP-bound form, which localizes diffusively throughout the cytoplasm, and the active GTP-bound form that accumulates in an asymmetric manner with a larger cluster at the leading pole (Leonardy et al., 2010; Zhang et al., 2010). This asymmetric localization of MglA-GTP is provided by MglB that is mostly localized at the lagging pole with only a small amount at the leading pole. MglB has GAP activity and binds to MglA in 2:1 stoichiometry, stimulating GTP hydrolysis by MglA, thus, excluding MglA-GTP from the lagging pole (Leonardy et al., 2010; Miertzschke et al., 2011; Zhang et al., 2010). The RomR/RomX complex is also bipolar, asymmetric and mostly localizes at the lagging cell pole (Fig. 14) (Szadkowski et al., 2019). RomR/RomX has MglA GEF activity and stimulates binding of MglA at the leading pole via two mechanisms, i.e. by stimulating accumulation of MglA-GTP, and by directly interacting with MglA-GTP (Keilberg et al., 2012; Leonardy et al., 2007; Szadkowski et al., 2019; Zhang et al., 2012).

MglA-GTP is essential, while RomR/RomX is conditionally required for the formation of Agl-Glt complexes. By increasing the concentration of MglA-GTP at the leading pole, RomR/RomX stimulates assembly of the Agl-Glt complexes and incorporation of MglA-GTP in these complexes. When the concentration of MglA-GTP in cells is increased by means of the Q82A substitution in MglA (which locks the protein in the GTP-bound form) or by absence of the MglB GAP, Agl-Glt complexes can be formed independently of RomR/RomX (Leonardy et al., 2010; Szadkowski et al., 2019). At the lagging pole MglB causes disassembly of the Agl-Glt complexes (Fig. 14). Further, as MglB co-occurs with large clusters of RomR/RomX at the lagging pole, its GAP activity was suggested to dominate over the recruitment role of the RomR/X complex at this pole (Szadkowski et al., 2019).

Moving uni-directionally, cells of *M. xanthus* occasionally stop and resume movement in the opposite direction. This event takes place on average every 8-10 minutes and are called reversals (Blackhart and Zusman, 1985). During reversals, both motility systems invert their polarity, hence, T4P and gliding motility complexes are now assembled at the new leading pole and the latter are disassembled at the new lagging pole (Jelsbak and Søgaard-Andersen, 2002; Mignot et al., 2005; Søgaard-Andersen, 2004). It was also shown that MglA-GTP, MglB, RomR and RomX switch the corresponding poles during reversals and this switch takes on average 30-60 seconds (Leonardy et al., 2007; Szadkowski et al., 2019; Zhang et al., 2010).

For the T4P-dependent motility the switch of the direction of movement also coincides with switch in PilB and PilT asymmetric localization, therefore, after reversal PilB stimulates T4P formation at the new leading pole (Bulyha et al., 2009).

1.2.3.2 Frz chemosensory system

Reversal events of *M. xanthus* cells are under the control of the Frz chemosensory system (Blackhart and Zusman, 1985). The Frz pathway includes the FrzCD MCP, the hybrid histidine kinase FrzE and the coupling protein FrzA that are homologous to CheA-CheY and CheW of *E. coli*, accordingly (Bustamante et al., 2004; McBride and Zusman, 1996). The three proteins are co-localized in multiple cytoplasmic clusters that are positioned over the nucleoid. Localization of FrzE in these clusters depends on FrzCD and FrzA (Kaimer and Zusman, 2016). The activity of FrzCD is modulated by methylation, which is catalyzed by FrzF, a methyl-transferase, and FrzG, a methyl esterase, and by upstream regulator, FrzB (Astling et al., 2006; Bustamante et al., 2004; Scott et al., 2008). The histidine kinase FrzE interacts with FrzCD using ATP as a phosphoryl-donor for autophosphorylation at a histidine residue (Inclan et al., 2008). Further, FrzE kinase transfers the phosphoryl group to its own response regulator (RR)-domain, and FrzZ and FrzX

response regulators (Fig. 15). Specifically, FrzE^{RR} acts as a phosphate sink that prevents noisy activation of the system at low stimulation levels. The phosphorylated version of FrzZ localizes at the leading pole and is proposed to increase a reversal frequency by means of lowering the concentration of MglA-GTP at the leading pole. Phosphorylated FrzX, in turn, localizes at the lagging pole and is suggested to help MglA to displace MglB from this pole during reversals. This displacement is only effective if the concentration of RomR reaches certain threshold (Guzzo et al., 2015; Guzzo et al., 2018; Kaimer and Zusman, 2016) (Fig. 15).

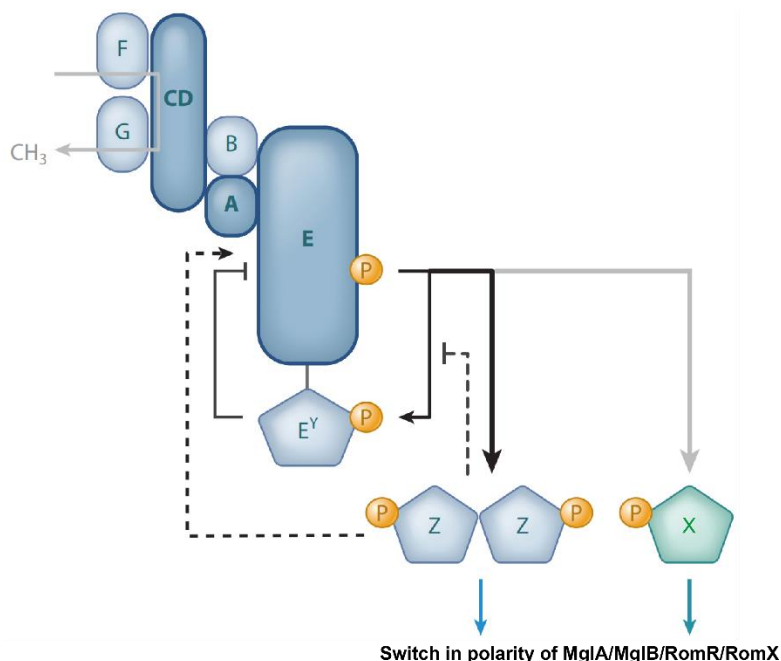


Figure 15 The Frz polarity module acts on the polarity module in *M. xanthus* (Schumacher and Søgaard-Andersen, 2017). Corresponding Frz proteins are labeled with the letters.

Mutations in Frz proteins can cause either hypo- or hyper-reversing phenotype. Cells with deleted FrzCD, FrzA, FrzE, FrzZ and FrzX demonstrate decreased reversal frequency with 1-2 reversals per hour (Blackhart and Zusman, 1985; Guzzo et al., 2018). In contrast, partial N-terminus truncation of FrzCD or a point mutation in the response regulator domain of FrzE cause hyper-reversing phenotype (Bustamante et al., 2004; Li et al., 2005). Although the signal that activates Frz system has not been identified yet, it is strongly suggested that the MglA/B/RomR/X polarity module acts downstream of the Frz pathway. Thus, a signal, transmitted via Frz system, causes eventually re-localization of the four proteins to the opposite poles.

1.2.4 Regulation of T4P-dependent motility in *M. xanthus*

Uni-directional movement is assured by the unipolar T4P extension, adhesion and retraction, where the latter process is stimulated by the EPS production. Reversal of *M. xanthus*

cell is associated with disassembly of functional T4aPM at the old leading pole and its reassembly at the new leading pole. Several mechanisms are involved in regulation of correct T4P function during movement and reversals in *M. xanthus*.

c-di-GMP regulation

Although *M. xanthus* genome does not contain obvious homologues of the Fim proteins of *Xanthomonas spp* and *P. aeruginosa*, c-di-GMP and related proteins have been shown to regulate T4P-dependent motility. However, in most cases, the precise mechanism is not known.

A two-component system consisting of the hybrid histidine kinase SgmT and the DNA-binding response regulator DigR, was found to be essential in regulating the composition of ECM. Absence of any of the two proteins leads to motility defect, which, in turn, is likely associated to the EPS (Overgaard et al., 2006; Petters et al., 2012).

An experiments with altered levels of intracellular c-di-GMP revealed that increased as well as decreased level of c-di-GMP in *M. xanthus* cells affects T4P-mediated motility phenotype. In particular, a 7-fold increase in the c-di-GMP level resulted in ≈ 2.5 times lower *pilA* expression, hence, lower PilA accumulation and surface T4P assembly, but not EPS production defect. Systematic inactivation of c-di-GMP related genes identified three genes whose inactivation leads to T4P-dependent motility defects. Thus, additionally to SgmT, lack of TmoK or DmxA caused increased EPS accumulation and subtle motility defect. TmoK is a histidine kinase with a catalytically inactive GGDEF domain, incapable of binding c-di-GMP. DmxA contains several TM domains, two GAF domains and GGDEF domain that binds c-di-GMP (Skotnicka et al., 2016). Precise regulatory mechanisms involving TmoK and DmxA are yet to determined.

FrzS

In 1993 FrzS protein, encoded right after proteins of the Frz chemosensory pathway, was identified to be a component, required for motility in *M. xanthus* (Shi and Zusman, 1993). Later it has been verified to function as T4P-dependent motility regulator, as lack of FrzS leads to severe reduction in colony expansion over time (Ward et al., 2000). Extensive studies of the FrzS-dependent motility regulation revealed that it mainly affects EPS production. It has been proposed that FrzS may activate EPS synthesis and secretion at the leading cell pole (Berleman et al., 2011).

A FrzS-GFP fusion localized in bipolar asymmetric fashion with higher protein amount at the leading pole. During reversals, the localization was switched and this dynamic protein accumulation was found to be regulated by the Frz chemosensory system (Mignot et al., 2007;

Ward et al., 2000). Moreover, co-occurrence of MglA GTPase and FrzS at the leading pole allowed to hypothesize the connection between two proteins that has been later confirmed. Thus, in absence of MglA, FrzS was localized in exclusively unipolar fashion and tandem affinity purification suggested the direct interaction between the two proteins (Mauriello, 2010).

SofG/BacP dependent regulation

Bulyha and colleagues were able to show that one of the primary functions of MglA is to sort PilB and PilT ATPases to opposite poles. Similar to eukaryotic cells, where regulation of motility and polarity is provided by more than one small GTPase, *M. xanthus* genome was searched for paralogs of MglA. Among two paralogs found, one, named SofG, was shown to be important for T4P-dependent motility. Interestingly, neither amount of surface T4P, nor level of EPS or LPS were affected in the absence of SofG, (Bulyha, 2010; Bulyha et al., 2013). The bipolarly localized PilM and PilC were not observed to change their localization in the absence of SofG, while PilB and PilT localization was shifted towards subpolar rather than mostly polar (Bulyha et al., 2013).

Localization of SofG was mostly unipolar and did not switch during reversals. The single cluster was shuttling in the subpolar region approaching the pole and dislocating from it again. In addition, SofG was found to interact with the cytoskeletal protein BacP, which forms filamentous patches in the polar regions. BacP, in turn, was found to impact localization of SofG, PilB and PilT. Finally, SofG GTPase activity was verified and observed to be important for its localization and function (Bulyha et al., 2013).

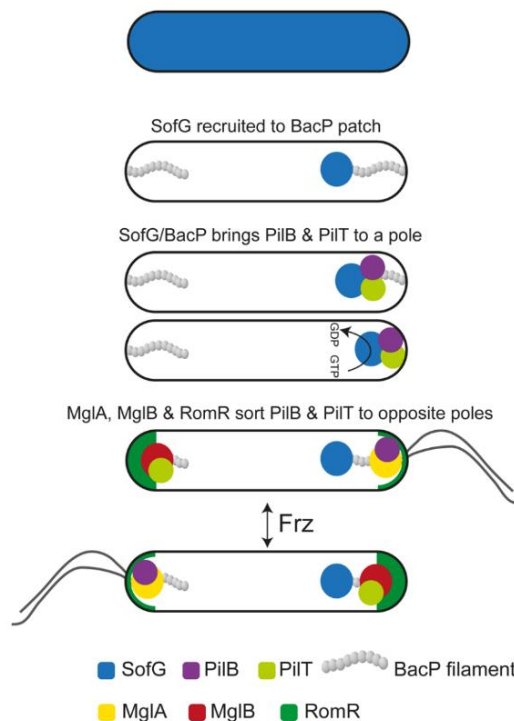


Figure 16 PiIB and PiIT are brought to the opposite cell poles by three hierarchically organized protein modules (Keilberg and Sogaard-Andersen, 2014).

In the current model, SofG is recruited to one of the two BacP polar patches, and together SofG and BacP stimulate polar accumulation of PiIB and PiIT. Next, MglA, whose localization and function depends on MglB and RomR/X, sorts PiIB and PiIT to the opposite poles. During reversals, all mentioned proteins except SofG and BacP, invert their polarity (Bulyha et al., 2013; Keilberg and Sogaard-Andersen, 2014) (Fig. 16).

1.3 Scope of this study

A few decades ago the small Ras-like GTPase MglA was shown to be crucial for gliding and T4P-dependent motility of *M. xanthus* (Hodgkin and Kaiser, 1979). Recent findings extended our understanding of the function of MglA in gliding motility, however less is known about the MglA-dependent regulation of T4P-dependent motility. The two paralogous GTPases MglA and SofG were shown to bring PiIB and PiIT to opposite poles (Bulyha et al., 2013). Here, performing further localization studies, we identify the role of MglA in localizing the bipolar stationary T4aPM components. Further, by systematically observing formation of T4P in mutants lacking proteins of the polarity module, we show that MglA is important for T4aP extension and, likely, essential for retractions. MglB, in turn, maintains T4aP asymmetry by excluding MglA from the lagging pole. We identify the SgmX TPR domain protein as an interaction partner of MglA. Using a combination of cell biological and biochemical approaches, we describe SgmX to stimulate formation of T4P

and confirm direct interaction between SgmX and MglA-GTP. Furthermore, by localizing SgmX in different genetic backgrounds as well as T4PM components in absence of SgmX, we propose SgmX to stimulate T4P extension via the PilB ATPase.

2 RESULTS

2.1 Roles of MglA, MglB & RomR in T4P dependent motility

2.1.1 MglA stimulates formation & function of T4P

The importance of MglA for T4P-dependent motility was shown 40 years ago (Hodgkin and Kaiser, 1979). Still the mechanism by which MglA stimulates T4P-dependent motility is not understood. Here, we first tested motility of $\Delta mglA$ strain on a soft surface, which is optimal for T4P-dependent motility. After 24h of incubation at 32° C, wild-type (WT) cells had formed the long flares at the colony edge, characteristic of T4P-dependent motility, while the $\Delta pilA$ strain had a flat colony edge. The colony edge of the $\Delta mglA$ mutant was also flat indicating that no T4P-dependent motility occurred (Fig. 17A). Further, we tested the mentioned strains for EPS accumulation using a colorimetric assay with Congo red that binds to EPS. It has been reported that mutants that lack T4P, are also defective in EPS accumulation (Bulyha, 2010). Thus, the $\Delta pilA$ mutant served as a negative control and, compared to the WT, did not bind Congo red. Cells of a $\Delta mglA$ mutant displayed a severe defect in EPS accumulation, but it was not abolished completely (Fig. 17A, right column). Thus, a mutant lacking MglA is impaired in T4P-dependent motility and EPS accumulation.

We performed immunoblot analysis to test for the accumulation of the 10 core components of the T4PM in $\Delta mglA$ cells compared to WT cells. The deletion mutant accumulated these proteins at levels similar to the WT (Fig. 17B).

To test whether the T4P are extended, formation of external T4P was analyzed by transmission electron microscopy (TEM). Exponentially grown cells were fixed and stained with 2% uranyl acetate. WT had unipolar T4P in 83% of cells and the remaining 17% of cells did not have T4P (Fig. 17C). Cells of the $\Delta pilA$ mutant, as expected, did not have T4P. Interestingly, 31% of $\Delta mglA$ cells possessed T4P at one pole, whereas the remaining 69% of cells were not piliated (Fig. 17C). The visual TEM observations were accompanied by the immunoblot analysis of the sheared T4P fractions. While the total cellular level of PilA was equal for WT and $\Delta mglA$ cells, considerably less PilA was detected in the sheared fraction of the $\Delta mglA$ cells (Fig. 17D, top and middle panels). This observation is consistent with our TEM data and indicates that MglA likely stimulates formation of T4P. Because T4P, assembled by the few examined $\Delta mglA$ cells do not allow any group cell movement, these data support that MglA has an essential role for the function of T4P.

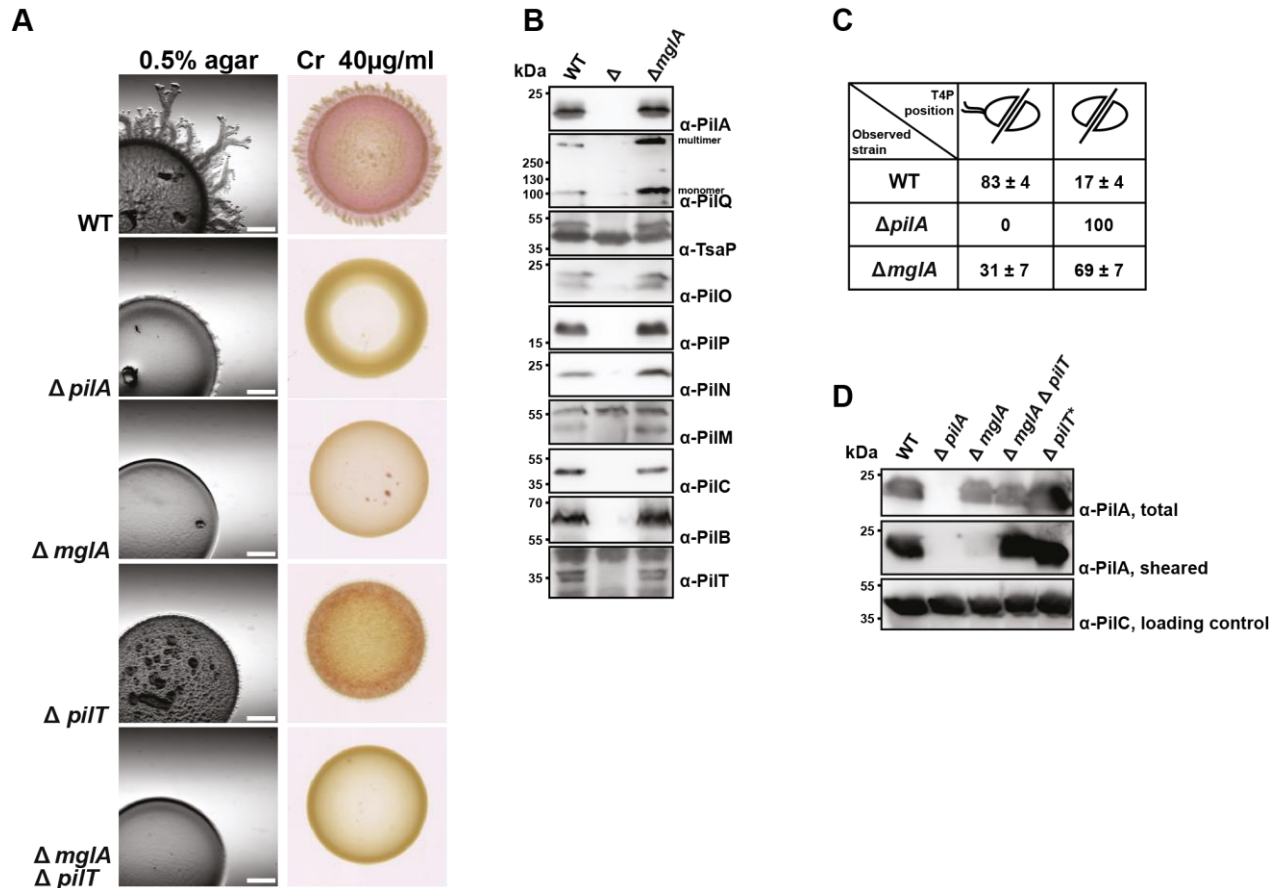


Figure 17 MglA is essential for T4P function, stimulates its formation and inhibits retraction

(A) Left column represents a test for T4P-dependent motility of indicated strains on 0.5% agar. Scale bar 500 μ m. Right column shows EPS accumulation in WT and selected mutants. Aliquots of 20 μ l cell suspensions at 7×10^9 cells/ml were spotted on 0.5% agar supplemented with 0.5% CTT and 40 μ g/ml Congo red (Cr) and incubated at 32 $^{\circ}$ C for 24 hours.

(B) Accumulation of the core T4P proteins in WT (first column) compared to Δ *mglA* (last column) strain. Single deletions of corresponding genes (indicated on the right by the specific antibodies used for detection) were used as a negative control (middle column). Total protein from the same number of cells was loaded and protein level was detected using antibodies specific for every indicated protein. Calculated size of the proteins (in kDa) are following: 23.4 (PilA), 98 (PilQ monomer) and ≥ 250 (PilQ multimer), 43.6 (TsaP), 22.8 (PilO), 21.3 (PilP), 24.8 (PilN), 42.3 (PilM), 45.1 (PilC), 62.5 (PilB), 40.7 (PilT).

(C) Summary of TEM observations of T4P localization in different strains. Numbers represent percentage of analyzed cells displaying indicated piliation phenotype \pm standard deviation, calculated based on three biological replicates. $N \geq 50$.

(D) Immunoblot analysis of whole cell extracts and sheared T4P fractions of corresponding strains. Cells were grown on 1% CTT/1.5% agar plates and taken samples were normalized by the cell mass. T4P were sheared and further precipitated using PEG6000/MgCl₂ containing buffer. Total protein from the same number of cells was loaded on the upper and lowest blots. Level of total and external PilA was detected using specific antibodies (top and second panels). *Sheared T4P fraction of Δ *pilT* was diluted 200 times due to non-retracting phenotype leading to massive external T4P overproduction. For the other indicated strains on the middle blot T4P were sheared from the same amount of cells and equally diluted. Lowest panel blot treated with PilC (T4P platform protein) antibodies used as a loading control.

T4P undergo cycles of extension and retraction and the amount of surface T4P can be modified by defects in each of the two processes. We speculated that MglA might not only stimulate assembly, but also affect retraction of T4P. In order to test this hypothesis, we took advantage of the $\Delta pilT$ deletion strain, which assembles a high number of T4P due to lack of the retraction ATPase (Yang et al., 2010). We combined a $\Delta mglA$ deletion with the $\Delta pilT$ deletion. The $\Delta mglA\Delta pilT$ mutant displayed an external T4P level that was higher than in the $\Delta mglA$ mutant. Yet the level of T4P assembled by the $\Delta mglA\Delta pilT$ strain was considerably lower than for $\Delta pilT$ mutant (Fig. 17D). This suggests the possibility of a minimal contribution of MglA in inhibiting T4P retraction. Importantly, the motility phenotype of $\Delta mglA\Delta pilT$ strain on soft agar was comparable to that of the $\Delta mglA$ mutant, supporting that the T4P formed by the double deletion strain are non-functional (Fig. 17A). This notion was additionally supported by the comparable phenotype of $\Delta mglA$ and $\Delta mglA\Delta pilT$ mutants with respect to the EPS production. The $\Delta pilT$ mutant showed high level of Congo red binding (Fig. 17A). Thus, MglA is essential for the T4P function, stimulates T4P extension and may minimally inhibit retraction.

2.1.2 MglB & RomR indirectly affect formation of T4P

The function of MglA is tightly connected to the three other polarity module proteins – MglB, RomX and RomR. The three proteins regulate localization and function of MglA, and each of these proteins plays a unique roles in regulating gliding. Function of RomX with respect to MglA is tightly connected to RomR and the two corresponding deletion mutants phenocopy each other in case of T4P-dependent and gliding motility (Szadkowski et al., 2019). Therefore, we included only RomR and MglB, but not RomX, in the current study.

A

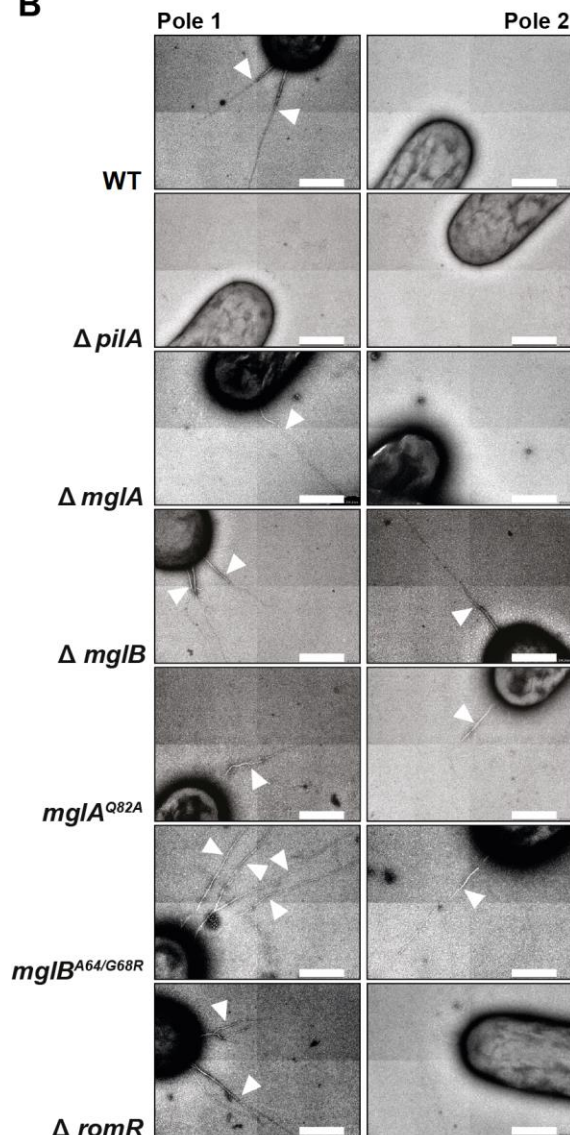
Observed strain	T4P position			
WT	83 ± 4	17 ± 4	0	
$\Delta pilA$	0	100	0	
$\Delta mglA$	31 ± 7	69 ± 7	0	
$\Delta mglB$	53 ± 3	10 ± 2	37 ± 3	
$mglA^{Q82A}$	47 ± 7	19 ± 6	34 ± 11	
$mglB^{A64/G68R}$	54 ± 8	17 ± 13	29 ± 11	
$\Delta romR$	37 ± 25	60 ± 29	3 ± 3	

Figure 18 Formation of T4P coincides with polar accumulation of MglA-GTP

(A) TEM observations of T4P localization (table) compared to the average positions of the MglA-GTP, MglB and RomR proteins inside the cells and relatively to each other (right panel) in corresponding strains. Color code of the proteins indicated at the legend above. Observed cells were divided in three groups based on no T4P formation, uni- or bipolar T4P assembly. Analysis of the TEM data was performed as for Fig. 17.

(B) Example of T4P localization in one cell per every observed strain. Two pictures in a line represent first and second poles of the same cell. Arrowhead point at the single pili found. Cell of $\Delta pilA$ shows no T4P, cells of WT, $\Delta mglA$ and $\Delta romR$ contain unipolar T4P and cells of $\Delta mglB$, $mglA^{Q82A}$ and $mglB^{A64/G68R}$ display T4P at both poles. Scale bar 500 nm.

B



In WT cells, MglA mostly localizes at the leading pole, while MglB and RomR display asymmetric bipolar localization with a large cluster at the lagging pole (Szadkowski et al., 2019) (Fig. 19, first row). Cells of a non-piliated $\Delta pilA$ strain show localization of MglB and RomR, similar to the WT, whereas MglA displayed a stronger asymmetry with 79% of $\Delta pilA$ cells compared to 32% of the WT cells having unipolar MglA localization (Fig. 19, second row).

If MglA stimulates T4P extension at the leading pole, then we would predict that mutants, in which MglA localizes at both poles, would have T4P at both poles. To test this prediction, we analyzed T4P formation in the $\Delta mglB$ mutant. MglA and RomR have been shown to localize in a mostly bipolar fashion without MglB (Keilberg et al., 2012; Zhang et al., 2012). Interestingly, cells of the $\Delta mglB$ mutant possessed T4P at both poles in 37% cells. In 53% of $\Delta mglB$ cells T4P were unipolar and 10% of cells did not show T4P at any of the poles (Fig. 18). Moreover, in an $mglA^{Q82A}$ mutant, in which MglA is locked in the GTP-bound form, all three proteins – MglA^{Q82A}, MglB and RomR - are shifted towards bipolarity (Fig. 19, third row) (Miertschke et al., 2011). 43% of $mglA^{Q82A}$ cells assembled T4P at both poles, and 47% and 19% of unipolar T4P and non-piliated cells, respectively (Fig. 18). Colocalization of MglB, MglA-GTP and T4P at two poles indicates no direct inhibitory role for MglB and supports the stimulatory function of MglA with respect to the T4P formation. Finally, an $mglB^{A64/G68R}$ mutant was tested for the localization of MglA/B/RomR proteins and formation of T4P. MglB^{A64/G68R} of *M. xanthus* corresponds to MglB^{A68/72R} of *T. thermophilus* and was described to have significantly decreased GAP activity and reduced interaction with MglA_{T.t}. The two MglB proteins share 28/52% of identity/similarity and MglB_{T.t} was used to study structural and functional characteristics of MglB alone and in complex with MglA (Miertschke et al., 2011). We observed similar localization of MglA, MglB^{A64/G68R} and RomR in $mglB^{A64/G68R}$ and $mglA^{Q82A}$ mutants (Fig. 19, last row). The three proteins localize more bipolar in cells of $mglB^{A64/G68R}$ mutant than in the WT cells. Further, comparable to $\Delta mglB$ and $mglA^{Q82A}$ mutants, a cell fraction of 29% had T4P at both poles, while 54% cells had unipolar T4P and 17% did not assemble T4P (Fig. 18). This observations support that MglA stimulates T4P extension. MglB, in turn, helps establishing T4P asymmetry in the WT strain, by excluding MglA from the lagging pole.

Finally, the $\Delta romR$ mutant was tested for T4P formation and position. RomR has been reported to be important for polar MglA accumulation and important for polar occurrence of MglB. Thus, MglA is mostly diffuse and MglB clusters more rarely appear at the pole in absence of RomR (Keilberg et al., 2012; Szadkowski, 2018; Zhang et al., 2012). 37±25% cells of $\Delta romR$ mutant contained T4P at one pole. A few cells had T4P at both poles and on average 60±29% of

cells did not have T4P at the poles. Of note, the $\Delta romR$ mutant is highly adhesive and, therefore, T4P difficult to image and count by TEM giving rise to considerable standard deviations (Fig. 18). Hence, the high amount of T4P formed in the $\Delta romR$ mutant supports that polar localization of MglA may not be strictly required for T4P extension.

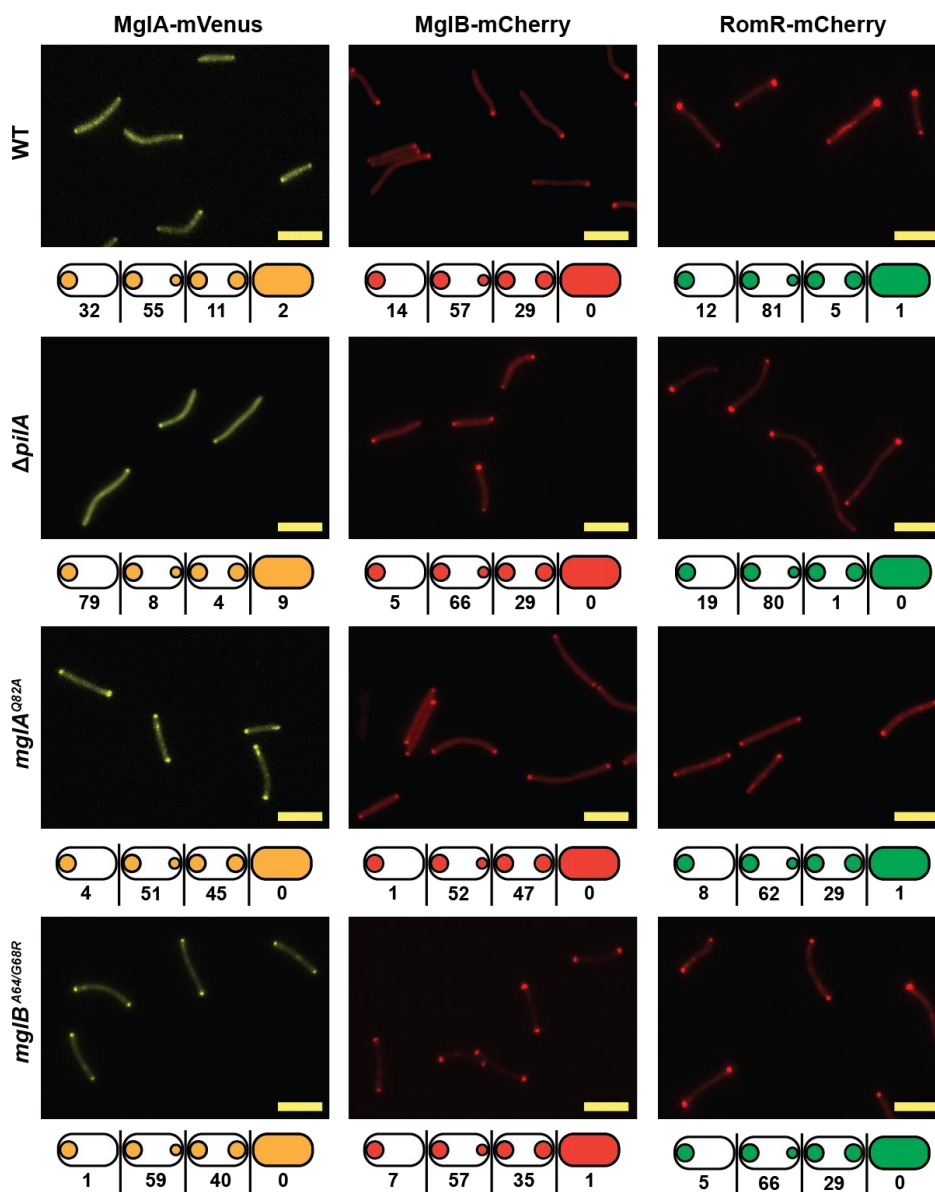


Figure 19 Localization of MglA, MglB and RomR in different genetic backgrounds.

Top panel for every genetic background represents field of cells from the microscopy snapshots. Numbers on the bottom panel represent percentage of cells with certain localization pattern. Localization patterns were defined as described in Materials and Methods 4.3.8. The fluorescence signal for each pole and cytoplasm was calculated. To distinguish between different localization patterns, the ω value that represents asymmetry between the polar clusters was calculated from the equation:

$$\omega = \frac{\text{total fluorescence at pole 1} - \text{total fluorescence at pole 2}}{\text{total fluorescence at pole 1} + \text{total fluorescence at pole 2}}$$

By definition, pole 1 is the pole with the highest fluorescence. The ω value is between 0 (bipolar symmetric localization) and 1 (unipolar localization). The localization patterns are binned from the ω values as follows: unipolar ($\omega > 0.9$), bipolar asymmetric ($0.9 > \omega > 0.2$) and bipolar symmetric ($\omega < 0.2$). Diffuse localization was determined when no polar signal was detected. The localization patterns observed are indicated in the schematics. $N \geq 150$. Scale bar 5 μm .

Altogether, we propose an indirect role of MglB for asymmetric T4P formation, which is achieved by excluding active MglA from the lagging cell pole. Although RomR targets MglA to the pole, it is not strongly affecting T4P formation.

Next, we analyzed the overall level of external T4P using the shear off assay. Independent of unipolar or bipolar T4P formation, or lower number of piliated cells in the $\Delta romR$ mutant, the four tested strains – $\Delta mglB$, $mglA^{Q82A}$, $mglB^{A64/G68R}$ and $\Delta romR$ had comparable level of PilA in both, total and sheared fractions (Fig. 20A).

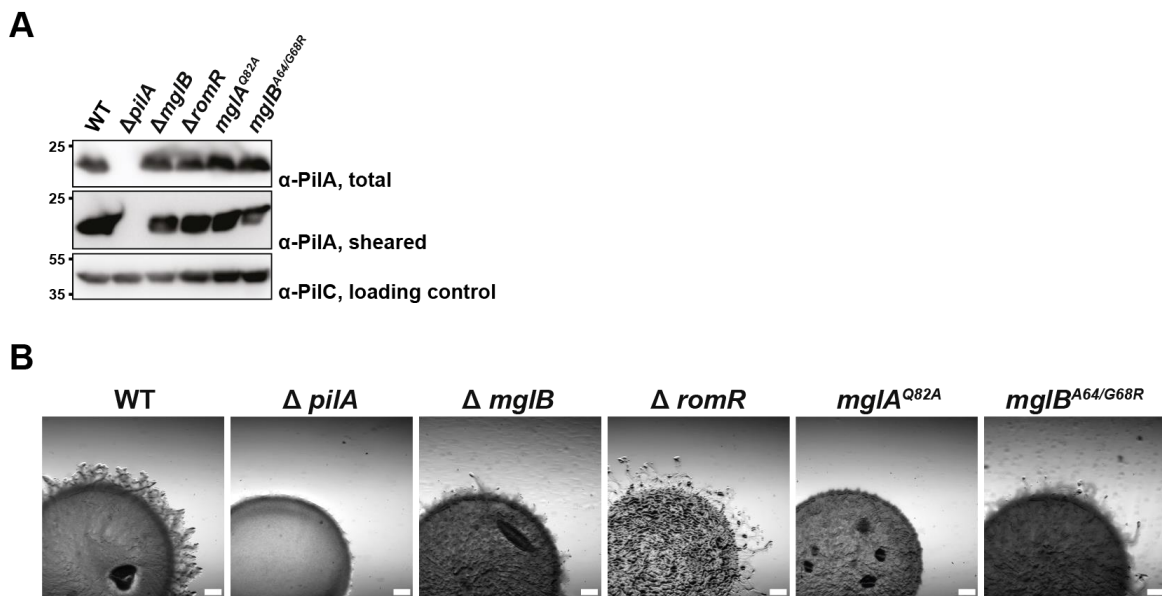


Figure 20 Strains with different T4P localization form the same amount of T4P but form colonies with different shape on 0.5% agar

(A) Immunoblot analysis of whole cell extracts and sheared T4P fractions of corresponding strains was done as for Fig. 17.

(B) T4P dependent motility phenotypes for corresponding strains obtained on the 0.5% agar. Scale bar 500 μm .

The soft agar motility assay showed different morphology of the colony edge for all tested strains. The four mutants ($\Delta mglB$, $\Delta romR$, $mglA^{Q82A}$, $mglB^{A64/G68R}$) displayed detectable movement, compared to the negative $\Delta pilA$ control, but none of the mutants formed similar to the WT strain flares (Fig. 20B). Moreover, the appearance of the colonies differed between each other. The colony of $mglA^{Q82A}$ cells expanded the least and did not form pronounced flares, however the ripply colony appearance of the $mglA^{Q82A}$ mutant compared to the smooth surface of

the $\Delta pilA$ mutant colony, indicates ability of cells to move. As expected, $\Delta mgIB$ and $mgIB^{A64/G68R}$ had similar phenotypes with misshaped flares at the colony edge. Deletion of $romR$ caused cells to form flares, longer and thinner than the ones of the WT colony (Fig. 20B). To better understand the nature of the motility differences we looked at single cells, moving by means of T4P only, for all strains of interest.

We took an advantage of the assay that Sun et al developed in order to observe the single *M. xanthus* cells moving by T4P (Sun et al., 2000). Cells of exponentially growing cultures were placed on polystyrene surface and coated with highly viscous 1% methylcellulose solution. Time lapse recordings of moving cells for 10 minutes with 20 sec intervals allowed cell velocity and reversal frequency to be calculated and compared between strains.

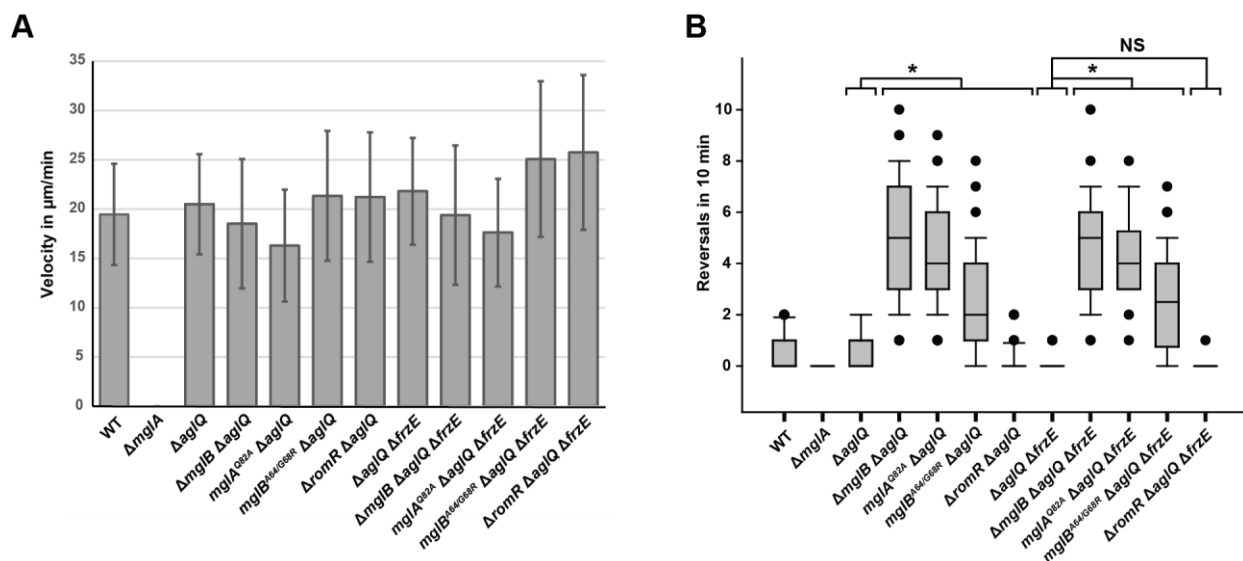


Figure 21 Velocity and reversals calculations for single cells of different strains moving by T4P

(A) Cell velocity for indicated strains. Single cells were tracked for 10 min. Bars presents velocity in $\mu\text{m}/\text{min}$ with calculated standard deviation. $N=600$ single time frames of 20 sec considering only moments when cell moves straight forward between the reversals. Only motile cells were analyzed.

(B) Reversal frequency counted in 10 minutes for indicated strains. The lower and upper boundaries of the boxes represent the 25% and 75% percentile, whiskers represent the 10% and 90% percentiles, respectively. Students' t-test was employed for statistical analysis and * marks significantly different values with $P<0.01$, while NS refers to no significant difference detected. $N\geq 50$.

In all tested strains the $agIQ$ gliding motility gene was deleted, focusing the analysis on T4P dependent motility exclusively. WT cells were imaged initially, however, later for the main course of the experiment, the single $agIQ$ deletion strain served as positive control, as this strain has fully functional T4P (Fig. 21A). Cells of the two strains – WT and $\Delta agIQ$ moved with comparable velocity of 19.5 ± 5 and $20.5\pm 5 \mu\text{m}/\text{min}$, respectively, suggesting that cells in our assay really move by T4P, since gliding motility is abolished by deletion of $agIQ$. Cells of $\Delta mgIA$ mutant

did not show any measurable movement and with only rare dislocation events. The average velocity of the different mutants was following: $18.5 \pm 7 \mu\text{m}/\text{min}$ ($\Delta aglQ \Delta mgIB$), $16.3 \pm 6 \mu\text{m}/\text{min}$ ($\Delta aglQ mgIA^{Q82A}$), $21.3 \pm 7 \mu\text{m}/\text{min}$ ($\Delta aglQ mgIB^{A64/68R}$) and $21.2 \pm 7 \mu\text{m}/\text{min}$ ($\Delta aglQ \Delta romR$). Velocity of mentioned strains varied between each other but did not show drastic changes for any particular strain (Fig. 21A). Importantly, we noticed that strains with T4P at two poles were incapable of moving straight forward for as long as cells with predominantly unipolar T4P. This observation is evidently reflected in the reversal frequency calculations. While WT and $\Delta aglQ$ cells reversed on average once every 10 minutes, cells with additional $\Delta mgIB$, $mgIA^{Q82A}$ and $mgIB^{A64/68R}$ genotypes demonstrated 5, 4 and 2 reversals during the same time period, respectively. Cells, carrying the three mentioned mutations are referred as hyper-reversing. The cells, lacking $romR$, were hypo-reversing with 0.1 reversal per 10 minutes. This is in agreement with previously reported study (Guzzo et al., 2015; Szadkowski et al., 2019) (Fig. 21B).

Reversals of *M. xanthus* cells are under control of the Frz chemosensory system (Blackhart and Zusman, 1985). In order to confirm that the hyper-reversing phenotype of the bipolarly piliated cells is induced by the unusual T4P formation, we deleted FrzE histidine kinase in all observed strains as a key component of the Frz pathway. Further, we used a double $\Delta aglQ \Delta frzE$ background as otherwise WT strain and compared its velocity and reversal frequency to the triple mutants with other gene deletions of interest. Hence, none of the strains could glide and any registered reversal did not refer to the function of Frz system.

The velocity of $\Delta aglQ \Delta frzE$ cells ($21.8 \pm 5 \mu\text{m}/\text{min}$) was comparable to previously observed velocities for WT and cells of the single $aglQ$ deletion. Moreover, all of the tested triple mutants moved similar to corresponding double mutants and to the control strains with calculated velocities of: $19.4 \pm 7 \mu\text{m}/\text{min}$ ($\Delta mgIB \Delta aglQ \Delta frzE$), $17.6 \pm 5 \mu\text{m}/\text{min}$ ($mgIA^{Q82A} \Delta aglQ \Delta frzE$), $25 \pm 8 \mu\text{m}/\text{min}$ ($mgIB^{A64/68R} \Delta aglQ \Delta frzE$) and $26 \pm 8 \mu\text{m}/\text{min}$ ($\Delta romR \Delta aglQ \Delta frzE$) (Fig. 21A). Reversal frequency of $\Delta aglQ \Delta frzE$ cells and $\Delta aglQ \Delta frzE \Delta romR$ cells was maximally close to 0 with rare reversal events in a few cells. Cells with $\Delta mgIB$, $mgIA^{Q82A}$ and $mgIB^{A64/68R}$ genotypes reversed almost equal without active Frz chemosensory system as with it – with on average of 5, 4 and 2.5 reversals in 10 minutes, respectively. The number of the reversals for $\Delta aglQ$ cells was significantly different from cells carrying $\Delta mgIB$, $mgIA^{Q82A}$, $mgIB^{A64/68R}$ and $\Delta romR$ genotypes. Whereas, reversal counts of cells of a double $\Delta aglQ \Delta frzE$ mutant were indifferent to ones of a triple $\Delta aglQ \Delta frzE \Delta romR$ mutant and both were significantly different from the $\Delta mgIB$, $mgIA^{Q82A}$ and $mgIB^{A64/68R}$ mutants (Fig. 21B).

The data, presented here, lead us to the following conclusions. First, a unipolar cluster of MglA-GTP is required for the continuous uni-directional cell movement. Second, bipolar accumulation of MglA-GTP leads to assembly of active T4P at two poles. Finally, T4P, simultaneously active at both poles, cause spatial disorientation of cells, accompanied by spontaneous frequent reversals. Likely, cells move uni-directionally while the number of T4P formed is higher at one of the poles. This becomes temporarily the leading pole. However, once the second pole assembles as many, and maybe even more T4P, the direction of movement is switched to the opposite.

2.2 Parts of T4PM depend on the polarity proteins but are not connected physically

We found that MglA has a crucial effect on formation and function of T4P, while MglB and RomR affect asymmetric formation of T4P indirectly. Every T4PM component has defined localization inside the cells. Here, the membrane proteins PilQ, PilO, PilC, PilP, PilN and the cytoplasmic PilM protein are mostly found at both poles, while the extension ATPase PilB and retraction ATPase PilT are mostly unipolar. We assumed that one or more of polarity module proteins might stimulate polar binding and/or proper sorting of some Pil proteins. Considering that MglA, MglB and RomR are cytoplasmic proteins we tested their effect on the localization of cytoplasmic PilB, PilT and PilM.

2.2.1 PilB localizes independently on MglA/MglB/RomR

Earlier observations, obtained by immunofluorescence, indicate predominantly unipolar localization of the PilB extension ATPase at the leading pole (Bulyha et al., 2013). Here, we constructed the C-terminal fluorescent fusion PilB-mCherry under control of the native promoter and introduced it by site specific recombination into the Mx8 *attB* site in the $\Delta pilB$ deletion mutant. This strain accumulated the protein at similar level as native PilB and complemented the motility defect of the $\Delta pilB$ deletion (Fig. 22).

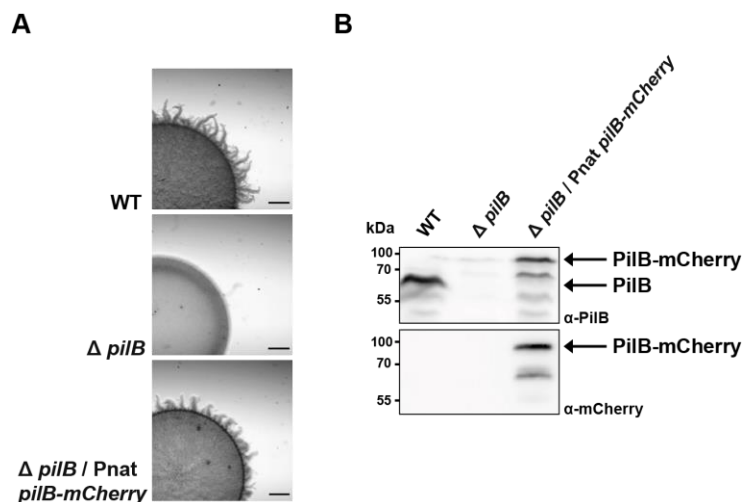


Figure 22 PilB-mCherry is active.

(A) Introduced at the attachment site P_{nat} -PilB-mCherry fluorescent fusion complements T4P dependent motility defect of $\Delta pilB$. Scale bar 500 μ m.

(B) PilB-mCherry accumulates as full-length protein (≈ 89.2 kDa) at comparable to WT PilB (62.5 kDa) level. Upper blot was probed with α -PilB, and lower with α -mCherry antibodies.

We combined the $\Delta pilB$ deletion with every genotype of interest ($\Delta mgIA$, $\Delta mgIB$, $\Delta romR$ and $mgIA^{Q82A}$) and transformed all obtained double mutants with vector expressing $pilB$ -mCherry. Prior to observing protein localization, we checked stability of PilB-mCherry fusion in every genetic background. The fusion proteins were accumulating at a similar level in all indicated strains (Fig. 23).

The careful analysis of the PilB-mCherry localization revealed four localization patterns observed for all tested strains. These are unipolar, bipolar asymmetric, bipolar symmetric and diffuse protein localization. As expected in the WT-like cells PilB-mCherry was mostly at one pole with 60% cells displaying a unipolar and 26% cells a bipolar asymmetric signal. The rest of the cells localized PilB-mCherry bipolar in 6% cases and diffuse in 8% cases, respectively. A similar localization of PilB-mCherry could be observed in a $\Delta mgIA$ and a $\Delta romR$ backgrounds (Fig. 24). Importantly, in the two mutants, $\Delta mgIB$ and $mgIA^{Q82A}$, which are capable of forming bipolar T4P, PilB-mCherry tended to localize more bipolarly. 50% and 16% of $\Delta mgIB$ and 39% and 19% of $mgIA^{Q82A}$ cells showed bipolar asymmetric and symmetric localization pattern of PilB-mCherry, respectively. For the rest of the cases, the 32% of $\Delta mgIB$ cells and 33% of $mgIA^{Q82A}$ cells displayed unipolar localization of PilB-mCherry, with few cells for each mutant showing diffuse signal (Fig. 24). Percentage of protein in cytoplasm did not vary strongly between the strains, indicating that difference in dominating localization patterns is due to re-location of the protein bound at the pole.

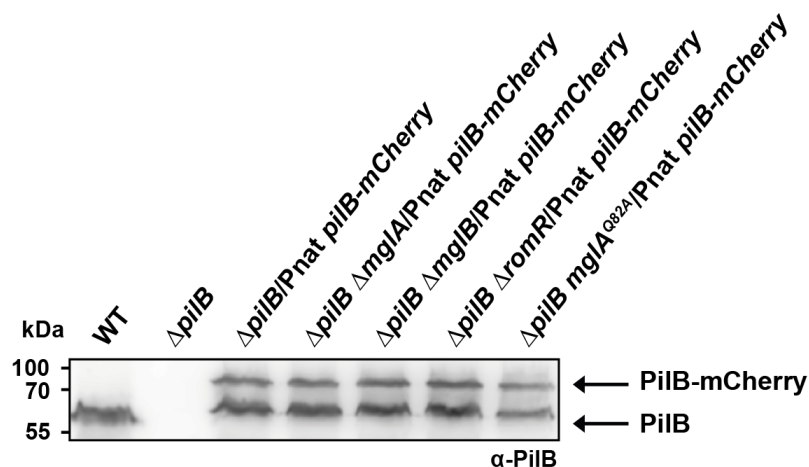


Figure 23 PilB-mCherry fusion stability.

Cells were grown in liquid culture and harvested. Total protein was separated by SDS-PAGE (protein from 7×10^7 cells loaded per lane) and analyzed by immunoblotting. Blot was probed with α -PilB antibodies.

We conclude that none of tested polarity proteins is directly involved in bringing PilB to the poles, however PilB follows localization of MglA-GTP. The data for the $\Delta mgIA$ strain supports previous observations, showing a unipolar PilB localization in this mutant (Bulyha et al., 2013). Bipolar PilB localization in $\Delta mgIB$ and $mgIA^{Q82A}$ strains is consistent with bipolar T4P formation that is, in turn, likely triggered by bipolar accumulation of MglA-GTP.

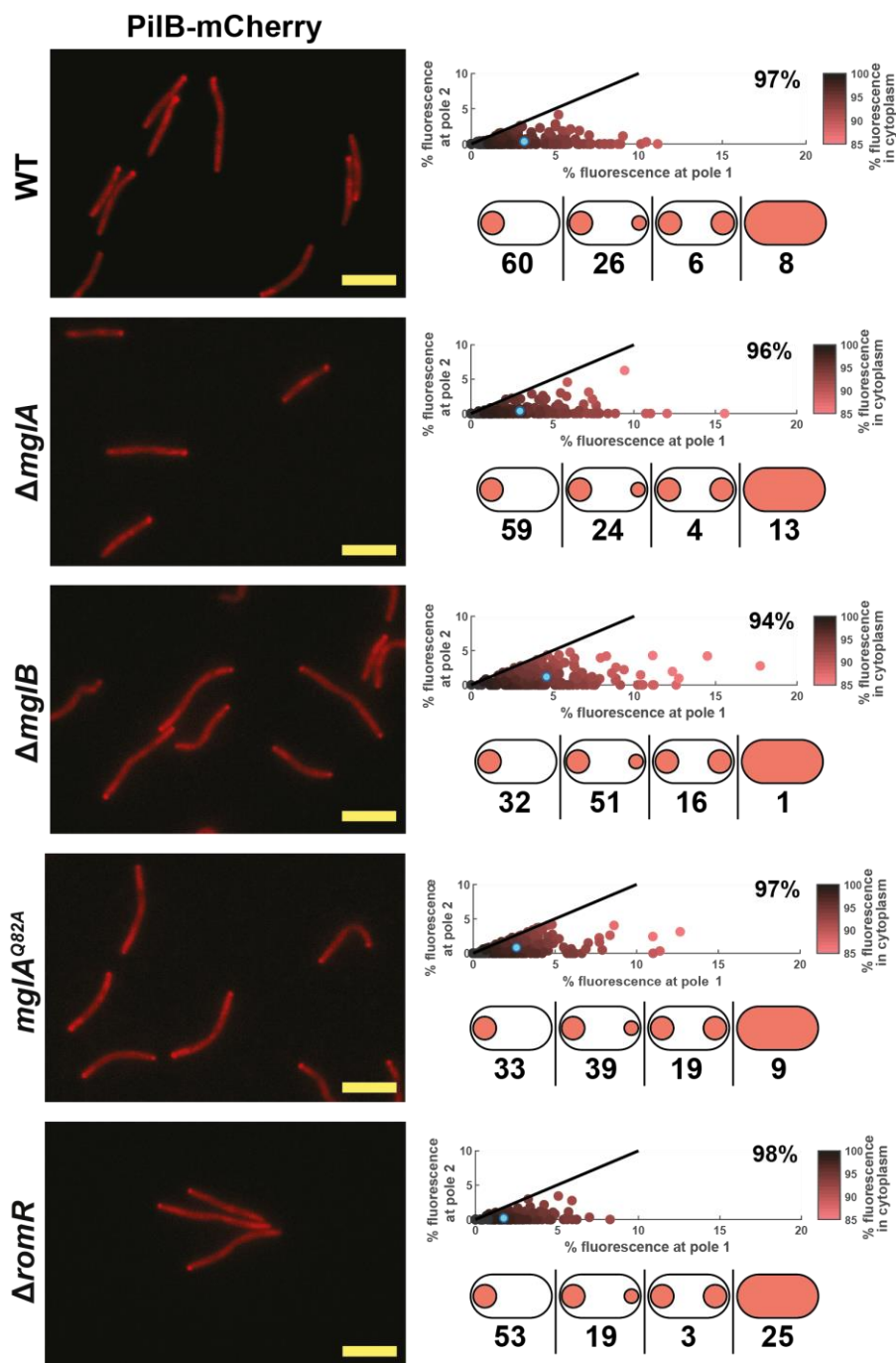


Figure 24 Localization of PilB-mCherry in different genetic backgrounds.

Left column represents images with snapshot of cells expressing PilB-mCherry in every indicated background. Scale bar 5 μ m.

The colour of the dots on the scatter plots and on schematic localization images below refer to the colour given to the protein on the models, shown in the Discussion part.

Scatter plots in the right column represent calculated fluorescence signal for the two poles and the cytoplasm of every analyzed cell. The cyan dot represents the mean protein localization. Number at the right top corner of the plots refers to mean fluorescence in cytoplasm. Numbers below the plots show percentage of cells with corresponding protein localization and calculated as for Fig. 19. $N > 150$.

2.2.2 PiIT localizes independently on MglA/MglB/RomR

To test localization of the PiIT retraction ATPase we created an N-terminal mCherry-PiIT fluorescence fusion. The full-length fusion was expressed from the *attB* site under control of the native *piIT* promoter. The protein accumulated close to native levels and complemented the motility defect of a $\Delta piIT$ mutant (Fig. 25). Sequentially, we introduced the fusion to the single $\Delta piIT$ deletion and all double deletion mutants containing genotypes of interest and verified similar accumulation level of mCherry-PiIT in all resulted strains (Fig. 26).

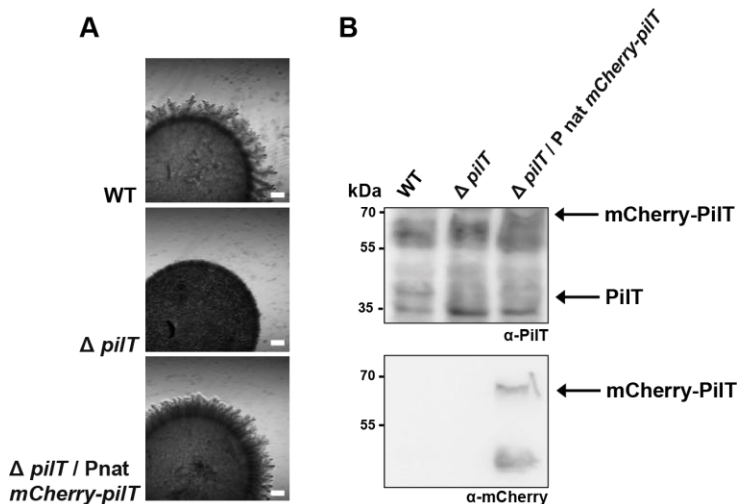


Figure 25 mCherry-PiIT is active.

(A) Introduced at the attachment site P_{nat} -mCherry-PiIT fluorescent fusion complements a T4P dependent motility defect of $\Delta piIT$ mutant. Scale bar 500 μm .

(B) mCherry-PiIT accumulates as full-length protein (≈ 67.4 kDa) at levels comparable to WT PiIT (40.7 kDa). Upper blot was probed with α -PiIT, and lower blot with α -mCherry antibodies.

The localization patterns described above were analyzed for the mCherry-PiIT fusion. In the WT strain mCherry-PiIT localized unipolar in 34% cells, bipolar asymmetric in 50% cells and bipolar symmetric in 16%. No cells with diffuse fluorescence signal were found. In absence of MglA or RomR the protein distribution shifted towards unipolarity with 56% and 48% cells of mentioned deletion strains having a cluster of mCherry-PiIT at one pole, respectively (Fig. 27). 7% cells of $\Delta mglA$ and $\Delta romR$ mutants showed bipolar symmetric mCherry-PiIT and 34 and 45% of the corresponding cells displayed bipolar asymmetric protein localization.

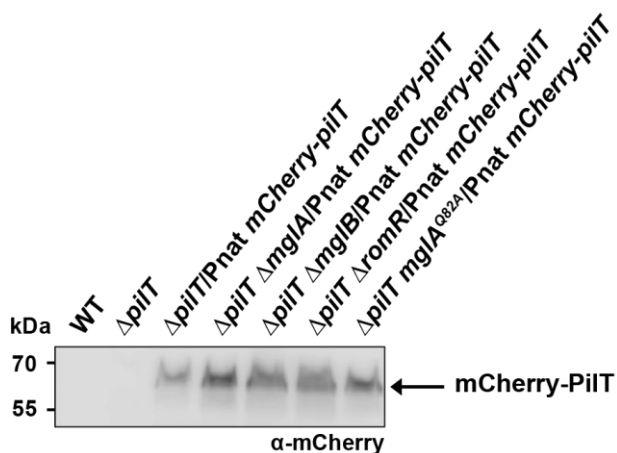


Figure 26 mCherry-PiIT fusion stability.

Immunoblot analysis was performed as for Fig. 17. Blot was probed with α -mCherry antibodies.

As in case of PilB-mCherry, both $\Delta mgIB$ and $mgIA^{Q82A}$ strains demonstrated more bipolar mCherry-PilT localization than the WT cells. Such that 65% and 24% cells of $\Delta mgIB$ had mCherry-PilT in asymmetric and symmetric bipolar fashion, accordingly, while 54% and 24% of $mgIA^{Q82A}$ cells showed the same localization patterns (Fig. 27).

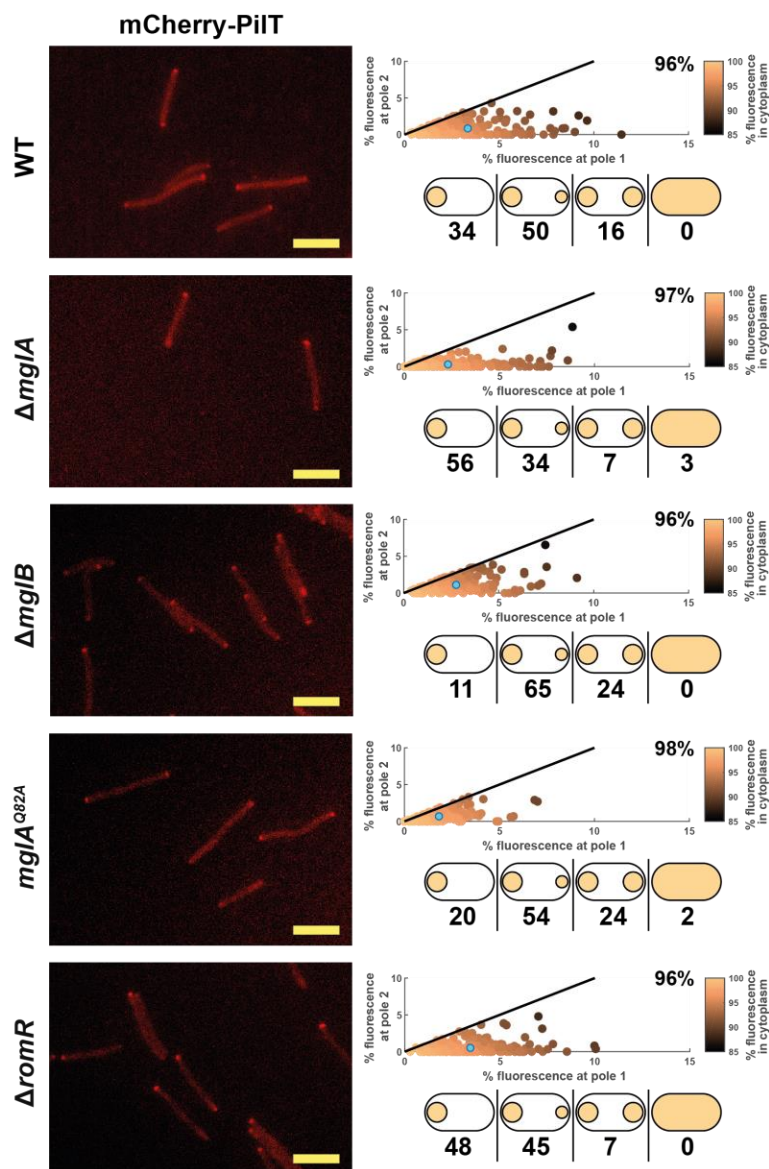


Figure 27 Localization of mCherry-PilT in different genetic backgrounds.

Localization studies performed and analyzed as for Fig. 19. N>150. Scale bar 5 μ m.

The mostly unipolar localization of mCherry-PilT in WT confirms the earlier observations for YFP-PilT, accumulating under control of the constitutively active *pilA* promoter (Bulyha et al., 2013). Moreover, localization of PilT is similar to that of the PilB extension ATPase, suggesting that for every T4P forming strain the two proteins localize at the necessary pole, thereby being able to stimulate the corresponding process to support dynamic formation of T4P. None of the polarity proteins is directly responsible for bringing PilT to the poles. However, in strains, where

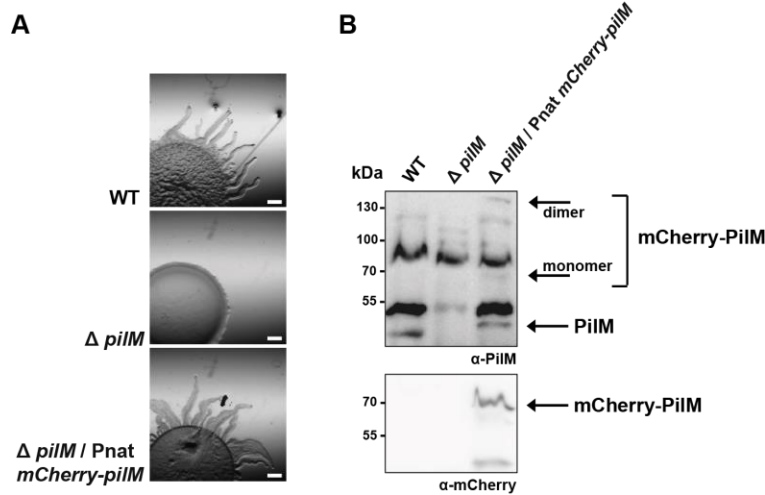
MglA-GTP stimulates bipolar T4P formation, PilT also localizes more bipolar than in strains with unipolar T4P, suggesting presence of an indirect regulation.

2.2.3 MglA regulates localization of PiIM

The last cytoplasmic protein of the T4PM is PiIM that has been previously described to be integrated in the pre-assembled T4P protein complexes located at both cell poles (Bulyha et al., 2009; Chang et al., 2016; Friedrich et al., 2014).

Figure 28 mCherry-PiIM is active.

(A) Introduced at the attachment site P_{nat} -mCherry-PiIM fluorescent fusion complements T4P dependent motility defect of $\Delta piIM$. Scale bar 500 μ m.



(B) mCherry-PiIM accumulates as full-length protein (\approx 69 kDa monomer and \approx 138 kDa dimer) at comparable to WT PiIM (42.3 kDa) level. Upper blot was probed with α -PiIM, and lower with α -mCherry antibodies.

We generated an N-terminal mCherry-PiIM fluorescence fusion that accumulates as a full-length protein, when expressed from the *attB* site. This fusion complemented the T4P-dependent motility defect of a $\Delta piIM$ deletion (Fig. 28). As previously done for PiIB and PiIT, we transformed the single $\Delta piIM$ deletion and double mutants of interest with a vector carrying *mCherry-piIM*. Controlled by the native promoter, the fluorescence protein accumulated at WT levels in every tested background (Fig. 29).

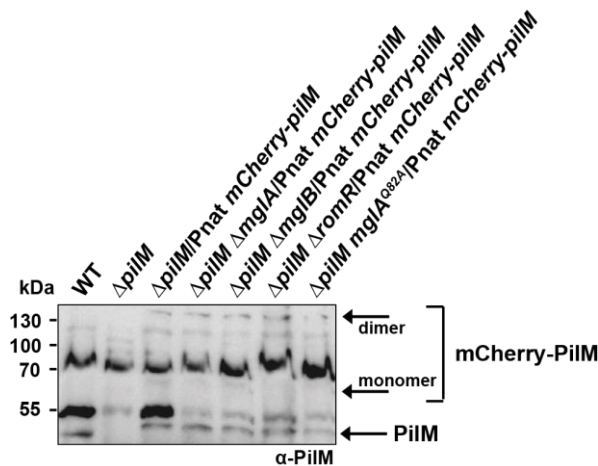


Figure 29 mCherry-PiIM fusion stability.

Immunoblot analysis was performed as for Fig. 17. Blot was probed with α -PiIM antibodies.

In WT-like cells mCherry-PiIM formed pronounced clusters, localized in unipolar (13%), bipolar asymmetric (62%) and bipolar symmetric

(24%) fashion with rare single cells containing diffuse signal (1%) (Fig. 30, upper row). Surprisingly, the percentage of cells with unipolar clusters grew drastically in absence of *mgIA*. In particular, 55% cells of a $\Delta mgIA$ mutant formed unipolar clusters, while 40% had bipolar asymmetric localization of PilM, and only 2% and 3% cells showed bipolar symmetric and diffuse signal, respectively. Localization of mCherry-PilM in absence of *mgIB*, *romR* or in a *mgIA*^{Q82A} mutant looked similar to the WT localization with predominantly bipolar symmetric and asymmetric protein distribution. Interestingly, cells of a $\Delta romR$ mutant, lacking polar accumulation of MglA, did not show as strong tendency for unipolar localization of mCherry-PilM as the $\Delta mgIA$ deletion strain, with only 25% cells bearing PilM at one pole (Fig. 30).

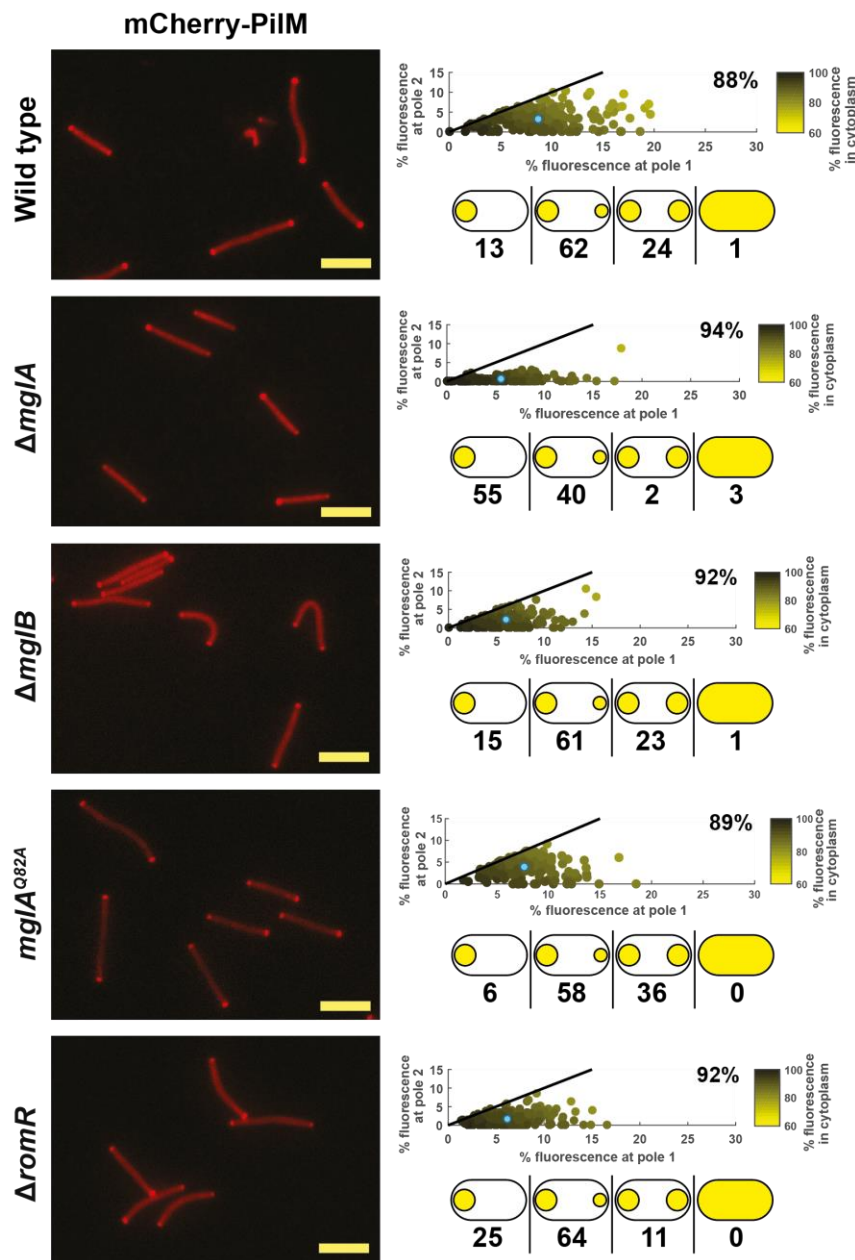


Figure 30 Localization of mCherry-PilM in different genetic backgrounds.

Localization studies performed and analyzed as for Fig. 19. N>150. Scale bar 5 μ m.

The observations, described above, demonstrate the ability of MglA to sort at least one of the stationary localized T4P proteins to both poles. Moreover, the similar localization of PilM in the WT and in the $\Delta romR$ strain suggests that a high concentration of MglA at the poles is not necessary to ensure PilM sorting. Although the mechanism of this sorting is yet to be understood, we speculate unipolar localization of PilM in $\Delta mglA$ cells might mediate assembly of T4P at one pole only in this mutant.

2.2.4 MglA and RomR regulate localization of PilQ

As the T4P is assembled in outside-in manner, PilM is the last protein to be incorporated into stationary T4P clusters (Friedrich et al., 2014). However, it is intriguing that MglA is the first identified regulator that helps any of the bipolar T4P components to localize correctly. Hence, we decided to test if this function of MglA also extends on the other T4P proteins existing in tandem with PilM at two cell poles. To address this question we tested the localization of the initial bipolar T4P machine component, the OM PilQ secretin protein.

For the purposes of the current study we created an endogenous C-terminal *pilQ*-sfGFP fluorescence fusion substituting the native copy of *pilQ* in the genome. PilQ-sfGFP accumulated in the view of monomers and multimers at the WT level and fully complemented the motility defect of *pilQ* deletion (Fig. 31). As before, we introduced the *pilQ*-sfGFP fusion into a $\Delta mglA$, $\Delta mglB$, $\Delta romR$ and $mglA^{Q82A}$ mutants to investigate its localization. As for PilB, PilT and PilM before, level of PilQ-sfGFP was constant for every strain used (Fig. 32).

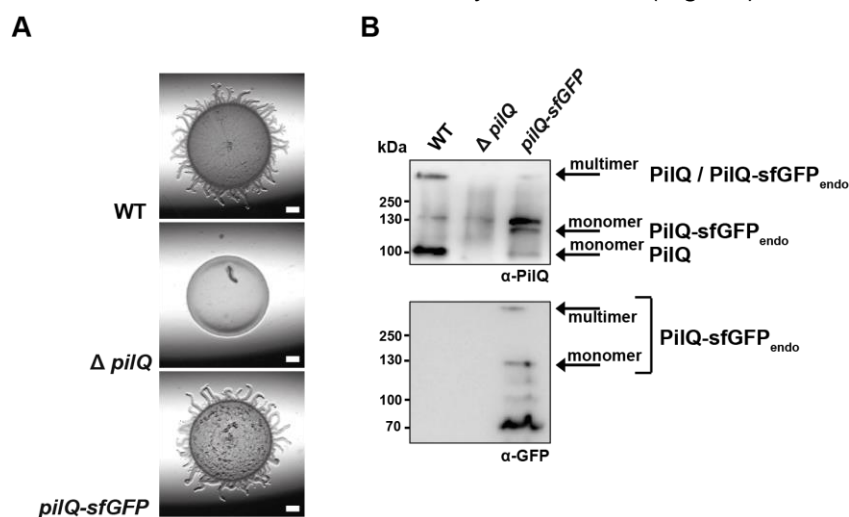


Figure 31 PilQ-sfGFP_(endo) is active.

(A) Introduced at the native site P_{nat}-PilQ-sfGFP fluorescent fusion complements T4P dependent motility defect of $\Delta pilQ$. Scale bar 500 μ m.

(B) PilQ-sfGFP accumulates as full-length protein (≈ 125.2 kDa) at comparable to WT PilQ (99 kDa) level and forms multimers (>250 kDa). Upper blot was probed with α -PilQ, and lower with α -GFP antibodies.

The localization of PilQ-sfGFP in otherwise WT cells was unipolar in 11% cases, bipolar asymmetric in 76% and bipolar symmetric in the rest 13% cells (Fig). Similar to mCherry-PilM the majority of cells had tendency to localize PilQ in either of bipolar patterns, supporting previous

observations describing PilQ as stationary bipolar component of the T4P machine. Next, we analyzed the localization of PilQ-sfGFP in a $\Delta mglA$ background and compared it to the WT localization and localization observed for mCherry-PilM. The localization patterns of PilQ clusters in $\Delta mglA$ were similar to the data we obtained for PilM in this background. PilQ-sfGFP localized unipolarly in 52% cells, while only 45% and 3% cells contain bipolar asymmetric and symmetric protein localization, respectively (Fig. 33).

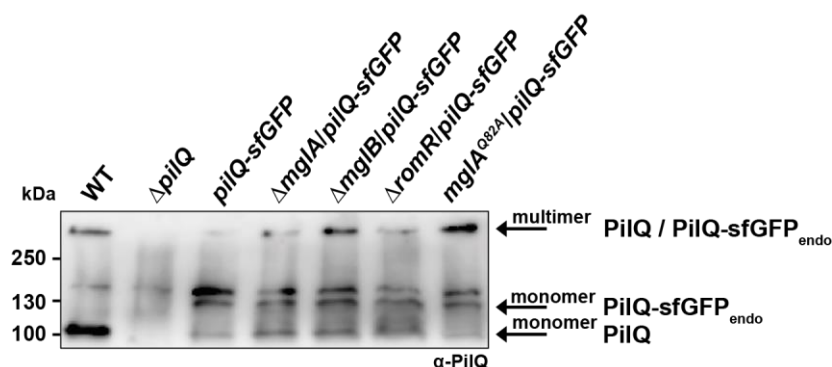


Figure 32 PilQ-sfGFP_{endogenous} fusion stability.

Immunoblot analysis was performed as for Fig. 17. Blot was probed with α -PilQ antibodies.

Similar to PilB, PilT and PilM, analyzed earlier, PilQ localized in a predominantly bipolar manner in the $\Delta mglB$ and $mglA^{Q82A}$ strains. Remarkably, the localization of PilQ was shifted towards a unipolar localization in a $\Delta romR$ similar to PilQ in a $\Delta mglA$ mutant. 50% of $\Delta romR$ cells accumulated PilQ-sfGFP at one pole only (Fig. 33). Visually the similarity of PilQ localization in absence of MglA and RomR points at the connection between these two proteins in bringing PilQ to the two poles. The role of RomR as a landmark protein for MglA would contribute to the possibility of a functional connection between the two regulators. However, PilM as the cytoplasmic part of the stationary T4PM complexes remained mostly bipolar in absence of *romR*, indicating a more complex mechanism involved in the MglA-dependent Pil proteins sorting or a separate role of RomR in this process.

Taking into account the observations acquired for the PilQ-sfGFP localization we confirm the prominent sorting effect of MglA regarding the bipolar T4PM proteins. Further, unipolar localization of PilB, PilT, PilM and PilQ in absence of *mglA* are in agreement with unipolar formation of T4P in a $\Delta mglA$ mutant. Moreover, the cytoplasmic levels of all observed proteins remained similar between the different mutants. This suggests that PilM and PilQ accumulated with double excess at one pole of $\Delta mglA$ cells. An increased protein accumulation could explain reduced number of T4P assembled in this strain. Although, a strong change of PilQ accumulation in the $\Delta romR$ strain brings significant complexity to the regulatory network, involving MglA and RomR, unipolar localization of PilQ likely explains the mostly unipolar formation of T4P in this mutant, despite the diffuse localization of MglA and bipolar PilM.

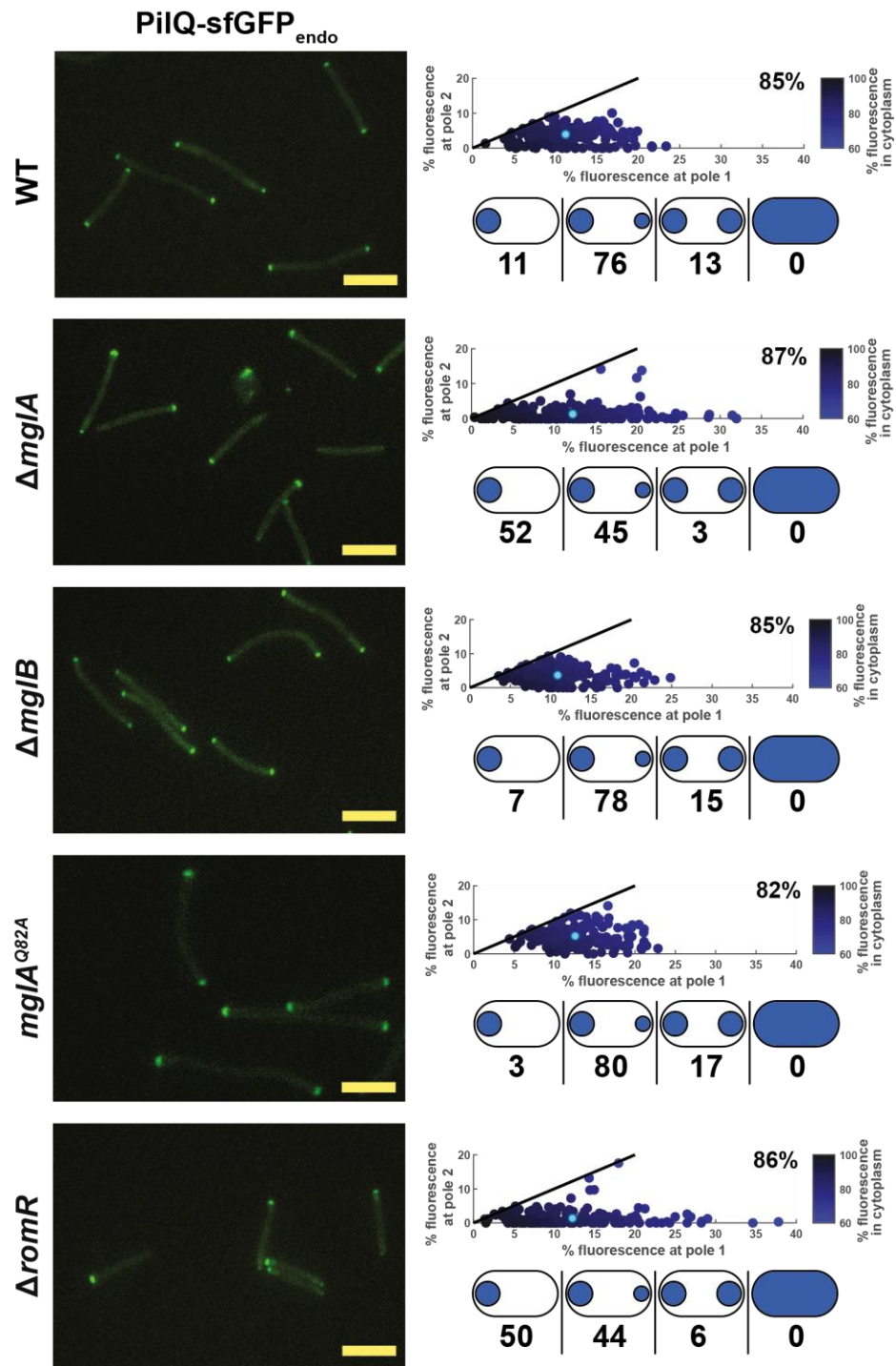


Figure 33 Localization of PilQ-dfGFP in different genetic backgrounds.

Localization studies performed and analyzed as for Fig. 19. N>150. Scale bar 5 μ m.

2.2.5 The polarity module does not interact to PilB/PilT/PilM in bacterial two hybrid assay

Taken together, the observed localization effects for all T4P proteins tested, are likely achieved by one or more protein-protein interactions that mechanically connect the MglA based regulatory scaffold to the T4PM. Therefore, we tested pairwise interactions between the polarity module parts MglA/B/RomR and the cytoplasmic parts of the T4PM PilB/T/M. In order to do that we took an advantage of the bacterial two hybrid system (BACTH) (Karimova et al., 1998). All six proteins were fused to the T25 and T18 fragments of the *Bordetella pertussis* adenylate cyclase in C- and N-terminal orientation. Further, by performing double transformations of *E. coli* BTH101 with pairs of obtained vectors we tested, first, self-interactions of all indicated proteins. MglB and RomR demonstrated self-interaction, while MglA did not interact with itself in any of the tested vector combinations, confirming earlier reported results and with that verifying the functionality of the assay (Keilberg, 2013; McLoon et al., 2016). As we expected, all three T4P proteins tested also self-interacted, supporting the predictions for PilB and PilT to form hexamers and PilM to form oligomeric ring-shaped structure as a part of pre-assembled polar complexes (Bischof et al., 2016; Chang et al., 2016; Jakovljevic et al., 2008) (Fig. 34A).

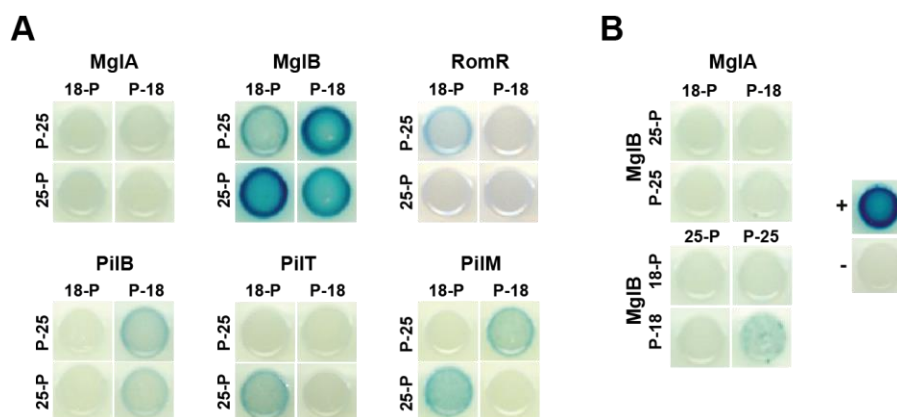


Figure 34 BACTH assay is functional for different polarity and T4P proteins.

(A) Self-interaction of the indicated proteins. Vectors obtained by fusing every indicated gene to T25 or T18 adenylate cyclase fragments of *B. pertussis* were co-transformed to *E. coli* BTH101 in all possible pairwise combinations. Blue colony (+) means presence of the interaction, while white colony (-) means no interaction detected. P letter marks protein of interest that is additionally indicated on the top.

(B) Test for the interaction of MglA with MglB.

Additionally, we verified previously identified interaction between MglA and MglB. In current study it occurred between the MglA-T25 and MglB-T18 (Fig. 34B).

As a next step, MglA, MglB and RomR were sequentially tested for the interaction with each of the Pil proteins and possible combinations were examined. None of the polarity proteins

revealed an interaction with any of T4PM proteins (Fig. 35). This could be interpreted differently. We reasoned that either an interaction between tested proteins has a highly transient nature and applied assay is not sensitive enough to detect it, or one or more other proteins are in between the T4PM and regulatory proteins of interest.

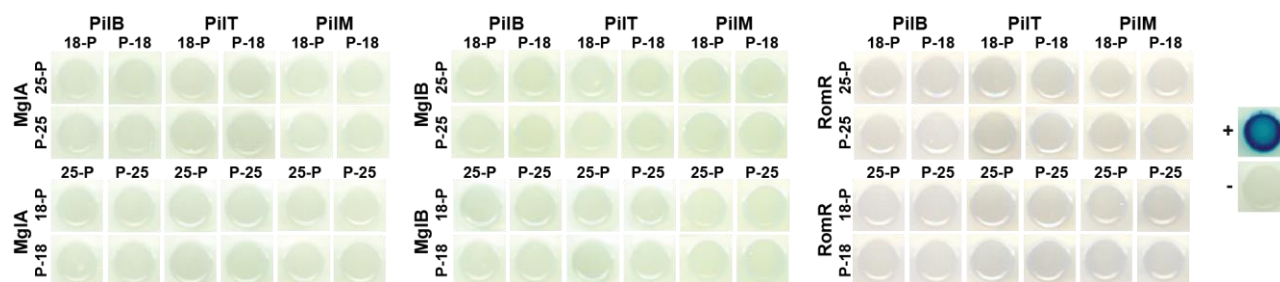


Figure 35 Polarity proteins do not interact with cytosolic T4P components in BACTH assay

Experiment was performed as for Fig. 34. None of the colonies show blue color indicating no interaction between indicated proteins.

2.3 Identification of SgmX

Among the three proteins of the polarity module, the function of MglA in establishing T4P asymmetry, stimulating its formation and function is strongly pronounced, whereas MglB and RomR are involved in all mentioned processes only indirectly. Therefore, we concentrated our work on looking for the proteins that directly connect MglA to the T4P machine. MglA homologues are widely represented in bacterial species, where they help to fulfil multiple functions (Keilberg et al., 2012; Milner et al., 2014; Salzer et al., 2015; Wuichet and Søgaard-Andersen, 2014). Among MglA-like proteins, studied to date, MglA from *Thermus thermophilus* has been described to localize T4P at the poles and, therefore, to spatially regulate T4P-associated DNA uptake (Salzer et al., 2015). Another homologous GTPase is found in the small deltaproteobacteria *Bdellovibrio bacteriovorus*, where it has an impact on T4P formation and prey invasion. The function of MglA in *B. bacteriovorus* is tightly connected to the RomR_{Bd} and both MglA and RomR_{Bd} interact with Bd2492 that is also required for prey invasion. The gene encoding Bd2492 is co-transcribed with two other genes – *bd2494* and *bd2495*, encoding essential proteins for the *B. bacteriovorus*. The same gene synteny was identified for *Bacteriovorax marinus* (BMS_0137-140) and *M. xanthus* (*mxan_5763-66*) with *mxan_5766* encoding homologue of Bd2492 (Milner et al., 2014).

In 2006 Youderian & Hartzell reported the results of *M. xanthus* transposon mutagenesis that aimed to determine genes involved in T4P-dependent and gliding motility. Gene *mxan_5766* was listed in the final gene table as an insertion in this gene impaired the T4P-dependent motility

(Youderian and Hartzell, 2006). We hypothesized that *M. xanthus* could have evolved a similar regulatory mechanism as found in *B. bacteriovorus*, with MglA functionally connected to MXAN_5766 to regulate T4P dependent motility.

2.3.1 Characterization of SgmX

Mxan_5766 encodes a large 1060 aa cytosolic protein that is predicted to have 5 and 3 tetratricopeptide (TPR) motifs at C- and N-terminus, respectively. No domains were predicted to be encoded by an intermediate (≈ 660 aa) region in between (Fig. 36A) (Milner et al., 2014). In 2006 the product of *mxan_5766* was named SgmX (from **S**ocial **g**liding **m**otility protein **X**), which we will use for the corresponding protein from now on (Youderian and Hartzell, 2006).

TPR repeats are on average 34 amino acids long, contain no invariant residues and share a consensus sequence, characterized by a pattern of small and large hydrophobic amino acids. TPR motifs are known to fold into TPR domains, described for proteins of eukaryotic and prokaryotic species. In different species, these proteins serve as an interaction scaffold for ligand compounds, proteins and multiprotein complexes. Typically, a TPR motif folds into a helix-turn-helix structure that is comprising the TPR domain. Often, TPR domain proteins oligomerize to extend the interaction surface for higher number of molecules (Zeytuni and Zarivach, 2012).

The *M. xanthus* gene synteny is similar to the one of *B. bacteriovorus* and includes *mxan_5763* and *mxan_5764*, encoding an OM protein with an Omp85 domain and an IM protein with a DUF490 domain, respectively. The two proteins are homologous to the components of translocation assembly module (Tam) that compose an autotransporter-secretion system (Selkrig et al., 2012). Unlike *B. bacteriovorus*, *M. xanthus* additionally encodes a putative Sec system ATPase MXAN_5765 by a gene positioned in between the *sgmX* and the *mxan_5763-4* genes. Downstream of *sgmX*, *mxan_5767* encodes for an Acetyl-CoA carboxylase domain protein, which was not characterized yet. SgmX and the products of all four flanking genes are relatively well conserved among myxococcales species (Fig. 36B).

The level of conservation of SgmX is highest for the TPR domain regions and decreases for the interdomain area (Fig. 36B). Although percentage of identity and similarity between SgmX and Bd2492 is just 7% and 10% respectively, parallels that were highlighted for regulatory pathways of the two species by Milner et al, 2014 and relation of SgmX to the T4P-dependent motility, predicted by Youderian & Hartzell (2006), made SgmX a promising candidate for the purposes of the current study. Additionally, proteins, homologous to SgmX, were found to often

co-exist with MglA, MglB, RomR/RomR, as well as to the proteins, potentially building the T4PM in other bacteria (Fig. 37).

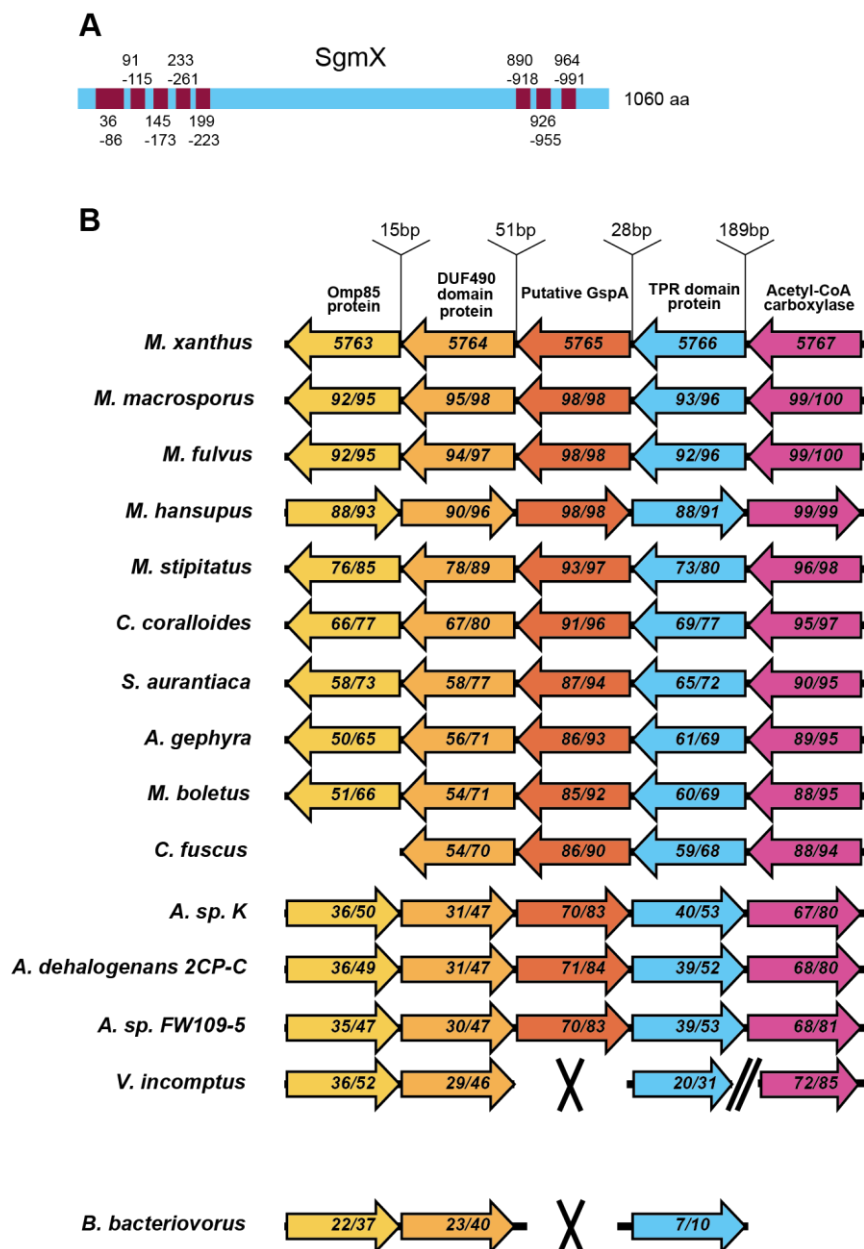


Figure 36 Bioinformatical analysis of SgmX

(A) Domain structure of SgmX, predicted by BlastP algorithm. Eight tetratricopeptide (TPR) motifs are marked in dark red and their amino acids coordinates indicated above and below.

(B) Conservation of *mxan_5763-5767* including the *sgmX* (*mxan_5766*) gene locus in myxococcales and *B. bacteriovorus*. Yellow, orange, peach, blue and rose arrows indicate genes. Same colors indicate homologous genes. Orientation of arrows corresponds to orientation of genes. Cross means lack of the corresponding gene and two bars indicate that the two genes are separated in the genome. Sequences, taken from the KEGG database, were aligned in pairwise manner using EMBOSS Needle software to obtain the % similarity/identity of SgmX to every protein of interest (indicated on every gene). Predicted domains described above. Distances between the *M. xanthus* genes noted on the top.

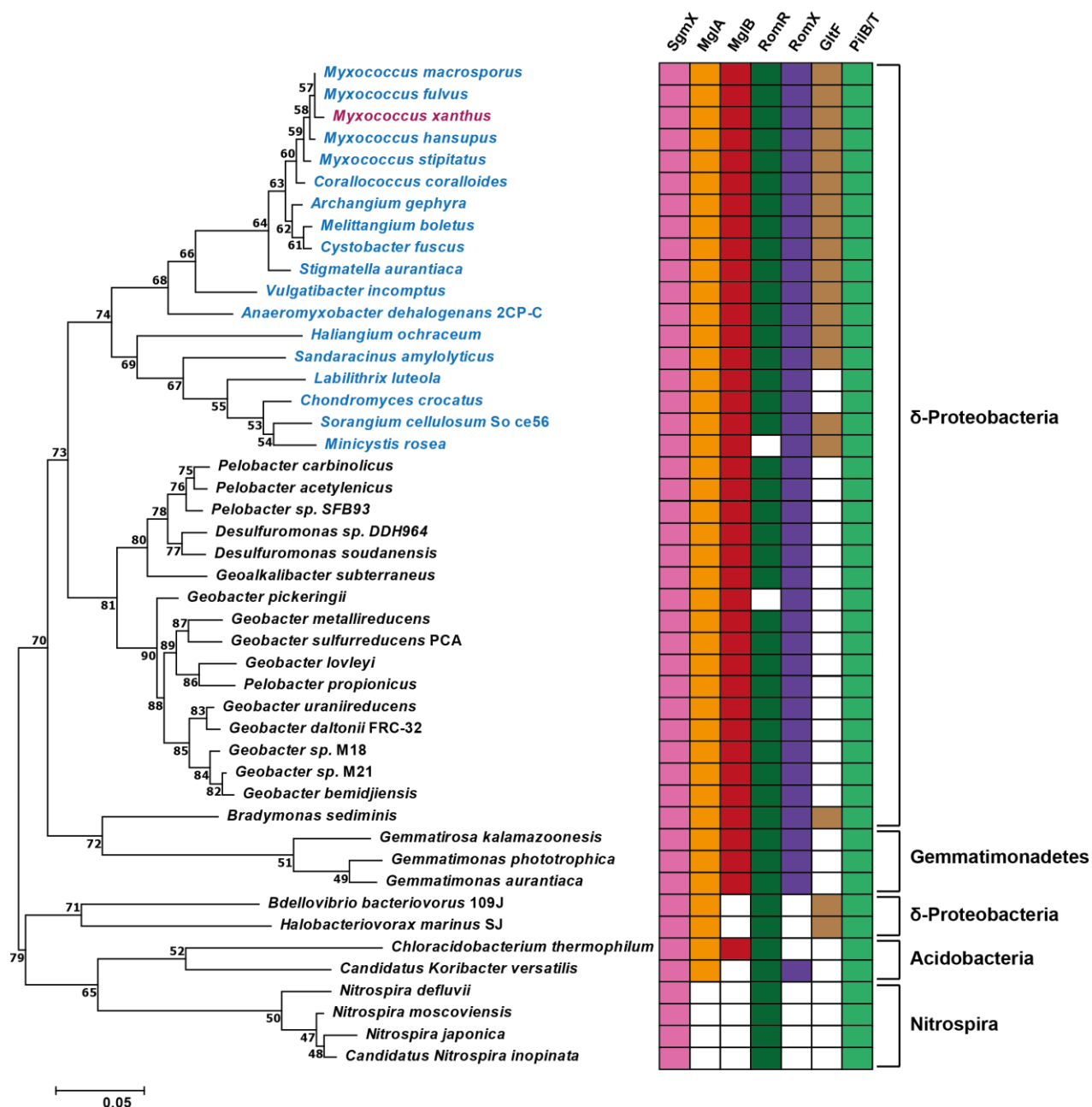


Figure 37 SgmX, MglA, MglB, RomR, RomX have similar genomic distribution among bacterial species and often co-exist with T4P-dependent motility system and gliding motility system.

Phylogenetic tree based on 16s RNA gene sequence was constructed using maximum likelihood. Sequences were obtained from KEGG Organisms database, and were aligned using ClustalW. The tree was built in MEGA7 software. Myxococcales species are marked with blue, *M. xanthus* is marked in red. Classes of indicated bacterial species represented on the right side. GltF protein represents the gliding motility machinery, PilB/T indicates the T4P-dependent motility machine. Scale bar represents 0.05 substitutions per amino acid site.

2.3.2 SgmX is important for T4P-dependent motility

In order to test whether SgmX is a novel motility regulator of *M. xanthus*, we generated an in-frame deletion mutant and tested it for T4P-dependent and gliding motility. On a 0.5% agar surface a ΔsgmX mutant formed a flat-edged colony, comparable to the ΔpilA negative control, suggesting lack of T4P-dependent motility for this strain (Fig. 38A, left column). As before for the ΔmglA mutant, we tested for accumulation of EPS by the cells of a ΔsgmX mutant. A colony of a ΔsgmX mutant did not display Congo red binding and looked equal to the ΔpilA negative control (Fig 41A, right column). To test gliding motility, we used a solid 1.5% agar surface. WT displayed well distinguishable single cells at the edge of the colony, while an *aglQ* deletion served as a negative control with no single cells outside of the colony. The colony edge of a ΔsgmX strain looked similar to the WT with numerous single cells moving outwards (Fig. 38A, two middle columns). Importantly, the T4P-dependent motility and EPS accumulation defects were restored by introducing an ectopic copy of *sgmX* under the control of its native promoter (500bp upstream), confirming no polar effect of *sgmX* deletion on the downstream genes (Fig. 38A, left and right columns). Additionally, we looked at the double $\Delta\text{aglQ}\Delta\text{sgmX}$ deletion in 1% methylcellulose-containing buffer to see if the motility defect could be complemented. No single cell movement was detected for $\Delta\text{aglQ}\Delta\text{sgmX}$ cells as previously reported for ΔmglA cells (data not shown). Therefore, SgmX is required for T4P-dependent but not for gliding motility.

Aiming to explain the lack of T4P-dependent motility in ΔsgmX background, we tested accumulation of the ten T4P components as previously performed for the *mglA* deletion. We found that all the proteins accumulated at the WT levels (Fig. 38B). Next, we looked at the T4P directly, using TEM and found no piliated cells of ΔsgmX strain. This observation was further confirmed by the shear off assay with subsequent immunoblot analysis of the total and sheared PilA, where the total cell fraction displayed a similar PilA accumulation as in the WT, whereas the sheared fraction was protein-free (Fig. 38C, D).

At last, we generated a non-retracting $\Delta\text{pilT}\Delta\text{sgmX}$ strain and compared its motility and surface T4P to the single *sgmX* and *pilT* deletions. The double deletion strain still showed movement by gliding motility and had a similar non-motile phenotype as the single *sgmX* deletion on T4P-favoring surface. Interestingly, the sheared PilA fraction of a $\Delta\text{pilT}\Delta\text{sgmX}$ mutant was easily detectable and comparable to the WT fraction (Fig. 38A, D). Yet, lack of motility and EPS production indicates that T4P formed by $\Delta\text{pilT}\Delta\text{sgmX}$ cells are not functional (Fig. 38A, first and last columns). Therefore, we conclude that SgmX is important for T4P formation and function.

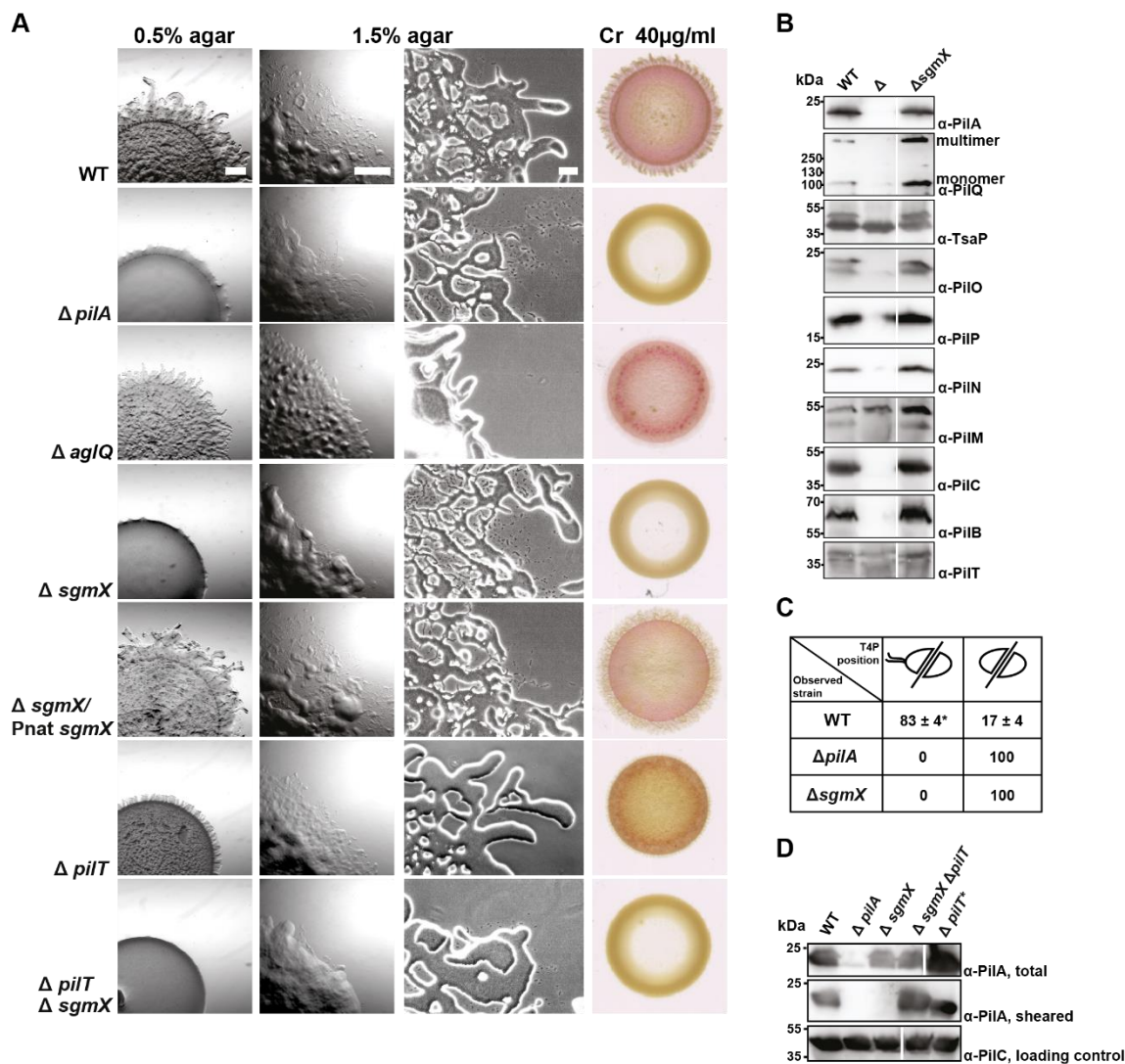


Figure 38 SgmX stimulates formation of T4P

(A) Cells of indicated genotypes move by means of T4P-dependent motility (0.5% agar, 24h) or gliding motility (1.5% agar, 24h). Left column displays the colony edge of cells moving by T4P. Two columns display the colony edge of single cells moving by gliding at different magnifications. Scale bars: 500 μ m for T4P-dependent motility; 500 μ m and 50 μ m left and right respectively for gliding motility. Right column shows EPS accumulation in WT and selected mutants that is detected as for the Fig. 17A.

(B) Immunoblot analysis of ten core T4P proteins accumulation in WT (left) compared to $\Delta sgmX$ (right) strains. Samples were prepared as for Fig. 17B. Tested proteins indicated on the right.

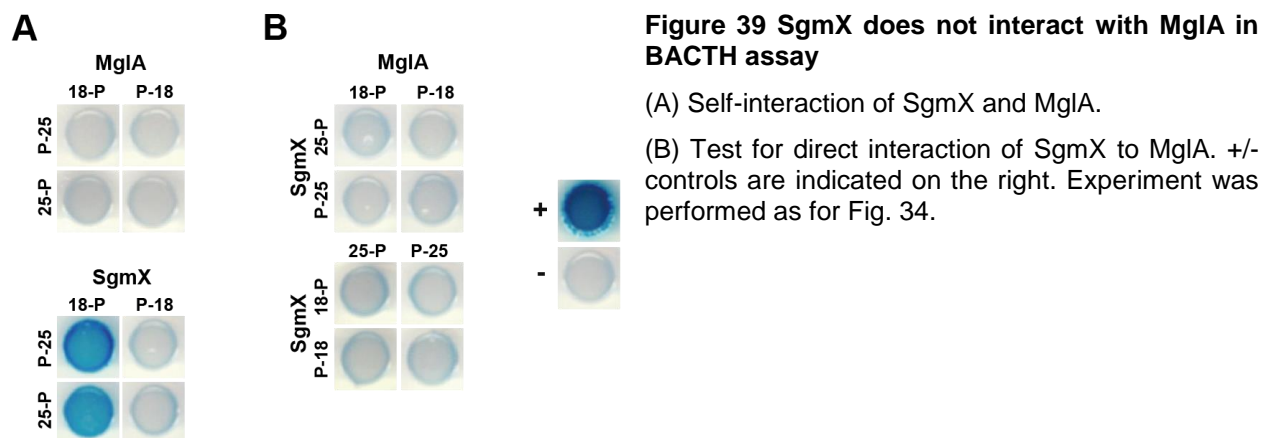
(C) TEM analysis of T4P formed by $\Delta sgmX$ cells. *Numbers represent percentage of cells analyzed displaying one of the three observed piliation phenotypes \pm standard deviation given by three biological replicates. $N \geq 50$.

(D) Immunoblot analysis of whole cell extracts and sheared T4P fractions of corresponding strains. Samples were collected and treated as for Fig. 17D. *Sheared fraction of the $\Delta pilT$ strain was diluted 200 times before loading.

The significant role of SgmX for the T4P-dependent motility was an important primary observation in context of the current study. As a next step we aimed to see if SgmX interacts with MglA and if those two proteins regulate T4P formation and function together.

2.3.3 SgmX interacts to MglA-GTP *in vitro*

In order to test direct interaction between SgmX and MglA we created BACTH vectors for *sgmX* and applied them in the assay. SgmX self-interacted in two vector combinations out of 4 tested, but did not interact with MglA in any of the cases (Fig. 39).



Keeping in mind that it might be difficult to capture transient protein-protein interaction using the BACTH system, we further purified SgmX and MglA and performed *in vitro* pull down experiments.

We used the previously published overexpression constructs for MglA-His₆ and His₆-MglB purification (Fig. 40A) (Zhang et al., 2010). We applied the reported purification protocols for both proteins and used pure MglA-His₆ and His₆-MglB to test the activity of MglA-His₆. For this purpose, a nonradioactive colorimetric assay was used. While His₆-MglB displayed no GTPase activity and an observed intrinsic GTPase activity of MglA-His₆ alone was minimal, MglA and MglB, mixed in a molar ratio of 1:2, showed high level of GTP hydrolysis. Calculated amount of phosphate, released per hour, was reaching 160 pmoles at highest concentrations of MglA-His₆ used, compared to only 14 pmole for MglA-His₆ alone (Fig. 40C).

As a next step, we created C-terminal Strep-tag version of SgmX under control of an IPTG-inducible promoter for overexpression and purification of the protein. SgmX-Strep was soluble and formed heat- and detergent-resistant dimers with a calculated size of 233.3 kDa by size exclusion chromatography (size of the monomer is ≈116.6 kDa). Dimer formation was also detectable on the SDS-PAGE (Fig. 40A, B).

Further, we pre-mixed MglA-His₆ with buffers containing GTP or GDP, or pure buffer and then added SgmX-Strep in equal molar concentration. After incubation, the protein mixtures were applied to a Ni²⁺-NTA resin, washed and proteins were eluted. SgmX-Strep alone or with added

GTP/GDP was used as a negative control and showed no binding to the Ni²⁺-NTA resin under any conditions tested (Fig. 41, upper part). Analysis of the elution fractions from experiments containing both MglA and SgmX detected the two proteins together only in the sample containing GTP, but not with GDP or no nucleotides added (Fig. 41, down part). This result confirmed SgmX to be an effector protein of MglA.

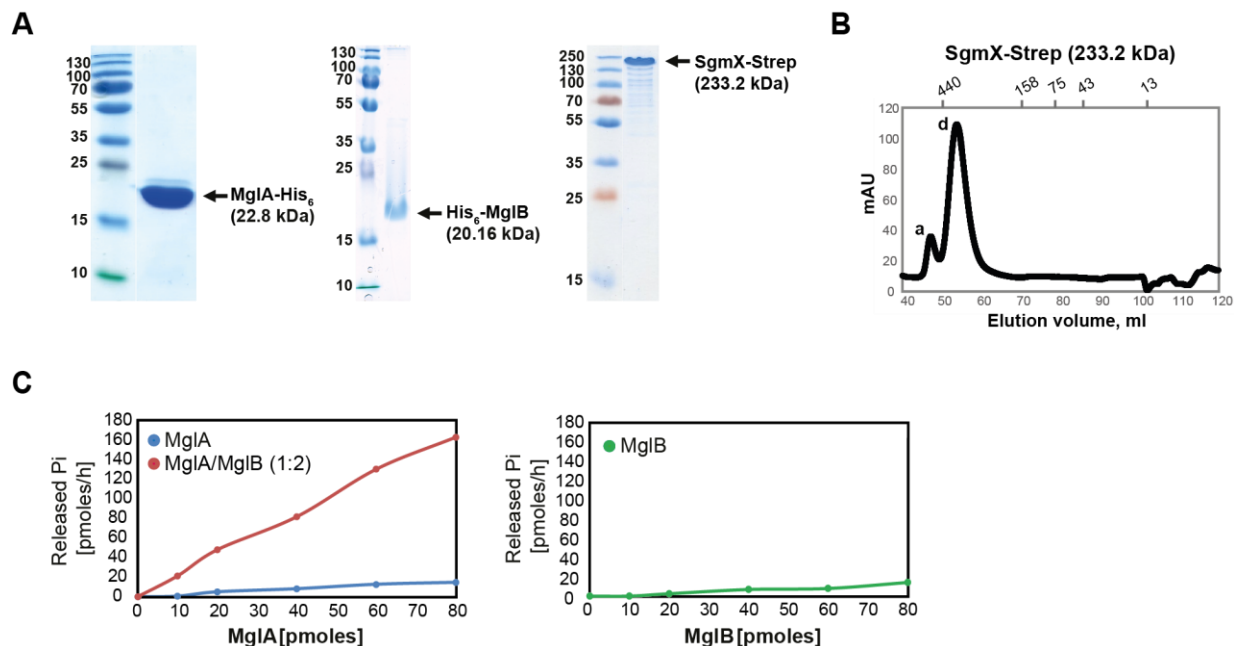


Figure 40 MglA-His₆ and SgmX-Strep are active *in vitro*

(A) SDS-PAGE analysis of purified MglA-His₆, His₆-MglB and SgmX-Strep. 15ng of the indicated proteins was separated by SDS-PAGE and gels stained with Instant Blue reagent. Calculated molecular weight of the proteins is indicated on the right. Molecular markers size are indicated on the left in kDa.

(B) SgmX-Strep forms dimers in solution. The diagram shows the elution profile of SgmX-Strep from size-exclusion chromatography (HiLoad 16/60 Superdex 200). Molecular markers size are indicated on the top. Peaks marked "a" and "d" correspond to aggregates and dimer, respectively.

(C) MglA is active in presence of MglB. Reactions were performed as described in Materials & Methods. Left plot represents the intrinsic GTPase activity curve (blue) of MglA-His₆ and the curve indicating GTPase activity of MglA-His₆ in presence of His₆-MglB (orange). Curves are created by plotting obtained values in pmoles released phosphate per hour against pmoles of MglA-His₆ (left plot) or His₆-MglB (right plot) taken. Amount of released phosphate, detected for the protein-free probe served as a background that was subtracted prior to creating the plots.

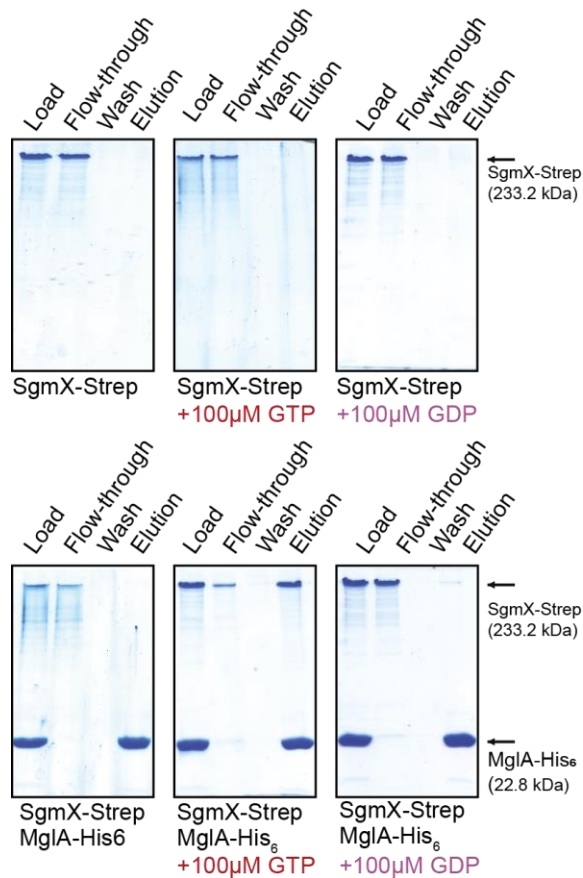


Figure 41 MglA-His₆ interacts to SgmX-Strep in presence of GTP *in vitro*.

SDS-PAGE analysis of protein fractions obtained in pull down experiments. For the top gels SgmX-Strep was pre-incubated with nucleotides and loaded on the column, washed and eluted. For the bottom gels, MglA-His₆ was pre-incubated with nucleotides, then SgmX-Strep was added. Samples before, after loading and the wash step were loaded in equal concentrations. The elution step was loaded in 3-fold concentration. Fractions analyzed marked above the gels, protein used below and protein sizes are shown on the right.

2.3.4 SgmX stimulates T4P formation downstream of MglA

Each - SgmX and MglA – stimulate T4P formation, however, the two deletion strains display different piliation phenotypes. We wanted to reveal the hierarchy of the two proteins in this process. In order to define it we created a double $\Delta mglA\Delta sgmX$ deletion and tested it for T4P formation. Unlike an *mglA* deletion and similar to the $\Delta sgmX$ strain, $\Delta mglA\Delta sgmX$ mutant did not show any T4P formed for the single cells examined by TEM, or in sheared T4P fraction analyzed by immunoblot (Fig. 42). Additionally, we took advantage of the strain containing the MglA^{Q82A} variant, which is locked in the active GTP-bound state and, hence, forming T4P upon constant MglA-GTP enforcement. We compared its piliation phenotype to the double $mglA^{Q82A}\Delta sgmX$ mutant. The newly generated strain showed the behavior of single $\Delta sgmX$ and a double $\Delta sgmX\Delta mglA$ deletions, forming no T4P (Fig. 42).

Thus, SgmX likely acts downstream of MglA-GTP in stimulating the formation of T4P in *M. xanthus*.

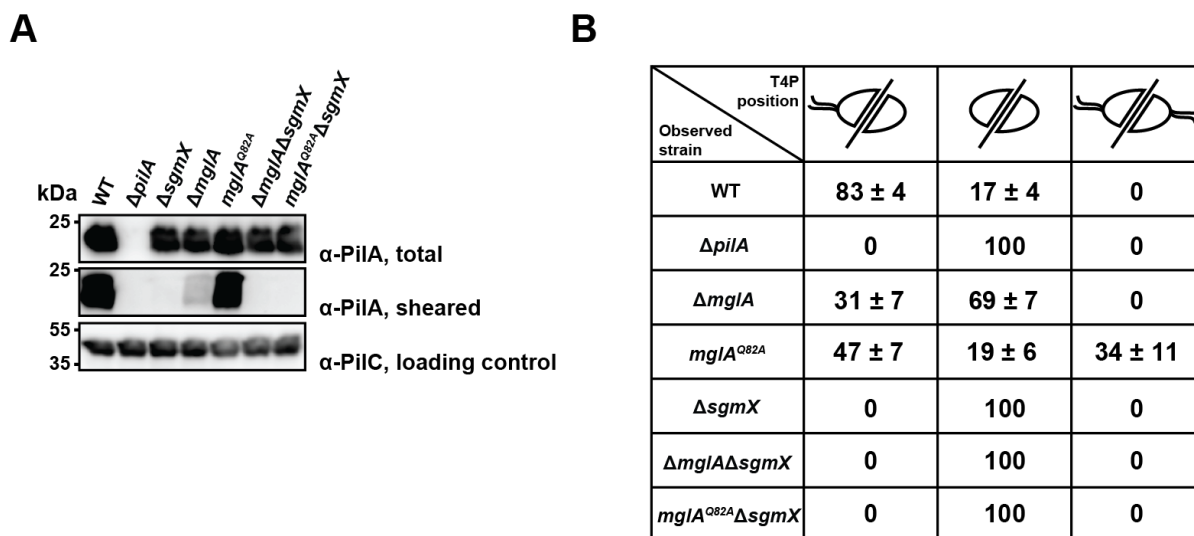


Figure 42 SgmX acts downstream of MglA for T4P formation

(A) Immunoblot analysis of whole cell extracts and sheared T4P fractions of corresponding strains. Samples were collected and treated as for Fig. 17D.

(B) T4P formation in indicated strains calculated based on TEM images. Numbers represent percentage of cells analyzed displaying one of the three observed piliation phenotypes ± standard deviation given by three biological replicates. N≥50.

2.3.5 SgmX stimulates polar binding of PilB

In order to understand the molecular mechanisms underlying the stimulatory role of SgmX for T4P dependent motility we used the fluorescence fusions of T4PM proteins, generated earlier, and tested their localization in a ΔsgmX background. Considering that SgmX interacts with MglA and the latter protein has an impact in sorting bipolar T4P components we assumed to see similar regulation effect by SgmX.

However, the two bipolar T4PM proteins analyzed – the cytoplasmic PilM and OM PilQ – localized in the WT-like fashion in absence of SgmX (Fig. 43), suggesting that MglA performs sorting of stationary T4P proteins independently of SgmX. Importantly, localization of PilB-mCherry strongly shifted towards a more diffuse localization in ΔsgmX strain, relatively to its WT localization, with 62% cells containing diffuse signal instead of 8% for the WT cells. The last T4P protein tested, PilT, located more unipolar in absence of SgmX, and, alike PilB, displayed a slight loss of polar binding. In particular, 65% cells of the ΔsgmX mutant compared to 34% cells of the WT strain had unipolar mCherry-PilT localization with cytoplasmic signal increasing from 96 to 98% in the deletion mutant (Fig. 43).

Thus, SgmX stimulates polar accumulation of the PilB ATPase that is key to T4P extension, and affects polar binding and asymmetric localization of the PilT retraction ATPase. However, no effect of SgmX on sorting the stationary bipolar T4PM clusters was observed.

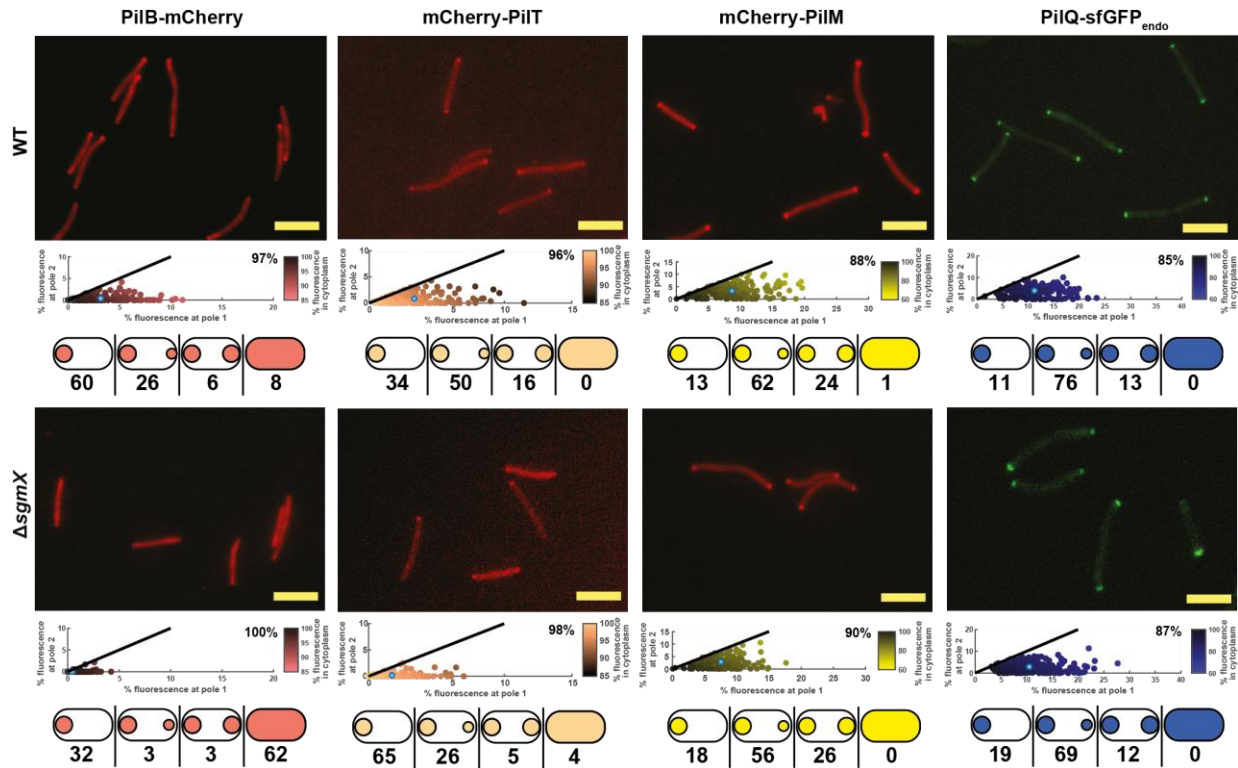


Figure 43 SgmX stimulates polar binding of PiIB-mCherry

Localization of fluorescence proteins indicated above in Δ *sgmX* background compared to the WT strain. Localization studies performed and analyzed as for Fig. 19. N>150. Scale bar 5 μ m.

2.3.6 SgmX regulates polar localization of MglA

Function of the T4PM is an output of SgmX dependent regulation, and MglA is its regulatory and interaction partner. We assumed that SgmX might affect not only correct localization of T4P proteins but also stimulate accumulation of sufficient amount of MglA at the poles. To test this idea, we looked at the localization of the endogenous fluorescence fusion MglA-mVenus in the WT compared to the Δ *sgmX* strain.

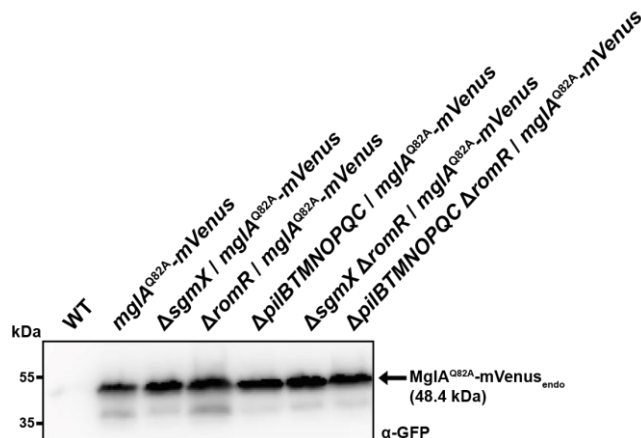


Figure 44 Stability of MglA^{Q82A}-mVenus in strains of indicated genotypes

Immunoblot analysis was performed as for Fig. 17. Blot was probed with α -GFP antibodies.

Dominating localization pattern of MglA-mVenus was similar in WT and in Δ *sgmX* cells, with most of the cells showing unipolar or bipolar asymmetric cluster position (Fig. 45A). Importantly, lack of SgmX led to an increase in number of cells with a diffuse MglA-mVenus signal from 2% to 35%. Fluorescence of the MglA-mVenus in the cytoplasm grew from 97% in the WT cells to 98% in the SgmX deficient cells. Assuming that SgmX serves as a bridge between MglA and the T4PM we hypothesized the absence of T4PM components to affect polar binding of MglA-mVenus similar to lack of SgmX. However, this was not the case as MglA-mVenus localized comparable to the WT strain in Δ *pilBTMNOPQC* background (Fig. 45A). Additionally, it has been previously reported and confirmed in the current study that RomR serves as a main landmark protein for MglA-mVenus at the pole. Lack of *romR* was sufficient to essentially eliminate polar localization of MglA (~100% cytoplasmic MglA-mVenus and 90% of the cells showing diffuse protein localization) (Fig. 45A). Yet, it is important to remember that MglA-mVenus represents a pool of protein including both GTP- and GDP-bound versions. Therefore, lack of localization differences of MglA-mVenus in the Δ *pilBTMNOPQC* mutant relatively to the WT strain, did not exclude the possibility that proteins of T4PM might be important only for localizing only one of the two versions of MglA. We assumed that the localization of an MglA-GTP would be likely affected in this case.

To differentiate between the localization of the WT MglA-mVenus and its GTP-bound version, we took advantage of the MglA protein carrying the Q82A substitution. MglA^{Q82A}-mVenus has been previously shown to localize in a pronounced bipolar fashion with additional clusters inside the cells representing gliding motility complexes. These are staying steady with respect to the substrate. Importantly, in a Δ *romR* background MglA^{Q82A}-mVenus still displayed minimal polar accumulation, accompanied by bright gliding motility complex clusters, shuttling along the cell body (Szadkowski et al., 2019). We were able to reproduce previously reported localization results for the MglA^{Q82A}-mVenus in both WT and Δ *romR* backgrounds (Fig. 45B). Further, we generated two new mutants, localizing MglA^{Q82A}-mVenus in absence of SgmX and T4PM proteins. Neither in Δ *sgmX* nor in Δ *pilBTMNOPQC* deletion strains could we observe drastic changes in localization of MglA^{Q82A}. In both backgrounds, the protein localized predominantly bipolar with clusters relocating between the poles and staying stationary with respect to the surface (Fig. 45B). Keeping in mind that for the constantly active MglA^{Q82A}, RomR served as a major but not essential polar determinant, we further combined a *romR* deletion with the two backgrounds of interest and analyzed localization of MglA^{Q82A}-mVenus in Δ *romR* Δ *sgmX* and Δ *romR* Δ *pilBTMNOPQC* strains. Remarkably, the minor polar binding of MglA^{Q82A}-mVenus, observed in cells of single Δ *romR* deletion, was completely abolished in two resulting double mutants. This effect shifted the general

protein localization towards mainly diffuse and unipolar, where every unipolar protein accumulation was a result of the shuttling FAs inside the cell, reaching the pole prior to a reversal. It is important to mention that every tested background accumulated equal amount of MglA^{Q82A}-mVenus (Fig. 44). Therefore, the localization differences were not due to lack or excess of the protein in cells. MglA-mVenus, localized in $\Delta romR \Delta sgmX$ and $\Delta romR \Delta pilBTMNOPQC$ strains showed equal patterns to its localization in the $\Delta romR$ mutant and was mainly diffuse (Fig. 45A).

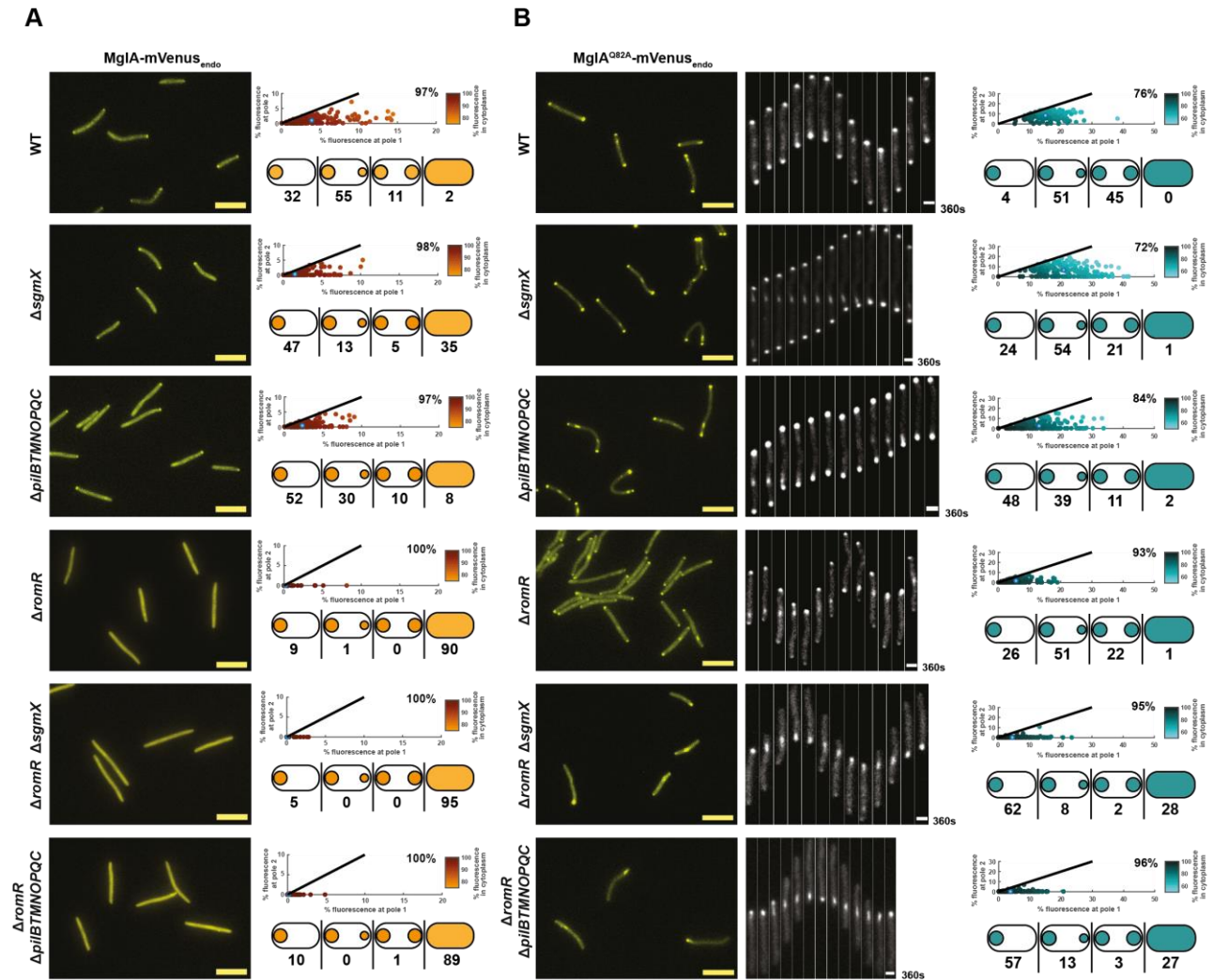


Figure 45 Localization of MglA and MglA^{Q82A} is regulated by SgmX

(A) Localization of MglA-mVenus in strains of indicated genotypes.

(B) Localization of MglA^{Q82A}-mVenus in strains of indicated genotypes. Left column shows field of steady cells. Middle column shows time-lapse microscopy of 6 minutes total with 30 sec intervals. Scatter plots and localization patterns indicated on the right. Localization studies performed and analyzed as for Fig. 19. N>150. Scale bar 5 μ m.

Based on the described observations it is tempting to assume that SgmX is a protein link between MglA-GTP and T4PM. Our data also suggest that RomR is the main polar recruitment factor of MglA-GTP and that SgmX and the T4aPM may also have minor roles in this recruitment.

2.3.7 SgmX localizes dynamically at the leading pole

SgmX is crucial for the formation of T4P, interacts with MglA-GTP and stimulates its polar accumulation. Moreover, it plays a role in polar binding of PilB. As MglA-GTP and PilB accumulate at the pole where T4P extension takes place, which for the WT cells is a leading pole, we hypothesized SgmX to localize at the leading pole as well.

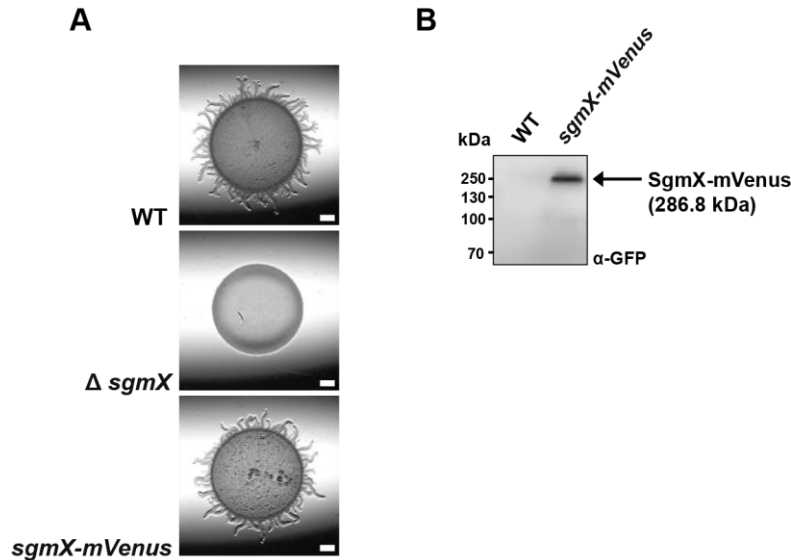


Figure 46 SgmX-mVenus_{endogenous} is active.

(A) Introduced at the native site *sgmX-mVenus* complements T4P dependent motility defect of Δ *sgmX*. Scale bar 500 μ m.

(B) SgmX-mVenus accumulates as full-length protein and runs as a heat- and detergent-resistant dimer (\approx 286.8 kDa). Blot was probed with α -GFP antibodies.

To test our hypothesis we created an endogenous SgmX-mVenus fluorescence fusion and substituted native *sgmX* with the *sgmX-mVenus* allele WT cells. Motility assay and immunoblot analysis confirmed the accumulation of the full-length SgmX-mVenus that formed dimers and complemented the motility defect caused by the *sgmX* deletion (Fig. 46).

Next, we looked at the localization of SgmX-mVenus in WT cells, as well as in the different deletion backgrounds. We verified stability of SgmX-mVenus in all used backgrounds (Fig. 47).

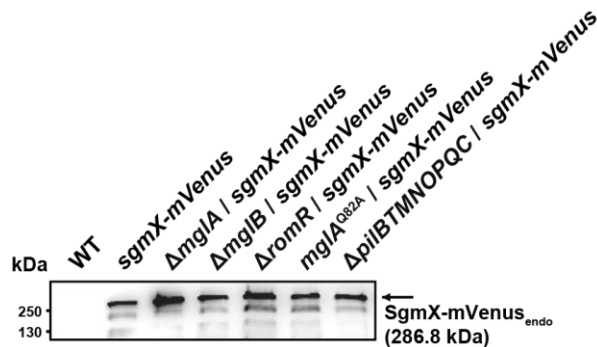


Figure 47 SgmX-mVenus fusion stability in indicated backgrounds.

Immunoblot analysis was performed as for Fig. 17. Blot was probed with α -GFP antibodies. Marker sizes are indicated on the right.

Confirming our prediction, SgmX-mVenus localized mainly unipolar, forming cluster at one pole only in 71% of the WT cells analyzed. The rest 27% and 2% cells displayed bipolar asymmetric and symmetric localization of SgmX, respectively, with no cells accumulating diffuse protein. In 5 minutes time-lapse recordings with 30 sec time frame intervals we observed that the

pole with a SgmX-mVenus cluster is the leading pole, and it switches its localization during reversals (Fig. 48, upper panel). Aiming to identify the polar protein target, as well as sorting factors for SgmX, we further analyzed its localization in absence of every single polarity module component, in a strain with the *mgIA*^{Q82A} variant and a strain, lacking the T4PM.

Keeping in mind the results described above, we hypothesized that MglA and/or one or more T4P proteins could affect localization of SgmX. Although the general distribution of SgmX-mVenus in the cells of $\Delta mgIA$ mutant was similar to its WT localization, we observed an increase in the cytoplasmic protein accumulation. The average fluorescence signal in the cytoplasm was 93% in a $\Delta mgIA$ mutant, compared to 67% in the WT. Although the *mgIA* deletion did not affect localization patterns of SgmX-mVenus drastically, the two mutants, forming bipolar T4P and accumulating MglA-GTP at two poles, consistently changed localization of SgmX-mVenus towards mostly bipolar. Thus, 40% and 58% cells of *mgIA*^{Q82A} mutant had bipolar asymmetric and symmetric clusters of SgmX-mVenus, respectively, while for the $\Delta mgIB$ cells the corresponding numbers were 33% and 61% for the same localization patterns. The cytoplasmic SgmX-mVenus signal increased in the absence of *mgIB* to 71% and in the *mgIA*^{Q82A} mutant to 78%. Bipolar localization of SgmX-mVenus remained steady during reversals (Fig. 48). Therefore, despite the effect of MglA on the polar binding of SgmX, in case of T4P formed at two poles, all three necessary proteins – MglA, PilB and SgmX – find themselves at two poles to stimulate the T4P assembly.

Considering that lack of MglA did not show a strong effect on localization of SgmX-mVenus, we assumed no significant changes of SgmX-mVenus localization in $\Delta romR$ cells either. Indeed, 85% cells localized SgmX-mVenus unipolar. Remarkably, strain lacking proteins of T4PM also did not show significant changes of SgmX localization. Both $\Delta romR$ and $\Delta pilBTMNOPQC$ mutants had an increased cytoplasmic amount of SgmX with 81% and 83%, respectively. Interestingly, cells of $\Delta pilBTMNOPQC$, which move by means of gliding motility only, contained SgmX-mVenus cluster at the correct, leading pole (Fig. 48). Therefore, neither PilB nor the T4PM *per se* bring SgmX to the pole to assure its proper function. Assumingly, some other protein or a group of proteins target SgmX to the poles. Despite the fact that neither MglA nor the T4P machine alone were essential for SgmX polar binding, the two deletion mutants displayed increased cytoplasmic signal of SgmX-mVenus. Hence, we hypothesized that MglA in combination with the T4PM could abolish polar localization of SgmX. To elucidate this possibility we generated a double $\Delta pilQ\Delta mgIA$ mutant, where lack of PilQ, as an initial component of the T4PM, leads to the accumulation defect of the rest stationary T4PM proteins, and localized SgmX-mVenus in the

generated strain. SgmX-mVenus displayed similar localization in the double $\Delta pilQ\Delta mgIA$ mutant as in the single $\Delta mgIA$ mutant with most of the cells showing unipolar clusters. Defects in the SgmX-mVenus polar binding, observed in a $\Delta mgIA$ and $\Delta pilBTMNOPQC$ backgrounds, were not additive and $\Delta pilQ\Delta mgIA$ mutant had 93% of cytoplasmic SgmX-mVenus as the cells of $\Delta mgIA$ (Fig. 48). Thus, likely one or more other compounds bind SgmX to the pole.

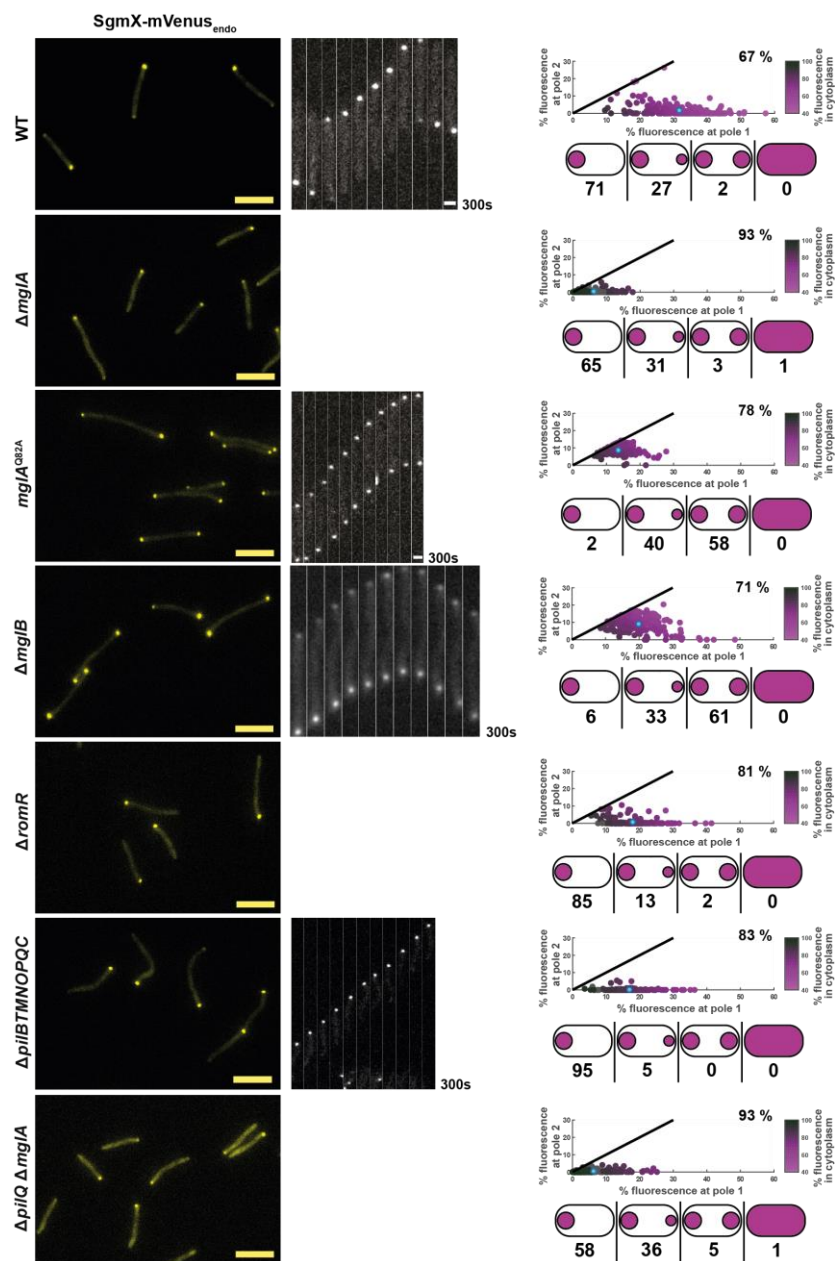


Figure 48 Localization of SgmX-mVenus in strains of indicated genotypes

Localization of SgmX-mVenus is unipolar and dynamic. Left column shows field of steady cells. Middle column shows time-lapse microscopy of 5 minutes total with 30 s intervals (displayed for the motile strains only). Scatter plots and localization patterns indicated on the right. Localization studies performed and analyzed as for Fig. 19. $N > 150$. Scale bar 5 μm .

2.3.8 MXAN_5763-5765 proteins are not essential in *M. xanthus*

We were not able to find a polar determinant of SgmX among polarity proteins or parts of the T4PM. As the system, described for *B. bacteriovorus*, served as an initial inspiration for our findings about SgmX, we searched for further clues in the study of Milner et al, 2014. TamAB-like proteins, encoded next to Bd2492 and described to be essential in *B. bacteriovorus*, were hypothesized to be associated with Bd2492 at the prey-invasive pole (Milner et al., 2014). In order to test whether there are similar protein connections occurring in *M. xanthus*, we deleted *mxan_5764* gene encoding the IM TamB-like protein. Taking into account that *M. xanthus* gene order is interrupted by *mxan_5765* inbetween *sgmX* and *tamAB*, we generated its in frame deletion as well. Finally, we constructed triple deletion mutant, lacking *mxan_5763-65* genes. None of the mentioned genes seemed to be essential in *M. xanthus* as all of them could be deleted easily. Further, all three strains moved similar to the WT on 0.5% agar, with respect to the T4P dependent motility (Fig. 49A). As a final test, we localized SgmX-mVenus in a $\Delta mxan_5764$ background. Similar to the WT, 93% analyzed cells of $\Delta mxan_5764$ mutant showed unipolar cluster that located at the leading pole and switched its position during reversals (Fig. 49B). Thus, MXAN_5763-65 proteins are not essential in *M. xanthus*, and do not influence T4P dependent motility or the localization of SgmX.

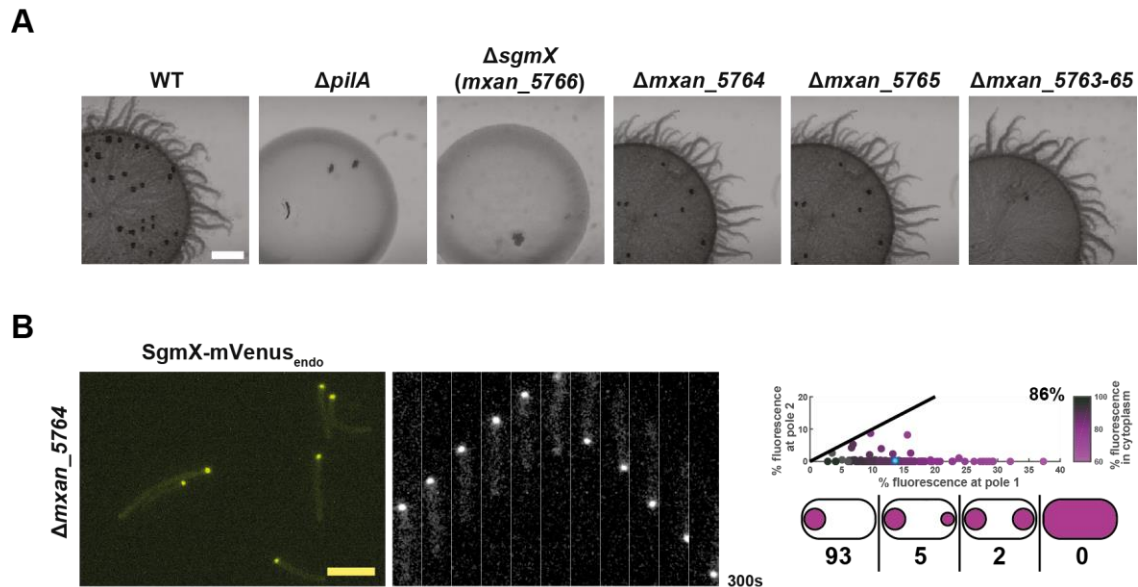


Figure 49 MXAN_5763-65 have no impact on T4P dependent motility and localization of SgmX.

(A) Cells of indicated strains moving by means or T4P on a 0.5% agar. Scale bar 1 mm.

(B) Localization of SgmX-mVenus in absence of DUF490 domain protein MXAN_5764. Snapshot (on the left) is followed by the time-lapse fluorescence microscopy (middle) and a scatter plot, representing protein localization, accompanied by the localization patterns in percentages (below the plot on the right). N=200. Scale bar 5 μ m.

2.4 Novel protein regulators might link MglA to the T4P machine

MglA together with SgmX stimulate formation and function of T4P in *M. xanthus*. However, not all the defects, caused by the *mglA* deletion, are also caused by the *sgmX* deletion. In particular, MglA distributes the stationary T4PM components between the two poles, while SgmX does not show this activity. SgmX, in turn, stimulates polar accumulation of PilB, which is not the case for MglA. Taken together, those findings clearly suggest that more proteins stand between MglA, SgmX and T4PM to regulate the mentioned processes. Trying to extend our view on regulatory network of interest, we combined an *in vivo* pull down experiments, using fluorescently tagged MglA, SgmX, PilM and PilB, with following up mass spectrometry analysis. Results of all performed screenings gave an idea of which other proteins might play role in asymmetric formation of functional T4P in *M. xanthus*.

2.4.1 T4P-dependent motility-related interaction candidates of MglA-mVenus

For performing the pull down experiments we used an *M. xanthus* strain, expressing MglA-mVenus from the native site, and cells, lacking *mglA*, as a negative control. Additionally, we included in our experiment a strain carrying MglA^{Q82A}-mVenus version, and a strain, expressing MglA-mVenus in the $\Delta mglB$ background. Strain producing MglA^{Q82A}-mVenus was involved in identifying maximal number of protein effectors of active MglA-GTP. The strain, lacking *mglB*, was used to keep more of the unbound MglA-mVenus protein for other potential interaction candidates, by eliminating the GAP as one of most prominent interaction partners of MglA.

Special procedure has been developed for identifying potential interaction partners that is briefly described below. Cells of all four strains were grown on 1% CTT/1.5% agar plates. Equal amounts of cells were harvested from plates, sonicated and the cell lysates, representing the total soluble protein content of *M. xanthus* cells, were taken for further pull down experiments. Lysates of all used strains were incubated with the GFP-Trap agarose beads (Chromotek) that have high affinity for the GFP protein and all its derivatives including mVenus. After incubation, beads were washed and proteins were eluted. Using sequential trypsinisation and C-18 purification, samples were prepared for subsequent LC/MS analysis. Then all peptides, were identified and counted. Samples, taken at different steps of the experiment, were analyzed by immunoblot to verify presence of full-length protein inside (Fig. 50A).

Based on the two biological replicates with two controls and six experimental samples, 451 proteins were identified as unique potential interaction partners (Fig. 50B). As unique proteins, we considered proteins, found in at least one out of three experimental samples (MglA^{WT}

-mVenus, MglA^{Q82A}-mVenus and Δ mglB/MglA^{WT}-mVenus), and in both biological replicates and not found in the negative control sample (Δ mglA). Further the iBAQ values of every identified protein in every experimental and control probe were calculated (iBAQ value is equal to the ratio of the protein intensity sum over the number of theoretically observable peptides). The protein abundance in the experiment compared to the control was expressed as a log2 fold change of the average iBAQ values. Significantly abundant proteins were identified by applying the Students' t-test on the groups of iBAQ values corresponding to the controls against the experiments.

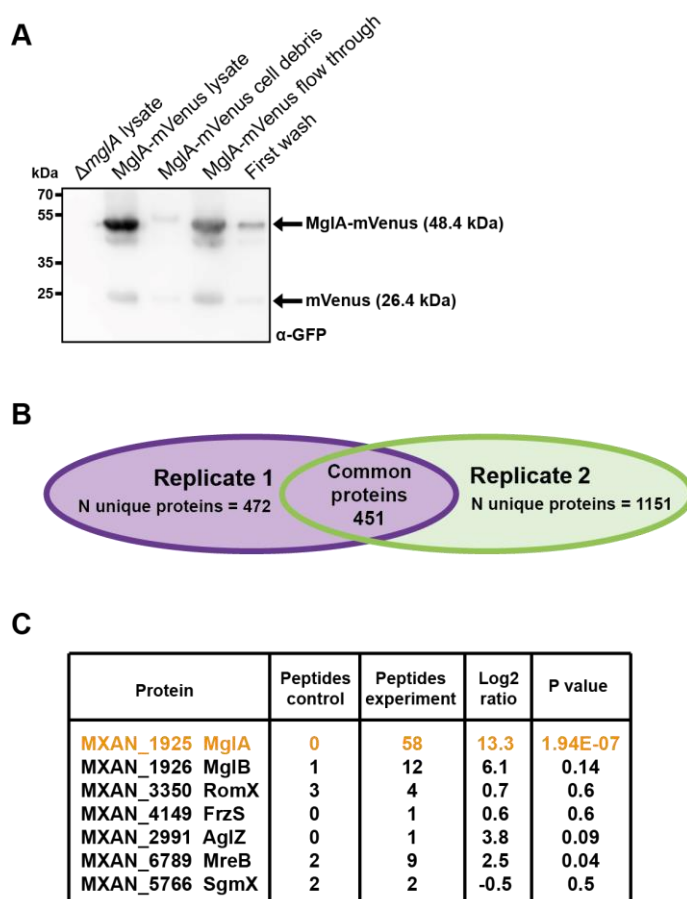


Figure 50 MglA-mVenus interacts with earlier verified interaction partners *in vivo*.

(A) Immunoblot analysis of indicated fractions, taken during pull down experiment. Equal amount of every sample was loaded on SDS-PAGE. Blot was probed with α -GFP antibodies. Proteins of interest indicated on the right with corresponding molecular sizes. Size of protein markers indicated on the left.

(B) Unique proteins found in each single biological replicate (left and right) and proteins that were common for two replicates (middle).

(C) Abundance of MglA and its previously reported interaction partners in the experimental samples compared to the control. Peptide counts represent an average number of peptides of a given protein identified in control/experimental sample, respectively. Log2 ratio is calculated for the average iBAQ value of a corresponding protein in experimental samples against the control sample. P values are obtained by applying the Students' t-test to the iBAQ values, obtained for control samples versus the ones of an experimental samples for every indicated protein. P values ≤ 0.05 correspond to the statistically significant difference of the protein enrichment in the experiment compared to the control.

MglA and several of its known interaction partners, including motility regulators and parts of either of the motility machineries, were found to be unique interaction partners of MglA-mVenus. Among them the FrzS protein, which regulates T4P-dependent motility by stimulating EPS production, and AglZ as a part of gliding motility engine. Two more proteins were abundant in the experimental samples compared to the negative control based on the log2 and P values, such as MglB GAP and MreB cytoskeletal protein. RomX that connects MglA to its polar landmark

RomR and SgmX, characterized in this study, were not shown to be unique or abundant in this experiment (Fig. 50C).

A few decades of studies directed on motility in *M. xanthus* allowed to identify a number of proteins related to either type of motility. While analyzing obtained interaction candidates of MglA-mVenus, we compared our list of significantly enriched proteins to all the information published to date. We highlighted all motility-related proteins and further concentrated on proteins, important for the T4P-dependent motility (Table 1, Table S1).

Table 1. Potential interaction partners MglA-mVenus and MglA^{Q82A}-mVenus, related to the T4P-dependent motility, based on *in vivo* pull down experiments. Color code differentiates cytosolic (blue) and membrane (red) proteins. MglA as bait protein is marked in orange. Log2 values represent the difference of the protein abundance in the experimental samples over the control samples. P values are calculated by the Students' t-test and are ≥ 0.05 .

Protein	Domain structure	Log2 ratio	P value
MXAN_1925 MglA	Mutual gliding-motility protein	13.30309	1.9419E-07
MXAN_5592 DigR	DNA-binding response regulator	5.010173	0.00225304
MXAN_7445 EpsE	Glycosyl transferase, group 1 family protein	2.368139	0.00263633
MXAN_5781 PilH	ABC transporter, ATP-binding protein	3.530964	0.0038174
MXAN_5783 PilA	Fimbrial protein	3.816996	0.00550006
MXAN_7441 EpsH	Glycosyl transferase, group 1	2.714014	0.00716108
MXAN_3084 Tgl	Social gliding motility protein	3.356178	0.0093663
MXAN_4640 SgmT	Sensor histidine kinase/response regulator	2.473498	0.01125545
MXAN_4150 SgmO	Uncharacterized protein	1.436243	0.01767954
MXAN_7448 EpsD	Glycosyl transferase, group 2 family protein	2.187312	0.01875134
MXAN_4619 WbgB	Glycosyl transferase, group 2 family protein	3.838369	0.019409
MXAN_5831 GlgP	Alpha-1,4 glucan phosphorylase	3.329449	0.032761
MXAN_4621 RfbC	Glycosyl transferase family protein	2.454814	0.03299122
MXAN_6696 DifA	Methyl-accepting chemotaxis protein DifA	2.028761	0.03308909
MXAN_4639 SgmS	TPR domain protein	1.028801	0.0333442
MXAN_7451 EpsA	Glycosyl transferase, WecB/TagA/CpsF family	2.894867	0.03356341
MXAN_5788 PilB	Type IV-A pilus assembly ATPase PilB	1.779798	0.03414731
MXAN_5333 SgmV	Glycosyl transferase, group 1	3.098093	0.0362334
MXAN_5775 PilN	Type IV pili biogenesis protein	2.959042	0.03803919
MXAN_2526 SgmH	Uncharacterized protein	1.39338	0.03971003
MXAN_1106 SgmC	PT repeat/DnaJ domain/tetratricopeptide repeat protein	0.994917	0.04236765
MXAN_5787 PilT	Twitching motility protein PilT	1.612725	0.04449004

Final list of protein candidates of interest contained 21 proteins with 16 of them predicted to be cytoplasmic and 6 membrane or periplasmic proteins (Table 1). It is important to note that a few T4PM components have been captured, including the IM proteins. As MglA is a cytoplasmic

protein, this result indicates that whole cascade of interaction partners might be captured by a bait protein in this experimental setup. Therefore, not all the proteins that were enriched in the experiments compared to the controls, will be direct interaction partners of MglA. Among the cytoplasmic proteins, encoded by genes of *pil* locus, we found PilB/PilT ATPases and PilH ATP-binding protein, serving as a part of poorly studied ABC efflux-transporter of *M. xanthus* (Wu et al., 1998). Identification of PilB supports the idea that MglA stimulates T4P formation/function via the extension ATPase. PilH has been shown to be essential for the T4P formation but its relation to the core Pil proteins remains unknown. Further, the SgmT and DigR pair of proteins were abundant in the experimental samples. SgmT and DigR compose the two-component system that regulates *M. xanthus* ECM composition and is involved in c-di-GMP signaling. Deletion of either of the genes leads to reduced T4P-dependent motility (Petters et al., 2012). DifA is an MCP of the Dif chemosensory pathway that, together with DifC and DifE, forms signaling complex, positively regulating formation of EPS (Black et al., 2010; Black et al., 2006). EpsA, -D, -E and -H are glycosyl transferases and clustered together with number of genes, involved in EPS biosynthesis in *M. xanthus* (Lu et al., 2005). SgmO, also named RasA, was shown to be important for development and social motility (Pham et al., 2005). The rest of the proteins, listed in Table 1, are predicted to have an impact on T4P-dependent motility by transposon mutagenesis, carried out in 2006, but has not been characterized in detail yet (Youderian and Hartzell, 2006).

2.4.2 PilB-mCherry & MglA-mVenus have common potential interaction partners

From the side of the T4PM we used the functional fluorescence fusion of PilB-mCherry for a similar experiment as described above for MglA-mVenus. We used $\Delta pilB$ /PilB-mCherry strain as a WT-like background and the $\Delta pilBTMNOPQC$ /PilB-mCherry strain in order to give a priority for identification of the novel potential interaction partners. The flow of the experiment was as described above. Single deletion of *pilB* was used as a negative control and the RFP-Trap agarose, specific for mCherry and its derivatives, was applied instead of the GFP-Trap. Fusion protein was abundant in the lysate and single PilB, as well as single mCherry protein, was enriched in resulted samples (Fig. 51A, Table 2).

A

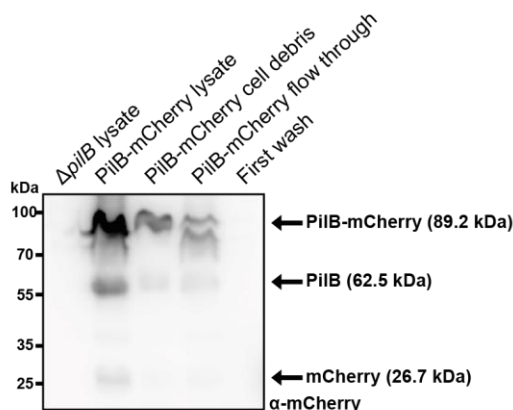
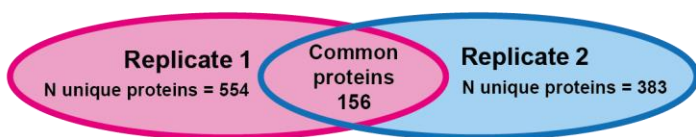


Figure 51 Results of the *in vivo* pull down for the PilB-mCherry.

(A) Immunoblot analysis of indicated fractions is generated as for Fig. 50A. Blot was probed with α -mCherry antibodies. Proteins of interest are indicated on the right with corresponding molecular sizes. Size of the protein markers indicated on the left.

(B) Unique proteins found in each single biological replicate (left and right) and proteins that were common for the two replicates (middle).

B



We found 156 unique protein candidates in the PilB-mCherry *in vivo* pull down; 70 of them were also unique for MglA-mVenus above (data not shown). Further statistical analysis, revealed the proteins, which were significantly enriched in the experimental samples compared to the controls. Nine of the enriched proteins, including the bait protein PilB, were previously described to be important for T4P-dependent motility (Youderian and Hartzell, 2006) (Table 2). Importantly, among the 9 proteins, we found MglA. Two more proteins, SgmO (MXAN_4150) and PilH, were abundant in the PilB-mCherry and MglA-mVenus experimental samples. The remaining 5 proteins were found in the MglA-mVenus pull down but were not unique or enriched. Among them the FrzS response regulator that is important for the EPS production and was reported to interact with MglA (Berleman et al., 2011; Mauriello, 2010). The last four proteins, MXAN_3506 (SgmL), MXAN_3759 (SgmM), MXAN_3797 (SgmN) and MXAN_4620 (SgmR) contain various predicted domains but were never studied with respect to motility in *M. xanthus* (Youderian and Hartzell, 2006) (Table 2). Interestingly, a few proteins, associated with gliding motility were also found as potential interaction partners of PilB-mCherry (Table S2). This can be due to the connection of PilB to the regulators, potentially controlling both motility systems.

Table 2. Potential interaction partners of PilB-mCherry, related to the T4P-dependent motility, based on *in vivo* pull down experiments. Table is generated as Table 1.

Protein	Domain structure	Log2 ratio	P value
MXAN_5788 PilB	Type IV-A pilus assembly ATPase	12.86519	7.24023E-06
MXAN_5781 PilH	Efflux ABC transporter, ATP-binding protein	3.141432	5.6841E-05
MXAN_4620 SgmR	Uncharacterized protein	1.132145	0.003202558

MXAN_4149 FrzS	Response regulator	2.829392	0.010906105
MXAN_3797 SgmN	Acyl-CoA dehydrogenase	1.058866	0.014830534
MXAN_4150 SgmO	Uncharacterized protein	1.508095	0.016514338
MXAN_1925 MglA	Mutual gliding protein	0.610231	0.030858497
MXAN_3759 SgmM	Carboxyl transferase domain protein	1.705166	0.038085435
MXAN_3506 SgmL	NAD-dependent epimerase/dehydratase family protein	0.832825	0.044436949

2.4.3 SgmX-mVenus & mCherry-PilM are not soluble in *in vivo* pull down

In the flow of the current study, the two more functional fluorescence fusions of cytoplasmic SgmX and PilM were created. However, our attempts to use them for *in vivo* pull downs were aborted as both proteins tended to stay in the insoluble fractions after sonication (Fig. 52). This could be due to a strong association of PilM and SgmX to the membrane components.

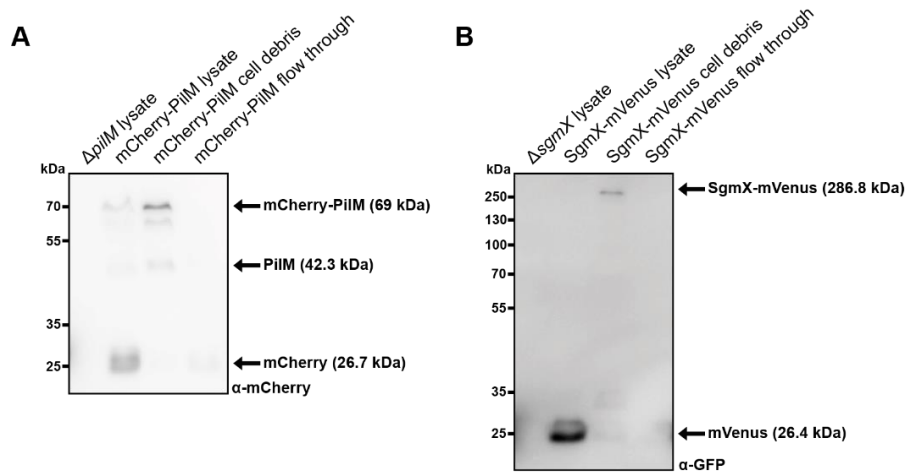


Figure 52 mCherry-PilM and SgmX-mVenus accumulate in cell debris after sonication.

Immunoblot analysis of indicated fractions was performed as for Fig. 50A. Blot was probed with α-mCherry (A) and α-mGFP (B) antibodies. Proteins of interest indicated on the right with corresponding molecular sizes. Size of protein markers indicated on the left.

3 DISCUSSION

Here, we aimed to elucidate the mechanism, executed by the MglA Ras-like GTPase to stimulate T4P-dependent motility in *M. xanthus*. The data presented reveal a number of observations that, taken together, allow to propose a sequence of events, triggering the unipolar formation of functional T4P. In particular, we show that presence of MglA-GTP in cells is important for extension and is essential for function of T4P. We elucidate that to induce these processes MglA sorts the stationary parts of the T4PM to the poles, assuring pre-assembly of the T4PMs at both poles. Next, we identify the TPR domain protein SgmX as an effector of MglA-GTP and provide evidence for their direct interaction. We further show that SgmX is crucial for the formation of T4P and acts downstream of MglA-GTP to stimulate the T4P extension. Our localization studies suggest that part of the function of SgmX is to bring PilB extension ATPase to the leading pole. Speculatively, upon binding GTP, MglA changes its conformation to the one that favours direct interaction with SgmX. This interaction is key for further stimulation of the T4P formation and function, which is likely happening via PilB. At the same time, MglB and RomR parts of the polarity module act indirectly to assure the formation of T4P at the correct pole. Thus, RomR (in complex with RomX) stimulates polar binding of MglA, whereas MglB, localizes asymmetrically and excludes MglA-GTP from one of the poles, indirectly inhibiting T4P formation at this pole.

Finally, applying a combination of the co-IP with an LC-MS we obtained first ideas of which other motility-related effectors might interact with MglA-GTP to regulate different aspects of (T4P-dependent) motility.

3.1 MglA has a diverse effects of the T4P formation and function

We experimentally verified that MglA is crucial for stimulating the T4P-dependent motility and also observed that it is important for the EPS production. Western-blot analysis revealed a WT accumulation of all the core T4PM components, showing a theoretical possibility for proper T4P formation, adhesion and retraction to occur. We proceeded with more careful analysis, in order to identify the aspects of the T4P-dependent motility that are affected by MglA.

Cells, lacking MglA, assemble less surface T4P than the WT ones. This observation was obtained by direct visualization of the T4P and confirmed by a western blot analysis of the sheared T4P. Additionally, absence of the PilT retraction ATPase, which normally causes increased formation of T4P, led to the 200 times lower amount of T4P formed in the $\Delta mglA$ background. Importantly, $\Delta romR$ mutant with diffuse MglA-GTP formed the WT amount of T4P and moved with sufficient speed. It is also remarkable as RomR is a part of the RomR/RomX protein complex,

which acts as a GEF and increases amount of active MglA in the cells. Finally, every mutant, accumulating MglA at the two poles, contained T4P at both poles. Taken together, these observations suggest that MglA can stimulate an extension of T4P at any of the poles and minimal presence of the MglA-GTP at the polar region is enough to fulfil this function. Yet, small amount of the T4P, formed by the $\Delta mglA$ cells, indicates that MglA is not essential for the extension process.

Neither of the T4P, formed by the cells of $\Delta mglA$ and $\Delta mglA\Delta pilT$ mutants triggered the motility and both strains were equally reduced EPS formation, suggesting that MglA is absolutely necessary for the function of the T4P. Additionally, lack of PilT led to an increased amount of the assembled T4P by the $\Delta mglA$ cells, and the T4P of the cells of single $\Delta mglA$ deletion could not retract. These findings demonstrate a certain effect of MglA to the retraction process, in addition to the assembly stimulation. However, we speculate that the latter function is likely predominant for the MglA.

Although the homologs of MglA are not widely studied in other bacteria, an effect of MglA on T4P was previously recorded. In *T. thermophilus* MglA together with its GAP MglB provide correct polar localization of the T4P (Salzer et al., 2015). MglA of predatory *B. bacteriovorus* localizes at the pole with T4P and stimulate its formation and function with respect to prey invasion (Milner et al., 2014). Bacterial species that do not contain MglA-like proteins use proteins of other types to stimulate T4P extension. In the *P. aeruginosa* and *Xanthomonas spp*, the GGDEF-EAL domain protein FimX and different PilZ domain-containing proteins are important for T4P assembly (Guzzo et al., 2013; Kazmierczak et al., 2006). Additionally, this function in *P. aeruginosa* was reported for the large FimV protein with multiple domains, for the FimL accessory protein and for the PilG response regulator. Lack of any of the mentioned proteins led to a decrease or absence of the detected surface pilin (Buensuceso et al., 2017; Inclan et al., 2016).

3.2 MglB & RomR indirectly affect localization of T4P

The pole, containing the large MglB/RomR amount does not form T4P in the WT case scenario. However, combined TEM and localization studies showed that functional T4P can co-occur with MglB and RomR at the pole. First, both proteins are accumulated at the low amounts at the leading pole in the WT cells. Second, mutants, carrying constitutively active MglA^{Q82A} version or MglB^{A64/G68R} version, which has reduced GAP activity, tended to extend the T4P at both poles and the MglB/RomR were also mostly bipolar in these two strains. Thus, neither of the two polarity proteins directly inhibits formation of the T4P.

However, we cannot say that MglB and RomR have no indirect role in stimulating the T4P-dependent motility. Cells of a $\Delta romR$ mutant reversed significantly less than the WT ones moving by means of T4P. Hence, RomR is involved in switch of the T4P formation between the poles, which normally co-occurs during reversals. On the other hand, cells lacking MglB, had less asymmetric MglA and formed T4P at both poles. This effect led to hyper-reversing phenotype and disability of cells to cover longer distances during T4P-dependent movement. Therefore, MglB is responsible for limiting the T4P formation by one pole and achieves it by preventing an accumulation of MglA-GTP at the lagging pole.

3.3 MglA affects localization of the T4PM proteins

In order to find a molecular basis for the MglA-dependent regulation, we kept in mind that the correct localization of the core T4PM proteins is essential for the proper function of T4P. Hence, we analyzed localization of the dynamic and stationary components of the machine in absence of MglA and other polarity proteins.

Our findings for localization of PilB and PilT in absence of MglA support earlier reports. The two proteins localized more unipolar in a $\Delta mglA$ cells, compared to the WT cells. Study of Bulyha et al declares that the two ATPases are also lacking WT-like spatial separation between the poles and are localized at the same and not the opposite poles in a $\Delta mglA$ mutant (Bulyha et al., 2013). We showed that PilB and PilT can co-exist at the same pole and the extended T4P at this pole will be functional. This was the case for the two mutants, $\Delta mglB$ and $mglA^{Q82A}$, assembling T4P at both poles, where PilB and PilT localized more bipolar than in the WT cells. Moreover, the speed of the two strains, moving by means of T4P, was comparable between each other and to the WT strain. Taken together, it means that the effect of MglA on polar distribution of PilB and PilT does not explain its function in stimulating the formation of functional T4P. Mentioned results rather speak of the role of MglA in establishing the asymmetry of T4P.

An unexpected effects were observed for the localization of stationary PilM and PilQ in different mutants. First, accumulation of PilM shifted strongly towards unipolar in a $\Delta mglA$ deletion. Aiming to see if this effect will be also true for the rest of stationary T4PM proteins we tested localization of the OM PilQ. In absence of MglA, PilQ became more asymmetric as well as PilM. Remarkably, lack of RomR resulted in similar PilQ localization as it is in a $\Delta mglA$ cells, whereas the shift of PilM towards unipolarity in $\Delta romR$ mutant was not as strong as it was observed for MglA-deficient mutant. Yet, the localization defects of PilM and PilQ suggest a sorting effect of MglA for the bipolar T4PM components. Moreover, this sorting likely depends on

the amount of active MglA at the poles, which is increased by RomR. However the localization defects of the stationary T4PMs are not crucial for proper extension/retraction of T4P and only affect the correct polarity of its formation.

MglA is not the only protein of *M. xanthus*, which is responsible for the sorting of T4PM proteins. Previous study described MglA as a part of regulatory mechanism, where a paralogous GTPase SofG, together with BacP bactofilin regulates localization of the T4P. To do so, BacP forms bipolar filaments and recruits SofG at one of the poles. This protein conformation recruits PilB and PilT from subpolar regions ensuring their polar accumulation. Importantly, shift of the PilB and PilT to the subpolar areas was not sufficient to decrease the amount of surface T4P (Bulyha et al., 2013).

Several cases of regulation of the localization of proteins that are involved in T4P biogenesis by the T4P assembly regulators are described for *P. aeruginosa*. The c-di-GMP binding protein FimX is brought to the T4P-forming pole by the core T4PM proteins, the OM PilQ secretin, the IM platform protein PilC and the PilF lipoprotein (Jain et al., 2017). In turn, polar FimX stimulates accumulation of PilB ATPase at the pole, and by means of this stimulation induces formation of T4P. Moreover, the FimV protein as a part of its function has been described to provide the correct localization of the PilMNOP proteins of the alignment complex and of the PilQ (Buensuceso et al., 2017). Another regulation effect was noted for the PilT localization in *P. aeruginosa*. There, the MreB cytoskeletal protein maintains formation of polar asymmetric clusters of PilT, supporting spatiotemporal occurrence of the T4P retraction (Cowles and Gitai, 2010).

MglA is a cytosolic protein, therefore, we do not assume it to bring all the membrane Pil components to the poles upon direct binding. Although the stationary T4PM parts contain cytoplasmic output PilM, an assembly of the machine happens in the outside-in manner and starts with PilQ. Thus, it is likely, that an unknown mechanism is used by MglA for the T4PM protein sorting and it involves membrane proteins. In this perspective, the MreB-dependent mechanism of placing PilT to the pole, mentioned for *P. aeruginosa*, attracted our special attention, as it is known that MglA interacts directly to MreB in *M. xanthus* to stimulate the gliding motility (Treuner-Lange et al., 2015). It is possible that this interaction is of high importance for sorting some of the T4PM proteins by MglA. This possibility will be tested in future experiments.

3.4 SgmX is a novel effector of MglA-GTP in stimulating the T4P-dependent motility

To further explain a role of MglA in triggering the function and stimulating the assembly of the T4P, we focused on the interaction partners, which could assist MglA in its function.

We did not observe any direct interaction between MglA, MglB and RomR to the proteins of T4PM in the BACTH assay. Therefore, an unknown accessory protein(s) could mechanically connect MglA to the machine. MglA of *B. bacteriovorus* stimulates T4P-dependent prey invasion by interacting with the TPR domain protein Bd2492 (Milner et al., 2014). A homologue of Bd2492, MXAN_5766 is encoded in the *M. xanthus* genome and was predicted to affect the T4P-dependent motility by transposon mutagenesis (Youderian and Hartzell, 2006). Hence, product of *mxan_5766*, named SgmX, was a promising candidate for functioning together with MglA in the context of current study.

In order to confirm or contradict our assumption of the function of SgmX, we generated an in frame deletion of *sgmX*. Then, for the obtained mutant we observed different parameters of the T4P-dependent motility that we previously examined for the $\Delta mglA$ strain. Cells of the $\Delta sgmX$ mutant moved well by gliding motility and were abolished in movement by T4P. Moreover, EPS accumulation level of the $\Delta sgmX$ cells was comparable to the one of the $\Delta pilA$ strain, serving as a negative control. Interestingly, no surface T4P was identified for the $\Delta sgmX$ deletion mutant, although the ten T4PM components accumulated at the WT level. We concluded, that SgmX is essential for the T4P formation. Lack of EPS is a common effect of absence of the core T4PM proteins that are essential for T4P formation (Bulyha, 2010). Additionally, no single cell movement was detected for cells of the $\Delta sgmX$ mutant on the 1% methylcellulose, hence, a T4P-dependent motility defect was not caused only by lack of EPS accumulation (data not shown). Therefore, we assumed that no EPS accumulation by a $\Delta sgmX$ is rather a consequence of loss of surface T4P.

A combined $\Delta sgmX\Delta pilT$ mutant was restored in the T4P formation to the WT-like level, however, this level was still about 200 times less than the amount of T4P formed by a $\Delta pilT$ mutant. Additionally, a double mutant was not restored in the EPS formation, which argues that the T4P formed are not functional. This experiment initially has a purpose to reveal if reduced T4P formation could be explained by an increased retraction rate. We reasoned that obtained observation argues that SgmX is not essential, but important for the formation of T4P. However, the drastic difference in detected surface T4P between $\Delta pilT$ and $\Delta sgmX\Delta pilT$ mutants likely supports the stimulatory role of SgmX for the extension process.

In presence of GTP, but not with addition of GDP or with no nucleotides, we could see SgmX-Strep to interact directly with MglA-His₆ *in vitro*. Cells of $\Delta mglA\Delta sgmX$ double deletion and of *mglA*^{Q82A} $\Delta sgmX$ mutant formed no T4P, equal to cells of a single $\Delta sgmX$ deletion. Summarizing these data we confirm that SgmX is an effector of MglA-GTP and stimulates T4P formation, acting downstream of MglA.

Primary function of the TPR domains is to create modules for the protein-protein interactions (Zeytuni and Zarivach, 2012). Thus, these proteins can link the two or more proteins for regulating various functions by a protein cascade, or to serve as an interaction surface, assuring direct interaction between different proteins. Regulation of the T4P formation by a TPR domain-containing protein, is known not only for *B. bacteriovorus*. Regulatory protein hub, working to stimulate the T4P assembly in *P. aeruginosa*, mainly relies on the large FimV protein. Cytoplasmic part of FimV possesses TPR domain that helps to recruit FimL accessory protein and components of the Chp chemosensory system. Importantly, all the proteins should co-localize in the polar area to perform further stimulation (Inclan et al., 2016).

SgmX is crucial for the T4P assembly and induces this process together with MglA. As the latter protein found mostly at the leading, T4P-containing, pole, we hypothesized SgmX to localize at the same pole. Indeed, generated SgmX-mVenus fluorescence fusion localized mainly at the leading pole and switched its position during reversals. This localization followed accumulation of MglA in the different mutants. Thus, SgmX tended to be bipolar in strains, extending the T4P and containing MglA-GTP at both poles. Moreover, strain, lacking the T4PM and moving by means of gliding motility localized SgmX together with MglA at the leading pole. Interestingly, polar binding of SgmX is decreased, but not abolished in absence of MglA. The same effect is also observed in the opposite situation, and MglA is more diffuse in the Δ *sgmX* mutant than in the WT. Finally, polar localization of the constantly active MglA^{Q82A}-mVenus version was minimally dependent on SgmX. Therefore, localization of SgmX and MglA-GTP at the leading pole is mutually dependent. However, it is likely that accumulation of SgmX at the pole also relies on yet unknown polar determinant.

The case of mutual regulation between the GTPase and its effectors for the local accumulation was earlier reported for the Rho-class GTPase Cdc42 of *Saccharomyces cerevisiae* and *Schizosaccharomyces pombe*. An effector protein of Cdc42, named p21-activated kinase (PAK) binds to the polarity scaffold protein (Bem1 or Scd2), which, in turn, binds to a Cdc42-directed GEF. PAK also associates with GTP-Cdc42 at the membrane and triggers local recruitment of GEF from the cytoplasm. The localized GEF activates more of Cdc42 and recruits more GEF from the cytoplasm. Like that a positive feedback loop is formed (Chiou et al., 2017; Kozubowski et al., 2008).

Bd2492 of the *B. bacteriovorus* was proposed to occur at the prey invasive pole upon binding a DUF490 domain containing protein, which was predicted to localize in the IM. This protein is encoded by the downstream gene *bd2494* and has a homologue, encoded by

mxan_5764 which is separated by only one gene from *sgmX* (Milner et al., 2014). However, we did not observe any localization change for SgmX in $\Delta mxan_5764$ background. Moreover, unlike the Bd2494 protein of *B. bacteriovorus*, product of *mxan_5764* was not essential in *M. xanthus*. Therefore, protein scaffolds of the two species contain similar proteins but differ in certain aspects.

Lack of SgmX did not cause sorting defects of the stationary T4PM proteins. However, less PilT accumulated at the pole in $\Delta sgmX$ mutant than in the WT, whereas PilB was mostly diffuse in absence of SgmX. These effects could partially explain decrease in the T4P formation.

As we mentioned above, polarly localized FimX of *P. aeruginosa* triggers the formation of T4P by stimulating polar binding of PilB. Additionally, FimX directly interacts to the PilB and serves as a part of protein cascade that achieves c-di-GMP-dependent stimulation of the T4P assembly (Jain et al., 2017). Another regulatory scenario is reported for the *N. punctiforme*. Here, the T4PMs are localized bipolar and need to be activated at one of the poles for triggering the T4P extension and directed movement. This activation function belongs to the HmpF protein that localizes dynamically and stimulates the formation of T4P at the pole where it accumulates. To do so it was proposed to directly interact to the PilB extension ATPase at one of the poles (Cho et al., 2017). Our localization studies suggest that MglA-dependent mechanism of *M. xanthus* can involve SgmX to either directly connect MglA-GTP to the PilB extension ATPase or to serve as a bridge between MglA-GTP and PilB at one pole. Although performed BACTH analysis did not reveal direct interaction of SgmX with PilB, future pull down experiments with purified proteins could be useful to test this idea.

3.5 MglA-based interaction scaffold

We showed that in order to properly assemble and retract the T4P at the leading pole, a complex of proteins act together (Fig. 53). In particular, brought about by RomR/RomX to the poles, and excluded by MglB from the lagging pole, MglA-GTP forms cluster predominantly at the leading pole. Here it directly interacts with SgmX, and together the two proteins stimulate extension of T4P. Likely, this protein complex acts via the PilB extension ATPase. Additionally, MglA induces the function of T4P, which can happen via SgmX or involve more effector proteins. Another important function of MglA is to sort the bipolar T4PM proteins, including PilM, PilN, PilO, PilP, PilC and PilQ, to two poles (Fig. 53). As SgmX does not have this activity, we speculate that MglA recruits an additional protein or complex of proteins to fulfil this function (Fig. 53, marked with X). Likely, this protein will be membrane-associated to physically reach the proteins of T4PM. As the two deletion mutants, $\Delta mglA$ and $\Delta sgmX$, were deficient in the EPS production and the

screen for interaction partners of MglA identified a few EPS-related proteins, it is also possible that MglA-GTP and/or SgmX interact to an additional regulator of the EPS level.

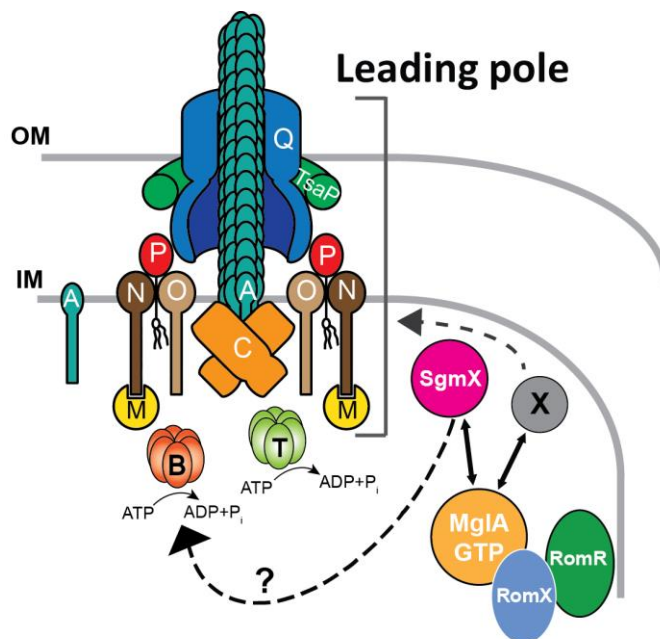


Figure 53 Protein-protein interactions that take place at the leading cell pole and assure stimulation of the functional T4P assembly by MglA. Single letters represent the corresponding components of the T4PM. An unknown effector(s) of MglA-GTP is marked with X. Solid arrow represents confirmed direct interaction. Dashed arrows indicate a direction of obtained effects, which occur by means of yet unknown protein-protein interactions. See the detailed description in the text.

3.6 SgmX-independent activity of MglA and its other potential effector proteins

Although MglA and SgmX are acting in concert to stimulate T4P formation, only lack of MglA leads to mislocalization of stationary proteins of the T4PM. Thus, the effect of MglA on T4PM sorting to the two cell poles appears to be independent of SgmX. We assumed that more protein/protein interactions support the MglA-dependent regulation of the T4P-dependent motility.

A global search for potential interaction candidates of MglA and examination of the proteins, known to be involved in T4P-dependent motility regulation and function, gave important results. Findings of this search provide additional evidence of the connection between MglA and PilB/PilT. Thus, both PilB and PilT are enriched in the MglA-mVenus containing samples, and MglA, in turn, is found to abundant among PilB-mCherry-bound proteins. Considering that MglA has an effect on T4P extension and function, and PilB is a key protein driving pilus extension, the connection of the two proteins was assumed to exist. Additionally, a number of the T4P formation regulators were shown to act via the extension ATPases. C-di-GMP-dependent regulation in *P.*

aeruginosa and *Xanthomonas* spp occurs via PilB; Hmp chemotaxis system of *N. punctiforme* likely acts on PilB at one of the poles (Cho et al., 2017; Guzzo et al., 2009; Jain et al., 2017).

Four proteins, identified by the co-IP-based search, are related to c-di-GMP in *M. xanthus*. For some time now it has been known that c-di-GMP participates in regulation of T4P function in a range of related species. For *P. aeruginosa*, *V. cholerae* and *Xanthomonas* spp, an extension ATPase can either directly, or via accessory proteins, bind c-di-GMP and with this stimulate T4P extension (Guzzo et al., 2013; Jain et al., 2017; Jones et al., 2015). In *M. xanthus* c-di-GMP has been verified to affect the transcription level of the *pilA* gene, encoding major pilin (Skotnicka et al., 2016). Although an activation cascade, operating via PilB to induce T4P formation, has not been shown for *M. xanthus*, capture compound pull down experiments, done by Skotnicka D. in 2016, revealed the PilT retraction ATPase and one of its paralogous proteins MXAN_0415 as potential c-di-GMP-binding proteins. Yet, binding of c-di-GMP has been further confirmed only for MXAN_0415, which was not shown to have an impact on T4P function (Treuner-Lange A., not published) (Skotnicka, 2016). Among the proteins we found as a result of co-IP experiments, SgmT and DigR represent a two-component system that regulates composition of ECM. Moreover, SgmT has been shown to bind c-di-GMP directly, however this function is separated from motility regulation by SgmT (Petters et al., 2012). Interestingly, in *B. bacteriovorus*, the TPR domain-containing protein Bd2492 interacts with MglA as well as the c-di-GMP receptor CdgA (Milner et al., 2014). Taken together, the published studies and our finding of SgmT and DigR to be connected to MglA, we speculate that c-di-GMP signaling might be connected to the motility of *M. xanthus* via MglA. Yet, it is not clear if the two regulatory processes would interfere.

A few more proteins, listed among the regulatory candidates, such as DifA MCP and EpsA/D/E,H glycosyl transferases are involved in regulation and biosynthesis of the EPS production (Lu et al., 2005). Deletion of *mglA* displayed partial loss of the EPS production as well as partial reduction in number of T4P formed. However, introducing cells of $\Delta mglA$ to the polystyrene surface covered with 1% methylcellulose did not trigger T4P-dependent motility of single cells. Described experimental conditions are known to complement the motility defect, given by a decrease in EPS production, hence, the crucial MglA-dependent regulation is centered on direct triggering of the formation and function of T4P (Hu et al., 2011). The connection between MglA and the Dif pathway as well as the Eps proteins would represent a side regulatory branch.

Among the proteins of the T4PM, an IM PilN and PilA appeared to be prominent candidates of the MglA-based regulatory network, however, due to their membrane localization we rather assume them to be pulled down in a complex with the cytoplasmic proteins. In particular,

PilB is known to interact directly with PilM, which, in turn, forms stable complex with PilN (Bischof et al., 2016; Friedrich et al., 2014). Although there is no interaction shown between PilA and PilN/O/C in the IM, we assume PilA-PilN direct interaction can occur in *M. xanthus*. Previously, similar interaction was confirmed between PilE major pilin and PilN of *N. meningitidis* (Georgiadou et al., 2012). Formation of PilA/PilN protein complex would explain enrichment of both proteins in analyzed MglA-mVenus-containing samples. Interestingly, the soluble ATP-binding part of the predicted ABC efflux transporter named PilH was captured among potential regulators by both, PilB and MglA. Proteins of the transporter are encoded by the genes, composing the *pil* locus, and were shown to be essential for T4P formation, hence, T4P-dependent motility (Wu et al., 1998). Generally, transporters of the ABC class are responsible for transmembrane transport of various substrates including drugs, sugars, amino acids and proteins (ter Beek et al., 2014). The precise function of the Pil efflux transporter in *M. xanthus* remains unclear. Yet we cannot exclude that the connection of MglA to the T4PM occurs via extra Pil regulators, among which we can consider the PilGHI transporter.

Finally, FrzS response regulator, which directly interacts and co-localizes with MglA, was pulled out by PilB-mCherry. Function of FrzS for the T4P formation and function is not essential, hence, we do not suggest PilB-FrzS interaction to be crucial to stimulate those processes (Berleman et al., 2011). Moreover, some proteins in this experiment were identified as interaction partners of other enriched components. Therefore, FrzS could be captured by the MglA that was also enriched in this experiment. Encoded next to FrzS, SgmO (MXAN_4149 and MXAN_4150, respectively), was abundant in MglA and PilB-containing samples. There is no regulatory mechanism proposed for SgmO, yet, similar to MglA, it was shown to stimulate T4P-dependent motility and be important for the development (Pham et al., 2005; Thomasson et al., 2002). Thus, SgmO may potentially link MglA with T4PM, conducting its stimulatory signal.

Remaining potential interaction partners of MglA and PilB contain various domains and are predicted to have an impact on T4P-dependent motility, but were not studied with respect to this function yet. Further systematic analysis could give clearer look on possible relation of identified proteins to MglA and its regulatory functions.

4 MATERIALS & METHODS

4.1 Chemicals and equipment

All the reagents, enzymes, antibiotics and kits used in this work are listed with their supplier in the Table 3. Technical devices, their application and manufacturer are listed in Table 4. Specific software used for data analysis with its manufacturer is listed in Table 5.

Table 3. Reagents, enzymes, antibiotics and kits used in this work

Reagents	Supplier
Chemicals	Roth (Karlsruhe), Merck (Darmstadt) Sigma-Aldrich (Taufkirchen)
Media components	Roth (Karlsruhe) Merck (Darmstadt) Difco (Heidelberg) Invitrogen (Darmstadt)
Oligonucleotides	Eurofins MWG Operon (Ebersberg) Invitrogen™ life technologies (Karlsruhe)
Agarose gel electrophoresis size standards 2-log DNA ladder	New England Biolabs (NEB) (Frankfurt a. M.)
Uranyl acetate	Plano GmbH (Wetzlar)
Electron microscopy grids	Plano GmbH (Wetzlar)
SDS gel electrophoresis size standards Pageruler™ Plus Prestained Protein Ladder	Pierce™ Thermo Scientific™ (Darmstadt)
Nitrocellulose membrane	GE Healthcare Europe GmbH (Freiburg)
Luminata Western HRP Substrate	Millipore Merck Chemicals GmbH (Schwalbach)
Rabbit antisera	Eurogentec (Seraing, Belgium)
Goat anti-rabbit IgG, goat anti-rabbit IgG DyLight 549	Pierce/Thermo Scientific (Dreieich)
Anti-GFP monoclonal antibody Anti-mCherry	Roche Diagnostics GmbH (Mannheim) BioVision
Anti-mouse with se, horseradish peroxidase linked	GE Healthcare Europe GmbH (Freiburg)
cOmpete his-tag purification resin	Roche (Mannheim)
GFP-Trap® RFP-Trap®	ChromoTek GmbH (Planegg-Martinsried)
Strep-Tactin® Suspension	IBA Lifesciences (Göttingen)
InstantBlue™	Expedeon (San Diego, CA)
GelRed® Nucleic Acid Gel Stain	Biotium (Fremont, CA)
Enzymes	
Restriction enzymes	Fermentas (St. Leon-Rot), New England Biolabs (Frankfurt a. M.)

Antarctic Phosphatase	New England Biolabs (NEB) (Frankfurt a. M.)
Phusion High-Fidelity DNA polymerase	Thermo Scientific (Dreieich)
Q5 High-Fidelity DNA polymerase	New England Biolabs (NEB) (Frankfurt a. M.)
5 PRIME MasterMix	5 PRIME GmbH (Hamburg)
T4 DNA Ligase	New England Biolabs (NEB) (Frankfurt a. M.)
Trypsin/Lys-C	Promega (Mannheim)
Antibiotics	
Kanamycin sulfate Ampicillin sodium sulfate Gentamycin sulfate Oxytetracycline dehydrate Streptomycin sulfate	Roth (Karlsruhe)
Kits	
NucleoSpin® Plasmid Kit NucleoSpin® Gel and PCR Clean-up Kit	Macherey-Nagel (Düren)
High Throughput Colorimetric GTPase Assays (inc. PiColorLock™)	Expedeon (San Diego, USA)

Table 4. Equipment used in this work

Application	Device	Manufacturer
Cell disruption	Branson Sonifier 250, UP200St, French pressure cell press	G. Heinemann (Schwäbisch Gmünd), Hielscher (Teltow), SLM instruments (Urbana, IL)
Centrifugation	Centrifuge 5424, Centrifuge 5424R, Multifuge X1R, Mega Star 1.6R, Avanti J-26 XP	Eppendorf (Hamburg), Thermo Scientific (Dreieich), VWR International GmbH (Darmstadt), Beckman Coulter (Krefeld)
PCR	Mastercycler, Mastercycler personal, Mastercycler epgradient, Mastercycler <i>nexus</i>	Eppendorf (Hamburg)
Thermomixer	Thermomixer F 1.5 Thermomixer C Thermomixer Compact	Eppendorf (Hamburg)
DNA illumination and documentation	E-BOX VX2 imaging system, GelStick Touch IMAGER	PeqLab (Eberhardzell) INTAS Science Imaging Instruments GmbH (Göttingen)
DNA illumination	UVT_20 LE, UB Transilluminator 312nm	Herolab (Wiesloch) INTAS Science Imaging Instruments GmbH (Göttingen)
Electroporation	GenePulser Xcell	Bio-Rad (München)
Protein electrophoresis	Mini-PROTEAN® 3 cell	Bio-Rad (München)
Western blotting	TransBlot®Turbo™ Transfer System	Bio-Rad (München)

Chemiluminescence detection	Luminescent image analyzer LAS-4000	Fujifilm (Düsseldorf)
Microscopes	DMI6000B Inverted microscope, DMi8 Inverted microscope, DM IRE2 Inverted microscope M205FA Stereomicroscope, JEM-1400 Plus Electron microscope	Leica (Wetzlar) Jeol GmbH (Freising)
Determination of optical densities, nucleic acids/protein absorption	Ultrospec 2100 pro Spectrophotometer, Nanodrop ND-1000 UV-Vis spectrophotometer	GE Healthcare Europe GmbH (Freiburg) Nanodrop (Wilmington)
Detection of absorption changes during colorimetric enzyme assay	Multifunktionsreared Infinite M200 Pro with Monochromatoroptics	Tecan Deutschland GmbH (Crailsheim)
Size exclusion chromatography	AKTA pure with Fraction collector F9-C (HiLoad 16/600 Superdex 200 pg)	GE Healthcare Europe GmbH (Freiburg)
Vacuum concentration	Savant SPD131DDA SpeedVac Concentrator	Thermo Scientific (Dreieich)
LC-MS	Q Exactive Plus	Thermo Scientific (Dreieich)

Table 5. Software used in this work

Application	Software	Supplier
Data analysis of microscopy pictures	Metamorph® v 7.7.5.0, ImageJ 1.51s	Molecular Devices (Union City, CA), Wayne Rasband (National Institutes of Health, USA)
Automatic detection of cells on the microscopy pictures	Oufti	Jacobs-Wagner Lab (Paintdakhi et al., 2016)
Calculation of fluorescence signals	MATLAB R2016b/R2018a	The MathWorks, Inc (Natick, USA)
Checking of DNA and proteins sequences, <i>in silico</i> cloning of plasmids and data management of DNA, protein and plasmid sequences	Vector NTI advance software, suite 11, DNASTAR	Invitrogen™ life technologies (Karlsruhe), DNASTAR, Inc (Madison, USA)

4.2 Media

E. coli cells were cultivated in Luria-Bertani (LB) liquid media or on LB agar plates with 1.5% agar concentration. *M. xanthus* cells were cultivated in CTT media or on CTT agar plates

with 1.5% agar concentration. Motility assays of *M. xanthus* cells were performed on A- or S-motility plates. Media composition is described in Table 6.

Table 6. Bacterial growth media used in this work

Media	Composition
<i>E. coli</i>	
Luria-Bertani (LB)	1% (w/v) tryptone, 0.5% (w/v) yeast extract 1% (w/v) NaCl
LB agar plates	LB medium, 1% (w/v) agar
<i>M. xanthus</i>	
CTT	1% (w/v) Bacto™ casitone 10 mM Tris-HCl pH 8.0 1 mM potassium phosphate buffer pH 7.6 8 mM MgSO ₄
CTT agar plates	CTT medium, 1.5% agar
STT soft agar	CTT medium, 0.5% agar
Motility assays	
Gliding motility plates (Hodgkin and Kaiser, 1977)	0.5% CTT 1.5% agar
T4P-dependent motility plates (Hodgkin and Kaiser, 1977)	0.5% CTT 0.5% agar
Microscopy media	
TPM agar	20% (v/v) CTT media 10 mM Tris-HCl pH 7.6 1 mM KH ₂ PO ₄ 8 mM MgSO ₄ 1.5% agar
Methylcellulose solution	10 mM MOPS pH 7.6 4 mM MgSO ₄ 2 mM CaCl ₂ 1% (w/v) Methylcellulose

For selection purpose appropriate antibiotics and compounds were added when needed (Table 7).

Table 7 Additives to the media used in this work

Additive	Final concentration	Dissolved in
<i>E. coli</i>		
Ampicillin sodium sulfate	100 µg/ml	H ₂ O

Kanamycin sulfate	50 µg/ml	H ₂ O
Streptomycin sulfate	20 µg/ml	H ₂ O
IPTG	0.2-0.5 mM	H ₂ O
5-Brom-4-chlor-3-indoxyl-β-D-galactopyranosid (X-gal)	40 µg/ml	Dimethylformamide
<i>M. xanthus</i>		
Kanamycin sulfate	50 µg/ml	H ₂ O
Oxytetracycline	10 µg/ml	0.1M HCl
Gentamycin sulfate	10 µg/ml	H ₂ O
Galactose	2.5%	H ₂ O

4.3 Microbiological methods

4.3.1 *E. coli* strains

Table 8 *E. coli* strains used in this work

Strain	Relevant characteristics	Source of reference
Mach1	$\Delta recA1398$ <i>endA1 tonA</i> $\phi 80\Delta lacZM15$ $\Delta lacX74$ <i>hsdR</i> ($r_K^- m_K^+$)	Invitrogen (Darmstadt)
Top10	$F^- mcrA \Delta(mrr-hsdRMS-mcrBC)$, $\phi 80/lacZ\Delta M15\Delta lacX74$, <i>recA1</i> , <i>araD139</i> $\Delta(ara-leu)7697$, <i>galU</i> , <i>galK</i> , <i>rpsL</i> (Str ^R) <i>endA1</i> , <i>nupG</i>	Invitrogen™ life technologies (Karlsruhe)
BTH101	$F^- cya-99$, <i>araD139</i> , <i>galE15</i> , <i>galK16</i> , <i>rpsL1</i> (Str ^R) <i>hsdR2</i> , <i>mcrA1</i> , <i>mcrB1</i>	Euromedex (Souffelweyersheim, France)
Rosetta 2 (DE3)	$F^- ompT$ <i>hsdS_B</i> ($r_B^- m_B^-$) <i>gal dcm</i> (DE3) pRARE2(Cm ^R)	Novagen/Merck (Darmstadt)
BL21 (DE3)	$F^- ompT$ <i>hsdS_B</i> ($r_B^- m_B^-$) <i>gal dcm</i> (DE3)	Invitrogen™ life technologies (Karlsruhe)

4.3.2 *M. xanthus* strains

M. xanthus strains used in this work listed in the Table 9. For strains containing plasmids integrated at the Mx8 attB site, the gene expressed including the promoter driving the expression is indicated in brackets. All fusions integrated in the native site are expressed from the native promoter of the corresponding gene.

Table 9 *M. xanthus* strains used in this work

Strain	Genotype	Source or reference
DK1622	Wild type	(Kaiser, 1979)
DK10410	$\Delta pilA$	(Wu and Kaiser, 1996)
SA4420	$\Delta mglA$	(Miertzschke et al., 2011)
SA3387	$\Delta mglB$	(Leonardy et al., 2010)
SA3300	$\Delta romR$	(Keilberg et al., 2012)
DK10409	$\Delta pilT$	(Wu and Kaiser, 1997)
DK10416	$\Delta pilB$	(Wu and Kaiser, 1997)
SA3002	$\Delta pilM$	(Bulyha et al., 2009)
DK8615	$\Delta pilQ$	(Wall et al., 1999)
SA6024	$\Delta pilBTMNOPOQC$	Carmen Friedrich
SA3011	$\Delta mglA \Delta pilT$	(Bulyha et al., 2013)
SA3833	$mglA^{Q82A}$	(Keilberg et al., 2012)
SA3954	$mglB^{A64/G68R}$	(Miertzschke et al., 2011)
SA5293	$\Delta aglQ$	(Jakobczak et al., 2015)
SA7101	$\Delta mglB \Delta aglQ$	This work
SA7107	$mglA^{Q82A} \Delta aglQ$	This work
SA7124	$mglB^{A64/G68R} \Delta aglQ$	This work
SA7110	$\Delta romR \Delta aglQ$	(Szadkowski et al., 2019)
SA7135	$\Delta aglQ \Delta frzE$	(Szadkowski et al., 2019)
SA7136	$\Delta mglB \Delta aglQ \Delta frzE$	This work
SA7148	$mglA^{Q82A} \Delta aglQ \Delta frzE$	This work
SA8447	$mglB^{A64/G68R} \Delta aglQ \Delta frzE$	This work
SA7147	$\Delta romR \Delta aglQ \Delta frzE$	This work
SA7125	$\Delta pilB P_{nat} pilB$ -mCherry (<i>attB</i> ::pAP12)	This work
SA7145	$\Delta pilB \Delta mglA P_{nat} pilB$ -mCherry (<i>attB</i> ::pAP12)	This work
SA8403	$\Delta pilB \Delta mglB P_{nat} pilB$ -mCherry (<i>attB</i> ::pAP12)	This work
SA7146	$\Delta pilB mglA^{Q82A} P_{nat} pilB$ -mCherry (<i>attB</i> ::pAP12)	This work
SA8460	$\Delta pilB \Delta romR P_{nat} pilB$ -mCherry (<i>attB</i> ::pAP12)	This work
SA8465	$\Delta pilT P_{nat} mCherry$ -pilT (<i>attB</i> ::pAP87)	This work
SA8466	$\Delta pilT \Delta mglA P_{nat} mCherry$ -pilT (<i>attB</i> ::pAP87)	This work
SA8467	$\Delta pilT \Delta mglB P_{nat} mCherry$ -pilT (<i>attB</i> ::pAP87)	This work
SA8468	$\Delta pilT mglA^{Q82A} P_{nat} mCherry$ -pilT (<i>attB</i> ::pAP87)	This work
SA8470	$\Delta pilT \Delta romR P_{nat} mCherry$ -pilT (<i>attB</i> ::pAP87)	This work
SA7130	$\Delta pilM P_{nat} mCherry$ -pilM (<i>attB</i> ::pAP16)	This work
SA8461	$\Delta pilM \Delta mglA P_{nat} mCherry$ -pilM (<i>attB</i> ::pAP16)	This work
SA8462	$\Delta pilM \Delta mglB P_{nat} mCherry$ -pilM (<i>attB</i> ::pAP16)	This work
SA8409	$\Delta pilM mglA^{Q82A} P_{nat} mCherry$ -pilM (<i>attB</i> ::pAP16)	This work
SA7174	$\Delta pilM \Delta romR P_{nat} mCherry$ -pilM (<i>attB</i> ::pAP16)	This work
SA7192	<i>pilQ</i> -sfGFP	This work
SA7193	$\Delta mglA, pilQ$ -sfGFP	This work
SA8451	$\Delta mglB, pilQ$ -sfGFP	This work

SA8459	<i>mgIA^{Q82A}, pilQ-sfGFP</i>	This work
SA8449	$\Delta romR, pilQ-sfGFP$	This work
SA7164	$\Delta sgmX$	This work
SA7175	$\Delta sgmX, P_{nat}sgmX (attB:pAP34)$	This work
SA7168	$\Delta pilT \Delta sgmX$	This work
SA8416	$\Delta mgIA \Delta sgmX$	This work
SA8417	<i>mgIA^{Q82A} $\Delta sgmX$</i>	This work
SA7170	$\Delta pilB \Delta sgmX P_{nat}pilB-mCherry (attB:pAP12)$	This work
SA8469	$\Delta pilT \Delta sgmX P_{nat}mCherry-pilT (attB:pAP87)$	This work
SA7171	$\Delta pilM \Delta sgmX P_{nat}mCherry-pilM (attB:pAP16)$	This work
SA8458	$\Delta sgmX pilQ-sfGFP (pAP37)$	This work
SA7195	<i>sgmX-mVenus (pAP35)</i>	This work
SA7196	$\Delta mgIA sgmX-mVenus (pAP35)$	This work
SA8440	$\Delta pilBTMNOQC sgmX-mVenus (pAP35)$	This work
SA8410	<i>mgIA^{Q82A} sgmX-mVenus (pAP35)</i>	This work
SA8448	$\Delta mgIB sgmX-mVenus (pAP35)$	This work
SA8442	$\Delta romR sgmX-mVenus (pAP35)$	This work
SA8446	$\Delta mgIA \Delta pilQ sgmX-mVenus (pAP35)$	This work
SA8185	<i>mgIA-mVenus</i>	(Szadkowski et al., 2019)
SA9845	$\Delta sgmX mgIA-mVenus$	Luis Carreira
SA8452	$\Delta pilA mgIA-mVenus$	This work
SA10013	<i>mgIB^{A64/G68R} mgIA-mVenus</i>	Luis Carreira
SA7150	$\Delta pilBTMNOQC mgIA-mVenus$	This work
SA7593	$\Delta mgIB mgIA-mVenus$	Luis Carreira
SA8183	<i>mgIA^{Q82A}-mVenus</i>	(Szadkowski et al., 2019)
SA7186	$\Delta sgmX mgIAQ82A-mVenus$	This work
SA7187	$\Delta pilBTMNOQC mgIAQ82A-mVenus$	This work
SA9898	$\Delta pilBTMNOQC \Delta romR mgIAQ82A-mVenus$	Luis Carreira
SA8191	$\Delta romR mgIAQ82A-mVenus$	(Szadkowski et al., 2019)
SA7169	$\Delta romR \Delta sgmX mgIAQ82A-mVenus$	This work
SA3963	<i>mgIB-mCherry</i>	Daniela Keilberg
SA8453	$\Delta pilA mgIB-mCherry$	This work
SA10199	<i>mgIA^{Q82A} mgIB-mCherry</i>	Luis Carreira
SA8471	<i>mgIB^{A64/G68R}-mCherry</i>	This work
SA7505	<i>romR-mCherry</i>	Luis Carreira
SA8450	$\Delta pilA romR-mCherry$	This work
SA9853	<i>mgIA^{Q82A} romR-mCherry</i>	Luis Carreira
SA10014	<i>mgIB^{A64/G68R} romR-mCherry</i>	Luis Carreira
SA8423	$\Delta mxan_5764$	This work
SA8438	$\Delta mxan_5765$	This work
SA8435	$\Delta mxan_5763-5765$	This work
SA8436	$\Delta mxan_5764 sgmX-mVenus (pAP35)$	This work

4.3.3 Cultivation and storage of bacterial strains

All used media and solutions were autoclaved at 121 °C for 20 min and 1 bar over pressure. Antibiotics and additives were filter sterilized by using 0.22 µm pore-size filters (Millipore Merck, Schwalbach) and added to the pre-cooled media at around 55 °C.

E. coli cells were cultivated on LB agar plates and strains were grown in liquid LB media with 230 rpm horizontal shaking or on agar plates at 37 °C. BTH 101 cells were grown on LB agar plates at 30 °C. Corresponding antibiotics were added when required. The optical densities of cultures were determined photometrically at 600 nm.

M. xanthus cells were cultivated on CTT agar plates at 32 °C in the dark. For the liquid cultures, cells were harvested from the plate, resuspended in volume of 1 ml of CTT and then transferred to the bigger volume of media. Liquid cultured were incubated with horizontal shaking 220 rpm at 32 °C. Liquid CTT and CTT agar was necessarily supplied with 10 µg/ml gentamycin to prohibit contaminations and additional supplements were added when necessary. The optical densities of *M. xanthus* cultures were determined photometrically at 550 nm.

For a short-term storage plates with *E. coli* and *M. xanthus* cells were stored up to four weeks at 4 °C and 18 °C respectively. Long-term stored glycerol stocks were made with overnight liquid culture for *E. coli* and exponentially growing liquid culture of *M. xanthus* with addition of 10% and 4% glycerol accordingly. All glycerol stocks were fast frozen in liquid nitrogen and stored at -80°C.

4.3.4 Bacterial two hybrid assay (BACTH)

The bacterial two-hybrid system (BACTH) was used to characterize protein-protein interactions in vivo (Karimova et al., 1998). The principle of BACTH is the catalytic domain of the adenylate cyclase (CyaA) from *Bordetella pertusis* which consists of two complementary fragments T18 and T25. The experiments were performed according to the manual enclosed by the manufacturer (Euromedex, Souffelweyersheim, France). Proteins of interest were co-expressed as fusions with the T25 and T18 fragments in the reporter strain BTH101 lacking the *cyaA* gene encoding the catalytic domain of the adenylate cyclase. Interaction between pair of proteins leads to the heterodimerization of these hybrid proteins what results in functional complementation between T25 and T18 fragments and, therefore, cAMP synthesis. cAMP in a complex with the catabolite activator protein (CAP) regulates gene expression in *E. coli* including genes involved in lactose and maltose catabolism. The BTH101 cells were co-transformed with the pair of recombinant plasmids (where one always contained T18 and another T25) and plated

on indicator media LB/X-Gal/IPTG with addition of kanamycin and ampicillin to reveal resulting Cya⁺ phenotype. Plates were incubated for 48 h at 30 °C; three representative clones from each transformation plate were resuspended in 500 µl of LB media, grown for 3 h and 5 µl spotted on fresh LB/X-Gal/IPTG plates containing appropriate antibiotics. The pictures of the plates were taken after 48 h incubation at 30 °C using Perfection V700 Proto scanner (Epson, Meerbusch). The blue colonies indicate positive interaction, while white colonies no interaction. The empty plasmids pKNT25 and pUT18C served as a negative control. The empty pKNT25 or pUT18C co-transformed with every experimental plasmid served as a quality control for plasmids containing tested proteins. The plasmids pKT25-zip and pUT18C-zip that encode for fusion proteins T25-zip and T18-zip (leucine zipper motifs appended to the T18 and T25 fragments) served as a positive control.

4.3.5 Motility assays for *M. xanthus*

For motility assays, 0.5% CTT plates supplemented with 0.5% and 1.5% agar for T4P-dependent and gliding motility respectively were prepared and kept at 32 °C in the dark for 24 h prior to the assay. *M. xanthus* cells from exponentially growing culture were harvested at 6000 rpm for 10 min and resuspended in 1% CTT to density of 7×10^9 cells/ml. 5 µl of cell suspensions were spotted on corresponding plates and incubated for 24 h in the dark at 32 °C. After the incubation whole colonies and colony edge were observed using Leica M205FA Stereomicroscope with CMOS camera for T4P-dependent motility and gliding motility and DM IRE2 Inverted microscope with Leica DFC280 camera for single gliding cells.

4.3.6 Methylcellulose-associated assay

For velocity of T4P-dependent motility and reversal frequency of single *M. xanthus* cells, 5 µl of exponentially growing cultures were spotted into a 24-well polystyrene plate (Falcon, New York, NY). After 10 min at RT, cells were covered with 500 µl of 1% methylcellulose solution (Table 5) and incubated at RT in the dark for 30 min. Subsequently, cells were visualized for 10 min at 20 s intervals at RT using a Leica DMI8 inverted microscope and imaged using a Leica DFC9000 GT camera. Individual cells were tracked using Metamorph 7.5 (Molecular Devices) and ImageJ 1.52b. For each cell, the distance moved per 20 s interval was determined and the total distance moved for 10 min and the speed per min calculated. For reversals, the number of reversals per cell per 10 min was determined.

4.3.7 Congo red dye binding assay

To determine an ability of *M. xanthus* to bind congo red dye plate assay was carried out. Cells from exponentially growing culters were harvested at 4700 rpm for 10 min and resuspended in 1% CTT to density of 7×10^9 cells/ml. 10 μ l aliquots of resuspension were spotted on 0.5% CTT supplemented with 0.5% agar and 40 μ g/ml congo red. Plates were incubated at 32 °C for 24h and images were recorded.

4.3.8 T4P shear-off assay

T4P were sheared from *M. xanthus* cells based on protocol from Wu and Kaiser (Wu and Kaiser, 1997) with following modifications. Briefly, cells were grown on 1% CTT/ 1.5% agar plates at 32 °C for 3 days and equal cell masses were scraped from plates for further experiment. Cells were resuspended in 1ml resuspension buffer (100 mM Tris-HCl pH 7.6 and 100 mM NaCl). 100 μ l aliquots were taken, harvested for 2 min at 13000 rpm at RT, resuspended in 200 μ l 1x SDS lysis buffer (10% (v/v) glycerol, 60 mM Tris-HCl; pH 6.8, 5 mM EDTA, 2% (w/v) SDS, 100 mM DTT, 0.005% bromphenol blue) and immediately denatured at 95°C for 10 min. These samples represented whole cell lysate fractions. The remaining cells were combined with lysate from 100 μ l aliquots, vortexed for 10 min at high speed and harvested for 20 min at 13000 rpm at 4°C. Supernatant was kept on ice and cells were resuspended in 800 μ l resuspension buffer, vortexed for 5 min at high speed and harvested again. Obtained supernatant was combined with previous one and resulted fractions were additionally harvested two times for 10 min at 13.000 rpm, 4°C. T4P precipitated overnight on ice using 200 μ l of 10 x precipitation buffer (20% PEG6000, 1 M MgCl₂, in resuspension buffer). Whole cell fraction and sheared fraction were analyzed by immunoblot with α -PilA antibodies and α -PilC antibodies as a loading control.

4.3.9 Microscopy and analysis of fluorescence microscopy images

For phase contrast and fluorescence microscopy, cells were treated, images recorded and analyzed as described (Szadkowski et al., 2019). Briefly, exponentially growing cells were placed on a thin 1.5% agarose pad buffered with TPM buffer (10 mM Tris-HCl pH 8.0, 1 mM potassium phosphate buffer pH 7.6, 8 mM MgSO₄) supplemented with 0.2% CTT on a glass slide and immediately covered with a coverslip, incubated for 30 min at 32 °C, and visualized at 32 °C using a temperature-controlled DM6000B microscope (Leica) with a Plan Apochromat 100x/NA 1.40 oil objective (Leica) and a Cascade II 1024 camera (Roper Scientific). Cells in phase contrast images were automatically detected using Oufi (Paintdakhi et al., 2016). Fluorescence signals in segmented cells were identified and analyzed using a custom-made Matlab v2016b (MathWorks)

script. The script divides a cell into three regions: polar region 1, polar region 2 and the cytoplasmic region. The polar regions are defined as the parts of a cell within a distance of 10 pixels, corresponding to 0.64 μm , from a tip of the cell. The cytoplasmic region includes all pixels of the cell with the exception of the polar regions. A polar cluster was identified when three or more connected pixels within a polar region had a fluorescence signal higher than a cell-specific threshold signal of two standard deviations above the average fluorescence signal in the cytoplasmic region. The fluorescence of a polar cluster was defined as the sum of the fluorescence signal of all connected pixels that exceeded the threshold value in that polar region. The cytoplasmic signal was defined as the sum of the fluorescence signal of all pixels between the two polar regions. For each cell with polar cluster(s), an asymmetry index (ω) was calculated as

$$\omega = \frac{\text{total fluorescence at pole 1} - \text{total fluorescence at pole 2}}{\text{total fluorescence at pole 1} + \text{total fluorescence at pole 2}}$$

By definition, pole 1 is the pole with the highest fluorescence. ω varies between 0 (bipolar symmetric localization) and 1 (unipolar localization). The localization patterns were binned from the ω values as follows: unipolar ($\omega > 0.9$), bipolar asymmetric ($0.9 > \omega > 0.2$) and bipolar symmetric ($\omega < 0.2$). Diffuse localization was determined when no polar signal was detected. For time-lapse epifluorescence microscopy, cells were prepared as described and recorded for 15 min with images captured every 30 s. Data were processed with Metamorph 7.5 and ImageJ 1.52b.

4.4 Molecular biology methods

4.4.1 Oligonucleotides and plasmids

Names and sequences of the oligonucleotides used in this work are listed in Table 10. Restriction sites indicated in bold. Nucleotides marked in blue show added sequences required for cloning. All plasmids used in this work are listed in Table 11.

Table 10 Oligonucleotides used in this work

Primer	Sequence (5'-3')	Purpose
PilB _{nat} fw	ATCCATATGGATGGC ACGGTGGTGACGGGC	Amplification of P _{PilB} - <i>pilB</i> to clone into pNG062
PilB _{nat} rev	ATCAGATCTTCGTTGATGCCTCTTCCTTGA	
PilB fw	GCGCTCTAGA AATGCCGGTCGACTCGGTG	
PilB rev	ATCAAGCTTGGTTGACTAGA AAGCGGTCCG	
PilM _{nat} fw	ATCCATATGTCCTGAAGTCCTACGCATGG	Amplification of P _{PilM} and <i>pilM</i> to clone into pNG063
PilM _{nat} rev	ATCAGATCTGCGTGACTCCGTCGAGAGGC	
PilM fw	ATCTCTAGAGCGAAGGGCAA ACTGGTACTC	

PilM rev	ATCAAGCTTTCAGGCCAGCTTGTGCGCCCG	
frzE A	ATCAAGCTTTGGCAAGGTCATCGAGACGC	In frame deletion of <i>frzE</i>
frzE B	TCTCAAGAAATCCCTCCTCGCGCAGGCCATCGACCGGC	
frzE C	TGGCCTGCGCGAGGAGGGATTTCTTGAGAGCCTCGGTG	
frzE D	ATCGAATTCGCTTCGTCCTGGGCAATGGT	
SgmX G	GTCAAGTACGGACTCCACGA	Verification of <i>sgmX</i> deletion
SgmX H	CGTCGGACAGCACCAACTGG	
SgmX BTH1	ATCTCTAGAGATGGACAAGAACAAGATCATC	Cloning of <i>sgmX</i> into BACTH vectors
SgmX BTH2	ATCGAATTCCTACAGGTAGCCGACCTTGCG	
SgmX BTH3	ATCGAATTCGCCAGGTAGCCGACCTTGCGCGC	
P _{nat} sgmX fw	ATCAAGCTTGAACGCCGAGGACCCGATTAC	Complementation of Δ <i>sgmX</i>
P _{nat} sgmX rev	ATCGAATTCCTACAGGTAGCCGACCTTGCG	
SgmX-mvA	ATCAAGCTTGCGGCGGAGGAGTGCGACGAG	Substitution of <i>sgmX</i> with endogenous <i>sgmX</i> - <i>mVenus</i>
SgmX-mvB	GGAGCCGCCGCCGCCAGGTAGCCGACCTTGCGCGC	
SgmX-mvC	ATCTCTAGATTGCACCCCGCGAGGTCCGGC	
SgmX-mvD	ATCGAATTCGAGGTCCACCTTGCTGCTCGT	
Venus/Cherry Fw	ATCGTCTAGAAGCAAGCGCCCAGGCGGG	
Venus/Cherry Rv	ATCGGAATTCGGGCGGGCGGGGCG	
PilQ-sfGFP A	ATCAAGCTTAGGGTGAAGGACGTGCTGAGT	Substitution of <i>pilQ</i> with endogenous <i>pilQ</i> - <i>sfGFP</i>
PilQ-sfGFP B	GGAGCCGCCGCCGCCAGAGTCTGCGCAATGGTCTG	
sfGFP Fw	GGCGGCGGCGGCTCCATGAGCAAAGGAGAAGAACTT	
sfGFP Rev	ATCTCTAGATTAGGATCCTTTGTAGAGCTC	
PilQ-sfGFP C	ATCTCTAGAGGGTTTCCCTTGCGTCCTCTT	
PilQ-sfGFP D	ATCGAATTCCTGGGTGAGGAGTTGGCGTA	
SgmX-Strep fw	ATCTCTAGAGACAAGAACAAGATCATCGAA	Overexpression of SgmX-Strep
SgmX-Strep rev	ATCAAGCTTTCACTTTTCGAACTGCGGGTGGCTCCACAGGTAGCCGACCTTGCGCGC	
PilT _{nat} fw	ATCCATATGGCTCCTTCCCTCCGCCAGGACC	Amplification of P _{PilT} and <i>pilT</i> to clone into pNG063
PilT _{nat} rev	ATCAGATCTGGGGGATGTCCTTCGGGGGA	
PilT fw	ATCTCTAGAGCCAACCTGCACCAGCTCCTC	
PilT rev	ATCAAGCTTCTAACGACCACCCGCTCCCC	
MglB ^{A/GR} -mChA	ATCAAGCTTAGGACGCGAACGCGAAGGTGG	Substitution of <i>mglB</i> ^{A64/G68R} with endogenous <i>mglB</i> ^{A64/G68R} - <i>mCherry</i>
MglB ^{A/GR} -mChB	GGAGCCGCCGCCGCCCTCGCTGAAGAGGTTGTCGAT	
MglB ^{A/GR} -mChC	ATCTCTAGACCCGGGAAGCCATGTCCTTCA	
MglB ^{A/GR} -mChD	ATCGAATTCCTCAGGTCGTAGCCCTGCTCCG	
5764 A	ATCAAGCTTGATGCACGCGGTGAGCTACAT	In frame deletion of <i>mxaN</i> ₅₇₆₄
5764 B	CAGCTTCAGCACGCTCCCCGACAAGACGAG	
5764 C	GGGAGCGTGCTGAAGCTGAGCTGGGAGGTC	
5764 D	ATCGAATTCCTCGTCCATGGGCTCCGAAACG	
5763-65 A	ATCAAGCTTCGGTCGCCTACGAGGAGCCC	In frame deletion of <i>mxaN</i> ₅₇₆₃₋₆₅
5763-65 B	GTACGTAGTCATGGGCTCGCCGACCTCGCGG	
5763-65 C	ATGACTACGTACGGGAGGCGATGGTGCGCATG	
5763-65 D	ATCGAATTCACCTCGCTGCGGAACACGT	
5763 G	CTGGTGTTGACGTGGAGGA	

5763 H	CCTCCGTCAGCTCATCCAGC	Verification of <i>mxan_5763-65</i> deletion
5765 A	ATCAAGCTTGCCCCGAGGACGTGGACACGC	In frame deletion of <i>mxan_5765</i>
5765 C	ATGACTACGTACCGGCTTTGTCTTCTCAGAGC	
5765 D	ATCGAATTCTCCACGTCCAGCTCGATGAC	
5765 G	CGCTGCTCGTCATCATCCAC	Verification of <i>mxan_5765</i> deletion
5765 H	AGGTTCTTCCCAGTGCATG	
attB right	GGAATGATCGGACCAGCTGAA	Primers used to verify integration at Mx8 phage attachment site
attB left	CGGCACACTGAGGCCACATA	
attP right	GCTTTCGCGACATGGAGGA	
attP left	GGGAAGCTCTGGGTACGAA	
M13 uni (-43)	AGGGTTTTCCAGTCACGACGTT	Sequencing of pBj114
M13 rev (-49)	GAGCGGATAACAATTCACACAGG	
pKT25fw	GGCGATTCGGTGACCGATTA	Sequencing of BACTH constructs
pKT25rv	GGGTTTTCCAGTCACGACG	
pKNT25 rev	CGCCACGGCCTTGATGCC	
pUT18forw	TCCGGCTCGTATGTTGTGTG	
pUT18rev -110	ATTCATGTCGCCGTCGTAGC	
pUT18Cfw	CTGGAAACGGTGCCGGCGTC	
pUT18Crev	GGGCTGGCTTAACATGCGGC	

Table 11 Plasmids used in this study

Plasmid	Description	Reference
pSWU30	Tet ^R , <i>attP</i>	(Wu and Kaiser, 1997)
pBj114	Kan ^R , <i>galk</i>	(Julien et al., 2000)
pSWU19	3 kb Smal-Smal <i>attP</i> fragment in pBGS18 at Dral sites, Kan ^R	(Wu and Kaiser, 1995)
pNG062	pSWU19; MCS-linker (GSAGSAAGSG)-mCherry	Nuria Gomez-Santos
pNG063	pSWU19; mCherry-linker (GSAGSAAGSG)-MCS	Nuria Gomez-Santos
pMAT135	Vector for overexpression, pET45b+ with cut region between XbaI and HindIII	Anke Treuner-Lange
pTM1	Overexpression MglA-His ₆	(Zhang et al., 2010)
pTM2	Overexpression His ₆ -MglB	(Zhang et al., 2010)
pDK56	MglA (pKT25)	Daniela Keilberg
pDK70	MglA (pKNT25)	(McLoon et al., 2016)
pDK76	MglA (pUT18)	Daniela Keilberg
pDK75	MglA (pUT18C)	(McLoon et al., 2016)
pDK55	MglB (pKT25)	Daniela Keilberg
pDK71	MglB (pKNT25)	(McLoon et al., 2016)
pDK77	MglB (pUT18)	Daniela Keilberg
pDK74	MglB (pUT18C)	(McLoon et al., 2016)

pSC57	PilB (pKT25)	Carmen Friedrich
pSC59	PilB (pKNT25)	Carmen Friedrich
pSC69	PilB (pUT18)	Carmen Friedrich
pSC70	PilB (pUT18C)	Carmen Friedrich
pSC58	PilT (pKT25)	Carmen Friedrich
pSC60	PilT (pKNT25)	Carmen Friedrich
pSC71	PilT (pUT18)	Carmen Friedrich
pSC72	PilT (pUT18C)	Carmen Friedrich
pSC73	PilM (pKT25)	Carmen Friedrich
pSC74	PilM (pKNT25)	Carmen Friedrich
pSC61	PilM (pUT18)	Carmen Friedrich
pSC62	PilM (pUT18C)	Carmen Friedrich
pAP29	SgmX (pUT18)	This work
pAP30	SgmX (pUT18C)	This work
pAP32	SgmX (pKT25)	This work
pAP31	SgmX (pKNT25)	This work
pLC20	pBj114; for <i>mglA</i> replacement by <i>mglA-mVenus</i> at native site	(Szadkowski et al., 2019)
pLC44	pBj114; for <i>mglA</i> replacement by <i>mglA^{Q82A}-mVenus</i> at native site	(Szadkowski et al., 2019)
pDK145	pBj114; for <i>mglB</i> replacement by <i>mglB-mCherry</i> at native site	Daniela Keilberg
pLC32	pBj114; for <i>romR</i> replacement by <i>romR-mCherry</i> at native site	Luis Carreira
pLC51	pBj114; for generation of in-frame deletion of <i>sgmX</i>	Luis Carreira
pBj Δ <i>aglQ</i>	pBj114; for generation of in-frame deletion of <i>aglQ</i>	(Sun et al., 2011)
pES2	pBj114; for generation of in-frame deletion of <i>mglA</i>	(Leonardy et al., 2010)
pAP12	pNG062; P _{nat} <i>pilB</i>	This work
pAP16	pNG063; P _{nat} <i>pilM</i>	This work
pAP19	pBj114; for generation of in-frame deletion of <i>frzE</i>	This work
pAP34	pSWU30; P _{nat} <i>sgmX</i>	This work
pAP35	pBj114; for <i>sgmX</i> replacement by <i>sgmX-mVenus</i> at native site	This work
pAP37	pBj114; for <i>pilQ</i> replacement by <i>pilQ-sfGFP</i> at native site	This work
pAP39	pMAT135; Overexpression SgmX-Strep	This work
pAP60	pBj114; for generation of in-frame deletion of <i>mxan_5765</i>	This work

pAP61	pBj114; for generation of in-frame deletion of <i>mxan_5763-65</i>	This work
pAP87	pNG063; P _{nat} <i>pilT</i>	This work
pAP88	pBj114; for <i>mgIB</i> replacement by <i>mgIB</i> ^{A64R} _{G68R} - <i>mCherry</i> at native site	This work
pAP89	pBj114; for generation of in-frame deletion of <i>mxan_5764</i>	This work

4.4.2 Plasmid construction

Genomic DNA of *M. xanthus* DK1622 and SA3952 was used to amplify DNA fragments. Plasmid constructs were transformed into *E. coli* Mach1 or TOP10 cells. Obtained plasmids were sequenced by Eurofins MWG Operon (Eldersber) company to verify their sequences correctness. Sequencing results were analyzed using ContigExpress from the VectorNTI advance suite 11 software (Invitrogen) or with SeqMan Pro from DNASTAR (DNASTAR) software package.

pAP12 (plasmid for expression of P_{nat}*pilB-mCherry* from the *attB* site): P_{nat} *pilB* (PilB_{nat} fw / PilB rev) fragment was amplified from genomic DNA of *M. xanthus* DK1622 and digested with NdeI +BamHI. Subsequently, fragment was cloned in pNG062 carrying C-terminal *mCherry* and sequenced.

pAP16 (plasmid for expression of P_{nat}*mCherry-pilM* from the *attB* site): P_{nat} (PilM_{nat} fw / PilM_{nat} rev) and *pilM* (PilM fw/PilM rev) fragments were amplified from genomic DNA of *M. xanthus* DK1622 and digested with NdeI+BglII and XbaI+HindIII, respectively. Subsequently, fragments were cloned in pNG063 carrying N-terminal *mCherry* and sequenced.

pAP19, pAP60, pAP61 and pAP89 (plasmid for generation of in-frame deletion of *frzE*, *mxan_5763-65*, *mxan_5765*, *mxan_5764*): up- (frzE A/frzE B; 5763-65 A/5763-65 B; 5765 A/5763-65 B; 5764 A/5764 B) and downstream fragments (frzE C/ frzE D; 5763-65 C/5763-65 D; 5765 C/5765 D; 5764 C/5764 D) were amplified from genomic DNA of *M. xanthus* DK1622. Subsequently, the AB and CD fragments were used as template for overlapping PCR (frzE A/ frzE D; 5763-65 A/5763-65 D; 5765 A/5765 D; 5764 A/5764 D) to generate the AD fragment. AD fragment was digested with HindIII+EcoRI, cloned in pBJ114 and sequenced.

pAP34 (plasmid for expression of P_{nat}*sgmX* from the *attB* site): P_{nat} *sgmX* fragment (P_{nat}*sgmX* fw/ P_{nat}*sgmX* rev) was amplified from genomic DNA of *M. xanthus*, digested with HindIII+EcoRI, cloned in pSWU30 and sequenced.

pAP35 (plasmid for *sgmX* replacement by *sgmX-mVenus* at native site): up- (SgmX-mvA/SgmX-mvB) and downstream fragments (SgmX-mvC/SgmX-mvD) were amplified from genomic DNA of *M. xanthus* DK1622. A fragment containing *mVenus* was amplified from plasmid pLC20 carrying *mgIA-mVenus* (Venus/Cherry Fw / Venus/Cherry Rv). Subsequently, AB and *mVenus* fragments were used as template for overlapping PCR (SgmX-mvA/Venus/Cherry Rv) to generate the AB-mVenus fragment. AB-mVenus and CD fragments were digested with HindIII+XbaI and XbaI+EcoRI, respectively. Fragments were cloned in pBJ114 and sequenced.

pAP37 (plasmid for *pilQ* replacement by *pilQ-sfGFP* at native site): up- (PilQ-sfGFP A/ PilQ-sfGFP B) and downstream fragments (PilQ-sfGFP C/ PilQ-sfGFP D) were amplified from genomic DNA of *M. xanthus* DK1622. A fragment containing *sfgfp* was amplified from plasmid pSC101 (Friedrich et al, 2014) (sfGFP Fw / sfGFP Rev). Subsequently, AB and *sfgfp* fragments were used as template for overlapping PCR (PilQ-sfGFP A/sfGFP Rev) to generate the AB-sfGFP fragment. AB-sfGFP and CD fragments were digested with HindIII+XbaI and XbaI+EcoRI, respectively. Fragments were cloned in pBJ114 and sequenced.

pAP39 (plasmid for overexpression of SgmX-Strep): *sgmX strep* fragment was amplified (SgmX-Strep fw/SgmX-Strep rev) from genomic DNA of *M. xanthus* DK1622; Strep tag was introduced using SgmX-Strep rev primes. Fragment was digested with XbaI+HindIII, cloned in pMAT135 (derivative of pET45-b+ lacking protein tag) and sequenced.

pAP87 (plasmid for expression of $P_{nat}mCherry-pilT$ from the *attB* site): P_{nat} (PilT_{nat} fw / PilT_{nat} rev) and *pilT* (PilT fw/PilT rev) fragments were amplified from genomic DNA of *M. xanthus* DK1622 and digested with NdeI+BglII and XbaI+HindIII, respectively. Subsequently, fragments were cloned in pNG063 carrying N-terminal *mCherry* and sequenced.

pAP88 (plasmid for *mgIB* replacement by *mgIB^{A64R G68R}-mCherry* at native site): up- (MgIB^{A/GR}-mChA / MgIB^{A/GR}-mChB) and downstream fragments (MgIB^{A/GR}-mChC/ MgIB^{A/GR}-mChD) were amplified from genomic DNA of *M. xanthus* SA3954. A fragment containing *mCherry* was amplified from plasmid pDK145 carrying *mgIB-mCherry* (Venus/Cherry Fw / Venus/Cherry Rv). Subsequently, AB and *mCherry* fragments were used as template for overlapping PCR (MgIB^{A/GR}-mChA/Venus/Cherry Rv) to generate the AB-mCherry fragment. AB-mCherry and CD fragments were digested with HindIII+XbaI and XbaI+EcoRI, respectively. Fragments were cloned in pBJ114 and sequenced.

pAP29-32 are bacterial two hybrid constructs containing SgmX. The gene was amplified from genomic *M. xanthus* DK1622 for cloning it in C- and N-terminal orientation (SgmX BTH1/2;

SgmX BTH 1/3). To be translated in the correct frame the *sgmX* derivatives contain one or two additional amino acid at the beginning and the end which additionally serves as a part of the linker for both *T18* and *T25* fragment fusions.

4.4.3 Construction of in-frame deletion mutants

To generate an in-frame deletion mutants previously described procedure of two-step homologous recombination was followed (Shi et al., 2008) (Fig. 55). Briefly, a combined AD fragment of ≈ 1000 -1600bp were created from up- and downstream flanking regions (AB and CD fragments). To do so, an AB fragment served as a template for CD. Further an AD fragment was transformed into pBj114 vector using HindIII/EcoRI cloning sites, and obtained plasmids were verified by sequencing. Correct vectors were transformed into appropriate *M. xanthus* background strains and clones containing an integration were Km resistant and selected by doing the PCR reaction using M13 fw and rev primers that bind pBj114. One clone from up- and downstream plasmid integration was used for the second step of homologous recombination. Plasmid pBJ114 contains the selection marker *galk* (galaktokinase) gene. The gene product Galk converts galactose into galactose-1-phosphate which cannot be metabolize by *M. xanthus* and accumulates up to toxic levels when cells are grown on media supplemented with galactose. Thus, only clones that undergo second homologous recombination lost plasmid are able to grown on media with galactose. For the second homologous recombination event cells were grown in CTT liquid shaking culture to exponential growth phase. Series of dilutions were plated on CTT agar plates supplemented with 10 $\mu\text{g/ml}$ gentamycin and 2.5% galactose. Galactose resistant and kanamycin sensitive clones were checked with PCR reaction using G (binds downstream of B primer) and H (binds upstream of C primer) primer pair. The GH fragment was amplified only in the WT.

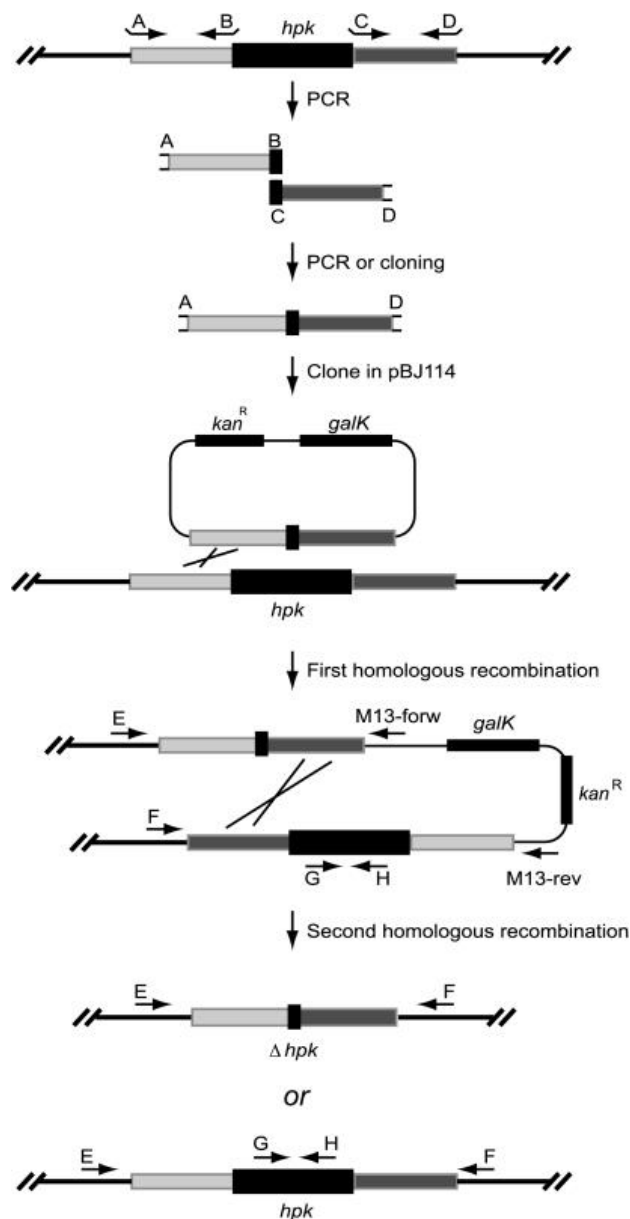


Figure 55 Strategy for in-frame deletion mutants construction.

First homologous recombination leads to up- or downstream plasmid integration in the genomic region of interest. Second homologous recombination enables loop out of vector (reconstitution) or vector with the region of interest (in-frame deletion). Details in the text. The figure is reproduced from Shi et al. (Shi et al., 2008).

4.4.4 DNA isolation of *E. coli* and *M. xanthus*

Plasmid DNA from *E. coli* was isolated using the NucleoSpin Plasmid QuickPure kit (Macherey-Nagel) following the instructions provided by the manufacturer. Concentration and purity of DNA was determined with the Nanodrop ND-1000 spectrophotometer. Crude genomic DNA for colony PCR of *M. xanthus* was prepared by resuspending cells taken from CTT agar plates in 80 μ l of H₂O and boiling the mixture at 96 °C for 10 min. One μ l of resulted cell suspension was used for PCR reactions. Crude genomic DNA for colony PCR of *E. coli* was obtained by directly adding cells from LB agar plate into PCR mixture.

4.4.5 Polymerase chain reaction

Amplification of specific DNA fragments was performed using Phusion High-Fidelity DNA Polymerase (Thermo Scientific™, Darmstadt) or Q5® Hot Start High-Fidelity DNA Polymerase (New England Biolabs, Frankfurt a. M.) was used in a total reaction volume of 50 µl. The colony PCR was performed used 5 PRIME MasterMix in total volume of 20 µl. The composition of the PCR reaction mix is described in Table 12.

Table 12 PCR reaction mix

Component	Volume	Final concentration
Cloning PCR with Phusion High-Fidelity DNA Polymerase		
Template DNA	1 µl	≈ 50 ng
10 µM primer (each)	1.5 µl	0.75 µM
10 mM dNTP mix	1.5 µl	0.3 mM
5 x Phusion GC buffer	10 µl	1x
5 x enhancer	10 µl	1x
Phusion DNA polymerase	0.5 µl	1 unit/50 µl reaction
ddH ₂ O	To 50 µl	
PCR with Q5® Hot Start High-Fidelity DNA Polymerase		
Template DNA	1 µl	≈ 50 ng
10 µM primer (each)	1.5 µl	0.75 µM
10 mM dNTP mix	1.5 µl	0.3 mM
5 x Q5 Reaction buffer	10 µl	1x
5 x Q5 High GC Enhancer	10 µl	1x
DMSO	2.5 µl	5% (v/v)
Q5 Hot Start High-Fidelity DNA	0.5 µl	1 unit/50 µl reaction
ddH ₂ O	To 50 µl	
Colony PCR		
Crude genomic DNA	1 µl	≈ 100 ng
10 µM primer (each)	1 µl	0.5 µl
5 PRIME MasterMix	10 µl	
DMSO	2 µl	10% (v/v)
ddH ₂ O	To 20 µl	

The PCR programs used in this work are represented in Table 13. Primer annealing temperature was adjusted depending on the GC content and elongation time was calculated based on the resulted DNA fragment length.

Table 13 PCR programs used in this work

Step	Temperature	Time	
Standard/check PCR			
Initial denaturation	98 °C	3 min	
Denaturation	98 °C	30 sec	35x
Primer annealing	5 °C below predicted melting temperature	30 sec	
Elongation	72 °C	1 min/kb – 5 PRIME MasterMix 30 sec/kb – Phusion/Q5 polymerase	
Final elongation	72 °C	3 min	
Hold	4 °C	∞	
Touch down PCR			
Initial denaturation	94 °C	3 min	
Denaturation	94 °C	30 sec	10x
Primer annealing	65 °C	30 sec	
Elongation	72 °C	1 min/kb or 30 sec/kb	
Denaturation	94 °C	30 sec	10x
Primer annealing	60 °C	30 sec	
Elongation	72 °C	1 min/kb or 30 sec/kb	
Denaturation	94 °C	30 sec	10x
Primer annealing	55 °C	30 sec	
Elongation	72 °C	1 min/kb or 30 sec/kb	
Final elongation	72 °C	3 min	
Hold	4 °C	∞	

4.4.6 Agarose gel electrophoresis

Nucleic acid fragments were separated by size on 1% agarose gels with 0.01% (v/v) ethidium bromide or GelRed® Nucleic Acid Gel Stain (Biotium) in TBE buffer (Invitrogen) at 120 V. When needed, DNA samples were pre-mixed with 5x DNA loading buffer (32.5% sucrose, 5 mM EDTA, 5 mM Tris-HCl pH 7.5, 0.15% bromophenol blue). The 2-log DNA ladder (NEB) was used as a size marker. Agarose gels were imaged using E-BOX VX2 imaging system (Peqlab) or GelStick Touch IMAGER (INTAS).

4.4.7 Restriction and ligation of DNA fragments

DNA fragments and backbone vectors (0.5-1 µg) were incubated with appropriate restriction endonucleases for 1h at 37 °C in 50 µl volume. For the fragments reaction was quenched by incubating for 10 min at 65 °C and then fragments were purified from mixture using NucleoSpin® Gel and PCR Clean-up Kit (Macherey-Nagel). Digested vectors were additionally treated with Antarctic phosphatase (total reaction volume 60 µl) for 1h at 37 °C and then separated by agarose gel electrophoresis. Digested vectors were cut out of the gel and purified using NucleoSpin® Gel and PCR Clean-up Kit (Macherey-Nagel).

Ligation reactions were performed using T4 DNA ligase from NEB in reaction volume of 20 µl. Ligations mixtures were incubated for 1-1.5h at RT and reaction was quenched by 10 min incubation at 65 °C. After inactivation, reaction tubes were cooled down on ice. PCR fragments were ligated into vectors using a 3- to 5-fold molar excess of insert DNA.

4.4.8 Preparation and transformation of chemically competent *E. coli* cells

Overnight cultures of *E. coli* were used to inoculate 150 ml LB medium. Cells were grown to an OD₆₀₀ of 0.5-0.7 and then harvested at 4700 rpm for 10 min at 4 °C. The cell pellet was resuspended in 30 ml ice cold 50 mM CaCl₂ solution and incubated for 15 min. Cells were once again pelleted as described before and resuspended in 4 ml CaCl₂ supplied with 16% glycerol. After 10 min incubation on ice, cells were aliquoted 100 µl and frozen in liquid nitrogen. Frozen aliquots were stored at -80 °C. One aliquot was used per transformation. Cells were thawed on ice and 20 µl of ligation mixture was added to the cells and mixed carefully. After incubation on ice for 15 min, cells were heat-shocked at 42 °C for 90 s. After 5 min incubation on ice, 1 ml LB-medium was added and cells were incubated for 1 h shaking at 37 °C. Then, cells were pelleted for 30 sec, the supernatant was discarded and cells were resuspended in 50 µl LB medium and plated on LB plates with appropriate antibiotics. Plates were incubated at 37 °C over night. Colonies were transferred to fresh agar plates and checked for the presence of the insert containing plasmid by PCR reaction.

4.4.9 Transformation of *E. coli* cells for BACTH system

The chemical competent cells of BTH101 *E. coli* were prepared as described in 4.4.8, aliquoted 300 µl and frozen in liquid nitrogen. For one transformation two plasmids were added to 50 µl cells one encoding for the T25 fragment (derivatives of pKNT25 or pKT25) and the other one encoding for the T18 fragment (derivatives of pUT18 or pUT18C). Normally ~100 ng of each

vector was used in one transformation. The cell suspension was plated on rich LB media in the presence of X-Gal (40 µg/ml), 0.5 M IPTG, 100 µg/ml ampicillin and 50 µg/ml kanamycin.

4.4.10 Preparation and transformation of electrocompetent *M. xanthus* cells

For transformation of *M. xanthus* cells, 2 ml of an overnight culture OD₅₅₀ 0.6-0.9 were harvested at 13,000 rpm for 2 min and the pellet was washed twice in 1 ml sterile ddH₂O and resuspended in 50 µl H₂O. 0.5 µg DNA for plasmids integrating at the Mx8 site and 1 µg of DNA for plasmids integrating at the endogenous site was added and the mixture was transferred into an electroporation cuvette. Cells were pulsed with 0.65 kV, 25 µF and 400 Ω. 1 ml CTT-medium was added and the cell suspension was transferred to a 25 ml Erlenmeyer flask and incubated at 32 °C, 230 rpm for 6h. For integration at the Mx8 site 50 and 200 µl of the culture were plated directly on CTT agar plates with the appropriate antibiotics. For the integration at the endogenous site the full transformation volume was pelleted, resuspended in 150 µl CTT media and plated on CTT agar plate supplied with 50 µg/ml kanamycin. Plates were incubated at 32 °C for 5-10 days and integration of the plasmid was verified by colony PCR.

4.5 Biochemical methods

4.5.1 Purification of proteins

SgmX-Strep and MglA-His₆ were expressed in *E. coli* BL21 (DE3), His₆-MglB was expressed in *E. coli* Rosetta. Cells of *E. coli* BL21 (DE3) transformed with pAP39 or pTM1 were scratched from LB agar plate and inoculated in 20 ml LB media containing appropriate antibiotic. Once the cultures grown at 37 °C reached OD₆₀₀ 0.5-0.7, 10 ml was taken for overexpression in 1L of LB media. For the His₆-MglB 10 ml of overnight culture was taken to inoculate in 1L. Large cultures were supplied with 0.5% sterile glucose solution. Cultures were shaking grown at 30 °C to the OD₆₀₀ 0.5-0.7 and protein expression was induced by adding 0.2 mM IPTG for SgmX-Strep and 0.5 mM IPTG for MglA-His₆ and His₆-MglB. Induction was carried out over night at 18 °C.

The cells were harvested by centrifugation at 10000 rpm for 10 min at 4 °C and cells with His-tagged proteins resuspended in 25 ml lysis buffer (50 mM Tris pH 7.5, 150 mM NaCl, 10 mM imidazole, 5% glycerol, 5mM MgCl₂ supplemented with EDTA-free protease inhibitors (Complete Protease Inhibitor Cocktail Tablet EDTA-free (Roche))). For cells with overexpressed SgmX-Strep the same buffer without Imidazole was used. Cells were lysed by French press and cell debris removed by centrifugation (48.385 x g, 4 °C, 30 min).

The cleared cell lysate with His-tagged proteins was pre-mixed for 1 hr with 1ml Ni²⁺-NTA-agarose preloaded with NiSO₄ as described by the manufacturer and pre-equilibrated in wash buffer A (50 mM Tris pH 7.5, 150 mM NaCl, 10 mM imidazole, 5% glycerol, 5mM MgCl₂) and sequentially loaded on a gravity column. The column was washed with 50 column volumes of column wash buffer. Proteins were eluted with elution buffer A (50 mM Tris pH 7.5, 150 mM NaCl, 5 mM MgCl₂, 500 mM imidazole) using a linear imidazole gradient from 50-500 mM. Fractions containing purified His-tagged proteins were combined and loaded onto a HiLoad 16/600 Superdex 200 pg (GE Healthcare) gel filtration column that was equilibrated with sterile de-gassed gel-filtration buffer (50 mM Tris pH 7.5, 150 mM NaCl, 5% glycerol, 5mM MgCl₂). Fractions containing His-tagged proteins were identified by SDS-PAGE, concentrated to a final volume of ≈1.5 ml, and frozen in liquid nitrogen and stored at -80 °C.

To purify SgmX-Strep, biotin affinity purification was used. Briefly, cells were lysed was pre-mixed for 1h with 1ml Strep-Tactin®XT Superflow® (IBA-lifesciences), pre-equilibrated with wash buffer B (50 mM Tris pH 7.5, 150 mM NaCl, 5% glycerol, 5mM MgCl₂) and sequentially loaded on a gravity column. The column was washed with 50 column volumes of wash buffer B. Protein was eluted with elution buffer B (150 mM Tris pH 7.5, 150 mM NaCl, 5% glycerol, 5mM MgCl₂, 2.5 mM Desthiobiotin). Elution fractions containing SgmX-Strep were loaded onto a HiLoad 16/600 Superdex 200 pg (GE Healthcare) gel filtration column equilibrated with sterile and de-gassed gel filtration buffer. Fractions with SgmX-Strep were identified by SDS-PAGE, concentrated to a final volume of ≈1.5 ml, and frozen in liquid nitrogen and stored at -80°C.

Concentration of all purified proteins was determined using Nanodrop ND-1000 UV-Vis spectrophotometer. For that purpose, specific for each protein molar extinction coefficient and molecular weight in daltons were calculated.

4.5.2 SDS polyacrylamide gel electrophoresis (SDS-PAGE)

To separate proteins under denaturing conditions SDS-PAGE (Laemmli, 1970) with 12% polyacrylamide gels was performed. To denature proteins, the protein samples were mixed with 1x loading buffer (10% (v/v) glycerol, 60 mM Tris-HCl pH 6.8, 2% (w/v) SDS, 100 mM DTT, 0.005% (w/v) bromophenol blue) and heated for 10 min at 95 °C directly before loading on the gel. Gel electrophoresis was performed in Bio-Rad electrophoresis chambers (BioRad, München) at 100-140 V in 1x Tris/Glycine SDS (TGS) running buffer from Bio-Rad. Size of proteins was determined by comparison to the protein marker, the PageRuler Prestained Protein Ladder from

Fermentas. Proteins were visualized by staining with InstantBlue™ protein staining solution (Expedeon).

4.5.3 Immunoblot analysis

Protein solutions or proteins from cell extracts were separated in the gel by SDS-PAGE and transferred to a nitrocellulose membrane using TransBlot® Turbo™ Transfer System from Bio-Rad at 1.3 A, 25 V for 7 min with transfer buffer (300 mM Tris and 300 mM Glycin, and 0.05% SDS, pH 9.0). After transfer the membrane was blocked in 5% non-fat milk powder (w/v) in 1 x TTBS buffer (0.05% (v/v) Tween 20, 20 mM Tris-HCl, 137 mM NaCl pH 7.0) for 2 h at RT. After washing with 1 x TTBS buffer, the primary antibody (rabbit) was added in proper dilutions (Table 14) in 1 x TTBS supplemented with 2% non-fat milk powder over night at 4 °C. Next, membranes were washed again with 1 x TTBS buffer and incubated with secondary anti-rabbit immunoglobulin G peroxidase conjugate (Sigma) in a dilution of 1:15000 or with secondary anti-mouse immunoglobulin G, horseradish peroxidase lined whole antibody (GE Healthcare) in a dilution 1:2000 for 1h at 4 °C. After washing with 1 x TTBS buffer the blot was developed with the Luminata Western HRP Substrate (Merck Millipore) and visualized with the luminescent image analyzer LAS-4000 (Fujifilm).

Table 14 Antibody dilutions used for immunoblotting

Antibody	α -PilA	α -PilB	α -PilC	α -PilM	α -PilN	α -PilO	α -PilP
dilution	1:5000	1:2000	1:5000	1:2000	1:2000	1:2000	1:2000

Antibody	α -PilQ	α -PilT	α -TsaP	α -GFP	α -mCherry
dilution	1:5000	1:2000	1:2000	1:2000	1:2500

4.5.4 GTPase assay

To test an activity of MglA-His₆ non-radioactive High Throughput Colorimetric GTPase Assay kit (Expedeon), based on malachite green was used. GTP hydrolysis was measured following the instructions provided by the manufacturer. Briefly, MglA-His₆ (final concentrations: 1, 2, 4, 6 and 8 μ M per reaction) mixed in 1:2 molar ratio to His₆-MglB (final concentrations: 2, 4, 8, 12 and 16 μ M per reaction) were pre-loaded with 0.5 mM GTP in reaction buffer (total volume 200 μ l) for 120 min at RT. GTPase reactions were terminated by adding 50 μ l of PiColorLock and after 2 minutes stabilized by adding 20 μ l Stabilizer. The reactions were transferred to 96-well plates (Greiner Bio-One) and color developed for 30 minutes. Absorption was measured at 600

nm at 37 °C using an Infinite M200 Pro plate-reader (Tecan) and the outcome calculated into released phosphate in $\mu\text{M}/\text{hour}$ based on the standard curve. Reaction mixtures for the standard curve were processed the same way as samples containing proteins and contained gradient concentrations of free phosphate in a range of 2.5-50 μM . Samples containing mentioned above concentrations of only MglA-His₆ or only His₆-MglB provided an intrinsic activity for each protein.

4.5.5 Pull down experiments

To test direct protein-protein interaction of MglA-His₆ to SgmX-Strep, 30 μM of MglA-His₆ was mixed with equal amount of SgmX-Strep and preloaded with GTP or GDP (final concentration: 100 μM) or incubated alone for 30 min at RT in gel filtration buffer (composition described in 4.5.1). SgmX alone or pre-incubated with nucleotides was used as a negative control. Further, 100 μl of a Ni²⁺-NTA-agarose resin previously equilibrated in gel filtration buffer was added and resulted samples were incubated in 1.5 ml Eppendorf tubes with slow rotation for 120 min at 4 °C. The resin was centrifuged at 2500 rpm for 2 min at 4 °C and flow through was taken out. Resin was washed four times with 1 ml of ice cold gel filtration buffer (when needed supplemented with corresponding amounts of nucleotides). Proteins were eluted with 100 μl of gel filtration buffer supplied with 400 mM imidazole. Fractions were analysed by dividing with SDS-PAGE and gel staining with InstantBlue™ (Expedeon).

4.5.6 Co-Immunoprecipitation (Co-IP)

To analyze possible interaction candidates of proteins of interest, functional fluorescence fusions of MglA, PilB, PilM and SgmX were expressed at native or Mx8 site of *M. xanthus*. To obtain sufficient amount of proteins cells containing MglA-mVenus_{endogenous}, PilB-mCherry, mCherry-PilM and SgmX-mVenus_{endogenous} and respective deletion mutants were grown on 1% CTT/ 1.5% agar plates at 32 °C for 2 days and equal cell masses (≈ 150 mg) were scraped from plates for further experiment. Cells were resuspended in 1.3 ml of resuspension buffer (50 mM Tris pH 7.5, 150 mM NaCl, supplemented with EDTA-free protease inhibitors (Complete Protease Inhibitor Cocktail Tablet EDTA-free (Roche))). *M. xanthus* cell suspensions were ultra-sonicated on ice for 30 s twice and centrifuged for 15 min at 15000 rpm, at 4 °C. 1 ml of clear cell lysates were pre-mixed to 15 μl of GFP- or RFP-Trap beads (depending on the fluorescence tag) (Chromotek) in 2 ml Eppendorf tubes, and resulted mixtures were incubated at slow rotation for 2.5 h at 4 °C.

After incubation beads were separated from the lysates and washed three times with 700 μl of 100 mM ammoniumbicarbonate (ABC) (Sigma-Aldrich) by 10 s vortexing and centrifuging

2.5 min at 2500 rpm RT. Next, 100 μ l elution buffer 1 (1.6 M urea, 100 mM ABC, 5 μ g/ml trypsin) was added, mixture was vortexed and incubated for 30 min at 1200 rpm shaking thermomixer at 27 °C. Beads were centrifuged and supernatant collected into fresh tubes. 40 μ l of elution buffer 2 (1.6 M urea, 100 mM ABC, 1 mM Tris(2-carboxyethyl)phosphin (TCEP)) was applied to the beads and after vortexing mixture was centrifuged and supernatant combined with the first part. Last step was repeated again and final combined supernatant had volume of 180 μ l. Reaction of peptide digestion was running overnight at RT and 40 μ l of iodoacetamid (final concentration 10 mM) were added at the morning. Samples were vortexed and incubated for 30 min in the dark.

Peptide samples were acidified by adding 150 μ l of 5% trifluoroacetic acid (TFA) with pH adjusted to <2. Peptide mixtures were desalted using solid-phase extraction (SPE) on C18-Microspin columns (Harvard Apparatus). SPE columns were prepared by adding acetonitrile (ACN), followed by column equilibration with 0.1% TFA. Peptides were loaded on equilibrated Microspin columns and washed twice with 5% ACN/0.1% TFA. After peptide elution using 50% ACN/0.1% TFA, peptides were dried in a rotating concentrator (Thermo Fischer Scientific), reconstituted in 0.1% TFA and subjected to LC-MS analysis.

4.5.7 Liquid chromatography-mass spectrometry (LC-MS)

LC-MS analysis of the peptide samples was carried out on a Q-Exactive Plus instrument connected to an Ultimate 3000 RSLC nano and a nanospray flex ion source (Thermo Scientific). Peptide separation was performed on a reverse-phase high-performance liquid chromatography (HPLC) column (75 μ m \times 42 cm) packed in-house with C18 resin (2.4 μ m). The peptides were loaded onto a PepMap 100 precolumn (Thermo Fischer Scientific) and eluted by a linear ACN gradient from 2–35% solvent B over 60 min (solvent A: 0.15% formic acid; solvent B: 99.85% ACN in 0.15% formic acid). The flow rate was set to 300 nl/min. The peptides were analyzed in positive ion mode. The spray voltage was set to 2.5 kV, and the temperature of the heated capillary was set to 300 °C. Survey fullscan MS spectra (m/z = 375–1500) were acquired in the Orbitrap with a resolution of 70,000 full width at half maximum at a theoretical m/z 200 after accumulation a maximum of 3×10^6 ions in the Orbitrap. Based on the survey scan up to 10 most intense ions were subjected to fragmentation using high collision dissociation (HCD) at 27% normalized collision energy. Fragment spectra were acquired at 17,500 resolution. The ion accumulation time was set to 50 ms for both MS survey and tandem MS (MS/MS) scans. To increase the efficiency of MS/MS attempts, the charged state screening modus was enabled to exclude unassigned and singly charged ions. The dynamic exclusion duration was set to 30 s.

Label-free quantification (LFQ) of the samples was performed using MaxQuant (Version 1.5.3.17) (Cox and Mann, 2008). For Andromeda database searches implemented in the MaxQuant environment, the protein databases for *M. xanthus* was downloaded from Uniprot and searches were performed using the protein database. The search criteria were set as follows: full tryptic specificity was required (cleavage after lysine or arginine residues); two missed cleavages were allowed; carbamidomethylation (C) was set as fixed modification; oxidation (M) and deamidation (N, Q) as variable modification. MaxQuant was operated with default settings with the “Match-between-run” option.

To calculate protein enrichment in co-IP experiments, intensity-based absolute quantification (iBAQ) values were calculated with MaxQuant (Schwanhauser et al., 2011). MaxQuant calculates protein intensities as a sum of all peptide intensities for a given protein. To obtain iBAQ values the protein intensity sum was divided by the number of theoretically observable peptides. Calculated iBAQ values were rescaled in order to compare different biological replicates.

4.6 Transmission electron microscopy

Transmission electron microscopy was used to visualize T4P essentially as described (Jakovljevic et al., 2008). Briefly, 50 μ l of exponentially growing *M. xanthus* cells were placed on Parafilm. A small piece of carbon-coated mica was dipped into the drop for 3-5 min, allowing cells to adsorb to the surface, excess liquid was soaked off, the film was placed briefly on a drop of distilled water, excess liquid was soaked off again, and the film transferred on a drop of 2% uranyl acetate (wt/vol) for 3-4 seconds and blotted dry. Transmission electron microscopy was performed on a JEOL JEM-1400 electron microscope at calibrated magnifications.

4.7 Bioinformatic analyses and statistics

BlastP (Boratyn et al., 2013) and Pfam v31.0 (pfam.xfam.org) (Finn et al., 2016) were used to identify and map TPR domains of SgmX. TMHMM v2.0 (Sonnhammer et al., 1998) was used to check for transmembrane helices with default gathering thresholds. % of identity/similarity between MXAN_5763-5767 and their homologs from other species were calculated using EMBOSS Needle software (Li et al., 2015) (pairwise sequence alignment). Sequences for the conservation figure were obtained from KEGG database (Kanehisa and Goto, 2000).

Statistical analyses were performed using a two-tailed Student’s t-test or a Mann-Whitney test for samples with unequal variances and distribution that did not pass the normality test.

5 SUPPLEMENTARY DATA

Table S1 T4P-dependent and gliding motility-related protein candidates, enriched in the experimental samples of *in vivo* pull down experiments for MglA-mVenus and MglA^{Q82A}-mVenus. Table is generated as Table 1 (Results 2.4.1).

Protein	Domain structure	Log2 ratio	P value
MXAN_1925 MglA	Mutual gliding-motility protein	13.30309	1.9419E-07
MXAN_5592 DigR	DNA-binding response regulator	5.010173	0.00225304
MXAN_7445 EpsE	Glycosyl transferase, group 1 family protein	2.368139	0.00263633
MXAN_6862 AgIR	MotA/TolQ/ExbB proton channel family protein	3.489604	0.00340864
MXAN_5781 PilH	ABC transporter, ATP-binding protein	3.530964	0.0038174
MXAN_5818 AgmR	Anion-transporting ATPase	4.05256	0.00429332
MXAN_6860 AgIS	Adventurous gliding motility protein	3.606151	0.00507145
MXAN_5783 PilA	Fimbrial protein	3.816996	0.00550006
MXAN_7441 EpsH	Glycosyl transferase, group 1	2.714014	0.00716108
MXAN_2539 GltB	Uncharacterized protein	3.780383	0.00866218
MXAN_3084 Tgl	Social gliding motility protein	3.356178	0.0093663
MXAN_4640 SgmT	Sensor histidine kinase/response regulator	2.473498	0.01125545
MXAN_6137 AgIU	Adventurous gliding motility protein	2.915598	0.01175971
MXAN_2541 GltC	Tetratricopeptide repeat protein	3.259955	0.01455276
MXAN_4866 AgmV	Uncharacterized protein	3.077041	0.0149559
MXAN_4150 SgmO	Uncharacterized protein	1.436243	0.01767954
MXAN_6607 AgmT	Hypothetical adventurous gliding motility protein	2.522072	0.01794014
MXAN_7448 EpsD	Glycosyl transferase, group 2 family protein	2.187312	0.01875134
MXAN_4619 WbgB	Glycosyl transferase, group 2 family protein	3.838369	0.019409
MXAN_3060 CglB	Adventurous gliding motility protein	2.786307	0.02881983
MXAN_5831 GlgP	Alpha-1,4 glucan phosphorylase	3.329449	0.032761
MXAN_4621 RfbC	Glycosyl transferase family protein	2.454814	0.03299122
MXAN_6696 DifA	Methyl-accepting chemotaxis protein DifA	2.028761	0.03308909
MXAN_4639 SgmS	TPR domain protein	1.028801	0.0333442
MXAN_7451 EpsA	Glycosyl transferase, WecB/TagA/CpsF family	2.894867	0.03356341
MXAN_5788 PilB	Type IV-A pilus assembly ATPase PilB	1.779798	0.03414731
MXAN_5753 AgIX	Transporter, MotA/TolQ/ExbB proton channel family	1.97046	0.03614421
MXAN_5333 SgmV	Glycosyl transferase, group 1	3.098093	0.0362334
MXAN_5775 PilN	Type IV pili biogenesis protein	2.959042	0.03803919
MXAN_2526 SgmH	Uncharacterized protein	1.39338	0.03971003
MXAN_1106 SgmC	PT repeat/DnaJ domain/tetratricopeptide repeat protein	0.994917	0.04236765
MXAN_5787 PilT	Twitching motility protein PilT	1.612725	0.04449004
MXAN_4869 AgIT	Adventurous gliding motility protein	1.880104	0.04516079

Table S2 T4P-dependent and gliding motility-related protein candidates, enriched in the experimental samples of *in vivo* pull down experiments for PilB-mCherry. Table is generated as Table 1 (Results 2.4.1).

Protein	Domain structure	Log2 ratio	P value
MXAN_5788 PilB	Type IV-A pilus assembly ATPase	12.86519	7.24023E-06
MXAN_5781 PilH	Efflux ABC transporter, ATP-binding protein	3.141432	5.6841E-05
MXAN_4620 SgmR	Uncharacterized protein	1.132145	0.003202558
MXAN_6137 AglU	Adventurous gliding motility protein	1.574147	0.003244169
MXAN_4149 FrzS	Response regulator	2.829392	0.010906105
MXAN_5753 AglX	Transporter, MotA/TolQ/ExbB proton channel family	0.84713	0.013733319
MXAN_3797 SgmN	Acyl-CoA dehydrogenase	1.058866	0.014830534
MXAN_4150 SgmO	Uncharacterized protein	1.508095	0.016514338
MXAN_1925 MglA	Mutual gliding protein	0.610231	0.030858497
MXAN_3759 SgmM	Carboxyl transferase domain protein	1.705166	0.038085435
MXAN_6862 AglR	MotA/TolQ/ExbB proton channel family protein	0.988438	0.039710686
MXAN_3506 SgmL	NAD-dependent epimerase/dehydratase family protein	0.832825	0.044436949

6 REFERENCES

Albers, S.V., and Jarrell, K.F. (2018). The Archaeum: An Update on the Unique Archaeal Motility Structure. *Trends Microbiol* 26, 351-362.

Alm, R.A., Bodero, A.J., Free, P.D., and Mattick, J.S. (1996a). Identification of a novel gene, *pilZ*, essential for type 4 fimbrial biogenesis in *Pseudomonas aeruginosa*. *J Bacteriol* 178, 46-53.

Alm, R.A., Hallinan, J.P., Watson, A.A., and Mattick, J.S. (1996b). Fimbrial biogenesis genes of *Pseudomonas aeruginosa*: *pilW* and *pilX* increase the similarity of type 4 fimbriae to the GSP protein-secretion systems and *pilY1* encodes a gonococcal PilC homologue. *Mol Microbiol* 22, 161-173.

Alm, R.A., and Mattick, J.S. (1997). Genes involved in the biogenesis and function of type-4 fimbriae in *Pseudomonas aeruginosa*. *Gene* 192, 89-98.

Ashton, A. (1993). Structural studies of the Lipopolisaccharide from *Myxococcus xanthus* and Lipopolisaccharide mutants. (Minneapolis, University of Minnesota).

Astling, D.P., Lee, J.Y., and Zusman, D.R. (2006). Differential effects of chemoreceptor methylation-domain mutations on swarming and development in the social bacterium *Myxococcus xanthus*. *Mol Microbiol* 59, 45-55.

Balagam, R., Litwin, D.B., Czerwinski, F., Sun, M., Kaplan, H.B., Shaevitz, J.W., and Igoshin, O.A. (2014). *Myxococcus xanthus* gliding motors are elastically coupled to the substrate as predicted by the focal adhesion model of gliding motility. *PLoS Comput Biol* 10, e1003619.

Banerjee, A., Ghosh, A., Mills, D.J., Kahnt, J., Vonck, J., and Albers, S.V. (2012). FlaX, a unique component of the crenarchaeal archaeum, forms oligomeric ring-shaped structures and interacts with the motor ATPase FlaI. *J Biol Chem* 287, 43322-43330.

Behmlander, R.M., and Dworkin, M. (1994). Biochemical and structural analyses of the extracellular matrix fibrils of *Myxococcus xanthus*. *J Bacteriol* 176, 6295-6303.

Belete, B., Lu, H., and Wozniak, D.J. (2008). *Pseudomonas aeruginosa* AlgR regulates type IV pilus biosynthesis by activating transcription of the *fimU-pilVWXYZ1Y2E* operon. *J Bacteriol* 190, 2023-2030.

Berleman, J.E., Allen, S., Danielewicz, M.A., Remis, J.P., Gorur, A., Cunha, J., Hadi, M.Z., Zusman, D.R., Northen, T.R., Witkowska, H.E., *et al.* (2014). The lethal cargo of *Myxococcus xanthus* outer membrane vesicles. *Front Microbiol* 5, 474.

Berleman, J.E., Chumley, T., Cheung, P., and Kirby, J.R. (2006). Rippling is a predatory behavior in *Myxococcus xanthus*. *J Bacteriol* 188, 5888-5895.

Berleman, J.E., and Kirby, J.R. (2007). Multicellular development in *Myxococcus xanthus* is stimulated by predator-prey interactions. *J Bacteriol* 189, 5675-5682.

Berleman, J.E., Scott, J., Chumley, T., and Kirby, J.R. (2008). Predatation behavior in *Myxococcus xanthus*. *Proc Natl Acad Sci U S A* 105, 17127-17132.

Berleman, J.E., Vicente, J.J., Davis, A.E., Jiang, S.Y., Seo, Y.E., and Zusman, D.R. (2011). FrzS regulates social motility in *Myxococcus xanthus* by controlling exopolysaccharide production. *PLoS One* 6, e23920.

Berleman, J.E., Zemla, M., Remis, J.P., Liu, H., Davis, A.E., Worth, A.N., West, Z., Zhang, A., Park, H., Bosneaga, E., *et al.* (2016). Exopolysaccharide microchannels direct bacterial motility and organize multicellular behavior. *ISME J* 10, 2620-2632.

Berry, J.L., and Pelicic, V. (2015). Exceptionally widespread nanomachines composed of type IV pilins: the prokaryotic Swiss Army knives. *FEMS Microbiol Rev* 39, 134-154.

Bertrand, J.J., West, J.T., and Engel, J.N. (2010). Genetic analysis of the regulation of type IV pilus function by the Chp chemosensory system of *Pseudomonas aeruginosa*. *J Bacteriol* 192, 994-1010.

Bhaya, D., Bianco, N.R., Bryant, D., and Grossman, A. (2000a). Type IV pilus biogenesis and motility in the cyanobacterium *Synechocystis sp.* PCC6803. *Mol Microbiol* 37, 941-951.

Bhaya, D., Takahashi, A., and Grossman, A.R. (2001). Light regulation of type IV pilus-dependent motility by chemosensor-like elements in *Synechocystis* PCC6803. *Proc Natl Acad Sci U S A* 98, 7540-7545.

Bhaya, D., Vaultot, D., Amin, P., Takahashi, A.W., and Grossman, A.R. (2000b). Isolation of regulated genes of the cyanobacterium *Synechocystis sp.* strain PCC 6803 by differential display. *J Bacteriol* 182, 5692-5699.

Bischof, L.F., Friedrich, C., Harms, A., Søgaard-Andersen, L., and van der Does, C. (2016). The Type IV Pilus Assembly ATPase PilB of *Myxococcus xanthus* Interacts with the Inner Membrane Platform Protein PilC and the Nucleotide-binding Protein PilM. *J Biol Chem* 291, 6946-6957.

Black, W.P., Schubot, F.D., Li, Z., and Yang, Z. (2010). Phosphorylation and dephosphorylation among Dif chemosensory proteins essential for exopolysaccharide regulation in *Myxococcus xanthus*. *J Bacteriol* 192, 4267-4274.

Black, W.P., Wang, L., Davis, M.Y., and Yang, Z. (2015). The orphan response regulator EpsW is a substrate of the DifE kinase and it regulates exopolysaccharide in *Myxococcus xanthus*. *Sci Rep* 5, 17831.

Black, W.P., Wang, L., Jing, X., Saldana, R.C., Li, F., Scharf, B.E., Schubot, F.D., and Yang, Z. (2017). The type IV pilus assembly ATPase PilB functions as a signaling protein to regulate exopolysaccharide production in *Myxococcus xanthus*. *Sci Rep* 7, 7263.

Black, W.P., Xu, Q., and Yang, Z. (2006). Type IV pili function upstream of the Dif chemotaxis pathway in *Myxococcus xanthus* EPS regulation. *Mol Microbiol* 61, 447-456.

Black, W.P., and Yang, Z. (2004). *Myxococcus xanthus* chemotaxis homologs DifD and DifG negatively regulate fibril polysaccharide production. *J Bacteriol* 186, 1001-1008.

Blackhart, B.D., and Zusman, D.R. (1985). "Frizzy" genes of *Myxococcus xanthus* are involved in control of frequency of reversal of gliding motility. *Proc Natl Acad Sci U S A* 82, 8767-8770.

Bonazzi, D., Lo Schiavo, V., Machata, S., Djafer-Cherif, I., Nivoit, P., Manriquez, V., Tanimoto, H., Husson, J., Henry, N., Chate, H., *et al.* (2018). Intermittent Pili-Mediated Forces Fluidize *Neisseria meningitidis* Aggregates Promoting Vascular Colonization. *Cell* 174, 143-155 e116.

Boratyn, G.M., Camacho, C., Cooper, P.S., Coulouris, G., Fong, A., Ma, N., Madden, T.L., Matten, W.T., McGinnis, S.D., Merezhuk, Y., *et al.* (2013). BLAST: a more efficient report with usability improvements. *Nucleic Acids Res* 41, W29-33.

- Bos, J.L., Rehmann, H., and Wittinghofer, A. (2007). GEFs and GAPs: critical elements in the control of small G proteins. *Cell* 129, 865-877.
- Briegel, A., Oikonomou, C.M., Chang, Y.W., Kjaer, A., Huang, A.N., Kim, K.W., Ghosal, D., Nguyen, H.H., Kenny, D., Ogorzalek Loo, R.R., *et al.* (2017). Morphology of the archaellar motor and associated cytoplasmic cone in *Thermococcus kodakaraensis*. *EMBO Rep* 18, 1660-1670.
- Buensuceso, R.N.C., Daniel-Ivad, M., Kilmury, S.L.N., Leighton, T.L., Harvey, H., Howell, P.L., and Burrows, L.L. (2017). Cyclic AMP-Independent Control of Twitching Motility in *Pseudomonas aeruginosa*. *J Bacteriol* 199.
- Bulyha, I. (2010). Regulation of type IV pili localization in *Myxococcus xanthus*. (Marburg, Philipps-University).
- Bulyha, I., Lindow, S., Lin, L., Bolte, K., Wuichet, K., Kahnt, J., van der Does, C., Thanbichler, M., and Søgaard-Andersen, L. (2013). Two small GTPases act in concert with the bactofilin cytoskeleton to regulate dynamic bacterial cell polarity. *Dev Cell* 25, 119-131.
- Bulyha, I., Schmidt, C., Lenz, P., Jakovljevic, V., Hone, A., Maier, B., Hoppert, M., and Søgaard-Andersen, L. (2009). Regulation of the type IV pili molecular machine by dynamic localization of two motor proteins. *Mol Microbiol* 74, 691-706.
- Burchard, R.P. (1982). Trail following by gliding bacteria. *J Bacteriol* 152, 495-501.
- Burrows, L.L. (2012). *Pseudomonas aeruginosa* twitching motility: type IV pili in action. *Annu Rev Microbiol* 66, 493-520.
- Bustamante, V.H., Martinez-Flores, I., Vlamakis, H.C., and Zusman, D.R. (2004). Analysis of the Frz signal transduction system of *Myxococcus xanthus* shows the importance of the conserved C-terminal region of the cytoplasmic chemoreceptor FrzCD in sensing signals. *Mol Microbiol* 53, 1501-1513.
- Campbell, E.L., Hagen, K.D., Chen, R., Risser, D.D., Ferreira, D.P., and Meeks, J.C. (2015). Genetic analysis reveals the identity of the photoreceptor for phototaxis in hormogonium filaments of *Nostoc punctiforme*. *J Bacteriol* 197, 782-791.
- Carbonnelle, E., Helaine, S., Nassif, X., and Pelicic, V. (2006). A systematic genetic analysis in *Neisseria meningitidis* defines the Pil proteins required for assembly, functionality, stabilization and export of type IV pili. *Mol Microbiol* 61, 1510-1522.
- Carbonnelle, E., Helaine, S., Prouvensier, L., Nassif, X., and Pelicic, V. (2005). Type IV pilus biogenesis in *Neisseria meningitidis*: PilW is involved in a step occurring after pilus assembly, essential for fibre stability and function. *Mol Microbiol* 55, 54-64.
- Carter, T., Buensuceso, R.N., Tammam, S., Lamers, R.P., Harvey, H., Howell, P.L., and Burrows, L.L. (2017). The Type IVa Pilus Machinery Is Recruited to Sites of Future Cell Division. *MBio* 8.
- Chang, Y.W., Kjaer, A., Ortega, D.R., Kovacicova, G., Sutherland, J.A., Rettberg, L.A., Taylor, R.K., and Jensen, G.J. (2017). Architecture of the *Vibrio cholerae* toxin-coregulated pilus machine revealed by electron cryotomography. *Nat Microbiol* 2, 16269.
- Chang, Y.W., Rettberg, L.A., Treuner-Lange, A., Iwasa, J., Søgaard-Andersen, L., and Jensen, G.J. (2016). Architecture of the type IVa pilus machine. *Science* 351, aad2001.
- Chau, R.M., Bhaya, D., and Huang, K.C. (2017). Emergent Phototactic Responses of Cyanobacteria under Complex Light Regimes. *MBio* 8.

- Chaudhury, P., Neiner, T., D'Imprima, E., Banerjee, A., Reindl, S., Ghosh, A., Arvai, A.S., Mills, D.J., van der Does, C., Tainer, J.A., *et al.* (2016). The nucleotide-dependent interaction of FlaH and FlaI is essential for assembly and function of the archaeellum motor. *Mol Microbiol* **99**, 674-685.
- Chen, I., and Dubnau, D. (2004). DNA uptake during bacterial transformation. *Nat Rev Microbiol* **2**, 241-249.
- Chiang, P., Habash, M., and Burrows, L.L. (2005). Disparate subcellular localization patterns of *Pseudomonas aeruginosa* Type IV pilus ATPases involved in twitching motility. *J Bacteriol* **187**, 829-839.
- Chiang, S.L., Taylor, R.K., Koomey, M., and Mekalanos, J.J. (1995). Single amino acid substitutions in the N-terminus of *Vibrio cholerae* TcpA affect colonization, autoagglutination, and serum resistance. *Mol Microbiol* **17**, 1133-1142.
- Chiou, J.G., Balasubramanian, M.K., and Lew, D.J. (2017). Cell Polarity in Yeast. *Annu Rev Cell Dev Biol* **33**, 77-101.
- Cho, Y.W., Gonzales, A., Harwood, T.V., Huynh, J., Hwang, Y., Park, J.S., Trieu, A.Q., Italia, P., Pallipuram, V.K., and Risser, D.D. (2017). Dynamic localization of HmpF regulates type IV pilus activity and directional motility in the filamentous cyanobacterium *Nostoc punctiforme*. *Mol Microbiol* **106**, 252-265.
- Claessen, D., Rozen, D.E., Kuipers, O.P., Sogaard-Andersen, L., and van Wezel, G.P. (2014). Bacterial solutions to multicellularity: a tale of biofilms, filaments and fruiting bodies. *Nat Rev Microbiol* **12**, 115-124.
- Clausen, M., Jakovljevic, V., Sogaard-Andersen, L., and Maier, B. (2009). High-force generation is a conserved property of type IV pilus systems. *J Bacteriol* **191**, 4633-4638.
- Coureuil, M., Mikaty, G., Miller, F., Lecuyer, H., Bernard, C., Bourdoulous, S., Dumenil, G., Mege, R.M., Weksler, B.B., Romero, I.A., *et al.* (2009). Meningococcal type IV pili recruit the polarity complex to cross the brain endothelium. *Science* **325**, 83-87.
- Cowles, K.N., and Gitai, Z. (2010). Surface association and the MreB cytoskeleton regulate pilus production, localization and function in *Pseudomonas aeruginosa*. *Mol Microbiol* **76**, 1411-1426.
- Cowles, K.N., Moser, T.S., Siryaporn, A., Nyakudarika, N., Dixon, W., Turner, J.J., and Gitai, Z. (2013). The putative Poc complex controls two distinct *Pseudomonas aeruginosa* polar motility mechanisms. *Mol Microbiol* **90**, 923-938.
- Cox, A.D., and Der, C.J. (2010). Ras history: The saga continues. *Small GTPases* **1**, 2-27.
- Craig, L., Forest, K.T., and Maier, B. (2019). Type IV pili: dynamics, biophysics and functional consequences. *Nat Rev Microbiol*.
- Craig, L., Pique, M.E., and Tainer, J.A. (2004). Type IV pilus structure and bacterial pathogenicity. *Nat Rev Microbiol* **2**, 363-378.
- Craig, L., Taylor, R.K., Pique, M.E., Adair, B.D., Arvai, A.S., Singh, M., Lloyd, S.J., Shin, D.S., Getzoff, E.D., Yeager, M., *et al.* (2003). Type IV pilin structure and assembly: X-ray and EM analyses of *Vibrio cholerae* toxin-coregulated pilus and *Pseudomonas aeruginosa* PAK pilin. *Mol Cell* **11**, 1139-1150.

Craig, L., Volkmann, N., Arvai, A.S., Pique, M.E., Yeager, M., Egelman, E.H., and Tainer, J.A. (2006). Type IV pilus structure by cryo-electron microscopy and crystallography: implications for pilus assembly and functions. *Mol Cell* 23, 651-662.

Darzins, A. (1993). The *pilG* gene product, required for *Pseudomonas aeruginosa* pilus production and twitching motility, is homologous to the enteric, single-domain response regulator CheY. *J Bacteriol* 175, 5934-5944.

Darzins, A. (1994). Characterization of a *Pseudomonas aeruginosa* gene cluster involved in pilus biosynthesis and twitching motility: sequence similarity to the chemotaxis proteins of enterics and the gliding bacterium *Myxococcus xanthus*. *Mol Microbiol* 11, 137-153.

Daum, B., and Gold, V. (2018). Twitch or swim: towards the understanding of prokaryotic motion based on the type IV pilus blueprint. *Biol Chem* 399, 799-808.

Daum, B., Vonck, J., Bellack, A., Chaudhury, P., Reichelt, R., Albers, S.V., Rachel, R., and Kuhlbrandt, W. (2017). Structure and in situ organisation of the *Pyrococcus furiosus* archaellum machinery. *Elife* 6.

DeLange, P.A., Collins, T.L., Pierce, G.E., and Robinson, J.B. (2007). PilJ localizes to cell poles and is required for type IV pilus extension in *Pseudomonas aeruginosa*. *Curr Microbiol* 55, 389-395.

Donnenberg, M.S., Zhang, H.Z., and Stone, K.D. (1997). Biogenesis of the bundle-forming pilus of enteropathogenic *Escherichia coli*: reconstitution of fimbriae in recombinant *E. coli* and role of DsbA in pilin stability--a review. *Gene* 192, 33-38.

Ducret, A., Fleuchot, B., Bergam, P., and Mignot, T. (2013). Direct live imaging of cell-cell protein transfer by transient outer membrane fusion in *Myxococcus xanthus*. *Elife* 2, e00868.

Ducret, A., Valignat, M.P., Mouhamar, F., Mignot, T., and Theodoly, O. (2012). Wet-surface-enhanced ellipsometric contrast microscopy identifies slime as a major adhesion factor during bacterial surface motility. *Proc Natl Acad Sci U S A* 109, 10036-10041.

Dunger, G., Llontop, E., Guzzo, C.R., and Farah, C.S. (2016). The *Xanthomonas* type IV pilus. *Curr Opin Microbiol* 30, 88-97.

Ellison, C.K., Dalia, T.N., Vidal Ceballos, A., Wang, J.C., Biais, N., Brun, Y.V., and Dalia, A.B. (2018). Retraction of DNA-bound type IV competence pili initiates DNA uptake during natural transformation in *Vibrio cholerae*. *Nat Microbiol* 3, 773-780.

Ellison, C.K., Kan, J., Dillard, R.S., Kysela, D.T., Ducret, A., Berne, C., Hampton, C.M., Ke, Z., Wright, E.R., Biais, N., *et al.* (2017). Obstruction of pilus retraction stimulates bacterial surface sensing. *Science* 358, 535-538.

Evans, K.J., Lambert, C., and Sockett, R.E. (2007). Predation by *Bdellovibrio bacteriovorus* HD100 requires type IV pili. *J Bacteriol* 189, 4850-4859.

Faure, L.M., Fiche, J.B., Espinosa, L., Ducret, A., Anantharaman, V., Luciano, J., Lhospice, S., Islam, S.T., Treguier, J., Sotes, M., *et al.* (2016). The mechanism of force transmission at bacterial focal adhesion complexes. *Nature* 539, 530-535.

Fink, J.M., and Zissler, J.F. (1989a). Characterization of lipopolysaccharide from *Myxococcus xanthus* by use of monoclonal antibodies. *J Bacteriol* 171, 2028-2032.

Fink, J.M., and Zissler, J.F. (1989b). Defects in motility and development of *Myxococcus xanthus* lipopolysaccharide mutants. *J Bacteriol* 171, 2042-2048.

- Finn, R.D., Coggill, P., Eberhardt, R.Y., Eddy, S.R., Mistry, J., Mitchell, A.L., Potter, S.C., Punta, M., Qureshi, M., Sangrador-Vegas, A., *et al.* (2016). The Pfam protein families database: towards a more sustainable future. *Nucleic Acids Res* **44**, D279-285.
- Friedrich, C., Bulyha, I., and Sogaard-Andersen, L. (2014). Outside-in assembly pathway of the type IV pilus system in *Myxococcus xanthus*. *J Bacteriol* **196**, 378-390.
- Fu, G., Bandaria, J.N., Le Gall, A.V., Fan, X., Yildiz, A., Mignot, T., Zusman, D.R., and Nan, B. (2018). MotAB-like machinery drives the movement of MreB filaments during bacterial gliding motility. *Proc Natl Acad Sci U S A* **115**, 2484-2489.
- Fulcher, N.B., Holliday, P.M., Klem, E., Cann, M.J., and Wolfgang, M.C. (2010). The *Pseudomonas aeruginosa* Chp chemosensory system regulates intracellular cAMP levels by modulating adenylate cyclase activity. *Mol Microbiol* **76**, 889-904.
- Georgiadou, M., Castagnini, M., Karimova, G., Ladant, D., and Pelicic, V. (2012). Large-scale study of the interactions between proteins involved in type IV pilus biology in *Neisseria meningitidis*: characterization of a subcomplex involved in pilus assembly. *Mol Microbiol* **84**, 857-873.
- Giltner, C.L., Habash, M., and Burrows, L.L. (2010). *Pseudomonas aeruginosa* minor pilins are incorporated into type IV pili. *J Mol Biol* **398**, 444-461.
- Giltner, C.L., Nguyen, Y., and Burrows, L.L. (2012). Type IV pilin proteins: versatile molecular modules. *Microbiol Mol Biol Rev* **76**, 740-772.
- Goldman, B.S., Nierman, W.C., Kaiser, D., Slater, S.C., Durkin, A.S., Eisen, J.A., Ronning, C.M., Barbazuk, W.B., Blanchard, M., Field, C., *et al.* (2006). Evolution of sensory complexity recorded in a myxobacterial genome. *Proc Natl Acad Sci U S A* **103**, 15200-15205.
- Gresock, M.G., Kastead, K.A., and Postle, K. (2015). From Homodimer to Heterodimer and Back: Elucidating the TonB Energy Transduction Cycle. *J Bacteriol* **197**, 3433-3445.
- Guzzo, C.R., Dunger, G., Salinas, R.K., and Farah, C.S. (2013). Structure of the PilZ-FimXEAL-c-di-GMP Complex Responsible for the Regulation of Bacterial Type IV Pilus Biogenesis. *J Mol Biol* **425**, 2174-2197.
- Guzzo, C.R., Salinas, R.K., Andrade, M.O., and Farah, C.S. (2009). PILZ protein structure and interactions with PILB and the FIMX EAL domain: implications for control of type IV pilus biogenesis. *J Mol Biol* **393**, 848-866.
- Guzzo, M., Agrebi, R., Espinosa, L., Baronian, G., Molle, V., Mauriello, E.M., Brochier-Armanet, C., and Mignot, T. (2015). Evolution and Design Governing Signal Precision and Amplification in a Bacterial Chemosensory Pathway. *PLoS Genet* **11**, e1005460.
- Guzzo, M., Murray, S.M., Martineau, E., Lhospice, S., Baronian, G., My, L., Zhang, Y., Espinosa, L., Vincentelli, R., Bratton, B.P., *et al.* (2018). A gated relaxation oscillator mediated by FrzX controls morphogenetic movements in *Myxococcus xanthus*. *Nat Microbiol* **3**, 948-959.
- Hager, A.J., Bolton, D.L., Pelletier, M.R., Brittnacher, M.J., Gallagher, L.A., Kaul, R., Skerrett, S.J., Miller, S.I., and Guina, T. (2006). Type IV pili-mediated secretion modulates *Francisella* virulence. *Mol Microbiol* **62**, 227-237.
- Han, X., Kennan, R.M., Parker, D., Davies, J.K., and Rood, J.I. (2007). Type IV fimbrial biogenesis is required for protease secretion and natural transformation in *Dichelobacter nodosus*. *J Bacteriol* **189**, 5022-5033.
- Harman, J.G. (2001). Allosteric regulation of the cAMP receptor protein. *Biochim Biophys Acta* **1547**, 1-17.

- Hartung, S., Arvai, A.S., Wood, T., Kolappan, S., Shin, D.S., Craig, L., and Tainer, J.A. (2011). Ultrahigh resolution and full-length pilin structures with insights for filament assembly, pathogenic functions, and vaccine potential. *J Biol Chem* 286, 44254-44265.
- He, K., and Bauer, C.E. (2014). Chemosensory signaling systems that control bacterial survival. *Trends Microbiol* 22, 389-398.
- Helaine, S., Carbonnelle, E., Prouvensier, L., Beretti, J.L., Nassif, X., and Pelicic, V. (2005). PilX, a pilus-associated protein essential for bacterial aggregation, is a key to pilus-facilitated attachment of *Neisseria meningitidis* to human cells. *Mol Microbiol* 55, 65-77.
- Helaine, S., Dyer, D.H., Nassif, X., Pelicic, V., and Forest, K.T. (2007). 3D structure/function analysis of PilX reveals how minor pilins can modulate the virulence properties of type IV pili. *Proc Natl Acad Sci U S A* 104, 15888-15893.
- Hendrick, W.A., Orr, M.W., Murray, S.R., Lee, V.T., and Melville, S.B. (2017). Cyclic Di-GMP Binding by an Assembly ATPase (PilB2) and Control of Type IV Pilin Polymerization in the Gram-Positive Pathogen *Clostridium perfringens*. *J Bacteriol* 199.
- Hengge, R. (2009). Principles of c-di-GMP signalling in bacteria. *Nat Rev Microbiol* 7, 263-273.
- Hobbs, M., and Mattick, J.S. (1993). Common components in the assembly of type 4 fimbriae, DNA transfer systems, filamentous phage and protein-secretion apparatus: a general system for the formation of surface-associated protein complexes. *Mol Microbiol* 10, 233-243.
- Hobley, L., Fung, R.K., Lambert, C., Harris, M.A., Dabhi, J.M., King, S.S., Basford, S.M., Uchida, K., Till, R., Ahmad, R., et al. (2012). Discrete cyclic di-GMP-dependent control of bacterial predation versus axenic growth in *Bdellovibrio bacteriovorus*. *PLoS Pathog* 8, e1002493.
- Hodgkin, J., and Kaiser, D. (1977). Cell-to-cell stimulation of movement in nonmotile mutants of *Myxococcus*. *Proc Natl Acad Sci U S A* 74, 2938-2942.
- Hodgkin, J., and Kaiser, D. (1979). Genetics of gliding motility in *Myxococcus xanthus* (Myxobacteriales): Two gene systems control movement. *Mol Gen Genetics* 171, 177-191.
- Hospenthal, M.K., Costa, T.R.D., and Waksman, G. (2017). A comprehensive guide to pilus biogenesis in Gram-negative bacteria. *Nat Rev Microbiol* 15, 365-379.
- Hu, W., Hossain, M., Lux, R., Wang, J., Yang, Z., Li, Y., and Shi, W. (2011). Exopolysaccharide-independent social motility of *Myxococcus xanthus*. *PLoS One* 6, e16102.
- Hu, W., Yang, Z., Lux, R., Zhao, M., Wang, J., He, X., and Shi, W. (2012). Direct visualization of the interaction between pilin and exopolysaccharides of *Myxococcus xanthus* with eGFP-fused PilA protein. *FEMS Microbiol Lett* 326, 23-30.
- Inclan, Y.F., Laurent, S., and Zusman, D.R. (2008). The receiver domain of FrzE, a CheA-CheY fusion protein, regulates the CheA histidine kinase activity and downstream signalling to the A- and S-motility systems of *Myxococcus xanthus*. *Mol Microbiol* 68, 1328-1339.
- Inclan, Y.F., Persat, A., Greninger, A., Von Dollen, J., Johnson, J., Krogan, N., Gitai, Z., and Engel, J.N. (2016). A scaffold protein connects type IV pili with the Chp chemosensory system to mediate activation of virulence signaling in *Pseudomonas aeruginosa*. *Mol Microbiol* 101, 590-605.
- Islam, S.T., and Mignot, T. (2015). The mysterious nature of bacterial surface (gliding) motility: A focal adhesion-based mechanism in *Myxococcus xanthus*. *Semin Cell Dev Biol* 46, 143-154.

- Jain, R., Sliusarenko, O., and Kazmierczak, B.I. (2017). Interaction of the cyclic-di-GMP binding protein FimX and the Type 4 pilus assembly ATPase promotes pilus assembly. *PLoS Pathog* 13, e1006594.
- Jakobczak, B., Keilberg, D., Wuichet, K., and Søgaard-Andersen, L. (2015). Contact- and Protein Transfer-Dependent Stimulation of Assembly of the Gliding Motility Machinery in *Myxococcus xanthus*. *PLoS Genet* 11, e1005341.
- Jakovljevic, V., Leonardy, S., Hoppert, M., and Søgaard-Andersen, L. (2008). PilB and PilT are ATPases acting antagonistically in type IV pilus function in *Myxococcus xanthus*. *J Bacteriol* 190, 2411-2421.
- Jelsbak, L., and Søgaard-Andersen, L. (2002). Pattern formation by a cell surface-associated morphogen in *Myxococcus xanthus*. *Proc Natl Acad Sci U S A* 99, 2032-2037.
- Johnson, M.D., Garrett, C.K., Bond, J.E., Coggan, K.A., Wolfgang, M.C., and Redinbo, M.R. (2011). *Pseudomonas aeruginosa* PilY1 binds integrin in an RGD- and calcium-dependent manner. *PLoS One* 6, e29629.
- Jones, C.J., Utada, A., Davis, K.R., Thongsomboon, W., Zamorano Sanchez, D., Banakar, V., Cegelski, L., Wong, G.C., and Yildiz, F.H. (2015). C-di-GMP Regulates Motile to Sessile Transition by Modulating MshA Pili Biogenesis and Near-Surface Motility Behavior in *Vibrio cholerae*. *PLoS Pathog* 11, e1005068.
- Jonsson, A.B., Nyberg, G., and Normark, S. (1991). Phase variation of gonococcal pili by frameshift mutation in *pilC*, a novel gene for pilus assembly. *EMBO J* 10, 477-488.
- Julien, B., Kaiser, A.D., and Garza, A. (2000). Spatial control of cell differentiation in *Myxococcus xanthus*. *Proc Natl Acad Sci U S A* 97, 9098-9103.
- Kahnt, J., Aguiluz, K., Koch, J., Treuner-Lange, A., Konovalova, A., Huntley, S., Hoppert, M., Søgaard-Andersen, L., and Hedderich, R. (2010). Profiling the outer membrane proteome during growth and development of the social bacterium *Myxococcus xanthus* by selective biotinylation and analyses of outer membrane vesicles. *J Proteome Res* 9, 5197-5208.
- Kaimer, C., and Zusman, D.R. (2016). Regulation of cell reversal frequency in *Myxococcus xanthus* requires the balanced activity of CheY-like domains in FrzE and FrzZ. *Mol Microbiol* 100, 379-395.
- Kaiser, D. (1979). Social gliding is correlated with the presence of pili in *Myxococcus xanthus*. *Proc Natl Acad Sci U S A* 76, 5952-5956.
- Kanehisa, M., and Goto, S. (2000). KEGG: kyoto encyclopedia of genes and genomes. *Nucleic Acids Res* 28, 27-30.
- Kaplan, H.B., Kuspa, A., and Kaiser, D. (1991). Suppressors that permit A-signal-independent developmental gene expression in *Myxococcus xanthus*. *J Bacteriol* 173, 1460-1470.
- Karimova, G., Pidoux, J., Ullmann, A., and Ladant, D. (1998). A bacterial two-hybrid system based on a reconstituted signal transduction pathway. *Proc Natl Acad Sci U S A* 95, 5752-5756.
- Karuppiah, V., and Derrick, J.P. (2011). Structure of the PilM-PilN inner membrane type IV pilus biogenesis complex from *Thermus thermophilus*. *J Biol Chem* 286, 24434-24442.
- Karuppiah, V., Hassan, D., Saleem, M., and Derrick, J.P. (2010). Structure and oligomerization of the PilC type IV pilus biogenesis protein from *Thermus thermophilus*. *Proteins* 78, 2049-2057.

- Kazmierczak, B.I., Lebron, M.B., and Murray, T.S. (2006). Analysis of FimX, a phosphodiesterase that governs twitching motility in *Pseudomonas aeruginosa*. *Mol Microbiol* 60, 1026-1043.
- Keane, R., and Berleman, J. (2016). The predatory life cycle of *Myxococcus xanthus*. *Microbiology* 162, 1-11.
- Keilberg, D. (2013). Regulation of motility and polarity in *Myxococcus xanthus*. (Marburg, Philipps-University).
- Keilberg, D., and Søgaard-Andersen, L. (2014). Regulation of bacterial cell polarity by small GTPases. *Biochemistry* 53, 1899-1907.
- Keilberg, D., Wuichet, K., Drescher, F., and Søgaard-Andersen, L. (2012). A response regulator interfaces between the Frz chemosensory system and the MglA/MglB GTPase/GAP module to regulate polarity in *Myxococcus xanthus*. *PLoS Genet* 8, e1002951.
- Khayatan, B., Meeks, J.C., and Risser, D.D. (2015). Evidence that a modified type IV pilus-like system powers gliding motility and polysaccharide secretion in filamentous cyanobacteria. *Mol Microbiol* 98, 1021-1036.
- Kirn, T.J., Bose, N., and Taylor, R.K. (2003). Secretion of a soluble colonization factor by the TCP type 4 pilus biogenesis pathway in *Vibrio cholerae*. *Mol Microbiol* 49, 81-92.
- Klausen, M., Aaes-Jorgensen, A., Molin, S., and Tolker-Nielsen, T. (2003). Involvement of bacterial migration in the development of complex multicellular structures in *Pseudomonas aeruginosa* biofilms. *Mol Microbiol* 50, 61-68.
- Kolappan, S., Coureuil, M., Yu, X., Nassif, X., Egelman, E.H., and Craig, L. (2016). Structure of the *Neisseria meningitidis* Type IV pilus. *Nat Commun* 7, 13015.
- Konovalova, A., Petters, T., and Søgaard-Andersen, L. (2010). Extracellular biology of *Myxococcus xanthus*. *FEMS Microbiol Rev* 34, 89-106.
- Korotkov, K.V., Sandkvist, M., and Hol, W.G. (2012). The type II secretion system: biogenesis, molecular architecture and mechanism. *Nat Rev Microbiol* 10, 336-351.
- Kozubowski, L., Saito, K., Johnson, J.M., Howell, A.S., Zyla, T.R., and Lew, D.J. (2008). Symmetry-breaking polarization driven by a Cdc42p GEF-PAK complex. *Curr Biol* 18, 1719-1726.
- Kuchma, S.L., Ballok, A.E., Merritt, J.H., Hammond, J.H., Lu, W., Rabinowitz, J.D., and O'Toole, G.A. (2010). Cyclic-di-GMP-mediated repression of swarming motility by *Pseudomonas aeruginosa*: the *pilY1* gene and its impact on surface-associated behaviors. *J Bacteriol* 192, 2950-2964.
- Kuchma, S.L., Griffin, E.F., and O'Toole, G.A. (2012). Minor pilins of the type IV pilus system participate in the negative regulation of swarming motility. *J Bacteriol* 194, 5388-5403.
- Laemmli, U.K. (1970). Cleavage of structural proteins during the assembly of the head of bacteriophage T4. *Nature* 227, 680-685.
- Lambert, C., Evans, K.J., Till, R., Hogley, L., Capeness, M., Rendulic, S., Schuster, S.C., Aizawa, S., and Sockett, R.E. (2006). Characterizing the flagellar filament and the role of motility in bacterial prey-penetration by *Bdellovibrio bacteriovorus*. *Mol Microbiol* 60, 274-286.
- Lambert, C., Fenton, A.K., Hogley, L., and Sockett, R.E. (2011). Predatory *Bdellovibrio* bacteria use gliding motility to scout for prey on surfaces. *J Bacteriol* 193, 3139-3141.
- Lancero, H., Caberoy, N.B., Castaneda, S., Li, Y., Lu, A., Dutton, D., Duan, X.Y., Kaplan, H.B., Shi, W., and Garza, A.G. (2004). Characterization of a *Myxococcus xanthus* mutant that is defective for adventurous motility and social motility. *Microbiology* 150, 4085-4093.

- Laventie, B.J., Sangermani, M., Estermann, F., Manfredi, P., Planes, R., Hug, I., Jaeger, T., Meunier, E., Broz, P., and Jenal, U. (2019). A Surface-Induced Asymmetric Program Promotes Tissue Colonization by *Pseudomonas aeruginosa*. *Cell Host Microbe* 25, 140-152 e146.
- Leech, A.J., and Mattick, J.S. (2006). Effect of site-specific mutations in different phosphotransfer domains of the chemosensory protein ChpA on *Pseudomonas aeruginosa* motility. *J Bacteriol* 188, 8479-8486.
- Leighton, T.L., Buensuceso, R.N., Howell, P.L., and Burrows, L.L. (2015). Biogenesis of *Pseudomonas aeruginosa* type IV pili and regulation of their function. *Environ Microbiol* 17, 4148-4163.
- Lemkul, J.A., and Bevan, D.R. (2011). Characterization of interactions between PilA from *Pseudomonas aeruginosa* strain K and a model membrane. *J Phys Chem B* 115, 8004-8008.
- Leonardy, S., Bulyha, I., and S ogaard-Andersen, L. (2008). Reversing cells and oscillating motility proteins. *Mol Biosyst* 4, 1009-1014.
- Leonardy, S., Freymark, G., Hebener, S., Ellehauge, E., and S ogaard-Andersen, L. (2007). Coupling of protein localization and cell movements by a dynamically localized response regulator in *Myxococcus xanthus*. *EMBO J* 26, 4433-4444.
- Leonardy, S., Miertzschke, M., Bulyha, I., Sperling, E., Wittinghofer, A., and S ogaard-Andersen, L. (2010). Regulation of dynamic polarity switching in bacteria by a Ras-like G-protein and its cognate GAP. *EMBO J* 29, 2276-2289.
- Li, W., Cowley, A., Uludag, M., Gur, T., McWilliam, H., Squizzato, S., Park, Y.M., Buso, N., and Lopez, R. (2015). The EMBL-EBI bioinformatics web and programmatic tools framework. *Nucleic Acids Res* 43, W580-584.
- Li, Y., Bustamante, V.H., Lux, R., Zusman, D., and Shi, W. (2005). Divergent regulatory pathways control A and S motility in *Myxococcus xanthus* through FrzE, a CheA-CheY fusion protein. *J Bacteriol* 187, 1716-1723.
- Li, Y., Sun, H., Ma, X., Lu, A., Lux, R., Zusman, D., and Shi, W. (2003). Extracellular polysaccharides mediate pilus retraction during social motility of *Myxococcus xanthus*. *Proc Natl Acad Sci U S A* 100, 5443-5448.
- Lu, A., Cho, K., Black, W.P., Duan, X.Y., Lux, R., Yang, Z., Kaplan, H.B., Zusman, D.R., and Shi, W. (2005). Exopolysaccharide biosynthesis genes required for social motility in *Myxococcus xanthus*. *Mol Microbiol* 55, 206-220.
- Luciano, J., Agrebi, R., Le Gall, A.V., Wartel, M., Fiegna, F., Ducret, A., Brochier-Armanet, C., and Mignot, T. (2011). Emergence and modular evolution of a novel motility machinery in bacteria. *PLoS Genet* 7, e1002268.
- Luo, Y., Zhao, K., Baker, A.E., Kuchma, S.L., Coggan, K.A., Wolfgang, M.C., Wong, G.C., and O'Toole, G.A. (2015). A hierarchical cascade of second messengers regulates *Pseudomonas aeruginosa* surface behaviors. *MBio* 6.
- Lyons, N.A., and Kolter, R. (2015). On the evolution of bacterial multicellularity. *Curr Opin Microbiol* 24, 21-28.
- Martin, P.R., Watson, A.A., McCaul, T.F., and Mattick, J.S. (1995). Characterization of a five-gene cluster required for the biogenesis of type 4 fimbriae in *Pseudomonas aeruginosa*. *Mol Microbiol* 16, 497-508.
- Mattick, J.S. (2002). Type IV pili and twitching motility. *Annu Rev Microbiol* 56, 289-314.

Mauriello, E.M. (2010). Cell polarity/motility in bacteria: closer to eukaryotes than expected? *EMBO J* 29, 2258-2259.

McBride, M.J., and Zusman, D.R. (1996). Behavioral analysis of single cells of *Myxococcus xanthus* in response to prey cells of *Escherichia coli*. *FEMS Microbiol Lett* 137, 227-231.

McCallum, M., Tammam, S., Khan, A., Burrows, L.L., and Howell, P.L. (2017). The molecular mechanism of the type IVa pilus motors. *Nat Commun* 8, 15091.

McDonough, K.A., and Rodriguez, A. (2011). The myriad roles of cyclic AMP in microbial pathogens: from signal to sword. *Nat Rev Microbiol* 10, 27-38.

McLoon, A.L., Wuichet, K., Hasler, M., Keilberg, D., Szadkowski, D., and Sogaard-Andersen, L. (2016). MglC, a Paralog of *Myxococcus xanthus* GTPase-Activating Protein MglB, Plays a Divergent Role in Motility Regulation. *J Bacteriol* 198, 510-520.

Merighi, M., Lee, V.T., Hyodo, M., Hayakawa, Y., and Lory, S. (2007). The second messenger bis-(3'-5')-cyclic-GMP and its PilZ domain-containing receptor Alg44 are required for alginate biosynthesis in *Pseudomonas aeruginosa*. *Mol Microbiol* 65, 876-895.

Merz, A.J., So, M., and Sheetz, M.P. (2000). Pilus retraction powers bacterial twitching motility. *Nature* 407, 98-102.

Meshcheryakov, V.A., and Wolf, M. (2016). Crystal structure of the flagellar accessory protein FlaH of *Methanocaldococcus jannaschii* suggests a regulatory role in archaeal flagellum assembly. *Protein Sci* 25, 1147-1155.

Miertzschke, M., Koerner, C., Vetter, I.R., Keilberg, D., Hot, E., Leonardy, S., Sogaard-Andersen, L., and Wittinghofer, A. (2011). Structural analysis of the Ras-like G protein MglA and its cognate GAP MglB and implications for bacterial polarity. *EMBO J* 30, 4185-4197.

Mignot, T. (2007). The elusive engine in *Myxococcus xanthus* gliding motility. *Cell Mol Life Sci* 64, 2733-2745.

Mignot, T., Merlie, J.P., Jr., and Zusman, D.R. (2005). Regulated pole-to-pole oscillations of a bacterial gliding motility protein. *Science* 310, 855-857.

Mignot, T., Merlie, J.P., Jr., and Zusman, D.R. (2007). Two localization motifs mediate polar residence of FrzS during cell movement and reversals of *Myxococcus xanthus*. *Mol Microbiol* 65, 363-372.

Milner, D.S., Till, R., Cadby, I., Lovering, A.L., Basford, S.M., Saxon, E.B., Liddell, S., Williams, L.E., and Sockett, R.E. (2014). Ras GTPase-like protein MglA, a controller of bacterial social-motility in Myxobacteria, has evolved to control bacterial predation by *Bdellovibrio*. *PLoS Genet* 10, e1004253.

Muller, F.D., Treuner-Lange, A., Heider, J., Huntley, S.M., and Higgs, P.I. (2010). Global transcriptome analysis of spore formation in *Myxococcus xanthus* reveals a locus necessary for cell differentiation. *BMC Genomics* 11, 264.

Munoz-Dorado, J., Marcos-Torres, F.J., Garcia-Bravo, E., Moraleda-Munoz, A., and Perez, J. (2016). Myxobacteria: Moving, Killing, Feeding, and Surviving Together. *Front Microbiol* 7, 781.

Nakane, D., and Nishizaka, T. (2017). Asymmetric distribution of type IV pili triggered by directional light in unicellular cyanobacteria. *Proc Natl Acad Sci U S A* 114, 6593-6598.

- Nan, B., Mauriello, E.M., Sun, I.H., Wong, A., and Zusman, D.R. (2010). A multi-protein complex from *Myxococcus xanthus* required for bacterial gliding motility. *Mol Microbiol* 76, 1539-1554.
- Navarro, M.V., De, N., Bae, N., Wang, Q., and Sondermann, H. (2009). Structural analysis of the GGDEF-EAL domain-containing c-di-GMP receptor FimX. *Structure* 17, 1104-1116.
- Ng, D., Harn, T., Altindal, T., Kolappan, S., Marles, J.M., Lala, R., Spielman, I., Gao, Y., Hauke, C.A., Kovacikova, G., et al. (2016). The *Vibrio cholerae* Minor Pilin TcpB Initiates Assembly and Retraction of the Toxin-Coregulated Pilus. *PLoS Pathog* 12, e1006109.
- Nguyen, Y., Sugiman-Marangos, S., Harvey, H., Bell, S.D., Charlton, C.L., Junop, M.S., and Burrows, L.L. (2015). *Pseudomonas aeruginosa* minor pilins prime type IVa pilus assembly and promote surface display of the PilY1 adhesin. *J Biol Chem* 290, 601-611.
- Nivaskumar, M., Bouvier, G., Campos, M., Nadeau, N., Yu, X., Egelman, E.H., Nilges, M., and Francetic, O. (2014). Distinct docking and stabilization steps of the Pseudopilus conformational transition path suggest rotational assembly of type IV pilus-like fibers. *Structure* 22, 685-696.
- Nunn, D.N., and Lory, S. (1991). Product of the *Pseudomonas aeruginosa* gene *pilD* is a prepilin leader peptidase. *Proc Natl Acad Sci U S A* 88, 3281-3285.
- O'Connor, K.A., and Zusman, D.R. (1991a). Behavior of peripheral rods and their role in the life cycle of *Myxococcus xanthus*. *J Bacteriol* 173, 3342-3355.
- O'Connor, K.A., and Zusman, D.R. (1991b). Development in *Myxococcus xanthus* involves differentiation into two cell types, peripheral rods and spores. *J Bacteriol* 173, 3318-3333.
- O'Toole, G.A., and Kolter, R. (1998). Flagellar and twitching motility are necessary for *Pseudomonas aeruginosa* biofilm development. *Mol Microbiol* 30, 295-304.
- Oliveira, N.M., Foster, K.R., and Durham, W.M. (2016). Single-cell twitching chemotaxis in developing biofilms. *Proc Natl Acad Sci U S A* 113, 6532-6537.
- Overgaard, M., Wegener-Feldbrugge, S., and Søgaard-Andersen, L. (2006). The orphan response regulator DigR is required for synthesis of extracellular matrix fibrils in *Myxococcus xanthus*. *J Bacteriol* 188, 4384-4394.
- Paintdakhi, A., Parry, B., Campos, M., Irnov, I., Elf, J., Surovtsev, I., and Jacobs-Wagner, C. (2016). Oufiti: an integrated software package for high-accuracy, high-throughput quantitative microscopy analysis. *Mol Microbiol* 99, 767-777.
- Parge, H.E., Forest, K.T., Hickey, M.J., Christensen, D.A., Getzoff, E.D., and Tainer, J.A. (1995). Structure of the fibre-forming protein pilin at 2.6 Å resolution. *Nature* 378, 32-38.
- Peabody, C.R., Chung, Y.J., Yen, M.R., Vidal-Ingigliardi, D., Pugsley, A.P., and Saier, M.H., Jr. (2003). Type II protein secretion and its relationship to bacterial type IV pili and archaeal flagella. *Microbiology* 149, 3051-3072.
- Pellicic, V. (2008). Type IV pili: e pluribus unum? *Mol Microbiol* 68, 827-837.
- Pérez-Burgos, M., García-Romero, I., Jung, J., Valvano, M.A., and Søgaard-Andersen, L. (2019). Identification of the lipopolysaccharide O-antigen biosynthesis priming enzyme and the O-antigen ligase in *Myxococcus xanthus*: critical role of LPS O-antigen in motility and development. *Mol Microbiol*.
- Pérez, J., Jimenez-Zurdo, J.I., Martinez-Abarca, F., Millan, V., Shimkets, L.J., and Muñoz-Dorado, J. (2014). Rhizobial galactoglucan determines the predatory pattern of *Myxococcus xanthus* and protects *Sinorhizobium meliloti* from predation. *Environ Microbiol* 16, 2341-2350.

- Persat, A., Inclan, Y.F., Engel, J.N., Stone, H.A., and Gitai, Z. (2015). Type IV pili mechanochemically regulate virulence factors in *Pseudomonas aeruginosa*. *Proc Natl Acad Sci U S A* 112, 7563-7568.
- Petters, T., Zhang, X., Nesper, J., Treuner-Lange, A., Gomez-Santos, N., Hoppert, M., Jenal, U., and Søgaard-Andersen, L. (2012). The orphan histidine protein kinase SgmT is a c-di-GMP receptor and regulates composition of the extracellular matrix together with the orphan DNA binding response regulator DigR in *Myxococcus xanthus*. *Mol Microbiol* 84, 147-165.
- Pham, V.D., Shebelut, C.W., Mukherjee, B., and Singer, M. (2005). RasA is required for *Myxococcus xanthus* development and social motility. *J Bacteriol* 187, 6845-6848.
- Planet, P.J., Kachlany, S.C., DeSalle, R., and Figurski, D.H. (2001). Phylogeny of genes for secretion NTPases: identification of the widespread *tadA* subfamily and development of a diagnostic key for gene classification. *Proc Natl Acad Sci U S A* 98, 2503-2508.
- Qi, Y., Xu, L., Dong, X., Yau, Y.H., Ho, C.L., Koh, S.L., Shochat, S.G., Chou, S.H., Tang, K., and Liang, Z.X. (2012). Functional divergence of FimX in PilZ binding and type IV pilus regulation. *J Bacteriol* 194, 5922-5931.
- Raetz, C.R., and Whitfield, C. (2002). Lipopolysaccharide endotoxins. *Annu Rev Biochem* 71, 635-700.
- Rakotoarivonina, H., Jubelin, G., Hebraud, M., Gaillard-Martinie, B., Forano, E., and Mosoni, P. (2002). Adhesion to cellulose of the Gram-positive bacterium *Ruminococcus albus* involves type IV pili. *Microbiology* 148, 1871-1880.
- Reindl, S., Ghosh, A., Williams, G.J., Lassak, K., Neiner, T., Henche, A.L., Albers, S.V., and Tainer, J.A. (2013). Insights into Flal functions in archaeal motor assembly and motility from structures, conformations, and genetics. *Mol Cell* 49, 1069-1082.
- Risser, D.D., and Meeks, J.C. (2013). Comparative transcriptomics with a motility-deficient mutant leads to identification of a novel polysaccharide secretion system in *Nostoc punctiforme*. *Mol Microbiol* 87, 884-893.
- Römling, U., Galperin, M.Y., and Gomelsky, M. (2013). Cyclic di-GMP: the first 25 years of a universal bacterial second messenger. *Microbiol Mol Biol Rev* 77, 1-52.
- Ruan, J. (2013). [Bergey's Manual of Systematic Bacteriology (second edition) Volume 5 and the study of Actinomycetes systematic in China]. *Wei Sheng Wu Xue Bao* 53, 521-530.
- Rumszauer, J., Schwarzenlander, C., and Averhoff, B. (2006). Identification, subcellular localization and functional interactions of PilMNOWQ and PilA4 involved in transformation competency and pilus biogenesis in the thermophilic bacterium *Thermus thermophilus* HB27. *FEBS J* 273, 3261-3272.
- Salzer, R., Herzberg, M., Nies, D.H., Joos, F., Rathmann, B., Thielmann, Y., and Averhoff, B. (2014a). Zinc and ATP binding of the hexameric AAA-ATPase PilF from *Thermus thermophilus*: role in complex stability, piliation, adhesion, twitching motility, and natural transformation. *J Biol Chem* 289, 30343-30354.
- Salzer, R., Joos, F., and Averhoff, B. (2014b). Type IV pilus biogenesis, twitching motility, and DNA uptake in *Thermus thermophilus*: discrete roles of antagonistic ATPases PilF, PilT1, and PilT2. *Appl Environ Microbiol* 80, 644-652.
- Salzer, R., Joos, F., and Averhoff, B. (2015). Different effects of MglA and MglB on pilus-mediated functions and natural competence in *Thermus thermophilus*. *Extremophiles* 19, 261-267.

- Savvides, S.N. (2007). Secretion superfamily ATPases swing big. *Structure* 15, 255-257.
- Schuerger, N., Nurnberg, D.J., Wallner, T., Mullineaux, C.W., and Wilde, A. (2015). PilB localization correlates with the direction of twitching motility in the cyanobacterium *Synechocystis* sp. PCC 6803. *Microbiology* 161, 960-966.
- Schumacher, D., and Søgaard-Andersen, L. (2017). Regulation of Cell Polarity in Motility and Cell Division in *Myxococcus xanthus*. *Annu Rev Microbiol* 71, 61-78.
- Schwanhausser, B., Busse, D., Li, N., Dittmar, G., Schuchhardt, J., Wolf, J., Chen, W., and Selbach, M. (2011). Global quantification of mammalian gene expression control. *Nature* 473, 337-342.
- Scott, A.E., Simon, E., Park, S.K., Andrews, P., and Zusman, D.R. (2008). Site-specific receptor methylation of FrzCD in *Myxococcus xanthus* is controlled by a tetra-trico peptide repeat (TPR) containing regulatory domain of the FrzF methyltransferase. *Mol Microbiol* 69, 724-735.
- Selkrig, J., Mosbahi, K., Webb, C.T., Belousoff, M.J., Perry, A.J., Wells, T.J., Morris, F., Leyton, D.L., Totsika, M., Phan, M.D., *et al.* (2012). Discovery of an archetypal protein transport system in bacterial outer membranes. *Nat Struct Mol Biol* 19, 506-510, S501.
- Shevchik, V.E., Robert-Baudouy, J., and Condemine, G. (1997). Specific interaction between OutD, an *Erwinia chrysanthemi* outer membrane protein of the general secretory pathway, and secreted proteins. *EMBO J* 16, 3007-3016.
- Shi, W., and Zusman, D.R. (1993). The two motility systems of *Myxococcus xanthus* show different selective advantages on various surfaces. *Proc Natl Acad Sci U S A* 90, 3378-3382.
- Shi, X., Wegener-Feldbrugge, S., Huntley, S., Hamann, N., Hedderich, R., and Søgaard-Andersen, L. (2008). Bioinformatics and experimental analysis of proteins of two-component systems in *Myxococcus xanthus*. *J Bacteriol* 190, 613-624.
- Shimkets, L.J. (1986a). Correlation of energy-dependent cell cohesion with social motility in *Myxococcus xanthus*. *J Bacteriol* 166, 837-841.
- Shimkets, L.J. (1986b). Role of cell cohesion in *Myxococcus xanthus* fruiting body formation. *J Bacteriol* 166, 842-848.
- Shimkets, L.J., and Kaiser, D. (1982). Induction of coordinated movement of *Myxococcus xanthus* cells. *J Bacteriol* 152, 451-461.
- Siewering, K., Jain, S., Friedrich, C., Webber-Birungi, M.T., Semchonok, D.A., Binzen, I., Wagner, A., Huntley, S., Kahnt, J., Klingl, A., *et al.* (2014). Peptidoglycan-binding protein Tsap functions in surface assembly of type IV pili. *Proc Natl Acad Sci U S A* 111, E953-961.
- Skerker, J.M., and Berg, H.C. (2001). Direct observation of extension and retraction of type IV pili. *Proc Natl Acad Sci U S A* 98, 6901-6904.
- Skotnicka, D. (2016). Regulation by cyclic di-GMP in *Myxococcus xanthus*. (Marburg, Philipps-University).
- Skotnicka, D., Petters, T., Heering, J., Hoppert, M., Kaeffer, V., and Søgaard-Andersen, L. (2016). Cyclic Di-GMP Regulates Type IV Pilus-Dependent Motility in *Myxococcus xanthus*. *J Bacteriol* 198, 77-90.
- Søgaard-Andersen, L. (2004). Cell polarity, intercellular signalling and morphogenetic cell movements in *Myxococcus xanthus*. *Curr Opin Microbiol* 7, 587-593.
- Sondermann, H., Shikuma, N.J., and Yildiz, F.H. (2012). You've come a long way: c-di-GMP signaling. *Curr Opin Microbiol* 15, 140-146.

Sonnhammer, E.L., von Heijne, G., and Krogh, A. (1998). A hidden Markov model for predicting transmembrane helices in protein sequences. *Proc Int Conf Intell Syst Mol Biol* 6, 175-182.

Starruss, J., Peruani, F., Jakovljevic, V., Søgaard-Andersen, L., Deutsch, A., and Bar, M. (2012). Pattern-formation mechanisms in motility mutants of *Myxococcus xanthus*. *Interface Focus* 2, 774-785.

Stingl, K., Muller, S., Scheidgen-Kleyboldt, G., Clausen, M., and Maier, B. (2010). Composite system mediates two-step DNA uptake into *Helicobacter pylori*. *Proc Natl Acad Sci U S A* 107, 1184-1189.

Strom, M.S., and Lory, S. (1987). Mapping of export signals of *Pseudomonas aeruginosa* pilin with alkaline phosphatase fusions. *J Bacteriol* 169, 3181-3188.

Sun, H., Zusman, D.R., and Shi, W. (2000). Type IV pilus of *Myxococcus xanthus* is a motility apparatus controlled by the frz chemosensory system. *Curr Biol* 10, 1143-1146.

Sun, M., Wartel, M., Cascales, E., Shaevitz, J.W., and Mignot, T. (2011). Motor-driven intracellular transport powers bacterial gliding motility. *Proc Natl Acad Sci U S A* 108, 7559-7564.

Sutherland, I.W., and Thomson, S. (1975). Comparison of polysaccharides produced by *Myxococcus* strains. *J Gen Microbiol* 89, 124-132.

Szabo, Z., Stahl, A.O., Albers, S.V., Kissinger, J.C., Driessen, A.J., and Pohlschroder, M. (2007). Identification of diverse archaeal proteins with class III signal peptides cleaved by distinct archaeal prepilin peptidases. *J Bacteriol* 189, 772-778.

Szadkowski, D. (2018). Identification and characterization of RomX and RomY, two novel motility regulators in *Myxococcus xanthus*. (Marburg, Philipps-University).

Szadkowski, D., Harms, A., Carreira, L.A.M., Wigbers, M., Potapova, A., Wuichet, K., Keilberg, D., Gerland, U., and Søgaard-Andersen, L. (2019). Spatial control of the GTPase MglA by localized RomR-RomX GEF and MglB GAP activities enables *Myxococcus xanthus* motility. *Nat Microbiol*.

Takhar, H.K., Kemp, K., Kim, M., Howell, P.L., and Burrows, L.L. (2013). The platform protein is essential for type IV pilus biogenesis. *J Biol Chem* 288, 9721-9728.

Tammam, S., Sampaleanu, L.M., Koo, J., Manoharan, K., Daubaras, M., Burrows, L.L., and Howell, P.L. (2013). PilMNOPQ from the *Pseudomonas aeruginosa* type IV pilus system form a trans-envelope protein interaction network that interacts with PilA. *J Bacteriol* 195, 2126-2135.

Tanaka, K., Nakasone, Y., Okajima, K., Ikeuchi, M., Tokutomi, S., and Terazima, M. (2012). Time-resolved tracking of interprotein signal transduction: *Synechocystis* PixD-PixE complex as a sensor of light intensity. *J Am Chem Soc* 134, 8336-8339.

ter Beek, J., Guskov, A., and Slotboom, D.J. (2014). Structural diversity of ABC transporters. *J Gen Physiol* 143, 419-435.

Thomassin, J.L., Santos Moreno, J., Guilvout, I., Tran Van Nhieu, G., and Francetic, O. (2017). The trans-envelope architecture and function of the type 2 secretion system: new insights raising new questions. *Mol Microbiol* 105, 211-226.

Thomasson, B., Link, J., Stassinopoulos, A.G., Burke, N., Plamann, L., and Hartzell, P.L. (2002). MglA, a small GTPase, interacts with a tyrosine kinase to control type IV pili-mediated motility and development of *Myxococcus xanthus*. *Mol Microbiol* 46, 1399-1413.

Treuner-Lange, A., Macia, E., Guzzo, M., Hot, E., Faure, L.M., Jakobczak, B., Espinosa, L., Alcor, D., Ducret, A., Keilberg, D., *et al.* (2015). The small G-protein MglA connects to the MreB actin cytoskeleton at bacterial focal adhesions. *J Cell Biol* 210, 243-256.

Vetter, I.R., and Wittinghofer, A. (2001). The guanine nucleotide-binding switch in three dimensions. *Science* 294, 1299-1304.

Wall, D., Kolenbrander, P.E., and Kaiser, D. (1999). The *Myxococcus xanthus pilQ* (*sgIA*) gene encodes a secretin homolog required for type IV pilus biogenesis, social motility, and development. *J Bacteriol* 181, 24-33.

Wang, F., Coureuil, M., Osinski, T., Orlova, A., Altindal, T., Gesbert, G., Nassif, X., Egelman, E.H., and Craig, L. (2017). Cryoelectron Microscopy Reconstructions of the *Pseudomonas aeruginosa* and *Neisseria gonorrhoeae* Type IV Pili at Sub-nanometer Resolution. *Structure* 25, 1423-1435 e1424.

Ward, M.J., Lew, H., and Zusman, D.R. (2000). Social motility in *Myxococcus xanthus* requires FrzS, a protein with an extensive coiled-coil domain. *Mol Microbiol* 37, 1357-1371.

Watnick, P.I., Fullner, K.J., and Kolter, R. (1999). A role for the mannose-sensitive hemagglutinin in biofilm formation by *Vibrio cholerae* El Tor. *J Bacteriol* 181, 3606-3609.

Weiss, R.L. (1971). The structure and occurrence of pili (fimbriae) on *Pseudomonas aeruginosa*. *J Gen Microbiol* 67, 135-143.

Welker, A., Cronenberg, T., Zollner, R., Meel, C., Siewering, K., Bender, N., Hennes, M., Oldewurtel, E.R., and Maier, B. (2018). Molecular Motors Govern Liquidlike Ordering and Fusion Dynamics of Bacterial Colonies. *Phys Rev Lett* 121, 118102.

Whitchurch, C.B., Alm, R.A., and Mattick, J.S. (1996). The alginate regulator AlgR and an associated sensor FimS are required for twitching motility in *Pseudomonas aeruginosa*. *Proc Natl Acad Sci U S A* 93, 9839-9843.

Whitchurch, C.B., Beatson, S.A., Comolli, J.C., Jakobsen, T., Sargent, J.L., Bertrand, J.J., West, J., Klausen, M., Waite, L.L., Kang, P.J., *et al.* (2005). *Pseudomonas aeruginosa fimL* regulates multiple virulence functions by intersecting with Vfr-modulated pathways. *Mol Microbiol* 55, 1357-1378.

Whitchurch, C.B., Leech, A.J., Young, M.D., Kennedy, D., Sargent, J.L., Bertrand, J.J., Semmler, A.B., Mellick, A.S., Martin, P.R., Alm, R.A., *et al.* (2004). Characterization of a complex chemosensory signal transduction system which controls twitching motility in *Pseudomonas aeruginosa*. *Mol Microbiol* 52, 873-893.

Wilde, A., and Mullineaux, C.W. (2017). Light-controlled motility in prokaryotes and the problem of directional light perception. *FEMS Microbiol Rev* 41, 900-922.

Wolfgang, M., Lauer, P., Park, H.S., Brossay, L., Hebert, J., and Koomey, M. (1998a). PilT mutations lead to simultaneous defects in competence for natural transformation and twitching motility in pilated *Neisseria gonorrhoeae*. *Mol Microbiol* 29, 321-330.

Wolfgang, M., Park, H.S., Hayes, S.F., van Putten, J.P., and Koomey, M. (1998b). Suppression of an absolute defect in type IV pilus biogenesis by loss-of-function mutations in *pilT*, a twitching motility gene in *Neisseria gonorrhoeae*. *Proc Natl Acad Sci U S A* 95, 14973-14978.

Wu, S.S., and Kaiser, D. (1995). Genetic and functional evidence that Type IV pili are required for social gliding motility in *Myxococcus xanthus*. *Mol Microbiol* 18, 547-558.

Wu, S.S., and Kaiser, D. (1996). Markerless deletions of *pil* genes in *Myxococcus xanthus* generated by counterselection with the *Bacillus subtilis sacB* gene. *J Bacteriol* 178, 5817-5821.

- Wu, S.S., and Kaiser, D. (1997). Regulation of expression of the *pilA* gene in *Myxococcus xanthus*. *J Bacteriol* 179, 7748-7758.
- Wu, S.S., Wu, J., Cheng, Y.L., and Kaiser, D. (1998). The *pilH* gene encodes an ABC transporter homologue required for type IV pilus biogenesis and social gliding motility in *Myxococcus xanthus*. *Mol Microbiol* 29, 1249-1261.
- Wuichet, K., and Søgaard-Andersen, L. (2014). Evolution and diversity of the Ras superfamily of small GTPases in prokaryotes. *Genome Biol Evol* 7, 57-70.
- Yang, F., Tian, F., Li, X., Fan, S., Chen, H., Wu, M., Yang, C.H., and He, C. (2014). The degenerate EAL-GGDEF domain protein Filp functions as a cyclic di-GMP receptor and specifically interacts with the PilZ-domain protein PXO_02715 to regulate virulence in *Xanthomonas oryzae* pv. *oryzae*. *Mol Plant Microbe Interact* 27, 578-589.
- Yang, R., Bartle, S., Otto, R., Stassinopoulos, A., Rogers, M., Plamann, L., and Hartzell, P. (2004). AglZ is a filament-forming coiled-coil protein required for adventurous gliding motility of *Myxococcus xanthus*. *J Bacteriol* 186, 6168-6178.
- Yang, Z., Duan, X., Esmaeilian, M., and Kaplan, H.B. (2008). Composition, structure, and function of the *Myxococcus xanthus* cell envelope. In *Myxobacteria: Multicellularity and Differentiation*, D.E. Whitworth, ed. (Washington, DC: ASM Press).
- Yang, Z., Geng, Y., and Shi, W. (1998). A DnaK homolog in *Myxococcus xanthus* is involved in social motility and fruiting body formation. *J Bacteriol* 180, 218-224.
- Yang, Z., Lux, R., Hu, W., Hu, C., and Shi, W. (2010). PilA localization affects extracellular polysaccharide production and fruiting body formation in *Myxococcus xanthus*. *Mol Microbiol* 76, 1500-1513.
- Yang, Z., Ma, X., Tong, L., Kaplan, H.B., Shimkets, L.J., and Shi, W. (2000). *Myxococcus xanthus dif* genes are required for biogenesis of cell surface fibrils essential for social gliding motility. *J Bacteriol* 182, 5793-5798.
- Yoshihara, S., Geng, X., and Ikeuchi, M. (2002). *pilG* Gene cluster and split *pilL* genes involved in pilus biogenesis, motility and genetic transformation in the cyanobacterium *Synechocystis* sp. PCC 6803. *Plant Cell Physiol* 43, 513-521.
- Yoshihara, S., Suzuki, F., Fujita, H., Geng, X.X., and Ikeuchi, M. (2000). Novel putative photoreceptor and regulatory genes Required for the positive phototactic movement of the unicellular motile cyanobacterium *Synechocystis* sp. PCC 6803. *Plant Cell Physiol* 41, 1299-1304.
- Youderian, P., and Hartzell, P.L. (2006). Transposon insertions of magellan-4 that impair social gliding motility in *Myxococcus xanthus*. *Genetics* 172, 1397-1410.
- Yuan, H., and Bauer, C.E. (2008). PixE promotes dark oligomerization of the BLUF photoreceptor PixD. *Proc Natl Acad Sci U S A* 105, 11715-11719.
- Yuen, A.S., Kolappan, S., Ng, D., and Craig, L. (2013). Structure and secretion of CofJ, a putative colonization factor of enterotoxigenic *Escherichia coli*. *Mol Microbiol* 90, 898-918.
- Zeytuni, N., and Zarivach, R. (2012). Structural and functional discussion of the tetra-trico-peptide repeat, a protein interaction module. *Structure* 20, 397-405.
- Zhang, Y., Franco, M., Ducret, A., and Mignot, T. (2010). A bacterial Ras-like small GTP-binding protein and its cognate GAP establish a dynamic spatial polarity axis to control directed motility. *PLoS Biol* 8, e1000430.

Zhang, Y., Guzzo, M., Ducret, A., Li, Y.Z., and Mignot, T. (2012). A dynamic response regulator protein modulates G-protein-dependent polarity in the bacterium *Myxococcus xanthus*. PLoS Genet 8, e1002872.

ACKNOWLEDGEMENTS

Above all I would like to express my genuine gratitude to my advisor, Prof. MD, PhD Lotte Søgaaard-Andersen for introducing the challenging yet fascinating world of protein regulation to me and helping me to find a path through this world. I deeply appreciate all the patient and necessary comments and advices she gave to me over past five years. Undoubtedly, my skills, knowledge and research in general evolved so much due to professional and careful guidance provided by me supervisor.

Next, I absolutely need to mention lovely postdocs that who helped me on the very first steps over my PhD time and further kept giving tips and hints at every troublesome moment. Thank you so much – Dr. Nuria Gómez-Santos, Dr. Magdalena Połatyńska, Dr. Beata Jakobczak.

I cannot imagine to go through this long way without people that were closest to me and supported me equally great in scientific as well as in life situations. Dearest Portuguese colleague of mine Luis Carreira, who arrived to the lab at the same time as I did and was fighting with every (motile and non-motile) dilemma side by side with me. Dobro, who watched my back and surrounded me with permanent help I could always count on. Sweet little Maria who studies and knows practically everything and can just give you a warm smile every time you need. Of course, Sofy, a real fighter, smart and strong woman who have been through darkest and brightest moments with me. No need to say that those people created very special atmosphere that was inspiring and cheering me up every day.

I would like to thank Steffi Lindow, Dr. Dorota Skotnicka, Dr. Anke Treuner-Lange and Dr. Dominik Schumacher for highly qualified scientific help I could ask for whenever it was needed. With their assistance I grew significantly in a professional way and the experiments I carried out were maximally informative and successful. Additionally I feel necessary to thank Dr. Timo Glatter for optimal solutions and help with performing co-IP and mass spectrometry experiments.

Of course I feel greatly thankful to the members of my thesis advisory committee, Dr. Simon Ringgaard, Prof. Dr. Martin Thanbichler and on the early stage Dr. Kristina Jonas for their careful attention, fruitful discussions and suggestions about my project. Special gratitude should be forwarded to the International Max Planck Research School that provided funding for this research.

Finally, no words can give a high enough value to my friends and family. I want to say how priceless was support given to me by Shankar, Bartosz and Tanya – here in Marburg, and Veta, Anna, Diana and Elena – back home. These amazing people never allowed me to doubt my ability

for finishing my PhD. And of course the one and the only – my loving mother. You gave me all your powers and care and I will never be able to pay back in full.

CURRICULUM VITAE**Personal data**

Name Anna Potapova
Date of birth May 21st 1991
Place of birth Ekaterinburg, Russia

Education

From 09/2014 PhD (Dr. rer. nat.) Philipps-University Marburg
Max Planck Institute for Terrestrial Microbiology, Marburg, Germany
Supervisor: Prof. MD, PhD Lotte Søgaard-Andersen

09/2012 – 06/2014 Master of Science
Pushchino State Institute of Natural Sciences, Pushchino, Russia
Supervisor: Dr. Maria Tutukina

09/2008 – 07/2012 Bachelor of Science
Ural Federal University named after the first President of Russia B.N.
Yeltsin, Ekaterinburg, Russia
Supervisor: Nikolay Firsov

09/2006 – 06/2008 Special center for study and science of Ural Federal University

Internships

06/2011 – 08/2011 Pre-degree practice in microbiology
G.K. Skryabin Institute of Biochemistry and Physiology of
Microorganisms, RAS, Pushchino, Russia

02/2014 – 03/2014 Research training in intermolecular interactions modeling
Centre for Genomic Regulation, Barcelona, Spain

List of publications

The small GTPase MglA in concert with the SgmX scaffold protein stimulate type IV pili formation and function in *Myxococcus xanthus*.

Potapova A, Szadkowski D, Carreira L & Søgaard-Andersen L (Manuscript in preparation).

Spatial control of the GTPase MglA by localized RomR–RomX GEF and MglB GAP activities enables *Myxococcus xanthus* motility.

Szadkowski D, Harms A, Carreira L, Wigbers M, Potapova A, Wuichet K, Keilberg D, Gerland U & Søgaard-Andersen L. Nature Microbiology 2019 May. doi: 10.1038/s41564-019-0451-4.

Structural modeling of the ExuR and UxuR transcription factors of *E. coli*: search for the ligands affecting their regulatory properties.

Tutukina MN, Potapova AV, Vlasov PK, Purtov UA & Ozoline ON. J Biomol Struct Dyn. 2016. V. 34 (10). 2296-2304.

Control of hexuronate metabolism in *Escherichia coli* by the two interdependent regulators, ExuR and UxuR: derepression by heterodimer formation.

Tutukina MN, Potapova AV, Cole JA & Ozoline ON. Microbiology. 2016. V. 162 (7). 1220-1231.

ERKLÄRUNG

Hiermit versichere ich, dass ich die vorliegende Dissertation mit dem Titel „Regulation of type IV pili formation and function by the small GTPase MglA in *Myxococcus xanthus*“ selbstständig verfasst, keine anderen als die im Text angegebenen Hilfsmittel verwendet und sämtliche Stellen, die im Wortlaut oder dem Sinn nach anderen Werken entnommen sind, mit Quellenangaben kenntlich gemacht habe.

Die Dissertation wurde in der jetzigen oder einer ähnlichen Form noch bei keiner anderen Hochschule eingereicht und hat noch keinen sonstigen Prüfungszwecken gedient.

Ort, Datum

Anna Potapova

EINVERSTÄNDNISERKLÄRUNG

Ich erkläre mich damit einverstanden, dass die vorliegende Dissertation

„Regulation of type IV pili formation and function by the small GTPase MglA in *Myxococcus xanthus*“

in Bibliotheken allgemein zugänglich gemacht wird. Dazu gehört, dass sie

von der Bibliothek der Einrichtung, in der ich meine Arbeit anfertigt habe, zur Benutzung in ihren Räumen bereitgehalten wird;

in konventionellen und maschinenlesbaren Katalogen, Verzeichnissen und Datenbanken verzeichnet wird;

im Rahmen der urheberrechtlichen Bestimmungen für Kopierzwecke genutzt werden kann.